THE UNIVERSITY
of EDINBURGH

Dissecting the Meiotic Defects of *Tex19.1*$^{-/-}$ Mouse Spermatocytes

James H. Crichton

For the Degree of Doctor of Philosophy

University of Edinburgh

August 2014

igmm
INSTITUTE OF GENETICS & MOLECULAR MEDICINE

Declaration

I declare that the work presented in this PhD thesis is my own except where otherwise stated. This work has not been submitted for any other degree.

James H. Crichton 14th of August, 2014

Acknowledgements

I am very grateful to many people without whom this work would not have been possible.

I've felt privileged to have been given the opportunity to conduct my PhD under the supervision of Ian Adams. His guidance and encouragement throughout this project have kept me feeling optimistic even on the darkest winter days, and his endless energy and enthusiasm have been an inspiration. I'd also like to thank Ian Overton, Richard Meehan and Andrew Jackson for all their input. I'm very grateful to a number of people for providing me with mice and reagents which have helped my work enormously: James Turner for the *Spo11* mutant mice, and Howard Cooke, Bernard de Massy, Scott Keeney, David Elliott, and James Ingles for antibodies. Shelagh Boyle's FISH wisdom has been of great benefit, as has the technical guidance of Donncha Dunican and Nick Gilbert. In particular, Matthew Pearson and Paul Perry's assistance with microscopy has been invaluable, and helped my days in the dungeon fly by. Thanks also to the members of the Chromosomes and Gene Expression section, the challenging and supportive atmosphere of which has provided a stimulating work environment. I owe a special thanks to Diana Best, Judith Reichmann, Marie MacLennan, Abby Wilson, David Read and Chris Playfoot for all their help, support and excellent tunes; making my time in the Adams lab an extremely enjoyable experience.

My family's encouragement and constant support through all the ups and downs has always been a great comfort and hugely motivational; thank you. Thanks also to all the friends I've made along the way, to David, Juan and Ruari for all the parties and everyone else for making them so much fun! Last but not least, thank you Rosie for keeping me fed, sane and happy.

"Mutability is our tragedy, but it's also our hope"

- Boethius

Abstract

The maintenance of genomic stability through suppression of retrotransposon activity is vital for the avoidance of potentially mutagenic genomic disruption caused by retrotransposition. Germline development is a particularly important phase for retrotransposon silencing as retrotransposition events here have the potential for transmission to the entire embryo, threatening the health of offspring. A collection of germline genome defence genes are required for the suppression of retrotransposons in the developing germline of male mice (e.g. *Tex19.1, Dazl, Mili, Miwi2, Gasz, Mov10l1, Mael, Dnmt3l*), all of which trigger meiotic prophase arrest when mutated. I have analysed the meiotic defects which arise in *Tex19.1*$^{-/-}$ male mice to contribute to the understanding of the fundamental mechanisms required for successful completion of meiosis and to investigate the involvement of retrotransposon silencing in this process.

The absence of TEX19.1 in male mice causes infertility; with failed chromosome synapsis in ~50% of pachytene nuclei and associated apoptosis, as well as individual univalent chromosomes in 67% of remaining nuclei progressing to metaphase I. Where studied, failed chromosome synapsis is a common feature of germline genome defence mutant spermatocytes. One aim of my studies has been to better understand the mechanism responsible for this failed chromosome synapsis. I have demonstrated that unlike *Mael*$^{-/-}$ spermatocytes, additional SPO11-independent DNA damage potentially attributable to retrotransposition is not detectable in *Tex19.1*$^{-/-}$ spermatocytes. Rather, the formation of meiotic DNA double strand breaks (DSBs) is dramatically reduced in early prophase to around 50%, resulting in a reduction in nuclear γH2AX signal, production of SPO11-oligonucleotide complexes and foci formation by early recombination proteins RPA, DMC1 and RAD51. Despite this early reduction, DSB frequency recovers to more normal levels shortly after in zygotene. I have shown that defective pairing of homologous chromosomes by meiotic recombination is likely responsible for the asynapsis previously reported. The initial reduction in DSB frequency could be sufficient to cause failed chromosome synapsis in this mutant, assuming that late-forming DSBs cannot participate effectively in promoting homologous pairing. Alternative hypotheses include altered positioning of DSBs in response to altered chromatin organisation relating to retrotransposon upregulation, misguiding the pairing of homologous chromosomes. Such a model of disruption could also extend to other germline genome defence mutants.

I have demonstrated that despite successful pairing of homologous chromosomes in a sub-population of *Tex19.1*$^{-/-}$ spermatocytes, subsequent progression of these cells through

pachytene is delayed. Numerous diverse features of progression are all delayed, including recombination, ubiquitination on autosomes and sex chromosomes, expression of the mid-pachytene marker H1t, and chromosome organisation. The delay identified is related to recombination therefore this feature is likely to stem from the initial defect in DSB formation early in prophase. While some delayed features are probably directly related to recombination, others are not. The coordinated delay observed may suggest the presence of a recombination-sensitive cell-cycle checkpoint operating to regulate progression through pachytene.

My research has also aimed to establish the cause of elevated univalent chromosomes not connected by chiasmata in metaphase I *Tex19.1*$^{-/-}$ spermatocytes. I have demonstrated that that absence of chiasmata is not due to failed crossover formation between synapsed chromosomes. Rather, the frequent observation of individual unsynapsed chromosomes during crossover formation suggests that some spermatocytes with low-level asynapsis are leaking through meiotic checkpoints and are unable to form a crossover before reaching metaphase. Therefore, again this later meiotic defect appears to stem from the initial defect in meiotic DSB formation, the consequences of which vary widely in severity. Remarkably the unsynapsed chromosomes present during crossover formation include both sex chromosomes, and autosomes. Tolerance of an unsynapsed autosome from pachytene into metaphase is an unusual observation in mice and this observation may aid the understanding of spermato cyte quality control mechanisms during this progression.

Together these findings have greatly advanced the understanding of the infertility incurred during meiosis in *Tex19.1*$^{-/-}$ male mice. These findings may also extend to benefit the understanding of other germline genome defence mutants. Diverse observations made during my investigations also reveal a potential system of coordinated progression through pachytene relating to meiotic recombination. The variable severity of the synapsis defects incurred in this mutant appears to have variable effects on spermatocyte survival and could also inform the understanding of meiotic checkpoint sensitivity.

Table of Contents

Declaration 2

Acknowledgements 3

Abstract 5

Table of Contents 7

List of Figures 13

Abbreviations 15

1 Introduction 17

1.1 Reproduction 18

1.2 Meiosis 18

1.3 The Synaptonemal Complex 21

1.3.1 Overview 21

1.3.2 Formation of the Synaptonemal Complex 22

1.3.3 The Chromosome Core 25

1.4 Cohesin 26

1.4.1 Sister Chromatid Cohesion 26

1.4.2 The Cohesin Complex 26

1.4.3 Addition and Removal of Cohesin in Mitosis 28

1.4.4 Additional Roles of Mitotic Cohesin 31

1.4.5 Meiotic Cohesin 31

1.4.6 Loading of Meiotic Cohesin 33

1.4.7 Role of Meiotic Cohesin 33

1.4.8 Removal of cohesin in meiosis 38

1.5 Recombination 39

1.5.1 SPO11 41

1.5.2 Recombination Hotspots 43

1.5.3 DSB Formation 45

1.5.4 DSB Processing 48

1.5.5 Early Recombination Proteins – Homology Search 50
1.5.6 Additional Mechanisms of Homolog Pairing 54
1.5.7 Intermediate Recombination Proteins – Joint Molecule Stabilisation 55
1.5.8 Late Recombination Proteins – Holliday Junction Resolution 57
1.6 The Pachytene Checkpoint 63
1.6.1 Meiotic silencing pathways: MSUC and MSCI 63
1.6.2 Mechanism of meiotic silencing 64
1.6.3 DNA Damage Pachytene Checkpoint 67
1.7 Role of Genome Defence Genes in Gametogenesis 68
1.7.1 Introduction to Retrotransposons 68
1.7.2 DNA methylation and transcriptional silencing 69
1.7.3 De novo DNA methylation 70
1.7.4 The piRNA retrotransposon silencing pathway 73
1.7.5 TEX19.1 in germline genome defence 79
1.7.6 How does retrotransposon activity cause infertility in males? 79
1.8 TEX19.1 and UBR2 81
1.9 Thesis Outline 84
2 Materials & Methods 86
2.1 Embryonic Stem Cell Culture 86
2.1.1 Freezing and Thawing Cells Stored in Liquid Nitrogen 86
2.1.2 Routine Cell Culture and Harvesting 86
2.1.3 Cell Counting 86
2.1.4 X-ray Irradiation 87
2.2 Animals 87
2.2.1 Animals Used 87
2.2.2 Genotyping Polymerase Chain Reaction (PCR) 87
2.2.3 Agarose Gel Electrophoresis 88
2.2.4 Drug Treatment 88

2.3 Gene Expression Analysis 89
2.3.1 RNA Isolation 89
2.3.2 cDNA Synthesis 90
2.3.3 qRT-PCR 90
2.3.4 Primer Design 91
2.4 SPO11 Oligonucleotide Assay 91
2.4.1 Preparation of Testes Lysates 91
2.4.2 Immunoprecipitation 92
2.4.3 Labelling and Resolving SPO11-Oligo Complexes 92
2.5 Imaging 93
2.5.1 Testis Spread Preparation 93
2.5.2 Antibody Staining 94
2.5.3 Spermatocyte Staging 95
2.5.4 Image Capture and Analysis 95
2.5.5 Metaphase Chromosome Spreading 96
2.5.6 Fluorescence *in situ* hybridisation (FISH) 97
3 Retrotransposon Activity Detection by Microarray and Involvement in *Tex19.1*$^{-/-}$ Meiotic Chromosome Asynapsis 100
3.1 Introduction 100
3.2 Results 102
3.2.1 Experimental Validation of Microarray Data Re-Annotated to Reveal Repetitive Element Expression 102
3.2.2 Investigating the Effect of Retrotransposon Activity on Events in *Tex19.1*$^{-/-}$ Spermatocyte Meiotic Prophase I 112
3.3 Discussion 118
3.3.1 Novel Retrotransposon Targets of HDAC1 Regulation in Identified in Mouse ESCs 119
3.3.2 TEX19.1 Regulation of Reterotransposon Activity 120
3.3.3 Mechanism of Chromosome Asynapsis in *Tex19.1*$^{-/-}$ Spermatocytes 121

4 Investigating the Cause of Homologous Chromosome Asynapsis in *Tex19.1*$^{-/-}$ Spermatocytes 124

4.1 Introduction 124

4.2 Results 127

4.2.1 Assessing the Nature of Asynapsed Chromosomes in *Tex19.1*$^{-/-}$ Spermatocytes 127

4.2.2 Investigating the Recruitment of Early Recombination Proteins in *Tex19.1*$^{-/-}$ Spermatocytes 132

4.2.3 Assessing DNA Double Strand Break Processing in *Tex19.1*$^{-/-}$ 138

4.2.4 Investigating DSB formation in *Tex19.1*$^{-/-}$ 141

4.3 Discussion 145

4.3.1 Caveats of Immunocytological Analysis 145

4.3.2 Meiotic Recombination Delay/Reduction and Chromosome Synapsis 146

4.3.3 Mechanisms of DSB Control 148

4.3.4 DSB Targeting and Chromosome Synapsis 150

5 Investigating Synapsed *Tex19.1*$^{-/-}$ Pachytene Spermatocytes for Defects Associated with Impaired Recombination 153

5.1 Introduction 153

5.2 Results 155

5.2.1 Do Recombination Defects Persist in *Tex19.1*$^{-/-}$ Synapsed Pachytene Spermatocytes? 155

5.2.2 Progression to Crossover Formation in *Tex19.1*$^{-/-}$ Pachytene Spermatocytes 159

5.2.3 Expression of Pachytene Sub-stage Markers and Events in *Tex19.1*$^{-/-}$ 161

5.2.4 Assessing MSCI in *Tex19.1*$^{-/-}$ 166

5.2.5 Investigating the Coordination of Delayed Pachytene Progression in *Tex19.1*$^{-/-}$ 167

5.3 Discussion 173

5.3.1 *Tex19.1*$^{-/-}$ Spermatocytes Survive Pachytene after Autosomal Synapsis is Achieved 173

5.3.2 Progression through Pachytene is Delayed in *Tex19.1*$^{-/-}$ Spermatocytes 174

5.3.3 Ubiquitination in *Tex19.1*$^{-/-}$ Pachytene Spermatocytes 176

6 Investigating the Source of Univalent Metaphase I Chromosomes in *Tex19.1*$^{-/-}$ Testes.... 179

6.1 Introduction 179

6.2 Results 181

6.2.1 Validating the Metaphase I Defect in Backcrossed *Tex19.1*$^{-/-}$ Spermatocytes... 181

6.2.2 Autosomal Crossover Formation in Pachytene *Tex19.1*$^{-/-}$ Spermatocytes ... 184

6.2.3 Autosomal Crossover Distribution..... 185

6.2.4 Autosomal Asynapsis as a Source of Univalent Metaphase I Chromosomes in *Tex19.1*$^{-/-}$ 187

6.2.5 Crossover Formation between Sex Chromosomes in *Tex19.1*$^{-/-}$ Spermatocytes 190

6.2.6 Sex Chromosome Asynapsis as a Source of Univalent Metaphase I Chromosomes 192

6.3 Discussion 194

6.3.1 Defects in Crossover Formation do not Cause Univalent Chromosomes in *Tex19.1*$^{-/-}$ Metaphase I Spermatocytes 194

6.3.2 Sex Chromosome Asynapsis in *Tex19.1*$^{-/-}$ Crossover-Forming Spermatocytes. 195

6.3.3 Autosomal Asynapsis in *Tex19.1*$^{-/-}$ Crossover-Forming Spermatocytes..... 196

7 Discussion 200

7.1 Defective Events in Early Recombination Cause Pachytene Chromosome Asynapsis in *Tex19.1*$^{-/-}$ 200

7.2 Defective Recombination Delays Progression of Synapsed *Tex19.1*$^{-/-}$ Spermatocytes through Pachytene 205

7.3 Pachytene Asynapsis Causes Univalent Chromosomes in *Tex19.1*$^{-/-}$ Metaphase I Spermatocytes 207

7.4 Retrotransposon Regulation and Fertility Through Evolution..... 208

7.5 Conclusion 209

Bibliography 212

Appendix 254

List of Figures

Figure 1-1. Mitotic and meiotic cell division. 19
Figure 1-2. Parallel progression of synaptonemal complex formation and recombination in meiotic prophase I 20
Figure 1-3. Assembly of the synaptonemal complex 22
Figure 1-4. Structure of the cohesin complex 27
Figure 1-5. Models of the maintenance and de-protection of cohesin in mitosis 29
Figure 1-6. Putative subunit composition of cohesin complexes 32
Figure 1-7. Anchorage of meiotic chromatin by cohesin determines axis length 37
Figure 1-8. Proteins and events involved in meiotic recombination 41
Figure 1-9. Connecting meiotic DSB sites to chromosome axes in *S. Cerevisiae* by Spp1 47
Figure 1-10. Strand invasion in meiotic recombination 52
Figure 1-11. Model for pre-leptotene DSB-independent pairing in mice 55
Figure 1-12. Sliding clamp model for MSH4-MSH5 stabilisation of meiotic joint molecules 56
Figure 1-13. Model of the antagonistic roles of RNF212 and HEI10 in meiotic DSB repair 61
Figure 1-14. MSUC triggers MSCI failure and meiotic arrest 64
Figure 1-15. Global DNA methylation loss triggers genome-defence gene activation during germline development 70
Figure 1-16. Expression patterns and mutant phenotypes of germline genome defence genes 73
Figure 1-17. The piRNA pathway 75
Figure 13-2. LTR retrotransposon targets of polycomb repressive complexes in ES cells. 104
Figure 3-3. Behaviour of different *RLTR4* retrotransposon microarray probe populations in *Ring1B*$^{-/-}$ single knockout ES cells. 106
Figure 3-4. A single rearranged copy of *RLTR4-int* is upregulated in *Ring1B*$^{-/-}$ single knockout ES cells. 107
Figure 3-5. Reanalysis of *Hdac1*$^{-/-}$ ES cell microarray data to assess rerotransposon expression. 109
Figure 3-6. qRT-PCR validation of retrotransposon expression changes in *Hdac1*$^{-/-}$ single knockout ES cells. 110
Figure 3-7. Physical association between HDAC1 and misregulated repetitive element sequences. 111
Figure 3-8. Effect of TEX19.1 on SPO11-independent meiotic DNA damage. 114
Figure 3-9. Effect of TEX19.1 on SPO11-independent recombination Foci. 116

Figure 4-1. Chromosome asynapsis in *Tex19.1*$^{-/-}$ pachytene spermatocytes 129
Figure 4-2. Synaptonemal complex formation in recombination-deficient spermatocytes . 131
Figure 4-3. Timing of early meiotic recombination protein recruitment 133
Figure 4-4. Early recombination protein localisation in zygotene spermatocytes 135
Figure 4-5. Early recombination protein localisation in leptotene spermatocytes 137
Figure 4-6. SPO11-oligonucleotide complex assessment 139
Figure 4-7. Embryonic stem cell sensitivity to DNA damage 140
Figure 4-8. γH2AX quantification in leptotene 142
Figure 4-9. MEI4 localisation leptotene 144
Figure 5-1. Early recombination protein localisation in pachytene spermatocytes 156
Figure 5-2. DNA damage levels in pachytene spermatocytes 158
Figure 5-3. Analysis of crossover-forming pachytene spermatocytes 160
Figure 5-4. Mid-pachytene progression of spermatocytes 162
Figure 5-5. UbH2A localisation to the sex body in pachytene 163
Figure 5-6. Mono- and poly-ubiquitin in pachytene spermatocytes 165
Figure 5-7. MSCI in pachytene spermatocytes 167
Figure 5-8. Synapsed pachytene spermatocyte axis length. 169
Figure 5-9. Pachytene autosomal axis length compared to DNA damage 171
Figure 5-10. Mid-pachytene progression of spermatocytes Lacking SPO11 172
Figure 6-1. Analysis of univalent metaphase I chromosomes 183
Figure 6-2. MLH1 analysis of crossover formation 185
Figure 6-3. Autosomal MLH1 distribution and positioning 187
Figure 6-4. Extent of asynapsis in *Tex19.1*$^{-/-}$ Spermatocytes 188
Figure 6-5. Autosomal asynapsis in MLH1 positive spermatocytes 189
Figure 6-6. Crossover formation between sex chromosomes 191
Figure 6-7. XY asynapsis in MLH1 positive spermatocytes 193
Figure 6-8. Model for generation of univalent chromosomes by low-level asynapsis 198
Figure 7-1. Model for shared mechanism of asynapsis in germline genome defence mutants 204

Abbreviations

µg	:	Microgram
µl	:	Microlitre
5mC	:	5-Methylcytosine
AE	:	Axial element
BSA	:	Bovine serum albumin
CE	:	Central element
ChIP	:	Chromatin immunoprecipitation
ChIP-seq	:	ChIP sequencing
CO	:	Crossover
DAPI	:	4,6-diamidino-2-phenylidole
DMEM	:	Dulbecco's modified Eagle's medium
DNA	:	Deoxyribonucleic acid
dpp	:	Days post partum
DSB	:	Double strand DNA break
E	:	Embryonic day
ESC	:	Embryonic stem cell
FCS	:	Foetal calf serum
FISH	:	Fluorescence in situ hybridisation
GMEM	:	Glasgow minimum essential medium
H2A	:	Histon 2A
H3K4	:	Histone 3 lysine 4
H3K9	:	Histone 3 lysine 9
HDAC	:	Histone deacetylase
IF	:	Immunofluorescence
IP	:	Immunoprecipitation
IR	:	Ionising radiation
JM	:	Joint molecule
kDa	:	Kilodalton

KO	:	Knockout
LE	:	Lateral element
LIF	:	Leukaemia inhibitory factor
LINE	:	Long interspersed nuclear element
LTR	:	Long terminal repeat
me2	:	Dimethyl
me3	:	Trimethyl
mg	:	Milligram
ml	:	Millilitre
MSCI	:	Meiotic sex chromosome inactivation
MSUC	:	Meiotic silencing of unsynapsed chromatin
NAHR	:	Non-allelic homologous recombination
NDR	:	Nucleotide depleted region
P	:	Postnatal day
PAR	:	Pseudoautosomal region
PBS	:	Phosphase buffer saline
PCR	:	Polymerase chain reaction
PFA	:	Paraformaldehyde
PGC	:	Primordial germ cell
piRNA	:	Piwi interactin RNA
qRT-PCR	:	Quantitative reverse transcription PCR
RNA	:	Ribonucleaic acid
SC	:	Synaptonemal complex
SCC	:	Sister chromatid cohesion
SINE	:	Short interspersed nuclear element
TdT	:	Terminal deoxynucleotidyl transferase
Tex19.1	:	Testis expressed gene 19.1
TF	:	Transverse filament
Ub	:	Ubiquitinated
WT	:	Wild type

Chapter 1:

Introduction

1 Introduction

1.1 Reproduction

Reproduction is a fundamental biological process central to a species' survival, evolution, and therefore life itself. Sexual reproduction requires the production of specialised germ cells (gametes) each containing half of the genetic information necessary to encode for healthy offspring. Fusion of two parental germ cells produces a zygote cell which will undergo patterned mitotic proliferation and differentiation to develop into a new organism and maintain its survival. The production of germ cells requires a specialised, meiotic, cell division and the preparation of each parent's contributing DNA for involvement in this new organism. Since every cell in an organism's body originates from the single zygote formed at its conception, the quality of DNA involved is of great importance, and as such many organisms employ strategies to protect the genomic integrity of germ cell DNA. My PhD has focussed on one of these genome defence mechanisms in particular and the effect of its disruption on germ cell production in male mice, in an attempt to better understand how germline genome defence influences fertility.

1.2 Meiosis

The DNA which comprises the genome is organised into chromosomal units which are typically present in a cell's nucleus in duplicate (diploid cells). The gametes are an exception to this as they contain a single copy of each chromosome (haploid cells). One copy of each chromosome in a diploid cell originates from each parental genome and is inherited via their gametes. These two parental copies of each chromosome are known as homologous chromosomes. During a mitotic cell division the genome is replicated and the two identical copies of every chromosome generated (these identical replicates are known as sister chromatids) are divided into opposite daughter cells (Figure 1-1). Meiosis is a specialised cell division involving a single round of DNA replication followed by two rounds of chromosome segregation. The first meiotic division involves an extended prophase during which numerous meiosis-specific events ensue, crucially generating a genetic exchange (crossover) between every pair of replicated homologous chromosomes by recombination, introducing genetic reorganisation and enabling homologous chromosome segregation into opposing daughter cells in metaphase I. The second meiotic division involves the segregation

of the remaining pairs of sister chromatids, resulting in the production of four genetically unique haploid gametes (Figure 1-1).

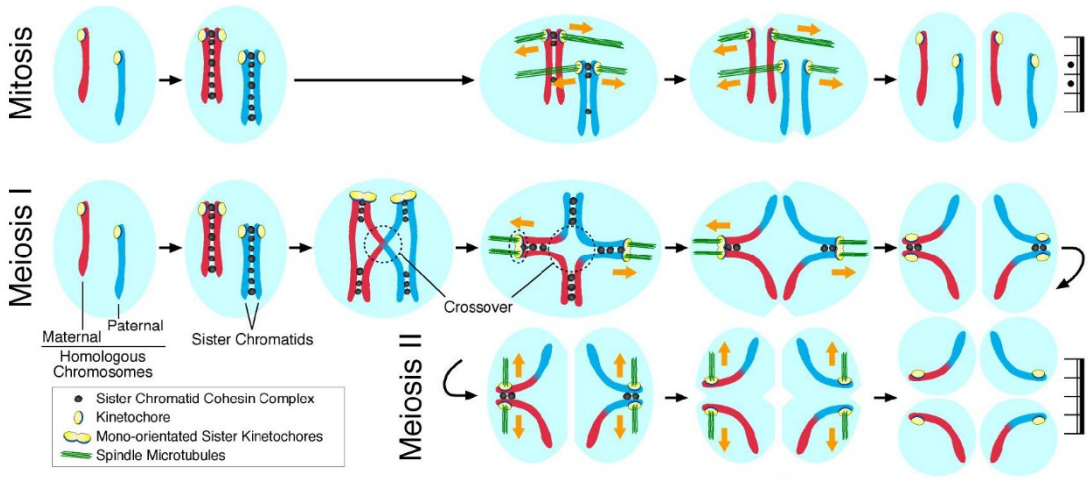

Figure 1-1. Mitotic and meiotic cell division.
Chromosomes are replicated and the duplicate "sister" chromatids are segregated during mitosis. In meiosis, chromosomes are replicated and the "homologous" chromosomes are segregated in the first division by a mechanism dependent on the formation of a genetic exchange (crossover) which connects the chromosomes (discussed in section 1.5). Sister chromatids are segregated in the second meiotic division. Cohesion is maintained between sister chromatids between replication and division by the cohesin complex (discussed in section 1.4). Modified image from Nobuaki Kudo.

Meiotic prophase I is a highly complex and dynamic stage which is divided into cytologically identifiable substages based on the formation of a meiosis-specific structure, the synaptonemal complex (SC), which occurs in parallel with homologous recombination (Figure 1-2). SC formation begins with the localisation of short filaments of proteinacious axial element (AE) providing anchorage for chromatin loops during leptotene. Hundreds of DNA double strand breaks (DSBs) are also generated across the genome in leptotene, initiating homologous recombination. These DSBs recruit successive recombination proteins which promote a search for equivalent sequence on the homologous partner chromosome (Moens et al., 2002). Axial element construction extends throughout the length of the chromosomes and axes of homologous chromosomes brought into close proximity by the homology search begin to synapse together in zygotene, with the formation of transverse filaments (TFs) extending from the AE to connect via a shared central element (CE) (Figure 1-2). Following synapsis AEs are commonly referred to as lateral elements (LEs). Every autosomal pair of homologous chromosome is completely synapsed at the pachytene stage of prophase. The X and Y sex chromosomes of male mice only synapse in a short region of shared homology known as the pseudosautosomal region (PAR). DSBs are repaired before

the end of pachytene, with a subpopulation ultimately repairing to form a genetic exchange termed a crossover, which physically links homologous chromosomes. This physical linkage is maintained by cohesin complexes which hold sister chromosomes together until cell divisions. Subsequent desynapsis of chromosomes proceeds in diplotene with the dissociation of the central element followed by axial element proteins (Figure 1-2). Cohesin complexes remain until correct bipolar alignment of homologous chromosomes is achieved by the spindle microtubules at the end of metaphase, at which point chromosome arm cohesin is removed, releasing homologous chromosomes to contract to opposite spindle poles (Figure 1-1) (Handel and Schimenti, 2010).

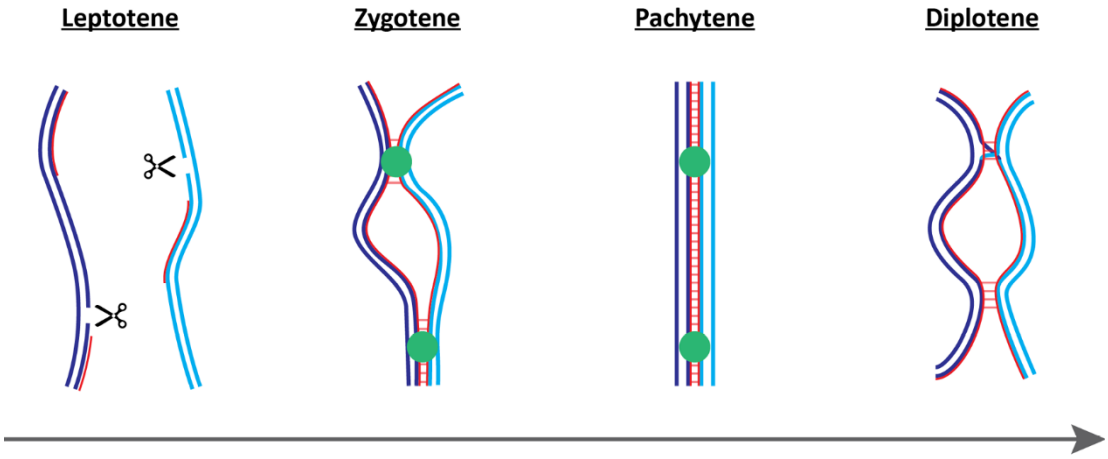

Figure 1-2. Parallel progression of synaptonemal complex formation and recombination in meiotic prophase I
Schematic depicts the simultaneous formation and dissolution of the synaptonemal complex and meiotic homologous recombination. Paired blue strands indicate replicated sister chromatids, light blue and dark blue distinguish homologous chromosomes. Axial element (red) begins to form in leptotene while DNA is cut generating double strand breaks (DSBs) (scissors). Formation of DSBs is shown on only one of the two sister chromatids for simplicity. Axial element extends along chromosome lengths in zygotene and DSBs recruit repair proteins. Axes begin to synapse with central element formation (horizontal red bars) between proximal chromosomes. Synapsis is complete in pachytene. DSBs repair before progression to diplotene and the chromosomes desynapse with the dissociation of the central element. Image modified from Crichton et al., 2014.

The timing and progression of meiosis is sexually dimorphic. In male mice quiescent prospermatogonia can differentiate into spermatogonial stem cells shortly after birth, which soon give rise to cells that participate in spermatogenesis (proliferating spermatogonia → meiotic spermatocytes → post-meiotic spermatids → sperm) throughout adult life. In females meiosis is initiated *in utero* but undergoes an arrest at the end of meiotic prophase a few days after birth and groups of these arrested oocytes are periodically selected to grow

and mature with each oestrous cycle. The final oocyte meiotic division is not completed until fertilisation (Ollinger et al., 2010).

1.3 The Synaptonemal Complex

1.3.1 Overview

The assembly and deconstruction of the SC is a feature central to meiotic prophase. Seven components of the mammalian SC have been identified to date. The AE is comprised of SYCP3 and SYCP2, while the CE consists of SYCP1, SYCE1, SYCE2, SYCE3 and TEX12 (Figure 1-3) (Fraune et al., 2012). SYCP3 is the main structural component of the axial element, and exists in two isoforms in mouse (30/33kD), the functional distinctions of which, if any, are currently unknown (Alsheimer et al., 2010). It contains an α-helical C-terminal domain thought to form coiled-coil structures and mediate homotypic or heterotypic protein interactions (Lammers et al., 1994), forms a tetramer and binds to double stranded DNA with its N-terminal sequences (Syrjänen et al., 2014). SYCP2 (173kD) also exhibits a short α-helical domain at its C-terminus (Offenberg et al., 1998) that is required for heterotypic interactions with both SYCP3 (Yang et al., 2006) and SYCP1, leading to a proposed role as the linker connecting the AE and the CE (Bolcun-Filas et al., 2007). SYCP1 (125kD) is the major component of the TF. It is a fibrillar molecule with a large, central α-helical domain which is likely to form coiled-coil structures mediating homotypic interactions (Meuwissen et al., 1992) between N-termini (Liu et al., 1996; Ollinger et al., 2005; Schmekel et al., 1996) and function in dimers (Costa et al., 2005). More recently, four proteins have been identified which depend of SYCP1 for their recruitment and are thus thought to localise specifically to the CE. These are SYCE1, SYCE2, SYCE3, TEX12 (Costa et al., 2005; Hamer et al., 2006; Schramm et al., 2011). These proteins are typically small (38, 19, 14, 12kD respectively) and other than TEX12 all possess predicted coiled-coil motifs.

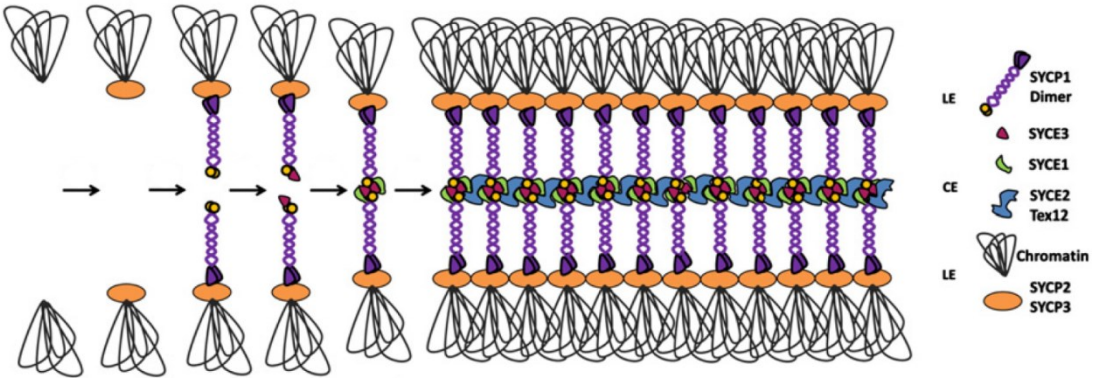

Figure 1-3. Assembly of the synaptonemal complex
Progressive localisation of synaptonemal complex (SC) components indicated. Lateral elements (LE) and central element (CE) marked. Image modified from Fraune et al., 2012.

1.3.2 Formation of the Synaptonemal Complex

The components of the synaptonemal complex are meiosis-specific, however transfection of genes encoding SC proteins into somatic cells has been informative with regards to how these structures form. This method has demonstrated that SYCP1 and SYCP3 possess the ability to self-assemble and form higher order structures (Ollinger et al., 2005; Yuan et al., 1998). The C-terminal domain of SYCP1 is essential for the formation of complexes in transfection experiments; with SYCP1 molecules lacking this domain remaining diffusely distributed. An important role for the N-terminus is also indicated by these experiments as SYCP1 lacking this domain has a reduced, but not abolished, ability to form higher order structures (Ollinger et al., 2005). Unlike SYCP3 and SYCP1, transfected SYCP2 is not capable of self-assembly (Winkel et al., 2009), but does however interact with SYCP3 if co-transfected, and modifies the higher-order complex constructed (Pelttari et al., 2001). Furthermore, SYCP2 interacts with SYCP1 and these proteins form complexes when co-transfected (Winkel et al., 2009). This data supports the roles of SYCP1 and SYCP3 as primary determinants of SC formation. There is currently no strong evidence for a direct interaction between SYCP1 and SYCP3, and the co-transfection experiments discussed have fuelled the hypothesis that SYCP2 behaves as a mediator between SYCP1 and SYCP3 during SC formation (Pelttari et al., 2001; Winkel et al., 2009).

Analysis of SC formation in mouse mutants has been informative as to the importance of the SC and the pattern of its assembly. SYCP3 and SYCP2 are the first components of the SC to localise, forming the AE during leptotene (Figure 1-2, Figure 1-3). In the absence of SYCP3, the AE does not appear to form, and SYCP2 does not localise to chromosomes

(Kolas et al., 2004; Yuan et al., 2000). Therefore SYCP3 is required for SYCP2 localisation. However, mice lacking the C-terminal domain of SYCP2 (referred to as *Sycp2*$^{-/-}$) required for its interaction with SYCP3 and SYCP1 are unable to recruit axial SYCP3 despite the truncated SYCP2 protein forming axial associations. Therefore the C-terminal domain of SYCP2 is needed for SYCP3 localisation and it appears that either SYCP3 doesn't need to be axial to promote SYCP2 localisation, or the truncated form of SYCP2 assumes abnormal properties enabling its independent axis-binding in this mutant. Analysis of a *Sycp2*$^{-/-}$*Sycp3*$^{-/-}$ double mutant mouse would help to resolve this (Winkel et al., 2009). In both the *Sycp3*$^{-/-}$ and *Sycp2*$^{-/-}$ mice SC formation is not apparent and mutant spermatocytes are unable to properly synapse homologous chromosomes, leading to an arrest of male meiosis during prophase (Yuan et al., 2000). However, although failing to properly synapse by complete CE formation, homologous chromosomes do pair up adjacent to one another in *Sycp3*$^{-/-}$ (Kolas et al., 2004) and SYCP1 is capable of forming short filaments which also co-localise with SYCP2 along chromosome axes in both mutants (Yang et al., 2006; Yuan et al., 2000). *Sycp3*$^{-/-}$ spermatocytes initiate recombination which proceeds further at synapsed regions, although DNA damage is unable to fully repair (Kolas et al., 2004; Yuan et al., 2000). Therefore SYCP3 is essential for complete synapsis and repair of meiotic DNA damage in spermatocytes.

Conversely, *Sycp3*$^{-/-}$ and *Sycp2*$^{-/-}$ female mice are able to pair and synapse homologous meiotic chromosomes and are ultimately fertile albeit with reduced litter sizes (Yang et al., 2006; Yuan et al., 2002). The reason for the dramatic sexual dimorphism of these mutant phenotypes is not currently understood. Although an AE does not form, SYCP1 filaments connect chromosomes in these mutants by what are proposed to be direct interactions with the axial DNA using the protein's C-terminal domain (Schramm et al., 2011). Furthermore, additional CE proteins are able to localise to this filament of SYCP1 (Schramm et al., 2011). *Sycp3*$^{-/-}$ oocytes complete recombination, with the marker of crossover formation MLH1 forming foci at similar or slightly elevated levels when compared to those of wild types. Despite this however, univalent chromosomes not linked to their homologous partner by chiasmata are commonly seen in *Sycp3*$^{-/-}$ diakinesis and metaphase I oocytes. These correlate with aneuploid zygotes generated by chromosome missegregation and are thought to be the cause of embryo loss in this mutant, causing the reduced litter size noted (Yuan et al., 2002). Phenotypic similarities suggest aneuploidy is also likely to be the cause of litter size reduction in *Sycp2*$^{-/-}$. The frequency of aneuploid conceptions increases with maternal age in *Sycp3*$^{-/-}$, accounting for growing reductions in litter size (Yuan et al., 2002). The cause of the univalent chromosomes in *Sycp3*$^{-/-}$, and likely *Sycp2*$^{-/-}$, is not entirely clear, however the

SYCP1 filaments formed in oocytes of both of these mutants are noted to contain gaps (Yang et al., 2006; Yuan et al., 2002) and in *Sycp3*$^{-/-}$ axes are extended to around double their wild-type length (Yuan et al., 2002). It is proposed that the abnormal axis and TF construction in these mutants leads to altered distribution of chiasmata and the frequent failure to form crossovers on smaller chromosomes, however the mechanism responsible is currently not well understood.

In the absence of the TF protein SYCP1 the AE appears to form normally and standard frequencies of early recombination proteins are recruited to axes in leptotene, indicating initiation of recombination. Indeed, homologous autosomes successfully pair next to one another and recruit more mature recombination proteins. However, chromosomes are unable to synapse by formation of a shared CE, holding them in close proximity, and retain a greater distance of separation than in WT pachytene. Furthermore, sex chromosomes fail to pair in mutant spermatocytes. Repair of meiotic DNA damage is also greatly perturbed and loss of SYCP1 causes infertility in both sexes, with spermatocytes largely arresting in pachytene (de Vries et al., 2005). Therefore formation of TFs is dispensable for the adjacent pairing of homologous chromosomes but appears to be important for meiotic recombination, possibly indicating a requirement for the TF to stabilise inter-homolog interactions to promote DSB repair mechanisms.

The central element (CE) proteins are also each vital for the proper synapsis of homologous chromosomes and fertility, although chromosome pairing and AE formation does take place in their absence (Bolcun-Filas et al., 2007, 2009; Hamer et al., 2008; Schramm et al., 2011). As with *Sycp1*$^{-/-}$ spermatocytes, DNA damage appears to be generated normally and can recruit early recombination proteins but is unable to repair and chromosomes cannot recruit markers of crossover formation in *Syce1*$^{-/-}$, *Syce2*$^{-/-}$, *Syce3*$^{-/-}$, or *Tex12*$^{-/-}$ (Bolcun-Filas et al., 2007, 2009; Hamer et al., 2008; Schramm et al., 2011). It is currently unclear if the lack of crossover markers and DSB repair in such mutant spermatocytes is due to defective recombination per se, or meiotic arrest prior to progression to latter stages of the recombination process. Curiously, localisation of SYCP1 and establishment of the TF is also greatly limited, but to a varying degree, between these mutants, as is the ability to form small regions of synapsis by CE construction. In *Syce2*$^{-/-}$ and *Tex12*$^{-/-}$ SYCP1 and SYCE1 localise in fragments between closely aligned axes, but this CE is unable to extend (Bolcun-Filas et al., 2007; Hamer et al., 2008; Schramm et al., 2011). Alternatively, in *Syce1*$^{-/-}$ and *Syce3*$^{-/-}$ spermatocytes SYCP1 localises faintly and discontinuously along the axes irrespective of partner alignment, CE formation is not

detected in either mutant by electron microscopy, and in *Syce3*$^{-/-}$ SYCE1 and SYCE2 fail to localise completely (Bolcun-Filas et al., 2009; Schramm et al., 2011). Therefore, SYCE1 and SYCE3 are required for the restriction of TF binding to aligned axes, while SYCE2 and TEX12 are required to promote the extension of CE formation (Figure 1-3). SYCE2 and TEX12 form a hetero-octameric complex (Davies et al., 2012; Hamer et al., 2006) and when co-transfected into cultured cells form a filamentous structure resembling the CE (Davies et al., 2012). While these properties of SYCE2 and TEX12 support their shared function in promoting CE polymerisation, these proteins are unable to co-immunoprecipitate (co-IP) with SYCP1 leading to proposals that other mediator proteins may be involved in this promotion (Hamer et al., 2006). SYCE3 is capable of interaction with SYCE2 and also SYCE1 (Schramm et al., 2011), while SYCE1 can interact with SYCP1 (Costa et al., 2005; Hamer et al., 2006). Hence it appears that during SC formation SYCE1 and SYCP1 interact in a SYCE3-dependent manner, before recruiting TEX12 and SYCE2 and proceeding to extend the SC. In summary the formation of the SC is central to meiotic prophase and occurs in stepwise manner beginning with AE formation by SYCP3 and SYCP2, followed by TF formation by SYCP1 which is restricted to aligned axes by SYCE1 and SYCE3 before SYCE2 and TEX12 promote the extension of the CE along the chromosomes (Figure 1-3). Perturbations to the formation of the SC typically remain compatible with the initial ability of homologous chromosomes to become aligned with one another in an organised fashion, but SC formation is vital for fertility and the promotion of recombination in spermatocytes.

1.3.3 The Chromosome Core

Although the assembly of the SC is becoming well understood, the underlying organisation of the DNA involved, and the role of the SC in influencing this organisation is still being uncovered. It is interesting to note that despite the failed formation of the AE in *Sycp2*$^{-/-}$ and *Sycp3*$^{-/-}$ meiocytes, portions of SYCP1 filament form accurately between chromosomes in the absence of these anchorage points, and recombination proteins are still successfully recruited to chromosomes in a linear pattern of foci. This axis which remains in the absence of the AE is termed the chromosome core and is constructed by the cohesin complex (Llano et al., 2012; Pelttari et al., 2001). The chromosome core is an anchorage point securing loops of chromatin along each homologous chromosome. The AE forms along the chromosome core and influences chromosome core organisation, as seen in *Sycp3*$^{-/-}$ in which axes approximately double in length and chromatin loop size is reduced (Novak et al., 2008). The initial establishment of the chromosome core however is achieved independently by the

cohesin complex and is initiated before the AE begins to form axis-associated patterns (Eijpe et al., 2003; Llano et al., 2012; Pelttari et al., 2001).

1.4 Cohesin

The cohesin complex plays a vital role in organising genomic DNA during both meiotic cell division and during mitotic divisions. It is through the mitotic study of cohesin that a great deal has been learned about the complex's structure and function. In this section I will begin by discussing mitotic cohesin before presenting what is known about the involvement of this protein complex during meiosis.

1.4.1 Sister Chromatid Cohesion

The haploid mouse genome consists of 2.5 billion base-pairs of DNA, split across 20 chromosomes. During every mitotic cell cycle both parental copies of the genome (homologous chromosome pairs) are replicated (pairs termed sister chromatids) and segregated into two daughter cells. The faithful transmission of an identical diploid genome into each daughter cell is vital for survival. This fundamental process requires that each chromosome within a nucleus can be separated from other DNA without becoming entangled, and can be distinguished from its sister copy. Before the onset of the anaphase to metaphase transition the kinetochores on each sister chromatid are separately attached to microtubules along which chromosomes migrate towards opposite spindle poles (Rieder and Salmon, 1998). Pairwise alignment of chromatids on mitotic spindles and the prevention of premature chromosome separation are achieved by an adherent force known as sister chromatid cohesion (SCC) which binds sister chromatids until anaphase. SCC is achieved by the cohesin complex.

1.4.2 The Cohesin Complex

Work in yeast has shown cohesin to be a hetero-tetrameric tripartite complex consisting of a core heterodimeric complex of two SMC proteins, SMC1 and SMC3, an α-kleisin subunit (RAD21 in mammalian mitotic cohesin), and an SCC3 protein (SA1 or SA2 in mammalian mitotic cohesin) (Nasmyth and Haering, 2009). The SMC proteins contain a 50nm intermolecular antiparallel coiled coil, separating a hinge domain and nucleotide-binding domain at either end to form a rod-shape (Figure 1-4A). Due to the antiparallel nature of the

SMC coiled-coil domain, the nucleotide binding domain is built from two halves consisting of the protein's N- and C-terminal amino acids (Haering et al., 2002; Hirano and Hirano, 2002). The hinge domains of SMC1 and SMC3 interact (Guacci et al., 1997; Michaelis et al., 1997), with their nucleotide-binding domains at the ends of this complex being brought together by RAD21 which interacts with their N- and C-terminals respectively to create a ring (Figure 1-4A), consistent with the electron micrograph images of the cohesin complex (Anderson et al., 2002; Haering et al., 2002). The SCC3 protein is added to the complex by binding to the C-terminus of the yeast Rad21 homologue (Tóth et al., 1999). All four of the proteins are essential for the establishment of SCC (Nasmyth and Haering, 2009). The ring complex formed by cohesin is widely thought to embrace both sister chromatids (Figure 1-4B), although alternative models for its binding have been proposed (Nasmyth and Haering, 2009).

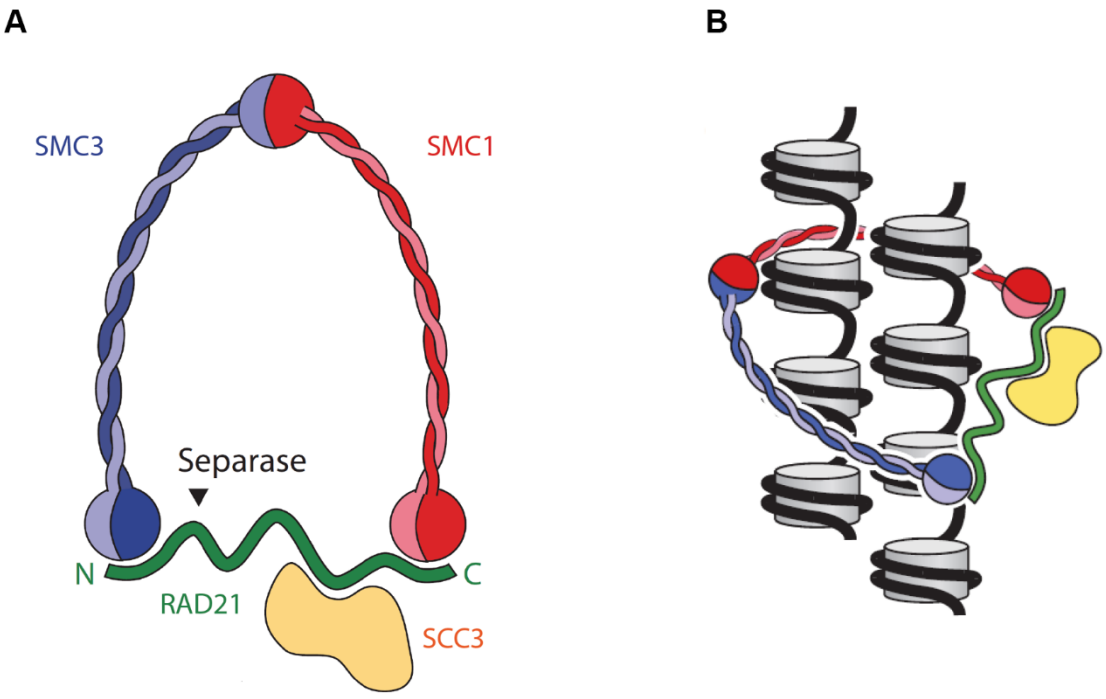

Figure 1-4. Structure of the cohesin complex
(A) SMC1 and SMC3 proteins form antiparallel coiled-coils, binding together to form a hinge domain. The N- and C- terminals of these proteins are connected by the α-kleisin subunit, RAD21, to create a ring. SCC3 (SA1 or SA2 in mammalian mitotic cohesin) binds to the C-terminus of RAD21. The "strong" version of the ring model predicts that sister chromatids (displayed as DNA (black) wrapped around nucleosomes (grey)) are embraced by a single cohesin ring. Schematics modified from Nasmyth and Haering, 2009.

1.4.3 Addition and Removal of Cohesin in Mitosis

The canonical function of cohesin is to maintain SCC from S-phase of the cell cycle, at which point the genome is replicated, until anaphase, when the sister chromatid copies are segregated. The release of cohesion by cohesin removal is tightly controlled and central to this function. The removal of mitotic cohesin in most eukaryotes takes place in two phases (Figure 1-1A), with 90% or more of chromatin-bound cohesin removed during prophase, leaving centromeric cohesin. The second phase of cohesin removal involves separase, a highly conserved cysteine protease, which cleaves the α-kleisin subunit (Figure 1-4A) to trigger sister-chromatid disjunction and the metaphase to anaphase transition (Pauli et al., 2008; Uhlmann et al., 1999, 2000; Waizenegger et al., 2000).

The loading of cohesin onto DNA is dependent on ATP hydrolysis (Arumugam et al., 2003; Hu et al., 2011) and is achieved by a complex of proteins termed "kollerin", consisting of SCC2 (NIPBL) and SCC4 (Ciosk et al., 2000; Nasmyth, 2011). Surprisingly, despite the central role for the cohesin complex in orchestrating sister chromosome segregation, cohesin associates with chromatin as early as telophase, during the separation of two daughter cells. The interaction between cohesin and chromatin does not become stabilised however until after DNA replication when a pair of sister chromatids is available to embrace, therefore until this point chromatin-loaded cohesin is unable to function in SCC (Gerlich et al., 2006). This stabilisation relies on the acetylation of SMC3 by ECO1, promoting the interaction between the SMC3 and the α-kleisin subunit, thought to reinforce the ring-structure (Chan et al., 2012; Ivanov et al., 2002; Rolef Ben-Shahar et al., 2008; Unal et al., 2008).

The first wave of cohesin removal is performed by a system termed the prophase pathway. This pathway is dependent on the multiple helical repeat containing protein, WAPL (Chatterjee et al., 2013; Ouyang et al., 2013). WAPL interacts with cohesin via the ATPase domain of SMC3 and PDS5, a binding partner of the α-kleisin subunit (Figure 1-5A) (Chatterjee et al., 2013; Ouyang et al., 2013). The ability of WAPL to catalyse the removal of cohesin is counteracted by SMC3-acetylation, and can be avoided by fusing the SMC3 and α-kleisin subunits, indicating that this joint of the cohesin complex is indeed the intended opening point by WAPL (Chan et al., 2012). Sororin, a binding partner of PDS5, is also key to the regulation of cohesin removal by the prophase pathway (Nishiyama et al., 2010). Phosphorylation of sororin by CDK1 allows WAPL to access PDS5 for prophase pathway removal of cohesin (Figure 1-5A) (Liu et al., 2013a). The purpose of the prophase

pathway has long remained elusive, as cohesin can also be removed by the secondary, separase-mediated, pathway. However, progress has been made by recent studies into the effects of WAPL depletion by RNAi and conditional deletion in cultured mammalian cells. WAPL-depleted cells exhibit persistent cohesin on chromosome arms due to an inability to remove these complexes by the prophase pathway. These cells exhibited reduced centromeric association of Aurora B, a kinase involved in correcting improper kinetochore-microtubule attachment (Foley and Kapoor, 2013), and a corresponding delay in chromosome alignment on the metaphase plate and frequent observation of lagging chromosomes in anaphase. Sister chromosomes were also frequently joined by DNA threads thought to indicate unresolved catenations. Aneuploidies accumulate in WAPL-deficient cells if the DNA-damage checkpoint is averted by p53 inactivation, and the level of cohesin on the chromosomes of daughter cells is reduced. Therefore prophase pathway removal of cohesin appears to facilitate the decatentation of chromosomes before mitosis, the direction of proteins required for chromosome biorientation, and the recycling of a pool of cohesin removed without cleavage, which can be utilised in daughter cells (Haarhuis et al., 2013; Tedeschi et al., 2013).

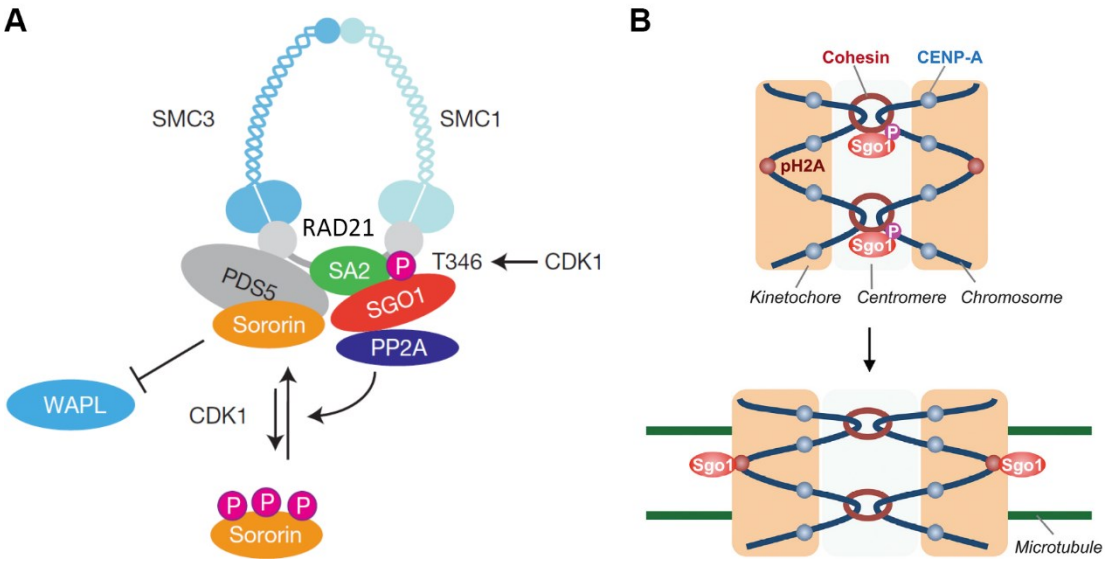

Figure 1-5. Models of the maintenance and de-protection of cohesin in mitosis
(A) Phosphorylation of sororin by CDK1 allows WAPL to access PDS5 for prophase pathway removal of cohesin. SGO1 bridges an interaction between centromeric cohesin and the phosphatase PP2A to maintain sororin in an unphosphorylated state, thereby protecting cohesin from prophase pathway removal. (B) SGO1 at centromeric cohesin is redistributed following the introduction of opposing tension between sister kinetochores by metaphase microtubules. Modified from Liu et al., 2013a and 2013b.

The preservation of centromeric cohesin in somatic cells is made possible by the shugoshin protein SGO1. SGO1 bridges an interaction between cohesin and the phosphatase PP2A (Figure 1-5A), allowing PP2A to maintain sororin in an unphosphorylated state, counteracting the kinase activity of CDK1 and preventing WAPL access to PDS5 (Liu et al., 2013a). The removal of cohesin at centromeres is dependent on the establishment of opposing tension between sister kinetochores, which triggers a redistribution of centromeric SGO1 (Figure 1-5B) (Liu et al., 2013b), allowing cohesin removal through cleavage by Separase, triggering the metaphase to anaphase transition.

The activity of Separase is tightly regulated, inhibited for much of the cell cycle through binding to its chaperone, Securin (Uhlmann et al., 2000). During mitosis, Separase is phosphorylated by CDK1 (Stemmann et al., 2001), inducing binding of Cyclin B/CDK1 (Gorr et al., 2005). Separase becomes fully activated following completion of metaphase chromosome biorientation. This event triggers the anaphase promoting complex's (APC) Cdc20 activator protein, allowing Cdc20 to recruit Cyclin B and securin to the APC, for ubiquitination and ultimately proteolysis (Musacchio and Salmon, 2007; Nasmyth, 2005). Liberated separase subsequently cleaves the α-kleisin subunits of cohesin complexes still bound to DNA in a DNA dependent manner, thus avoiding soluble cohesin associated with chromosomes (Hauf et al., 2001; Sun et al., 2009; Uhlmann et al., 1999). This opening of the remaining bound cohesin rings allows chromosome disjunction.

In summary cohesin is initially loaded to DNA by the kollerin complex prior to DNA replication. The chromatin-association of cohesin is then stabilised by ECO1-mediated acetylation of SMC3. The prophase and separase pathways of cohesin removal are highly regulated and involve the interaction of numerous accessory proteins and the cohesin complex. Initial cohesin removal on chromosome arms by the prophase pathway is catalysed by WAPL which relies on phosphorylated sororin to promote cohesin access; cohesin access is conversely counteracted by SMC3 acetylation. Centromeric cohesin meanwhile is protected by SGO1 which maintains sororin in an unphosphorylated state. SGO1 localisation is altered in response to opposing kinetochore tension provided by metaphase microtubules, causing cohesin to become unprotected and susceptible to removal by separase-mediated cleavage of the α-kleisin subunit, releasing sister chromosomes.

1.4.4 Additional Roles of Mitotic Cohesin

In addition to the canonical function of cohesin in sister chromatid cohesion, additional functions have also been identified in mitosis. Mitotic cohesin has been found to widely colocalise with CTCF binding, a DNA binding protein with enhancer blocking function and boundary element activity. The binding of cohesin to these sites is dependent on CTCF which in-turn is sensitive to DNA methylation. This association indicates connections between transcriptional regulation and cohesin distribution, as well as epigenetic influence over localisation (Parelho et al., 2008). Such a role for cohesin is further supported by the human developmental disorders, Cornelia de Lange Syndrome and Roberts Syndrome, in which patients exhibit altered transcriptional profiles and typically possess mutations in cohesin subunits or related proteins (Skibbens et al., 2013).

Cohesin mutant cells also display increased sensitivity to DNA damage, and DNA-damage dependent loading of functional cohesin to chromosomes after S-phase has been demonstrated in WT cells (Mehta et al., 2013). Cohesin binding to DNA therefore appears to play a role in the repair of DNA damage. Cohesin has also been shown to promote DNA repair by recombination between sister chromatids and suppress recombination between homologous chromosomes (Covo et al., 2010). Hence, it is clear that the global establishment of chromatin anchors achieved by cohesin binding has broader cellular implications than simply enabling chromosome segregation, and is also relied upon by other core cellular processes.

1.4.5 Meiotic Cohesin

As cells undergo two divisions during meiosis, the chromosome cohesion necessary to achieve this differs from that required in mitosis. As in mitosis, meiotic cohesin is initially present throughout the length of the chromosomes. However, in meiosis I, the metaphase to anaphase transition only requires the removal of arm cohesin to release chiasmata holding homologous chromosomes together. Centromeric cohesin remains until anaphase of meiosis II, at which point sister chromosomes segregate.

As well as dynamic distinctions, the composition of meiotic cohesin complexes also differs somewhat from those in mitosis, with the introduction of a suite of additional and alternative subunits enabling the formation of numerous distinct meiotic cohesin complexes (Lee and Hirano, 2011). SMC3 remains in mammalian meiosis, as does SMC1, and an

additional SMC1 isoform is present, called SMC1β. Except for a unique, basic DNA binding C-terminal motif, SMC1β is highly homologous to SMC1 (referred to in meiosis as SMC1α) (Revenkova et al., 2001). In addition to the α–kleisin RAD21, meiocytes possess the homologs REC8 and RAD21L (Eijpe et al., 2003; Ishiguro et al., 2011). The SA1 and SA2 cohesin subunits are not detectable in meiosis by immunofluorescence, but appear to be replaced by a meiosis-specific homolog, STAG3 (Pezzi et al., 2000; Prieto et al., 2001). It is not yet clear which of the many different potential combinations of cohesin complexes are present in meiosis, though co-immunoprecipitation experiments have led to a list of putative cohesin complexes present in mouse testes (Figure 1-6) (Lee and Hirano, 2011).

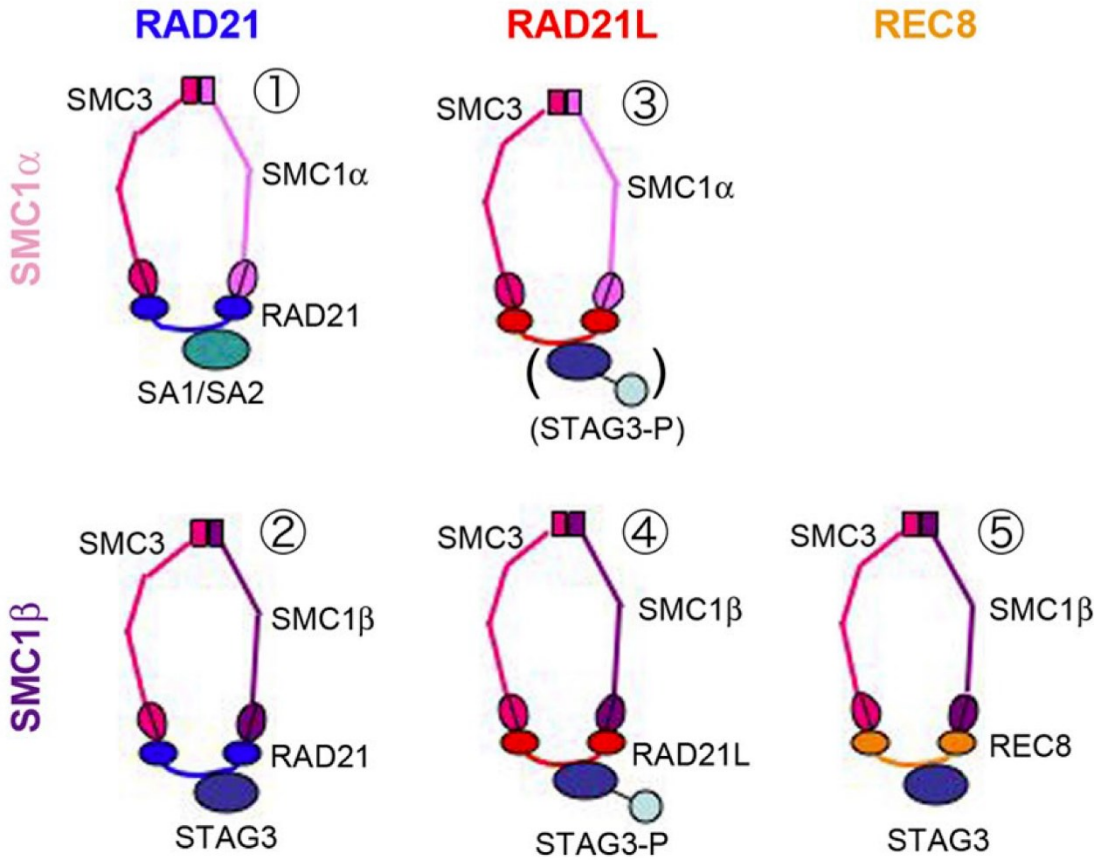

Figure 1-6. Putative subunit composition of cohesin complexes
Putative cohesin complexes present in mouse testes indicated by endogenous co-IP (Lee and Hirano, 2011). Figure taken from Lee and Hirano., 2011.

1.4.6 Loading of Meiotic Cohesin

Curiously, the loading of meiotic mammalian cohesin appears to begin with REC8, which is detected in rat spermatocytes by immunofluorescence shortly before pre-meiotic S-phase, and begins to form axial filaments shortly after this stage, prior to the detection of SMC3 and SMC1β which coincides with localisation of axial element proteins SYCP2 and SYCP3 (Eijpe et al., 2003). This may reflect a staggered loading of cohesin subunits onto chromatin.

Studies in yeast and plants indicate that the kollerin complex (NIPBL/SCC4), in addition to its role in mitotic cohesin loading, is also required for normal loading of cohesin to meiotic chromosomes (Lin et al., 2011; Sebastian et al., 2009). NIPBL and SCC4 are credited with the ability to load SMC proteins to chromatin (Hirano, 2006). The focal co-localisation of NIPBL and SCC4 on meiotic chromosomes at leptotene, and subsequent extension across the axes of zygotene meiocytes is consistent with this role during these stages of mouse meiosis (Kuleszewicz et al., 2013; Visnes et al., 2013). Kollerin in spermatocytes undergoes a wave of axial depletion and pericentromeric relocation in pachytene following meiotic DSB repair. This results in a pattern of Kollerin enrichment sharing very little overlap with cohesin or alteration to the dynamics of other SMC proteins. Therefore this relocation of Kollerin does not appear to be associated with further loading of cohesin, but rather suggests an alternative role for Kollerin at this stage in male germ cells (Kuleszewicz et al., 2013; Visnes et al., 2013). The mechanism of this relocation and the complex's subsequent role are currently not known.

1.4.7 Role of Meiotic Cohesin

STAG3, SMC3 and SMC1β all localise to meiotic chromosomes in leptotene and in addition to REC8 they coat chromosome arms and centromeres into metaphase I, then associate with centromeres from anaphase I to metaphase II, consistent with a role in sister chromatid cohesion (Eijpe et al., 2000a, 2003; Garcia-Cruz et al., 2010; Revenkova et al., 2004). Absence of STAG3, REC8 and SMC1β have all been demonstrated to reduce meiotic sister chromatid cohesion, supporting the involvement of these subunits in chromosome-segregation associated meiotic cohesin complexes (Llano et al., 2014; Revenkova et al., 2004; Xu et al., 2005). In addition to the fundamental role of cohesin in maintenance of sister chromatid cohesion during meiosis, it is becoming apparent that the role of cohesin in structuring chromatin has multiple implications unique to meiosis. However, the presence of

multiple homologs in the case of some subunits does present potential for functional redundancy.

RAD21L appears in spermatocytes at pre-meiotic S-phase, simultaneous with the appearance of REC8 and is detectable on axial elements from leptotene, extending along chromosome axes as prophase proceeds. The patterns of axial RAD21L localisation reported by some authors consist of numerous foci with a distribution curiously mutually exclusive to that of REC8, however other authors report continuous axial staining (Herrán et al., 2011; Ishiguro et al., 2011; Lee and Hirano, 2011), the distinctions between which may be technical and are currently unresolved. The observation of the alternating α-kleisin pattern has triggered theories of a cohesin "bar-code" which might direct the pairing of homologous chromosomes based on REC8- and RAD21L-controlled domains (Ishiguro et al., 2011). Indeed, RAD21L has recently been revealed to promote a degree of homologous chromosome pairing which occurs in meiosis independent of recombination (Ishiguro et al., 2014). Interestingly, the phenotype of *Rad21l*$^{-/-}$ mice is sexually dimorphic, with only male mice suffering infertility, while females display a normal capacity to produce offspring in their youth following mating to non-mutant males. Spermatocytes arrest in a zygotene-like stage following fragmented AE formation, defective homologous chromosome pairing and synapsis. Recombination is initiated by the formation of DSBs in *Rad21l*$^{-/-}$ but these are not repaired and spermatocytes arrest before the formation of crossovers. SMC3, SMC1β, REC8 and RAD21 subunits appear to load onto chromosomes at normal levels in mutant spermatocytes, but STAG3 and SMC1α levels are reduced. *Rec8*$^{-/-}$ spermatocytes do not feature this reduction in STAG3, demonstrating an important role for RAD21L in STAG3 binding. There is, however, no detectable reduction in sister chromatid cohesion in *Rad21l*$^{-/-}$ (Herrán et al., 2011). Indeed, the TEV protease mediated cleavage of REC8 in the growth phase of mouse oocytes triggers chiasmata resolution indicating that the remaining non REC8-containing cohesin complexes (i.e. RAD21L- or RAD21-containing cohesin) are insufficient to maintain bivalent chromosome associations (Tachibana-Konwalski et al., 2010). Wild type RAD21L protein gradually dissociates from chromosome axes from late pachytene stage and becomes enriched close to centromeres and over the sex body. Localisation close to centromeres and over XY chromosome axes is maintained into metaphase I and centromere-associate signals are still observed in anaphase II, further opposing a role in SCC as cohesion is lost by this stage but the protein remains associated (Herrán et al., 2011; Lee and Hirano, 2011). The relocation from pachytene axes coincides with the appearance of the mitotic α-kleisin RAD21 on axes of meiotic chromosomes, the pattern of which rarely overlaps with that of RAD21L or REC8, indicating that RAD21 may

replace these proteins at this stage (Herrán et al., 2011). The timing of this exchange appears to correlate with crossover formation however a role for RAD21 in meiotic recombination has not yet been demonstrated (Lee and Hirano, 2011). RAD21 largely dissociates from chromosome arms in metaphase I and, like RAD21L, becomes enriched at the centromeres. RAD21 is not detectable on meiotic chromosomes after meiosis I, indicating that it is not involved in the maintenance of SCC during meiosis II (Parra et al., 2004; Xu et al., 2004). The role of RAD21 during meiotic prophase is currently unclear, although it is proposed to confer some SCC in meiotic prophase I (Llano et al., 2012). In summary, the α-kleisin cohesin subunits RAD21 and RAD21L do not contribute greatly to SCC although a minor involvement is possible. Rather, the localisation patterns of these proteins and mutant phenotype of *Rad21l*$^{-/-}$ indicate that they are primarily involved in other processes, including a requirement for RAD21L to synapse spermatocyte chromosomes.

The other meiosis-specific α-kleisin, REC8, is required for fertility in both male and female mice. In the absence of REC8 the axial element appears to form normally, and some nuclei appear to pair homologous chromosomes. However, sister chromatid cohesion is clearly defective, with sister axial separation visible by SYCP3 staining and synapsis indicated by SYCP1 largely taking place between sister chromatids rather than homologues (Xu et al., 2005). Therefore REC8-mediated cohesion seems necessary to promote synapsis between homologous chromosomes rather than sisters. Recombination is initiated with DSB formation in *Rec8*$^{-/-}$ though the frequency of early recombination intermediates (RAD51/DMC1 foci) in zygotene nuclei is lower than those in WT mice suggesting an effect on DSB formation. The level of cohesin subunits SMC3 and RAD21 on chromosomes is unaltered in *Rec8*$^{-/-}$ demonstrating that despite the requirement for REC8 to achieve SCC it is not needed for cohesin association with DNA (Xu et al., 2005).

SMC3 and SMC1β largely colocalise during meiosis, associating with the axial element from leptotene, through prophase and becoming enriched near the centromeres from diplotene to metaphase I. Following this, the two proteins continue to associate with centromeres until anaphase II, consistent with a role in sister chromosome cohesion. SMC1α alternatively is present throughout the nucleus in leptotene before localising in a punctate pattern along chromosome axes between zygotene and diplotene, but failing to concentrate at the centromeres as like the other SMC cohesin subunits, and is not detected beyond diplotene (Revenkova et al., 2001). The meiotic study of cohesins which also have roles in mitosis is limited by the difficulty of generating mutants without causing restrictive somatic defects preceding meiosis. Among these are the SMC proteins SMC3 and SMC1α. SMC1β however,

is an isoform of SMC1 specific to meiosis. In the absence of SMC1β male and female mice are both infertile, with meiosis arresting at different stages. Spermatocytes form axial elements approximately half the length of those seen in WT mice, indicating a role for SMC1β in AE formation. The distance to which the chromatin loops extend from the shortened *Smc1β*$^{-/-}$ axes is double that of WT spermatocytes, indicating the presence of fewer axial anchorage sites for chromatin in the axis and consistent with a role for SMC1β in AE formation (Figure 1-7). Although some chromosomes successfully synapse in the mutant spermatocytes, many do not, and cells arrest in pachytene. Recombination is initiated but chromosomes fail to form crossovers and lack chiasmata when forced into metaphase I by okadaic acid treatment. Furthermore a reduction in centromeric cohesion is apparent in such metaphase I nuclei indicating a role for SMC1β in SCC (Revenkova et al., 2004). Mutant oocytes suffer similar defects though do not arrest at pachytene and recruit MLH1 foci to form crossovers, albeit at a reduced frequency. However, chiasmata positioning becomes terminalised during metaphase, oocytes become increasingly aneuploid through meiosis and this defect becomes more severe with age, demonstrating a role for SMC1β in the maintenance of SCC (Hodges et al., 2005). Furthermore the levels of STAG3 observed on metaphase chromosomse arms by immunofluorescence is greatly reduced, consistent with lower levels of arm cohesin to secure chiasmata positioning (Hodges et al., 2005). This observation of chiasmata terminalisation and loss is remarkably similar to the phenomenon of maternal age-related aneuploidy in humans, which appears to be associated with the loss of chiasmata over time, which must be maintained for years following their formation *in utero* until ovulation. As such, age-dependent loss of cohesion similar to that observed in *Smc1β*$^{-/-}$ is commonly claimed to be the cause of this defect (Chiang et al., 2010; Lister et al., 2010). Therefore SMC1β is involved in maintaining SCC required for faithful chromosome segregation and for controlling the anchorage of chromatin loops into the chromosome core. The meiotic functions of SMC1α and SMC3 however, remain to be determined.

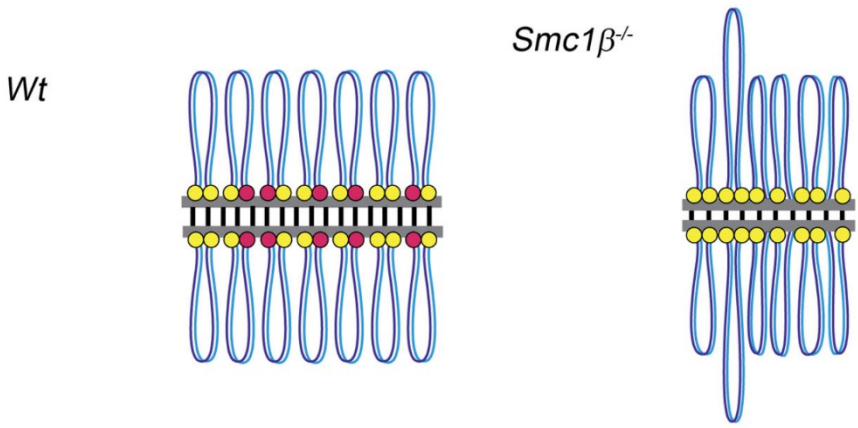

Figure 1-7. Anchorage of meiotic chromatin by cohesin determines axis length
Wild type chromosomes (blue) are thought to be anchored in the chromosome core by combinations of cohesin complexes containing SMC1α (yellow) and SMC1β (red). In *Smc1β*$^{-/-}$ only chromatin anchorage provided by SMC1α-containing cohesin complexes remain, causing increased extension of some chromatin loops and a shortening of synaptonemal complex length (AE=grey, CE=black). Model modified from Novak et al., 2008.

Deletion of STAG3 also has a significant effect of mouse meiosis, though at least in spermatogenesis this is less dramatic than that of the *Rad21L Rec8* double-null. This is somewhat surprising as both RAD21L and REC8 participate in cohesin complexes where the only SCC3 subunit is STAG3 (Lee and Hirano, 2011), hence a phenocopy might be expected. This implies a compensatory mechanism, however this is not performed by SA1 or SA2 and is currently not understood (Llano et al., 2014). *Stag3*$^{-/-}$ spermatocytes arrest at a zygotene-like stage after the formation of greatly shortened, but complete, axial elements which achieve a limited degree of synapsis. The levels of SMC3, RAD21 and RAD21L localisation appear similar to WT, though SMC1β and REC8 levels are reduced, indicating that STAG3 is only required for the localisation of a limited range of cohesin subunits. The reduction in axis length in *Stag3*$^{-/-}$ may be partly due to the reduction in SMC1β (Figure 1-7), but as the shortening is so extreme and SMC1β is only reduced, not absent, it is likely that a reduction in SMC1α-containing cohesin complexes in *Stag3*$^{-/-}$ also contributes to this phenotype. By cytological analysis of centromere pairing in *Stag3*$^{-/-}$ it is clear that the cohesion connecting sister centromeres is also compromised in *Stag3*$^{-/-}$, and forcing spermatocytes into metaphase I by okadaic acid treatment exacerbates this separation enabling the identification of all 80 centromeres rather than 20 centromeric tetramers. These spermatocytes initiate recombination by forming meiotic DSBs and recruit early recombination proteins RAD51 and DMC1, though these are reduced in frequency and do not dissociate, indicating reduced DSB frequency and failed DNA repair (Llano et al., 2014).

The *Stag3*$^{-/-}$ phenotype is the greatest effect yet seen by the loss of a single cohesin subunit in mouse meiosis supporting the major involvement of STAG3 in meiotic cohesin complexes.

The initial localisation of cohesin to the meiotic chromosome axis enables the establishment of a chromosome core, anchoring loops of chromatin, around which the synaptonemal complex is subsequently constructed. The organisation of chromosomes into the chromosome core, which extends through their length similar to the axial element, can be observed by immunostaining of cohesin subunits in *Sycp3*$^{-/-}$ spermatocytes which lack an AE, and so called "SC-null" mice (*Sycp3*$^{-/-}$*Sycp1*$^{-/-}$). This structure provided by cohesin is sufficient for the localisation of DSB repair foci and even limited chromosome synapsis by localisation of SYCP1 in *Sycp3*$^{-/-}$ spermatocytes (Kouznetsova et al., 2011; Pelttari et al., 2001). Chiasmata formation however is largely abolished in spermatocytes lacking SC, but with an intact chromosome core (Kouznetsova et al., 2011). Furthermore, in the absence of REC8 and RAD21L cohesin subunits, but not in single mutants for these genes, cohesin is unable to localise and consequently the axial element is unable to form. SYCP3 and SYCP2 only localise in a few very short leptotene-like filaments, demonstrating the key role of cohesin and the chromosome core for SC formation. However, the absence of the REC8 and RAD21L α-kleisin subunits is not enough for cells to lose sister chromatid cohesion after S-phase, with the remaining α-kleisin RAD21 presumably sufficient to maintain this in leptotene exemplifying the cohesin subunit redundancy available in meiosis (Llano et al., 2012).

Therefore in addition to involvement in providing SCC which is essential for the maintenance of chiasmata and balanced chromosome segregation, various cohesin subunits possess additional and alternative functions in processes influencing chromosome pairing, meiotic recombination, chromosome core organisation and chromosome synapsis. Diverse localisation patterns of cohesin subunits imply that the meiotic function of these proteins may extend further still and remain to be understood.

1.4.8 Removal of cohesin in meiosis

Unlike in mitosis, only one mechanism of cohesin removal has currently been shown to operate during meiosis. Separase activity is essential for the removal of REC8 and resolution of chiasmata in oocytes demonstrating that the release of meiotic arm cohesion depends on the activity of the separase pathway (Kudo et al., 2006). Furthermore, the expression of a mutant variant of REC8, REC8-N, which cannot be cleaved by separase prevents

chromosome segregation spermatocytes (Kudo et al., 2009). Therefore the separase pathway of cohesin α-kleisin subunit cleavage is essential for the removal of cohesin providing arm cohesion, and REC8 appears to be the major target of this activity. In contrast to mitotic cells, the prophase pathway has not been shown to play a role in cohesin removal in meiosis. The mechanisms facilitating the dynamics of the cohesin subunits without major implications in cohesion and chromosome segregation however remain poorly understood.

As cohesin removal must be limited to chromosome arms during the first meiotic division, this requires protection of centromeric cohesin. Similarly to mitotic cohesion which is defended from prophase-pathway removal, meiotic cohesin is protected by a shugoshin protein. In the absence of SGO2, REC8 is completely removed from metaphase I chromosomes at the onset of anaphase resulting in meiocytes with 40 individualised chromatids in metaphase II and causing infertility in both male and female mice (Llano et al., 2008). SGO2 localises to the centromere from diplotene and persists as a band between sister centromeres during prophase II, but relocates to a focus at each centromere in metaphase II. This relocation of SGO2 in metaphase II is dependent on the tension exerted on sister centromeres by the metaphase II spindles and has been proposed to leave cohesin unprotected therefore susceptible to cleavage by separase (Gómez et al., 2007; Lee et al., 2008). SGO2, via the phosphatase PP2A, combats the removal of centromeric cohesin in meiosis I by opposing phosphorylation of REC8 (Ishiguro et al., 2010; Katis et al., 2010). It has recently been revealed that unlike SGO2, PP2A continues to colocalise with REC8 at metaphase II oocyte centromeres and inhibition by Ci-I2PP2A at this stage leads to the failed opposition to REC8 phosphorylation (Chambon et al., 2013), thus presenting an alternative/additional mechanism via which cohesin protection is ultimately lost in metaphase II.

1.5 Recombination

Meiotic recombination is a remarkable process involving the endogenous generation of widespread DNA damage across the genome by SPO11 (Figure 1-8) (Baudat et al., 2000; Romanienko and Camerini-Otero, 2000). The distribution of these breaks follows patterns of enrichment across the genome (Smagulova et al., 2011) promoted by guidance mechanisms (Brick et al., 2012). The repair of much of this DNA damage is performed in a manner which promotes the homologous pairing of chromosomes using the recombinases RAD51 and

DMC1 (Figure 1-8) (Cloud et al., 2012; Yoshida et al., 1998) rather than repairing damage using the sister chromatid. The inter-homolog interactions at the break site associate with a sequence of recombination proteins involved in stabilising interactions and promoting repair. Ultimately DNA damage is repaired, with a limited number of breaks repairing via a crossover-forming route which generates a genetic exchange between homologs (Figure 1-8) that is required for the segregation of homologous chromosomes in metaphase I (Eaker et al., 2002). Segregation of homologous chromosomes is an event which is unique to and essential for meiosis, enabling the balanced division of the genome once before sister chromatids are separated in metaphase II to produce haploid (1n) germ cells from the 4n precursor genome.

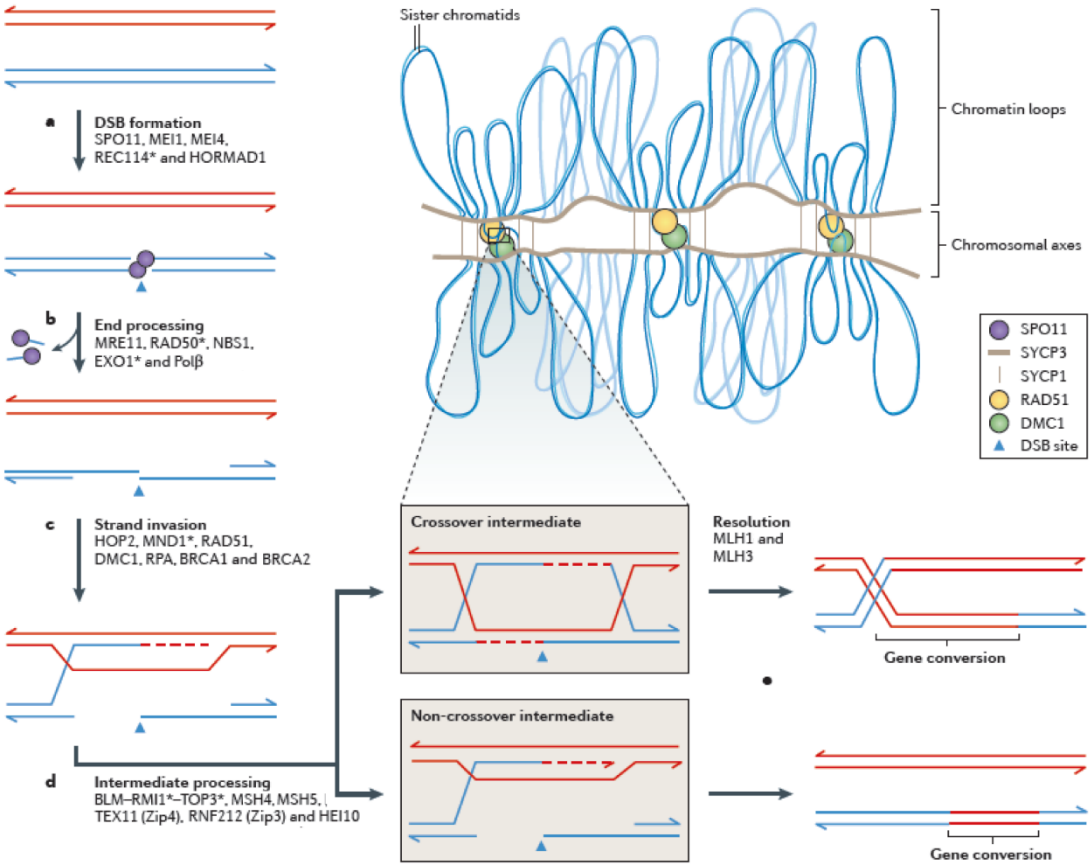

Figure 1-8. Proteins and events involved in meiotic recombination
Replicated homologous chromosomes represented as red and blue strands. (a) Formation of a DNA double strand break (DSB) initiates meiotic recombination. (b) DSBs are resected to produce ssDNA, releasing SPO11-oligonucleotide complexes. (c) ssDNA at the bread site invades a complementary sequence on a homologous chromosome to form a joint molecule (JM) by interactions with various early recombination proteins. (d) Intermediate recombination proteins are involved in stabilising inter-homolog interactions and promoting DSB repair either by the crossover or non-crossover forming route. Homologous sequence is used as a template to repair the damaged chromosome. Crossover intermediates form a double Holliday junction between homologs, while non-crossovers involve a single-end strand invasion. (e) DSB repair is resolved in pachytene, with both repair products containing a region (a few base pairs to a few hundred base pairs) around the DSB which is transferred chromosomes and defined as a gene conversion. Chromatin loops and the chromosome axis in zygotene are displayed in the top left. Most recombination proteins localise to the chromosome axis, as shown for RAD51 and DMC1. Proteins involved in these processes are discussed in detail in the text. Proteins marked with asterisks are predicted to be involved. Image modified from Baudat et al., 2013.

1.5.1 SPO11

Recombination is initiated in leptotene by the formation of double stranded DNA breaks (DSBs) across the genome by the highly conserved topoisomerase-like putative endonuclease SPO11 (Keeney et al., 1997). While abundant DSB are clearly detectable in WT spermatocytes by immunostaining for recombination proteins, these are greatly reduced

in spermatocytes lacking SPO11. Axial elements form, but homologous chromosome pairing and synapsis is severely defective and spermatocytes and oocytes arrest in late prophase (Baudat et al., 2000; Romanienko and Camerini-Otero, 2000). Using the chemotherapeutic drug cisplatin to artificially generate DSBs in *Spo11*$^{-/-}$ spermatocytes demonstrated a partial rescue of the failed chromosome pairing observed in this mutant. Therefore it is the ability of SPO11 to form DSBs which is vital for chromosome pairing, and the nature of these DSB is not peculiar to SPO11 but can be imitated by exogenous mechanisms (Romanienko and Camerini-Otero, 2000). A single report has achieved immunostaining to assess the meiotic localisation of SPO11. This indicated the focal appearance of SPO11 in leptotene spermatocytes, the majority of signals failing to colocalise with the forming axis and proposed to be generating DSB. SPO11 then becomes enriched at the synapsed portions of chromosomes in zygotene and pachytene, where its purpose is currently unclear, before dissociating from chromosomes in diplotene (Romanienko and Camerini-Otero, 2000).

SPO11 binds DNA as a dimer (Nichols et al., 1999) which remains bound following DSB formation until removal by endonucleolytic cleavage, releasing SPO11 in a covalently bound complex with a short oligonucleotide strand from the DNA break point (Figure 1-8b) (Neale et al., 2005). Two isoforms of mouse SPO11 exist, α and β, with distinct meiotic expression patterns and apparent genomic targets. *Spo11β* expression is largely restricted to leptotene and zygotene spermatocytes, the stages at which most DSBs are generated. In contrast, *Spo11α* expression is very low in early meiosis, peaks around pachytene/diplotene and persists into spermatid stages. The SPO11β isoform alone is sufficient for fertility in females and for autosomal synapsis in male mice, however the majority of DSBs generated in the PAR depend on SPO11α (Kauppi et al., 2011), indicating distinctions between the roles and targeting of the two SPO11 isoforms.

The level of DSB formation by SPO11 varies greatly during prophase indicating tight regulation of its activity, with mouse spermatocytes consistently forming 200-300 DSBs per nucleus (Kauppi et al., 2013a) in early meiotic prophase, distributed across the autosomes. SPO11 protein levels do not appear to be the limiting factor, with a large excess of protein remaining unbound to DNA (Neale et al., 2005), however the frequency of DSBs generated is altered by changes in *Spo11* expression (Cole et al., 2012; Kauppi et al., 2013b). Therefore it appears that only a limited proportion of SPO11 protein is active, the mechanisms involved in controlling this activity are in the process of being uncovered. The activity of the kinase ATM, recruited to meiotic DSB sites, is required to restrict the level of SPO11-DSBs generated. In *Atm*$^{-/-}$ spermatocytes DSB levels are increased 10-fold and the pool of excess SPO11 protein is greatly depleted as it is involved in DSB formation (Lange

et al., 2011). Curiously a reduction in *Spo11* content to heterozygousity is sufficient to rescue the asynapsis and prophase arrest incurred (Barlow et al., 1998; Bellani et al., 2005; Lange et al., 2011). Alternatively, in *Hormad1*$^{-/-}$ spermatocytes a reduction in DSBs formed is incurred (Daniel et al., 2011). Both HORMAD1 and ATM will be discussed in greater detail in section 1.6.2. Furthermore, an additional bout of DSB formation takes place in pachytene on the unsynapsed arms of sex chromosomes and as well as autosomes in the event of defective synapsis (Kauppi et al., 2013b). Together these data demonstrate the existence of factors which promote or limit DSB formation by SPO11, as well as temporal restriction to when unpaired homologous chromosomes receive DSBs. It is possible that feedback mechanisms control SPO11-DSB formation, influenced initially by factors including ATM and HORMAD1, then later in prophase by chromosome synapsis.

1.5.2 Recombination Hotspots

It has long been known that the formation of DSBs by SPO11 is not randomly distributed across the genome, but enriched at genetic hotspots. In *S. cerevisiae* these hotspots coincide with transcriptional promoters (Wu and Lichten, 1994). When tested, the transcriptional activity of the adjacent promoter was not found to be required; however the binding of transcription factors can influence DSB formation (Nicolas, 1998). Hotspot location is also associated with the accessibility of chromatin structure, as demonstrated by correlation with DNAse I hypersensitivity sites indicative of open chromatin (Wu and Lichten, 1994). Furthermore, active DSB initiation sites can lose their activity when inserted into a "cold" genomic region with low DSB activity (Borde et al., 1999). Similarly, targeting Spo11 to Gal4 binding sites generates DSBs adjacent to the binding site but is unable to do so if located within domains of low natural DSB activity such as centromere-associated regions (Robine et al., 2007). Open chromatin conformations have been detected at many DSB sites (Hirota et al., 2007), and the binding of a DSB-promoting transcription factor in *S. pombe* has been demonstrated to promote chromatin reorganisation (Mizuno et al., 1997), potentially making loci more structurally favourable to DSB-formation. Therefore the DSB-forming potential of a locus in yeast is influenced in a DNA sequence-independent manner by the structure of neighbouring chromatin.

Until fairly recently recombination hotspots in higher eukaryotes were largely identified by cytological and genetic analysis (Arnheim et al., 2007; Buard and de Massy, 2007; Lynn et al., 2004; Martinez-Perez and Colaiácovo, 2009). Genetic methods of genome-wide hotspot mapping have included (1) pedigree analysis, in which parents and offspring within

families (humans) or crossed inbred strains (mice) are genotyped at polymorphisms to generate genetic maps, enabling construction of sex-specific or even individual maps at low resolution (20-100kb). (2) Single-sperm genome wide genotyping of single nucleotide polymorphisms (SNPs) is a new technique allowing detection of recombination events in individual cells. (3) Analysis of linkage-disequilibrium within a population indicates the likelihood of two alleles being inherited together i.e. the chance of a CO event between them. This approach can be applied to natural population of non-model organisms, but can only provide population-averaged maps (Baudat et al., 2013).

Genetic assessment of CO formation in humans has revealed that, as seen in yeast, these are non-randomly distributed. Human CO hotspots exist in non-genic clusters 1-2kb in size and separated by 50-100kb regions with no or low CO activity (McVean et al., 2004; Myers et al., 2005). A sequence motif has even been identified in a large proportion of human hotspots (Myers et al., 2008) indicating some degree of direction at a DNA sequence level. CO activity in humans also varies over large multiple Mb-long domains showing high ("jungle") or low ("desert") rates of CO formation (Kong et al., 2002). Analysis of genetic diversity revealed ~25,000 CO hotspots in humans (Myers et al., 2005). Studies in mice also led to the initial identification of hotspots with similar constraints to those in humans, and a comparison between those of rats, mice and humans revealed a shared correlation with features such as GC-content, CpG density, repetitive elements and neutral mutation rate (Jensen-Seaman et al., 2004).

Interestingly, CO activity varies between populations and sexes in humans (Kong et al., 2010; Lynn et al., 2004) as well as strains and sexes in mice (Paigen et al., 2008). This variation has proved valuable in the identification of factors influencing the use of recombination hotspots. Cis-acting factors such as differences in DNA sequence at hotspots have been shown to affect hotspot activity (Paigen et al., 2008), and work in both humans and mice has also demonstrated the involvement of trans-acting factors (Grey et al., 2009; Neumann and Jeffreys, 2006; Paigen and Petkov, 2010; Parvanov et al., 2009). This has led to the identification of PRDM9, a powerful trans-acting hotspot promoter (Baudat et al., 2010; Myers et al., 2010; Parvanov et al., 2010), which contains a KRAB protein-protein binding domain (Birtle and Ponting, 2006), a PR/SET domain that can trimethylate histone 3 lysine 4 (Hayashi et al., 2005), and an array of zinc fingers.

Recent technical advances have enabled the interrogation of the genome-wide DSB sites rather than relying largely on genetic inference of crossover sites. This can be achieved by precipitating chromatin bound to early recombination proteins (DMC1, RAD51 ChIP-seq

analysis) (Smagulova et al., 2011) and by sequencing of the short SPO11-bound oligos produced following the resection of meiotic DSB sites (Pan et al., 2011). These analyses have demonstrated that in addition to DSBs repairing to generate COs genomic hotspots, as largely demonstrated genetically, the initial formation of DSBs is also restricted to hotspots (Smagulova et al., 2011). However, interestingly the potential of all DSB sites to form COs is not equal, indicating a further level of regulation during their repair (Serrentino and Borde, 2012). It is the distribution of DSBs which PRDM9 is primarily charged with monitoring. PRDM9 binds to hotspots via its zinc-finger, a fast evolving domain differing between mouse strains, leading to the promotion of distinct profiles of recombination hotspots (Brick et al., 2012). Strain-specific polymorphisms in *Prdm9* are also major contributors to hybrid sterility; a mechanism which renders the offspring of genetically diverging parents sterile and is implicated in the process of speciation (Auton et al., 2012; Mihola et al., 2009). It is curious to note that DSB hotspots in the pseudoautosomal region of the sex chromosomes appear to be independent of PRDM9, demonstrating that while it plays prominent role on mouse autosomes, alternative mechanisms are capable of acting elsewhere (Brick et al., 2012). This is also another example of the PAR behaving differently during to other regions of the genome during DSB formation, in addition to the distinct timing of DSB formation and reliance on the SPO11-α isoform (Kauppi et al., 2011). Therefore this may indicate that the DSB formation by the SPO11-α isoform occurs via PRDM9-independent means, while SPO11-β targeting is PRDM9-dependent.

Mouse *Prdm9* expression coincides with the initiation of meiosis and is essential for fertility (Hayashi et al., 2005). In the *Prdm9*$^{-/-}$ spermatocytes recombination is initiated however chromosome synapsis and the progression of meiotic recombination is impaired, and germ cells ultimately arrest in late prophase (Hayashi et al., 2005). ChIP-seq analysis of the DSB profiles in *Prdm9*$^{-/-}$ testes revealed that in the absence of PRDM9-dependent H3K4me3, DSBs are formed at gene promoters marked with PRDM9-independent H3K4me3 (Brick et al., 2012). The cause of infertility in this mutant is currently unknown, but theories include perturbed ability to repair DSBs due to inappropriate localisation (Brick et al., 2012), and mis-expression of essential meiotic genes due to the altered H3K4me3 profile (Hayashi et al., 2005).

1.5.3 DSB Formation

The occurrence of DSBs at H3K4me3-marked locations in the presence and absence of PRDM9 in mice indicates that this histone modification is associated with the targeting of

DSBs. The link between H3K4me3 and the meiotic recombination machinery, as well as how the PRDM9-generated H3K4me3 sites (~15% of the total cellular H3K4me3) are normally distinguished from other similarly modified location, is not known. Advances in the understanding of the involvement of H3K4me3 in recombination in yeast may prove relevant. The trimethylation of H3K4 in *S.cerevisiae* is exclusively carried out by the Set1 complex, which includes the methyltransferase subunit Set1 and the PHD-finger subunit Spp1 which regulates the H3K4me3 state (Dehé et al., 2006). In addition to its interaction with the Set1 complex components Spp1 also binds to Mer2 in the chromosome axis, which exists in a complex with the eukaryotically conserved Mei4 and Rec114 proteins (Figure 1-9) (Acquaviva et al., 2013; Kumar et al., 2010; Sommermeyer et al., 2013). Mer2 appears to be regulated in meiosis through CDK-dependent phosphorylation, but possesses unclear biochemical function and is not widely conserved (Henderson et al., 2006). Mei4 is predicted to contain conserved α-helical and coiled-coil domains at its N-terminus, likely involved in protein-protein interactions. Rec114 meanwhile is predicted to contain a conserved domain with β-sheet structure likely to be part of a structural domain of unknown biochemical function (Kumar et al., 2010). DSB formation typically involves DNA in chromatin loops (Blat et al., 2002), however the processing of DSB repair occurs at the chromosome axis in both yeast and mammals. The connection between H3K4me3 in the chromatin loop and DSB repair proteins located in the axis is provided by Spp1, which is thought to tether these locations together in yeast (Figure 1-9). Indeed the binding of Spp1 to cold DSB regions by generating Gal4 fusions of Set1 and Spp1 proteins and inserting UAS_{GAL} binding sites in appropriate genomic locations demonstrated that this is sufficient to stimulate DSB formation (Acquaviva et al., 2013).

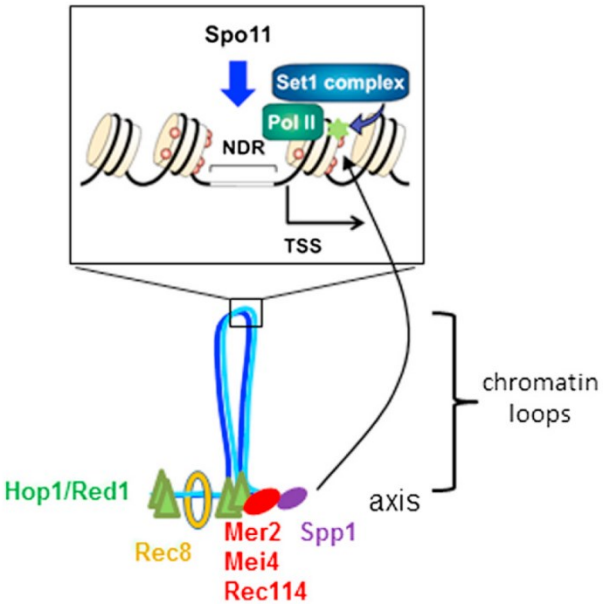

Figure 1-9. Connecting meiotic DSB sites to chromosome axes in *S. Cerevisiae* by Spp1
Most of the Spo11-accessible locations in *S. cerevisiae* are in nucleosome depleted regions (NDR) upstream of transcription start sites (TSSs). The Set1 complex interacting with RNA Pol II promotes H3K4me3 (green star) at the nucleosome downstream of the Spo11 recruitment site. The Spp1 protein, is localized to the chromosome axis through interaction with Mer2, and is able to bind H3K4me3 (arrow). This interaction promotes the tethering of the chromatin loop to the axis and Spo11 interaction with the Rec114/Mei4/Mer2 complex (RMM complex). The association of the RMM complex to the axes depends on the proteins Red1 and Hop1 and is influenced by the cohesin Rec8. Schematic modified from de Massy, 2013.

Mouse MEI4 and REC114 interact and MEI4 forms ~300 cytologically apparent foci localised to chromosome axes, which are most abundant in leptotene (Kumar et al., 2010). A comprehensive analysis of mouse REC114 is yet to be published. The localisation of MEI4 is upstream of SPO11 as demonstrated by normal appearance in *Spo11*$^{-/-}$. It has not yet been reported though whether or not this localisation is dependent on PRDM9 activity, or whether these foci mark DSB hotspot loci. MEI4 foci are not seen to co-localise with those formed by proteins involved in the early stages of DSB repair such as RPA, RAD51 or DMC1 indicating a temporal and/or spatial distinction in the loading of these proteins (Kumar et al., 2010). *Mei4*$^{-/-}$ mice are infertile. Mutant spermatocytes assessed cytologically are negative for early recombination proteins RAD51, DMC1 and RPA, and feature greatly reduced levels of γH2AX staining. Furthermore chromosome synapsis is defective. These features are consistent with an inability to generate meiotic DSBs in *Mei4*$^{-/-}$ (Kumar et al., 2010) and are strongly reminiscent of the *Spo11*$^{-/-}$ phenotype. These findings demonstrate a clear role for MEI4 and indicate that REC114 is also likely to be involved in mouse meiotic DSB formation (Figure 1-8). It will be interesting to uncover the extent of the similarity between mechanisms of meiotic DSB formation in yeast and higher eukaryotes, and specifically to

reveal whether H3K4me3 plays a similar role in enabling the tethering of hotspot DNA to the chromosome axis.

MEI1, a protein absent from yeast, but conserved in vertebrates and required for mouse fertility, also appears to have a role in the formation of meiotic DSBs (Libby et al., 2002, 2003). Mice carrying *Mei1* mutations fail to synapse their homologous chromosomes and feature cytological γH2AX signals similar to those seen in *Spo11*$^{-/-}$ as well as an absence of detectable RAD51 foci, indicating a lack of meiotic DSBs (Libby et al., 2002, 2003). Furthermore the defects incurred by *Mei1* mutation are epistatic to those in *Dmc1*$^{-/-}$ (Reinholdt and Schimenti, 2005), a mutant unable to repair DSBs which will be discussed shortly. Therefore while many components of the meiotic recombination pathway are shared with yeast, this is not always the case. However, the structure and function of MEI1 is not yet known and has been speculated to compensate for the absence of other yeast proteins required for DSB formation but lacking in vertebrates (Libby et al., 2003).

1.5.4 DSB Processing

One of the earliest signals of DSB formation in leptotene is the phosphorylation of histone variant H2AX at serine 139 (Mahadevaiah et al., 2001; Rogakou et al., 1998) by the kinase ATM (Bellani et al., 2005), in chromatin surrounding break sites. As previously mentioned, the appearance of this phosphorylated form of H2AX (γH2AX) is a widely used marker of DSB formation in both meiotic and mitotic cells. γH2AX staining persists through prophase, eventually dissociating from autosomes completely during pachytene. Autosomal γH2AX staining exists in two varieties of distinct focal pattern, namely small-foci (S-foci) which are SPO11-dependent, restricted to the chromosome axis and colocalise with recombination proteins, and loop-associated-foci (L-foci) which are SPO11-independent and extend in flare-like domains into chromatin loops (Chicheportiche et al., 2007). Despite the association between γH2AX and meiotic DNA damage, H2AX is not required for the repair of DSBs or homologous chromosome synapsis (Fernandez-Capetillo et al., 2003). The requirement for H2AX in irradiated somatic cells to facilitate the repair of damaged DNA implies that γH2AX play may a redundant role in the repair of meiotic DNA damage (Celeste et al., 2002). Potential candidates to compensate for the absence of H2AX include the other H2 histones; H2A and H2B which also become phosphorylated and largely colocalise with γH2AX in meiosis (Baarends et al., 2007).

Following the formation of meiotic DSBs the ends of the broken DNA are processed to enable their repair by homologous recombination. This processing involves the release of

covalently bound SPO11-oligonucleotide complexes by endonucleolytic activity, followed by exonucleolytic degradation of the same strand (Figure 1-10). The strands ultimately undergo a homology search to identify their partner homologous chromosome and use this as a template to repair the DNA damage. The endonucleolytic cleavage is asymmetric, generating products of distinct length from each side of the DSB, and is most likely catalysed by MRE11 (Figure 1-8b), as in yeast (Neale et al., 2005). Mre11 is a component of the MRN complex (consisting of Mre11, Rad50 and Nbs1) with single strand endonuclease activity. Certain *Mre11* mutants, including those lacking their endonuclease activity cannot remove Spo11 from DSB ends in yeast (Keeney, 2001). Mouse MRE11 is most strongly detectable during leptotene and zygotene, and is present throughout the nucleus at these stages before localising to the sex body during pachytene and diplotene (Eijpe et al., 2000b; Goedecke et al., 1999). The embryonic lethality caused by deletion of any member of the MRN complex in mammals, due to their key somatic functions, has complicated the study of mutation in meiosis (Stracker et al., 2004). The study of mice with hypomorphic mutations in *Mre11,* which support viability, has revealed delayed oocyte progression through leptotene and zygotene, while DSBs are being processed, as well as altered meiotic progression in males. Chromosome synapsis is defective in around half the oocytes and spermatocytes and localisation of the early recombination protein RAD51 is reported to be normal at early meiotic stages, indicating unaltered DSB frequency, however this marker and also γH2AX persist in pachytene with particularly strong enrichment along individual chromosomes despite their successful synapsis. Surprisingly the frequency of crossovers formed is reduced in the *Mre11* hypomorph and despite these defects the mutants are fertile at a sub-normal level (Cherry et al., 2007). The synaptic defects and abnormal meiotic progression may be caused by delayed performance of the homology search as a result of defective DSB processing, as would be predicted from findings in yeast mutants. The apparently normal level of RAD51 in early meiosis however is not consistent with defective DSB resection. Therefore while there is certainly a role from MRE11 in mouse meiosis, and this appears likely to influence recombination, the details of its involvement are not currently clear, due to potential phenotypic complication caused by residual activity remaining in hypomorphic mutants. The study of a meiosis-specific mutant will be an informative step towards better understanding the role of MRE11 in mouse meiosis.

The additional exonucleolytic degradation of the 5' strands at DSBs is predicted to be primarily mediated by exonuclease 1 (EXO1) due to its somatic function and findings in yeast (Hunter, 2011). However *Exo1*$^{-/-}$ mice are not defective in homologous chromosome

pairing (Wei et al., 2003), leading to suggestions that other nucleases may compensate for its absence (Hunter, 2011).

Surprisingly, DNA polymerase β (Pol β) is also involved in the very early events of DSB processing (Kidane et al., 2010). Pol β is an enzyme with both polymerase and deoxyribose phosphate (dRP) lyase activities and is not thought to participate in the replication of genomic DNA but is known to function in base excision repair (Sobol and Wilson, 2001). Pol β forms axis-associated foci during meiosis, which are detectable between zygotene and late pachyene (Jonason et al., 2001; Plug et al., 1997a) and dependent on SPO11 (Kidane et al., 2010). Mice with a conditional deletion of *Pol* β^{flox} in the primordial germ cells mediated by TNAP-(Cre) subsequently lack Pol β in the descendants of these cells, which include meiocytes (Kidane et al., 2010). These meiocytes are severely defective in chromosome synapsis and both spermatocytes and oocytes arrest in prophase. DSB formation is normal in the absence of Pol β as indicated by the similar localisation of γH2AX in mutant leptotene spermatocytes as WTs, however abnormally high levels of SPO11-dependent γH2AX in zygotene mutant spermatocytes indicates defective DSB repair. Assessment of SPO11-oligo complex levels in mutant testes revealed a dramatic reduction (at least 3-fold), indicating a severe defect in the efficiency of SPO11 removal from the DSB site. Consistent with this, the frequency of foci formed by ssDNA–binding early recombination proteins is reduced in the *Pol β* mutant (Kidane et al., 2010). Therefore it appears that Pol β is required for the timely removal of SPO11 from DSBs to promote the progression of DNA repair and homologous synapsis. How the protein functions in this process is currently unclear.

1.5.5 Early Recombination Proteins – Homology Search

The formation of the 3' ssDNA overhangs at DSB sites stimulates the recruitment of a collection of ssDNA-binding proteins which promote the meiotic homology search, an event largely responsible for the accurate pairing of homologous chromosomes in meiotic prophase. These proteins are heavily studied cytologically, where they are recognised as axis-associated foci. It is the frequency of such foci which has informed the estimates of DSB frequency in many organisms including mice. The first protein interacting with these strands appears to be replication protein A (RPA), a heterotrimeric protein which is thought to be involved in DNA damage recognition and the recruitment of repair machinery (Zou et al., 2006). Due to its central role in DNA repair in mitotic cells RPA is essential for viability, impeding the study of its requirement in meiosis (Dodson et al., 2004). Despite its early

predicted role in meiosis, RPA foci are often only detectable at relatively low frequencies during leptotene (~100 foci) before peaking during zygotene, somewhat after DSB formation, at 200-300 foci and steadily dissociating towards mid-pachytene as DNA is repaired (Moens et al., 2002; Plug et al., 1997b). However, in a mutant mouse with impaired loading of other meiotic ssDNA binding proteins (RAD51, DMC1), RPA can be detected at the leptotene stage (Yang et al., 2008). This suggests that either the loading of other ssDNA binding proteins temporarily displaces RPA in meiosis, or these similarly located proteins impair the ability to recognise RPA protein bound.

The recombinase RAD51 and its meiosis-specific homolog DMC1 are eukaryotic homologs of the bacterial protein RecA (Aboussekhra et al., 1992; Bishop et al., 1992). RAD51 and DMC1 localise to meiotic DSBs, forming 200-300 foci in mouse leptotene and early zygotene spermatocytes, then dissociating as DNA repairs into mid-pachytene (Barlow et al., 1997; Moens et al., 2002). Rad51 and Dmc1 have been mechanistically studied in detail in budding yeast, where they form nucleoprotein filaments on ssDNA which search for and swap strands with homologous double stranded DNA (dsDNA) to form joint molecules (JM) (Figure 1-8, Figure 1-10). RAD51 and DMC1 have been seen to localise to distinct domains and have been proposed to bind to opposite ends of the DSB (Figure 1-10) (Hunter and Kleckner, 2001). In addition to its meiotic function, Rad51 also acts directly in JM formation in mitotic recombination, where the sister chromosome is commonly invaded as a template for repair (Schwacha and Kleckner, 1997; Sheridan and Bishop, 2006; Shinohara et al., 1992; Tsubouchi and Roeder, 2006). Yeast lacking Rad51 are defective in the formation of Dmc1 foci, which are much fainter than in WT, and are found to generate abnormally high levels of inter-sister rather than inter-homolog JMs (inter-homolog/inter-sister JMs in WT = 4.8/1, and *rad51Δ* =1/3.9) (Bishop, 1994; Schwacha and Kleckner, 1997; Shinohara et al., 1997). Separation of function mutants in *Rad51* and *Dmc1* have demonstrated that only the ability Rad51 to form nucleoprotein filaments is needed during meiosis, as its JM forming capacity is dispensable for recombination. The JM forming capacity of Dmc1 however is vital for meiotic recombination (Cloud et al., 2012). Therefore it appears that Rad51 acts as a cofactor for Dmc1 activity, promoting its localisation and directing strand invasion towards homologous chromosomes rather than sisters.

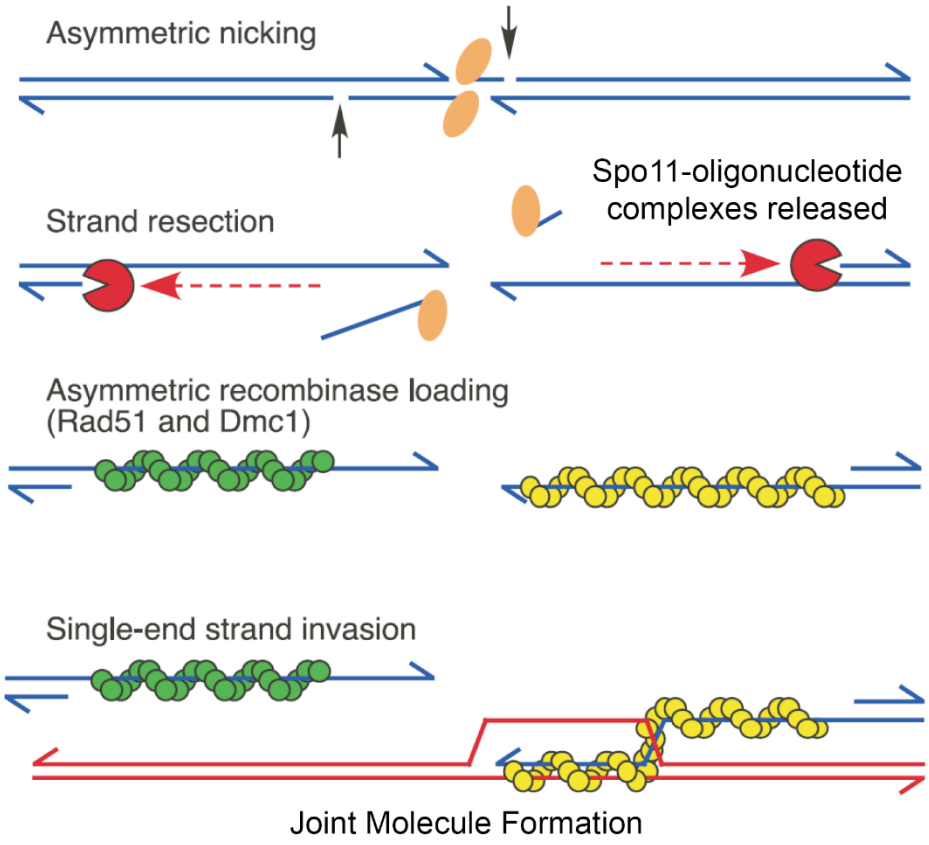

Figure 1-10. Strand invasion in meiotic recombination
DNA downstream of DSBs generated by SPO11 (orange oval) is nicked and subsequently resected to reveal ssDNA strands and release SPO11 in a complex with the covalently bound oligonucleotide sequence from the break site. DMC1 and RAD51 (yellow and green, specific organisation of filaments not shown) form filaments on the ssDNA and appear to perform distinct role in promoting single strand invasion of the homologous chromosome to produce a joint molecule and initiate repair. Model modified from Neale et al., 2005.

The somatic function of RAD51 in mammals has prevented the study of null-mutations in meiosis due to early embryonic lethality (Lim and Hasty, 1996). *Dmc1*$^{-/-}$ mice are infertile. *Dmc1*$^{-/-}$ spermatocytes are able to recruit RAD51 during meiosis, however they cannot perform a successful homology search and arrest in prophase with unsynapsed chromosomes and high levels of axial RAD51 foci indicating unrepaired DSBs (Pittman et al., 1998). Some inter-sister DNA repair may take place in the absence of DMC1 though this remains limited, indicating persistent inhibition of this repair mechanism. Therefore DMC1 is essential for the meiotic homology search in mice and it appears likely based on the analysis of this mutant and cytological assessment in WT meiosis, that the functions of DMC1 and RAD51 are conserved from budding yeast.

The recruitment and function of RAD51 and DMC1 during meiosis also requires a variety of cofactors. The breast cancer susceptibility gene *Brca2* is essential in mice for

embryonic viability but transgenic mutant embryos with poor expression in the gonads are viable but infertile, demonstrating a germline function for the protein (Sharan et al., 2004). BRCA2 contains several ssDNA binding motifs and stimulates recombination in mitotic environments by direct interaction with RAD51 (Holloman, 2011; Yang et al., 2002). A specific interaction has also been demonstrated between DMC1 and BRCA2 via an alternative domain to that interacting with RAD51 (Thorslund et al., 2007), thus demonstrating distinct interactions between BRCA2 and both RAD51 and DMC1 in meiosis. *Brca2*-deficient spermatocytes are unable to complete synapsis and arrest in prophase. These mutant spermatocytes initiate recombination, with normal levels of γH2AX detected in leptotene, however this damage is not repaired and persists in the asynapsed nuclei. The recruitment of RAD51 and DMC1 is severely impaired, with the frequency of axial foci greatly reduced but their levels of cellular protein unchanged. Unlike RAD51 and DMC1, RPA foci are abundant on the chromosomes of the mutant indicating that RPA recruitment is independent of BRCA2 (Sharan et al., 2004). BRCA1 also plays a key role in the DNA damage response has been shown to interact with RAD51, however unlike BRCA2 this interaction is thought to be indirect (Boulton, 2006). Homozygous *Brca1* mutations are only compatible with life when combined with heterozygous mutations in *p53*. Such male mice are infertile, with spermatocytes displaying greatly diminished levels of RAD51 foci, but the localisation of normal levels of DMC1, and unrepaired DNA damage in pachytene (Xu et al., 2003). The precise role of BRCA1 in meiotic recombination remains to be elucidated. In addition to the BRCA proteins, male mice also require the germ cell specific gene *Tex15* for proficient loading of RAD51 and DMC1 and meiotic chromosome synapsis, but not meiotic DSB formation or the loading of RPA (Wang et al., 2001; Yang et al., 2008). However, the structure of TEX15 and the mechanism of its involvement in recombination have not yet been reported.

Further cofactors are also required for the activity of RAD51 and DMC1 after loading to the DSB, such as HOP2 and MND1 (Petukhova et al., 2003; Pezza et al., 2014). HOP2-MND promotes the stability of RAD51 and DMC1 filaments on ssDNA *in vitro* and promotes the capture of potential partner chromosomes to facilitate the homology search and JM formation (Chi et al., 2007; Pezza et al., 2007, 2010). In the absence of HOP2 meiotic DSBs are generated and RPA, RAD51 and DMC1 localise to chromosomes, but very little synapsis occurs (Petukhova et al., 2003). HOP2's partner MND1 is also required for mouse fertility, however many *Mnd1*$^{-/-}$ spermatocytes achieve complete synapsis and repair meiotic DSBs. This repair has been proposed to take place by an alternative pathway, utilising the recombinase activity of HOP2 rather than DMC1, and does not result in crossover formation

(Pezza et al., 2014). Therefore it is possible that the meiotic arrest reported in primary spermatocytes arises due to chromosome segregation defects in metaphase I. In summary, the recruitment of RAD51 and DMC1 to meiotic DSBs is central to the formation of inter-homolog JMs. This recruitment involves a number of cofactors including BRCA1, BRCA2 and TEX15 and the subsequent activity of RAD51 and DMC1 appears to be dependent on further factors including HOP2 and MND1 (Figure 1-8).

1.5.6 Additional Mechanisms of Homolog Pairing

It is interesting to note that in addition to the homology search driven by recombination, additional mechanisms also appear to contribute to the pairing of homologous chromosomes. In *S. cerevisiae* telomeric attachments to cytoplasmic motors thought to be mediated by SUN proteins through the nuclear envelope drive rapid meiotic prophase chromosome movements (RPM). Mutations in SUN genes in yeast cause defects in RPMs and in chromosome pairing (Koszul and Kleckner, 2009). A similar vigorous movement of chromosomes is seen in a variety of eukaryotes and is thought to eliminate unwanted chromosomal associations and entanglements, though the mechanisms involved vary between organisms (Koszul and Kleckner, 2009). It was recently shown that a significant amount of homolog chromosome pairing precedes DSB formation in mice, and curiously this pairing remains SPO11-dependent though does not require the protein's ability to make DSBs (Boateng et al., 2013). SUN1, a protein required for telometic attachment to the nuclear envelope is also required for pre-DSB homolog pairing in mice. Pairing at homologous telomeres is maintained into prophase and is thought to be important for the initiation of synapsis (Boateng et al., 2013). Therefore it has been proposed that the recombination-driven homology search in mice serves to proofread and stabilise the pre-DSB pairing of homologous chromosomes (Figure 1-11).

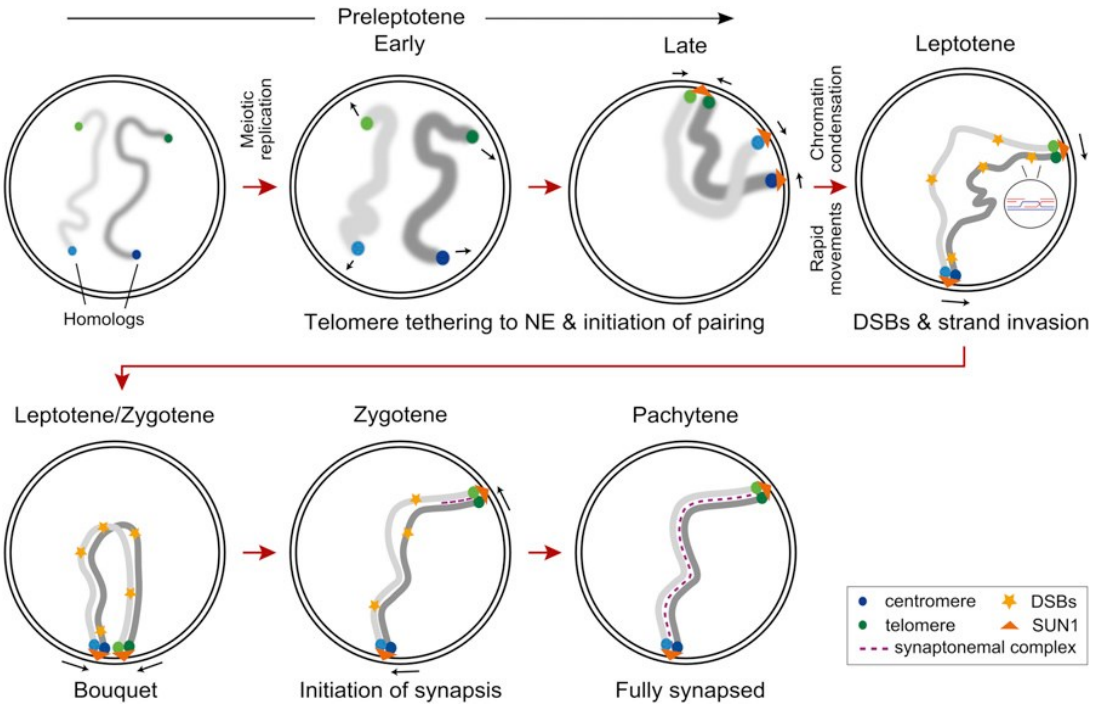

Figure 1-11. Model for pre-leptotene DSB-independent pairing in mice
Telomeres tethered to the nuclear envelope in late pre-leptotene by SUN1 is thought to facilitate homolog pairing subtelomeric regions. Upon entry to prophase pairing at interstitial (non-telomeric sites) is lost to allow the removal of unwanted interactions, though telomeric pairing is maintained at a minimum of one end. Homologous recombination is proposed to proofread these preliminary pairings. Model taken from Boateng et al., 2013.

In addition to this mechanism, the mutually exclusive staining patterns for the meiotic cohesin α-kleisin subunits REC8 and RAD21L have also been noted along homologous chromosomes of mouse spermatocytes and proposed to act as a barcode for homolog recognition (Ishiguro et al., 2011), thus implying a DSB-independent pairing mechanism. Finally, disruption to centromeric clustering into shared heterochromatic regions before leptotene has also been proposed to perturb chromosome synapsis (Takada et al., 2011). Therefore, while homologous recombination is the main driving force behind the search for homologous chromosomal partners other meiotic processes are coming to light which contribute to the promotion of this search.

1.5.7 Intermediate Recombination Proteins – Joint Molecule Stabilisation

As chromosomes synapse following homologous pairing and formation of JMs, early recombination proteins RAD51 and DMC1 are replaced by intermediate recombination proteins MSH4 and MSH5 (Moens et al., 2002). MSH4 and MSH5 are cytologically

recognised from zygotene, wherein they commonly colocalise with RPA and form ~150 foci before steadily dissociating in pachytene (Kneitz et al., 2000; Moens et al., 2002). MSH4 and MSH5 are mammalian homologs of the *E. coli* mismatch repair gene *MutS*. In *E. coli*, MutS recognises and binds to mismatched nucleotides and subsequently interacts with MutL and the endonuclease MutH which nicks hemimethylated DNA in the region of the mismatch to stimulate repair of the newly synthesised strand. Several eukaryotic homologs of these proteins exist and many of these are involved in mismatch repair. *Msh4 and Msh5* expression however is largely restricted to reproductive tissues (Her et al., 1999; Kneitz et al., 2000). In the absence of MSH4 or MSH5 mice are infertile. Recombination is successfully initiated and RAD51 recruited to chromosome axes, but chromosome pairing is defective and germ cells arrest in prophase, indicating a requirement for these proteins to stabilise inter-homolog JM interactions (Edelmann et al., 1999; Kneitz et al., 2000; Moens et al., 2002; de Vries et al., 1999). MSH4 and MSH5 form a heterodimeric complex. The observation that the asynapsis caused by the absence of MSH5 is more severe than in *Msh4*$^{-/-}$ spermatocytes, and unchanged in *Msh4*$^{-/-}$*Msh5*$^{-/-}$ double mutants, indicates that MSH5 is epistatic to MSH4 (Kneitz et al., 2000). MSH4 and MSH5 have been shown to recognise the Holliday Junction formed during the repair of JMs, and form a sliding clamp embracing the adjacent homologous duplex arms, thereby stabilising their interaction (Figure 1-12) (Snowden et al., 2004).

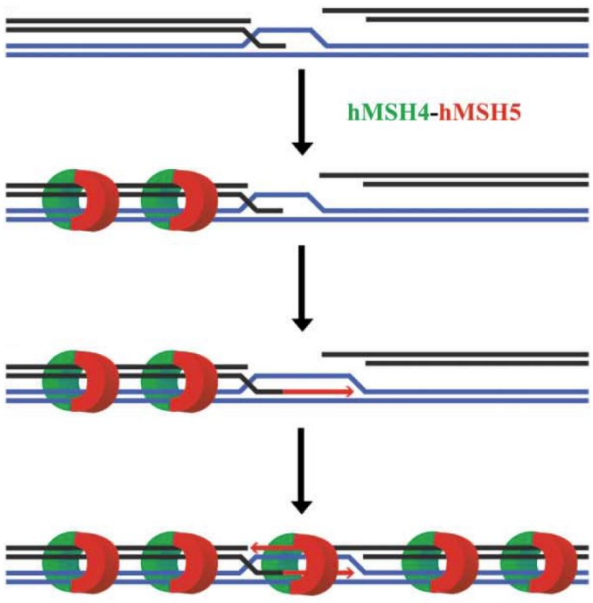

Figure 1-12. Sliding clamp model for MSH4-MSH5 stabilisation of meiotic joint molecules
The MSH4 and MSH5 complex recognises Holliday junctions and forms a sliding clamp that embraces adjacent homologous chromosomes, stabilising the initial inter-homolog interaction. A double Holliday junction would facilitate the loading of additional sliding clamps. Model taken from Snowden et al., 2004.

1.5.8 Late Recombination Proteins – Holliday Junction Resolution

Meiotic DSBs are ultimately repaired by homologous recombination one of two ways: (1) to produce a non-crossover (~90% of DSBs), where invasion is limited to a single strand which returns to its chromosome of origin after repair, or (2) a crossover (~10% of DSBs), where Holliday Junctions are generated at both ends of the break site and resolved to produce recombinant chromosomes by exchanging flanking DNA. Crossovers (COs) generate a stable inter-homologue connection which manifest as chiasmata in metaphase I and are required for homologous chromosome bi-orientation and segregation in combination with cohesin.

Crossover formation is largely dependent on two proteins homologous to the *E. coli* MutL protein, MLH1 and MLH3 (MLH: MutL homologue) (Eaker et al., 2002; Edelmann et al., 1996; Lipkin et al., 2002). MLH1 and MLH3 form a dimer which has recently been shown to function as an endonuclease, preferentially binding to Holliday Junctions and making single-stranded breaks in supercoiled DNA (Ranjha et al., 2014; Rogacheva et al., 2014). MLH1 and MLH3 form foci on synapsed meiotic chromosomes in pachytene, the frequency and distribution of which closely correspond with that of chiasmata visible in metaphase (Anderson et al., 1999; Lipkin et al., 2002). MLH1 and MLH3 are dependent on each other for their localisation (Lipkin et al., 2002). In the absence of MLH1 or MLH3 homologous chromosomes are able to synapse and repair DSBs, but are defective in chromosome segregation as very few bivalent chromosomes are held together by chiasmata in metaphase, resulting in meiotic arrest (Eaker et al., 2002; Lipkin et al., 2002).

CO distribution is tightly controlled, with at least one required on every pair of homologous chromosomes to facilitate balanced segregation. Typically around 23 crossovers/chiasmata are formed per spermatocyte. The formation of one CO between a pair of homologs inhibits the formation of another in the proximal chromatin by a process known as crossover interference. Hence, chromosomes with multiple COs are typically the largest (Anderson et al., 1999). The domain of CO inhibition by interference is dependent on a chromosome's axis length rather than its genetic size per se, as CO frequency on a particular chromosome can differ between oocyte and spermatocytes consistent with differences in axis length (Kleckner et al., 2003).

Although the majority of COs are lost in the absence of MLH1 or MLH3 in mice (the Class I crossover pathway), a small number of chromosomes do generate chiasmata. These chiasmata are generated by an alternative pathway dependent on the MUS81 endonuclease (Class II crossover pathway), similarly capable of resolving Holliday Junctions

(Chen et al., 2001). Unlike MLH1/3-dependent COs, those generated by MUS81 are insensitive to interference, and in *S. cerevisiae* the class II crossover pathway does not depend on MSH4/MSH5 (de los Santos et al., 2003). MUS81 is absent from Figure 1-8 as it is speculated that this pathway may resolve single rather than double Holliday junctions (Baudat et al., 2013), which are not included, and the understanding of the class II pathway in mice is currently limited. Interestingly the absence of MUS81 does not cause infertility in mice, and the number of chiasmata remains unaltered due to a compensatory increase in MLH1/3 resolved DSBs (~3 additional foci per nucleus) (Holloway et al., 2008).

Several factors have been identified which contribute towards deciding the repair fate of recombination intermediates. The helicase BLM (Bloom's syndrome mutated) exists in a complex with topoisomerase IIIα and BLAP75 in mitotic cells, where it is thought to localise to Holliday junctions to promote their dissolution (Wu et al., 2006; Yin et al., 2005). During meiosis BLM forms approximately 200 axis-associated foci during zygotene, which colocalise with RPA at DSBs and steadily dissociate during prophase consistent with DNA repair (Moens et al., 2002). Curiously, the dissociation of BLM from chromosome axes in pachytene is dependent on MLH3 and MUS81 (Holloway et al., 2008, 2010). While the significance of this is not clear it is interesting to note this unusual relationship with the resolution machinery (Holloway et al., 2010). Spermatocytes lacking BLM generate elevated levels of chiasmata despite recruiting normal frequencies of MLH1 foci, suggesting a role in restricting the CO formation by the Class II, MUS81 pathway (Holloway et al., 2010).

ZIP4H (TEX11) was identified as a male germ cell specific interaction partner of the MRN complex subunit NBS1. TEX11 appears to be orthologous to the *S. cerevisiae* and *A. thaliana* protein Zip4 (ZIP4H: Zip4 homologue) which influences levels of meiotic CO formation. ZIP4H is cytologically detected from late stage spermatogonia, through leptotene and zygotene, before diminishing into pachytene. ZIP4H does not localise to discrete domains, but is diffuse. Male mice lacking ZIP4H are fertile but display a delay in DSB repair, with normal levels of DMC1 foci detected in leptotene indicating normal DSB formation, but abnormally high levels persisting in pachytene (Adelman and Petrini, 2008). Despite this delay in DSB repair the proportion of pachytene spermatocytes in late, MLH1-positive, stages of recombination are unchanged between WT and *Zip4h*$^{-/-}$. Co-staining spermatocytes for MLH1 and RAD51 revealed an elevated proportion of pachytene spermatocytes decorated with both types of foci, demonstrating CO formation occurring in parallel with ongoing repair of immature DSBs, suggesting defective repair processing. The frequency of autosomal MLH1 foci localised to chromosome axes in *Zip4*$^{-/-}$ was subtly reduced (from 23.5 to 21.2). In spite of this reduction, analysis of CO positioning revealed a

relaxation of CO interference, with more double COs on single autosomes typically arising in closer proximity. Length of chromosome axes containing multiple COs was unchanged in this mutant, therefore the effects on CO formation are likely a direct involvement of ZIP4H in recombination. Metaphase I spermatocytes contain an increased number of achiasmate autosomes and sex chromosomes, resulting in chromosome segregation defects and increased apoptosis at this stage (Adelman and Petrini, 2008). Zip4 orthologues contain TPR motifs which are likely to drive protein interactions (Blatch and Lässle, 1999; Perry et al., 2005), leading to suggestions that these proteins promote CO formation through recruitment of recombination factors (Adelman and Petrini, 2008). The direction of ZIP4H to DSBs through its interaction with the MRN complex is an attractive possibility. Persistent immature recombination intermediates at pachytene is a feature observed in both *Zip4h*$^{-/-}$ and *Mre11* mouse mutants, however the absence of this feature from the hypomorphic mouse mutant of the *Nbs1* component of the MRN complex, and the contrasting increase in COs in both *Nbs* and *Mre11* mutants demonstrates that these three mutants do not phenocopy (Adelman and Petrini, 2008; Cherry et al., 2007). Therefore while the relationship between these proteins and their functional significance in mouse meiotic recombination is not completely understood, it is clear that they (ZIP4H, MRE11 and NBS1) all influence CO formation.

RNF212 is a mammalian homolog of the *S. cerevisiae* meiotic factor Zip3. RNF212 possesses a RING-finger domain, typical of enzymes that catalyse protein modification by the addition of ubiquitin-like molecules, and is implicated as an E3 enzyme for SUMO modification (Deshaies and Joazeiro, 2009; Reynolds et al., 2013). Expression in mice is exclusive to meiocytes and RNF212 forms ~150 axial foci around the transition between leptotene-zygotene stages of meiotic prophase. Surprisingly only ~30% of RNF212 foci colocalise with MSH4, indicating that it is not present at all intermediate recombination foci. The frequency of foci drops considerably in pachytene, until only one or two remain on each chromosome pair by mid-pachytene, the majority of which now colocalise with MSH4. The subset of recombination intermediates with which RNF212 interacts in pachytene also shows high colocalisation with MLH1. The pattern and frequency of RNF212 is unchanged in *Msh3*$^{-/-}$ mice which are unable to make COs, therefore RNF212 is marking CO precursors in pachytene rather than CO products. CO formation is largely abolished in *Rnf212*$^{-/-}$, with no detectable MLH1/3 foci localising despite proficient chromosome synapsis, and high levels of univalent chromosomes at metaphase I, rendering the mutant mice infertile. Despite initially normal levels of MSH4 foci in *Rnf212*$^{-/-}$ zygotene spermatocytes, in latter stages focus frequency was reduced, particularly in mid-pachytene. Similarly the levels of ZIP4H

foci are reduced in this mutant. Therefore RNF212 is required to stabilise a proportion of MSH4 foci as well as ZIP4H. In addition to the cytological instability, cellular protein levels of MSH4 and ZIP4H are dramatically reduced in *Rnf212*$^{-/-}$(Reynolds et al., 2013). RNF212 localisation to DSB sites is therefore proposed stabilise homologous interactions by enhancing MSH4 and ZIP4H association, thereby promoting the formation of Holliday junctions and subsequent CO formation (Reynolds et al., 2013). How this stabilisation is achieved is not currently clear, though it is proposed to be mediated by SUMOylation of MSH4/5 (Reynolds et al., 2013).

The mouse orthologue of HEI10 (The Human Enhancer of Invasion 10) is a further example of an E3 ligase involved in meiotic CO formation (Ward et al., 2007). *Hei10* is strongly expressed in testes and mutant mice are defective in chromosome segregation at metaphase I, resulting in infertility in both sexes. *Hei10* mutant spermatocytes recruit normal frequencies of RAD51 foci in zygotene, indicating normal progression of early recombination (Ward et al., 2007), however MSH4 persists on chromosomes and RNF212 is seen to localise to the majority of DSBs rather than a limited subset (Qiao et al., 2014). This has led to the proposal of antagonistic function of RNF212 and HEI10 in the stabilisation of recombination proteins at CO and NCO sites (Figure 1-13) (Qiao et al., 2014) possibly influencing the balance of SUMO and ubiquitin modifications of these recombination proteins. In addition to the apparent role of HEI10 in influencing the designation of NCO and CO formation in zygotene, HEI10 is also required for the formation of CO-specific complexes containing MLH1, MLH3 and CDK2 in synapsed pachytene spermatocytes (Ward et al., 2007). HEI10 forms axial foci in pachytene which largely colocalise with these CO-specific complexes, and this localisation is restricted by MLH3, with HEI10 forming numerous foci at this stage in *Mlh3*$^{-/-}$ spermatocytes (Qiao et al., 2014). Therefore HEI10 is thought to act in two phases, first to restrict RNF212 localisation to MSH4-marked DSBs in zygotene to restrict potential CO formation, before later HEI10 is directed by MLH3 (and possibly MLH1) to promote MSH4 and RNF212 dissociation and implementation of the final stages of CO formation (Figure 1-13) (Qiao et al., 2014).

CDK2 is a member of the cyclin dependent kinsase family of proteins which regulate the cell cycle both in mitosis and meiosis. CDK2 is essential for the completion of meiotic prophase in mice (Ortega et al., 2003) and as mentioned previously, CDK2 typically forms axial foci at interstitial points which colocalise with MLH1 in pachytene (Ashley et al., 2001). The phosphorylation of CDK2 appears to trigger the progression from the pachytene to diplotene stage of spermatogenesis (Liu et al., 2014). It has therefore been

proposed that CDK2 acts as a link between the meiotic DNA repair machinery and the cell cycle (Liu et al., 2014).

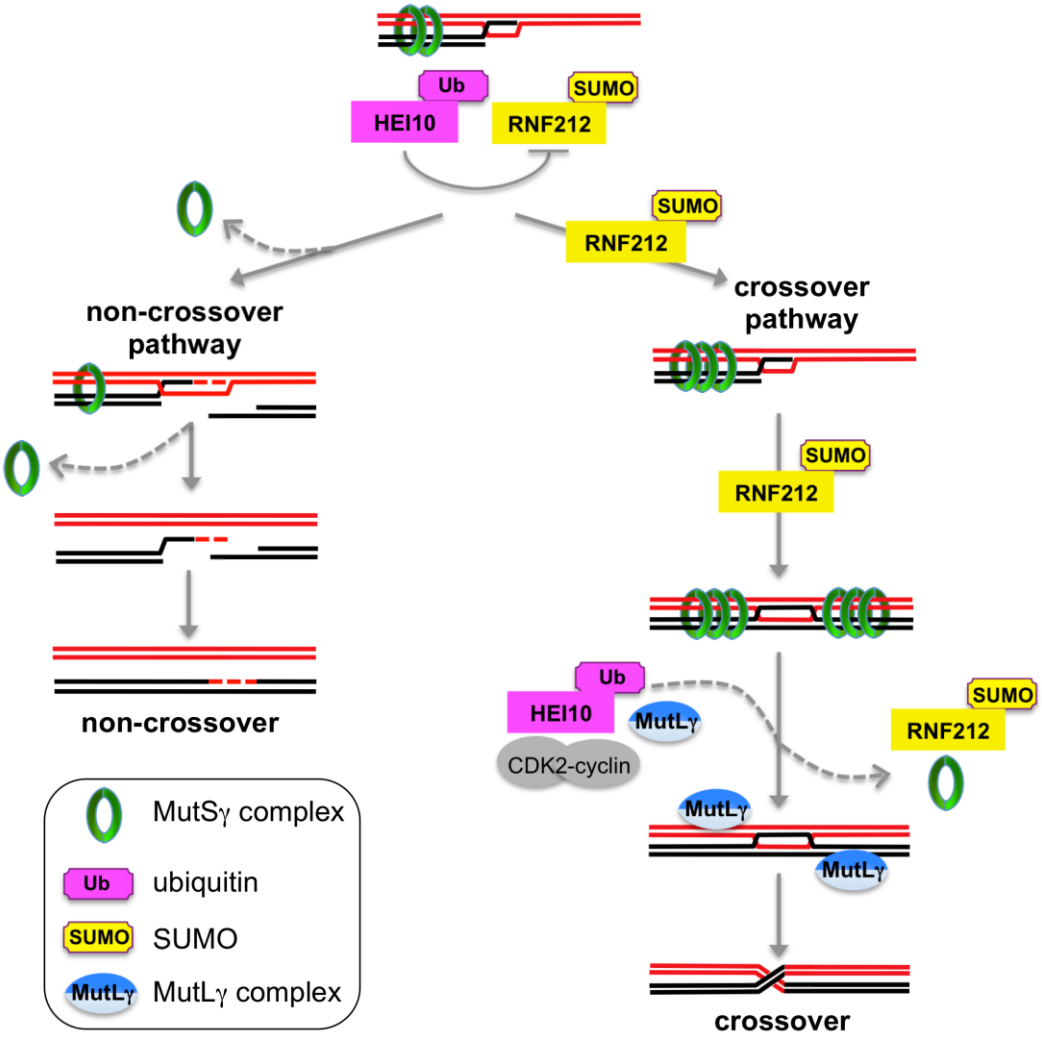

Figure 1-13. Model of the antagonistic roles of RNF212 and HEI10 in meiotic DSB repair
The MutSγ complex (MSH4 and MSH5) initially bind and stabilise most homologous interactions at invaded DSB site, promoting synapsis. The balance of HEI10-mediated ubiquitination and RNF212-mediated SUMOylation at this site (targets unknown) determines the stability of the MutSγ complex after synapsis. Some sites will accumulate sufficient RNF212 to stabilise MutSγ, which facilitates the formation of crossover intermediates. MutSγ dissociates from other sites allowing repair to progress towards non-crossover formation. The balance of RNF212 and HEI10 is again involved in the displacement of MutSγ to allow the association of MutLγ proteins (MLH1 and MLH3) and resolution of repaired DSBs to produce crossovers. Model from Qiao et al., 2014.

The Pachytene Checkpoint 2 protein (Pch2) is a crucial component of the synapsis checkpoint in *S. cerevisiae* and *C. elegans*, promoting the elimination of meiocytes with defective chromosome synapsis and/or recombination. In mice the orthologue of *Pch2, Trip13* (thyroid hormone receptor interacting protein) is involved in meiotic recombination (Li and Schimenti, 2007). Two hypomorphic mutants of *Trip13* have been generated which

fail to demonstrate a role for mouse TRIP13 in promoting the elimination of defective meiocytes, but do display meiotic phenotypes which differ in severity consistent with the reduction in expression of *Trip13* in each mutant, and ultimately result in infertility in both sexes (Li and Schimenti, 2007; Roig et al., 2010). *Trip13* is expressed in a variety of embryonic and adult tissues including testes (Li and Schimenti, 2007) (specifically spermatogonia, spermatocytes and spermatids) and oocytes (Li and Schimenti, 2007; Roig et al., 2010). *Trip13* mutants with a more moderate phenotype (*Trip13*$^{mod/mod}$) synapse homologous autosomes but feature an 11% reduction in SC length, indicating a role for TRIP13 in ensuring structurally normal SC formation (Roig et al., 2010). Furthermore, *Trip13*$^{mod/mod}$ ability to successfully synapse the XY chromosomes at their limited region of homology (PAR) was reduced, with many sex chromosomes failing to synapse in spermatocytes. Synapsis defects are amplified in the more severe *Trip13* mutant (*Trip13*$^{sev/sev}$) with chromosomes pairing successfully and initiating but failing to complete synapsis, arresting in a partially synapsed zygotene-like state typically with asynapsis restricted to chromosome termini (Roig et al., 2010). Both *Trip13* mutants are defective in the removal of HORMAD1 and HORMAD2 (Roig et al., 2010; Wojtasz et al., 2009), two proteins which typically dissociate from chromosome axes at sites of synapsis. The mouse HORMAD proteins influence multiple processes in meiosis, including the detection of asynapsis, as will be discussed shortly. Both mutants display defective recombination early in meiosis, with a dramatic reduction in RAD51 foci but normal levels of DMC1 foci and normal levels γH2AX indicating WT DSB frequency. RPA focus frequency is increased in the mutant leptotene spermatocytes, with additional foci thought to mark the RAD51-deficient DSBs (Roig et al., 2010). The repair of DSBs is also delayed, with DMC1, BLM and γH2AX persisting at abnormally high levels in pachytene, indicating a requirement for TRIP13 in ensuring the timely repair of meiotic DSBs (Li and Schimenti, 2007; Roig et al., 2010). MLH1 foci were not detected in *Trip13*$^{sev/sev}$ spermatocytes likely due to them failing to reach the necessary stage of maturity as the result of a male-specific checkpoint, but were present in *Trip13*$^{sev/sev}$ oocytes and *Trip13*$^{mod/mod}$ spermatocytes and often observed on chromosomes still decorated with abnormally high levels of immature DSB markers (Li and Schimenti, 2007; Roig et al., 2010). MLH1 foci frequency in both *Trip13*$^{mod/mod}$ spermatocytes and *Trip13*$^{sev/sev}$ oocytes is reduced and the frequency of chromosomes lacking crossovers increased. Furthermore, the positioning of MLH1 foci is subject to weaker CO interference in *Trip13*$^{mod/mod}$ spermatocytes. Therefore TRIP13 promotes the loading of RAD51 but not DMC1 onto meiotic DSBs, structural formation of the SC, chromosome synapsis, and the repair of DSBs by both CO and NCO pathways. Little is known about how

TRIP13 performs these diverse meiotic functions however, other than that is belongs to the AAA^{+}-ATPase family of proteins, and its role in regulating HORMAD1/2 dissociation is at least partially involved (Roig et al., 2010; Wojtasz et al., 2009).

1.6 The Pachytene Checkpoint

The synapsis of homologous chromosomes and repair of DNA damage are key events for the completion of prophase I and further progression through meiosis. Surveillance mechanisms related to these events exist in pachytene, providing a meiotic checkpoint at this stage. While chromosome synapsis and DSB repair are interlinked, defects in these processes appear to trigger distinct checkpoints at a similar stage (Burgoyne et al., 2009).

1.6.1 Meiotic silencing pathways: MSUC and MSCI

Chromosome asynapsis triggers the transcriptional silencing of chromatin involved by a process known as Meiotic Silencing of Unsynapsed Chromatin (MSUC) (Turner et al., 2005). A related process also occurs in WT pachytene spermatocytes on the unsynapsed XY chromosomes (Turner et al., 2004), resulting in the formation of a heterochromatic sex body (Solari, 1974) and the silencing of XY protein-coding gene expression (Song et al., 2009). This process is known as Meiotic Sex Chromosome Inhibition (MSCI) and the transcriptional silencing achieved is essential for male mouse fertility (Figure 1-14) (Royo et al., 2010).

H2AX is the key effector of these meiotic silencing pathways. In the absence of H2AX MSCI fails and spermatocytes arrest in pachytene (Fernandez-Capetillo et al., 2003). γH2AX becomes enriched at the sex body in pachytene spermatocytes. In spermatocytes with unsynapsed autosomes, γH2AX is sequestered at these sites and γH2AX localisation to the sex body is correspondingly reduced. Such a reduction of γH2AX at the sex body is associated with failed MSCI and subsequent pachytene spermatocyte arrest (Figure 1-14) (Mahadevaiah et al., 2008). Failed MSCI is therefore likely accountable for the shared pachytene arrest observed in response to asynapsis in many mutant mouse spermatocyte phenotypes (Barchi et al., 2005; Mahadevaiah et al., 2008). MSUC also takes place during female meiosis, where it also promotes apoptosis, presumably via transcriptional silencing of genes essential to further progression. However the female MSUC response is only active in response to low levels of asynapsis and does not function in response to high levels (Kouznetsova et al., 2009). As MSCI does not take place in oocytes, and impaired MSCI

appears to be the main cause of pachytene arrest in asynapsed spermatocytes undergoing MSUC, female meiotic progression is less sensitive to MSUC. Furthermore, MSUC is dispensable for the removal of defective oocytes suggesting that is has a limited input as a quality control mechanism in female meiosis (Kouznetsova et al., 2009)

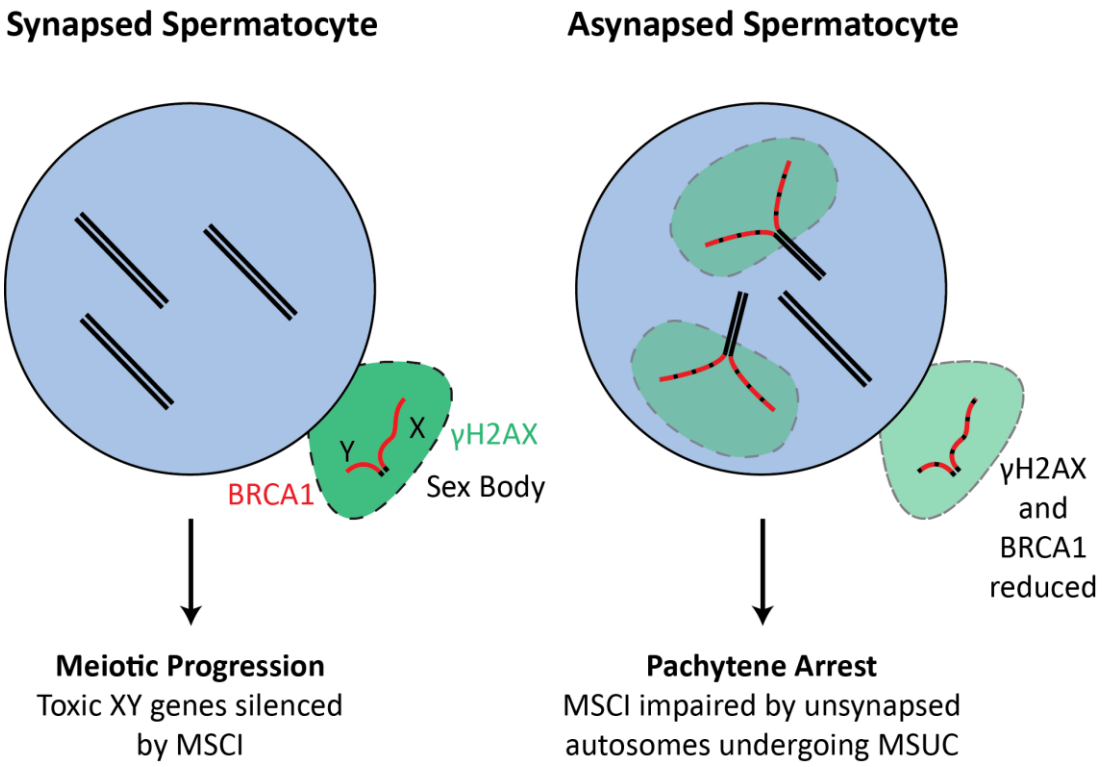

Figure 1-14. MSUC triggers MSCI failure and meiotic arrest
Transcriptional silencing of sex chromosomes by MSCI is essential for spermatocyte progression through pachytene. Asynapsed autosomes are silenced by MSUC, sequestering γH2AX and BRCA1, reducing the cells ability to simultaneously undergo MSCI. MSCI failure results in expression of toxic XY genes and meiotic arrest in mid-pachytene. Modified from Turner, 2007

1.6.2 Mechanism of meiotic silencing

H2AX can be phosphorylated at serine 139 by three PI3-K like kinases: Ataxia Telangiectasia Mutated (ATM), ATM Rad3-Related (ATR), and DNA-dependent Protein Kinase (DNA-PK) (Sedelnikova et al., 2003).These are key DNA damage sensors in mitosis, where ATM is recruited and activated by DSBs, ATR by RPA-coated ssDNA, and DNA-PK is directed to DSBs by the Ku proteins of the non-homologous end joining pathway (NHEJ) of DNA repair (Jackson and Bartek, 2009; Shiloh, 2003). In addition to H2AX these kinases also possess numerous other targets. *DNA-PK* mutants are fertile and do not display any abnormalities in the meiotic phosphorylation of H2AX (Bellani et al., 2005) indicating that it

is not responsible for this event in mice. ATM is essential for the initial wave of H2AX phosphorylation in response to DSB formation (by SPO11 or by irradiation). However, *Atm*$^{-/-}$ spermatocytes still display γH2AX at the sex body in pachytene indicating that MSCI is promoted by an alternative kinase (Bellani et al., 2005). ATR has long been implicated in both MSCI and MSUC due to its localisation to unsynapsed chromosome axes during meiosis and colocalisation with γH2AX during pachytene, as well as the association between its aberrant localisation and MSCI failure in *Brca1* mutant spermatocytes (Turner et al., 2004, 2005). The embryonic lethality caused by *Atr* deletion however has precluded the study of fertility in null mice (Brown and Baltimore, 2000). Two germline conditional knockouts of *Atr* have recently been generated, one triggered at the initiation of silencing, the other at the establishment of MSCI by an MSCI-dependent strategy (Royo et al., 2013). This analysis has revealed that ATR is dispensible for H2AX phosphorylation in leptotene, but mutant spermatocytes with pre-MSCI *Atr* deletion possess a dramatic reduction in γH2AX at zygotene, and sex body-associated γH2AX in pachytene is essentially absent. γH2AX is turned over rapidly during the early stages of meiotic prophase and ATR is essential for the re-phosphorylation apparent in late-zygotene/pachytene (Royo et al., 2013). Deletion of *Atr* after MSCI is established causes dramatic depletion of ATR protein levels and an absence of ATR at the sex chromosomes in late pachytene, demonstrating that ATR is unstable and is being constantly recruited to unsynapsed chromatin. Despite the absence of ATR in late pachytene this post-MSCI conditional mutant possesses a normal pattern of γH2AX at the sex chormosomes, indicating that ATR is not required for the maintenance of MSCI (Royo et al., 2013).

Several other factors involved in the establishment of MSCI and MSUC have also been identified. BRCA1 (Breast Cancer 1, early onset) is a tumour suppressor protein implicated in a wide range of processes (Boulton, 2006). In WT spermatocytes BRCA1 is first detected as foci on forming axial elements in leptotene as punctate staining which remains on unsynapsed and recently synapsed chromosomes in zygotene before becoming restricted to the unsynapsed arms of the XY chromosomes in pachytene (Turner et al., 2004). The localisation of BRCA1 during leptotene still occurs in *Spo11*$^{-/-}$ and is shed following non-homologous synapsis, indicating that this localisation is DSB-independent (Mahadevaiah et al., 2008). BRCA1 is required for the localisation of ATR to unsynapsed chromosome axes and subsequent H2AX phosphorylation in both MSCI and MSUC. As such, mouse *Brca1* mutant spermatocytes fail to undergo silencing (Turner et al., 2004, 2005). Furthermore it is interesting to note that the recruitment of BRCA1 to meiotic chromosomes is SYCP3-dependent, revealing a role for the synaptonemal complex in

meiotic silencing (Kouznetsova et al., 2009). It is not currently clear whether BRCA1-mediated recruitment of ATR to unsynapsed chromatin is direct or indirect.

During WT pachytene, ATR is initially detected primarily on the axes of the unsynapsed sex chromosomes before the cytological signal spreads to the XY chromatin loops as the stage progresses (Keegan et al., 1996; Moens et al., 1999). The initial localisation of ATR to the XY axes is sufficient to stimulate H2AX phosphorylation in this region, but the spread of ATR and thus γH2AX through XY chromatin is dependent on MDC1 (Ichijima et al., 2011). MDC1 (mediator of DNA checkpoint 1) is a binding partner of γH2AX, required for the formation of the sex body and establishment of MSCI (Ichijima et al., 2011). Therefore sex body formation occurs in two steps: initial localisation of ATR and γH2AX to XY axes, followed by their spread to chromatin loops.

The HORMA (Hop1, Rev7, and Mad2) domain proteins HORMAD1 and HORMAD2 localise along the length of the chromosome axes beginning in leptotene and steadily dissociate from axes during synapsis, so that in pachytene spermatocytes HORMAD1 and 2 only remain on the unsynapsed arms of the sex chromosomes (Wojtasz et al., 2009), similarly to other components of the meiotic silencing pathways (e.g. BRCA1). HORMAD1 and HORMAD2 are both required for normal levels of BRCA1 and ATR at unsynapsed axes (Daniel et al., 2011; Wojtasz et al., 2012). However, unlike *Brca1* mutant spermatocytes which fail to localise ATR to unsynapsed chromatin, ATR signal in *Hormad2*$^{-/-}$ spermatocytes is restricted to foci along the axes, largely colocalising with markers of DSBs (Wojtasz et al., 2012). Correspondingly, HORMAD1 and HORMAD2 are both required for MSCI (Daniel et al., 2011; Wojtasz et al., 2012). This demonstrates the existence of distinct DNA damage- and asynapsis-related ATR recruitment mechanisms (Wojtasz et al., 2012). ATR and BRCA1 colocalise at these DSB-associated foci in *Hormad2*$^{-/-}$ suggesting that the initial recruitment of ATR at these sites relies on BRCA1 (Wojtasz et al., 2012). The HORMAD proteins are therefore proposed to promote the recruitment of ATR to asynapsed chromosome axes and an asynapsis-sensitive checkpoint, but not the recruitment of ATR to sites of DNA damage. In support of this model, deletion of HORMAD2 promotes survival of *Spo11*$^{-/-}$ oocytes, but not *Dmc1*$^{-/-}$ oocytes which contain asynapsed axes without and with abundant unrepaired DSBs respectively (Wojtasz et al., 2012).

In addition to phosphorylated H2AX several other histone modifications are also associated with MSCI. Histones H3 and H4 undergo deacetylation at the sex body (Khalil et al., 2004). The addition of acetyl groups to lysine residues neutralises the positive charge in histone tails, weakening the interactions between histones and DNA, and increasing DNA

accessibility, decompaction, and often transcriptional activity (Bannister and Kouzarides, 2011; Musselman et al., 2012; Zentner and Henikoff, 2013). Therefore the deacetylation of XY chromatin is consistent with transcriptional silencing. The mono-ubiquitination of histone H2A (UbH2A) is also observed at the sex body and unsynapsed autosomal arms (Baarends et al., 2005). The localisation of UbH2A on meiotic chromosomes is dependent on ATR (Royo et al., 2013) and consistent with this, its spread to XY chromatin requires MDC1 (Ichijima et al., 2011). The role for UbH2A at the sex body however is unclear, as it is not required for MSCI (Lu et al., 2010).

In summary a secondary wave of H2AX phosphorylation at unsynapsed chromosomes by the ATR kinase appears to cause MSUC/MSCI. ATR relies on BRCA1 for recruitment to DSBs and unsynapsed axes, as well as the HORMAD proteins for recruitment specifically to unynapsed chromatin. The establishment of MSUC on unsynapsed autosomes sequesters factors involved in transcriptional silencing from the sex chromosomes, impairing MSCI and resulting in toxic expression of XY transcripts which trigger meiotic arrest in asynapsed spermatocytes.

1.6.3 DNA Damage Pachytene Checkpoint

In addition to pachytene arrest due to failed MSCI in spermatocytes, DNA damage also appears to trigger meiotic arrest by a distinct mechanism in pachytene (Li and Schimenti, 2007). The majority of mutant spermatocytes with persistent high levels of DNA damage in pachytene typically also display failed chromosome synapsis and as such trigger the MSCI-dependent pachytene checkpoint. In contrast, *Trip13*$^{mod/mod}$ spermatocytes achieve complete synapsis but are unable to repair numerous DSBs (Li and Schimenti, 2007; Roig et al., 2010). These spermatocytes appear to undergo MSCI successfully and also recruit MLH1 in the majority of pachytene cells (Roig et al., 2010), a feature of late pachytene not reported in mutants with MSCI-related arrest. Progression of these spermatocytes to diplotene however is greatly reduced and most spermatocytes are thought to undergo meiotic arrest in pachytene. A similar DNA damage checkpoint sensitive to endogenous unrepaired DNA damage and exogenous damage has also been identified in oocytes. This checkpoint in oocytes is dependent on checkpoint kinase 2 (CHK2) signalling to p63 and p53. Arrest in oocytes can be averted by *Chk2* mutation or combined deletion of *p63* and heterozygous deletion of *p53* (Bolcun-Filas et al., 2014). However *Chk2* or *p53* mutations were not found to rescue the arrest of spermatocytes with persistent DNA damage but complete chromosome

synapsis, indicating that the mechanism of the meiotic DNA damage checkpoint in males is different from that in females.

1.7 Role of Genome Defence Genes in Gametogenesis

One group of genes required for mammalian meiosis are those involved in germline genome defence (Crichton et al., 2013). These genes are involved in silencing retrotransposons however the mechanistic basis for their meiotic requirement is poorly understood.

1.7.1 Introduction to Retrotransposons

Retrotransposons are a highly abundant form of repetitive element, composing around 40% of the sequenced mammalian genome (Lander et al., 2001; Mouse Genome Sequencing Consortium et al., 2002). Retrotransposons are a major driver of genetic alteration and as such contribute greatly to evolution as well as pathogenic genomic instability. Retrotransposons can generate new mutations by retrotransposition into pre-existing genetic information in the host genome, and their repetitive nature promotes their involvement in recombination-mediated chromosomal deletions and rearrangements capable of influencing the expression of nearby genes (Romanish et al., 2010). The mammalian genome contains three main classes of retrotransposon: long interspersed nuclear elements (LINEs), short interspersed nuclear elements (SINEs) and long terminal repeat (LTR) retrotransposons, each of which possess distinct properties.

LINE-1 is the major family of LINE retrotransposons in mammals and accounts for ~17% of the sequenced genome. LINE-1 encodes two proteins: ORF1 encodes a nucleic acid binding protein with chaperone activity, and ORF2 encodes an endonuclease and reverse transcriptase. Both of these proteins are required for LINE-1 retrotransposition. SINEs account for ~10% of the sequenced genome and are non-autonomous elements, relying on LINE-1-encoded proteins for their retrotransposition. LTRs, also known as endogenous retroviruses (ERVs), possess a typical retroviral structure, with protein coding *gag*, *pol*, *pro* and occasionally *env* genes, flanked by long terminal repeats which act as promoters. There are approximately 150 different types of ERV, together composing around 9% of the human and mouse genomes. Similar to LINE elements, LTRs are often autonomous, relying on their encoded proteins for retrotransposition (Crichton et al., 2013; Ollinger et al., 2010).

For retrotransposon propagation to be successful, and for genomic rearrangements to have maximal impact, retrotransposition events must take place in the developing germline and hence become transmitted to every copy of the offspring's genome. As such, hosts have developed mechanisms for silencing retrotransposon activity in the germline, acting at both transcriptional and post-transcriptional levels, to maximise the integrity of the parental genome transmitted. Surprisingly, mutant mice that de-repress retrotransposons in the germline often also have problems progressing through meiosis (Crichton et al., 2013).

1.7.2 DNA methylation and transcriptional silencing

DNA methylation, which primarily occurs at cytosine residues of CpG dinucleotides, is one of the most abundant chromatin modifications present in mammalian genomes (Cedar and Bergman, 2012; Deaton and Bird, 2011; Reddington et al., 2013). DNA methylation at gene promoters is associated with transcriptional repression, although this association is affected by the density of CpG dinucleotides. Promoters with a high density of CpGs tend to be unmethylated and transcriptionally active, while promoters with a low density of CpGs are typically methylated regardless of whether they are transcriptionally active or not. The main class of promoters where methylation is associated with transcription have an intermediate density of CpGs and tend to be methylated and repressed in a tissue-specific manner (Meissner et al., 2008; Weber et al., 2007). DNA methylation could potentially act to repress transcription by recruiting 5-methylcytosine (5mC) reader proteins (Hendrich and Bird, 1998; Lewis et al., 1992; Prokhortchouk et al., 2001) or by directly obstructing the binding of transcription factors to the DNA (Wiench et al., 2011). In general, DNA methylation is recruited to promoters that have already been silenced by other mechanisms, and acts as a secondary modification to stabilise the repressed state (Deaton and Bird, 2011). However, a small group of genes have been identified that appear to use DNA methylation as a primary mechanism to silence expression (Hackett et al., 2012). During their migration to the developing gonad primordial gem cells initiate a phase of global demethylation that activates the expression of many of these methylation-sensitive genes prior to meiotic entry (Figure 1-15) (Hackett et al., 2012; Hajkova et al., 2002; Seki et al., 2005). Genes involved in suppressing retrotransposons are highly enriched within this group of methylation-sensitive genes, and their co-ordinate regulation by DNA methylation might represent a developmental coupling between expression of germline genome defence mechanisms and the potential for retrotransposon activity in multiple hypomethylated cell types (Hackett et al., 2012; Reichmann et al., 2013). This group of genes has been termed germline genome

defence genes (Hackett et al., 2012). Many of these methylation-sensitive germline genome-defence genes are required for progression through meiotic prophase (Figure 1-16) (Crichton et al., 2013). Setting up an appropriate DNA methylation status in the developing germline appears to be a prerequisite to allow appropriate gene expression for progression through meiotic prophase.

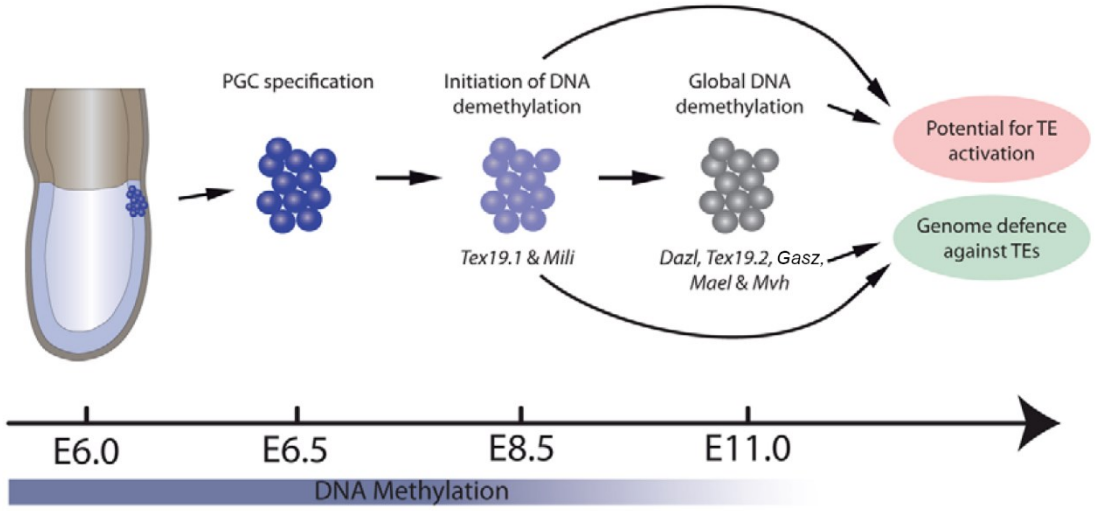

Figure 1-15. Global DNA methylation loss triggers genome-defence gene activation during germline development
At E6.25, PGCs are specified from epiblast cells that have already acquired global de novo methylation. At E8.5, DNA demethylation is initiated in PGCs, activating some 'early' genome defence genes (*Tex19.1* and *Mili*). At E11.5, genome-wide erasure of DNA methylation leads to expression of other genome-defence genes, which can suppress activity of transposable elements (TE) de-regulated by loss of methylation during reprogramming. The coupling of genome-defence genes to potential TE activation through a common regulatory mechanism, DNA methylation, ensures that genomic integrity is maintained during erasure of DNA methylation in the germline. Copied from Hackett et al., 2012.

1.7.3 De novo DNA methylation

Following global erasure of DNA methylation in developing germ cells, new methylation marks are established, at least some of which are sex-specific (imprinted genes). Timing of *de novo* methylation differs dramatically between spermatogenesis and oogenesis: *de novo* methylation in male germ cells occurs in late foetal development, long before meiosis is initiated; whereas in females *de novo* methylation occurs during postnatal oocyte growth while the oocyte is arrested in the dictyate stage of meiotic prophase (Figure 1-15). Thus the global level of DNA methylation during early meiotic prophase differs with gender (Crichton et al., 2014; Smallwood and Kelsey, 2012).

De novo methylation marks are written onto DNA by the DNA methyltransferases DNMT3A and DNMT3B, which have partially overlapping target loci (Kaneda et al., 2004; Kato et al., 2007; Okano et al., 1999). Although mutations in either *Dnmt3a* or *Dnmt3b* result in hypomethylation at specific imprinted genes and/or repetitive sequences in spermatocytes and oocytes, these defects do not impair progression through meiosis (Kaneda et al., 2004; Kato et al., 2007; Yaman and Grandjean, 2006). DNMT3A and DNMT3B both interact with the partially homologous but catalytically dead protein, DNMT3L (Hata et al., 2002), which stimulates their activity (Suetake et al., 2004). *Dnmt3l* is highly expressed in embryonic gonocytes (peaking at E15.5) (La Salle et al., 2007). The absence of DNMT3L results in reduced *de novo* DNA methylation at redundant target loci unaffected by the absence of DNMT3A or DNMT3B alone, including *LINE-1* and the abundant LTR retrotransposon *IAP* (Intracisternal A Partical) in prospermatogonia (Bourc'his and Bestor, 2004). Expression of *LINE-1* and *IAP* is greatly increased in prospermatogonia in male *Dnmt3l*$^{-/-}$ mice, meiotic entry is delayed, and meiotic progression is abnormal. The *Dnmt3l*$^{-/-}$ spermatocytes are defective in synaptonemal complex formation, with widespread asynapsis and non-homologous synapsis resulting in failure to progress to pachytene (Bourc'his and Bestor, 2004). Early recombination proteins RAD51 and RPA successfully localise to chromosome axes in *Dnmt3l*$^{-/-}$ spermatocytes, indicating that the synapsis defects are not the result of failure to initiate meiotic recombination (Mahadevaiah et al., 2008). Rather, asynapsis in *Dnmt3l*$^{-/-}$ spermatocytes appears to represent the impaired ability of meiotic chromosomes to successfully search for or recognise their homologous partner. The meiotic arrest of the *Dnmt3l*$^{-/-}$ spermatocytes is due to impaired MSCI as a result of the chromosome asynapsis discussed (Mahadevaiah et al., 2008).

A number of other mouse mutants with DNA methylation defects also suffer defective chromosome synapsis and meiotic prophase arrest in spermatocytes. These include mutations in *Lsh*, a putative accessory factor for *de novo* DNA methyltransferases, and *Miwi2*, a piRNA-binding protein required for *de novo* DNA methylation in the male germline (Carmell et al., 2007; Myant and Stancheva, 2008; Zeng et al., 2011). Therefore the meiotic progression defects in *Dnmt3l*$^{-/-}$ spermatocytes appear likely to be due to altered DNA methylation. The changes in DNA methylation in *Dnmt3l*$^{-/-}$ spermatocytes are also associated with some changes in histone modifications. Global levels of histone H4 acetylation and histone H3 acetylation, which are associated with active chromatin, normally decrease during early meiotic prophase in wild-type spermatocytes. However, this decrease is delayed in *Dnmt3l*$^{-/-}$ spermatocytes with levels of acetylated H3 and H4 remaining high in zygotene (Webster et al., 2005). The opposite change was observed in H3K9me2, a

modification associated with transcriptional repression, which is globally reduced in zygotene *Dnmt3l*$^{-/-}$ spermatocytes (Webster et al., 2005). Together these changes in histone modifications indicate that globally there is more decompacted, transcriptionally active or permissive chromatin present in zygotene *Dnmt3l*$^{-/-}$ spermatocytes. It is not currently clear whether the chromosome asynapsis and meiotic arrest of *Dnmt3l*$^{-/-}$ spermatocytes is the result of transcriptional de-repression of retrotransposons, aberrant regulation of meiotic gene expression, or changes in chromatin structure perturbing homologous chromosome synapsis (Crichton et al., 2013).

In contrast to spermatocytes, DNMT3L does not function until after recombination and synapsis is complete in oocytes, and is not required for these meiotic events (Bourc'his et al., 2001; La Salle et al., 2004). Although oocytes are globally hypomethylated compared to spermatocytes while they progress through early meiotic prophase, the DNA methylation that is present in meiotic oocytes does seem to play an important role in allowing meiotic prophase to proceed normally. *Lsh* is required for DNA methylation at repetitive elements and some single copy genes during development (Dennis et al., 2001; Sun et al., 2004). DNA methylation is reduced at *IAP* retrotransposon sequences in *Lsh*$^{-/-}$ oocytes, and *IAP* expression is greatly increased in *Lsh*$^{-/-}$ ovaries (De La Fuente et al., 2006). *Lsh*$^{-/-}$ oocytes successfully recruit the early recombination protein RAD51 to chromosome axes indicating normal initiation of recombination, but synapsis of homologous chromosomes is defective (De La Fuente et al., 2006), reminiscent of *Dnmt3l*$^{-/-}$ spermatocytes. Therefore it appears that DNA methylation is required for successful chromosome synapsis in oocyte prophase, and reducing DNA methylation levels is associated with defects in chromosome synapsis during meiosis in male and female germ cells.

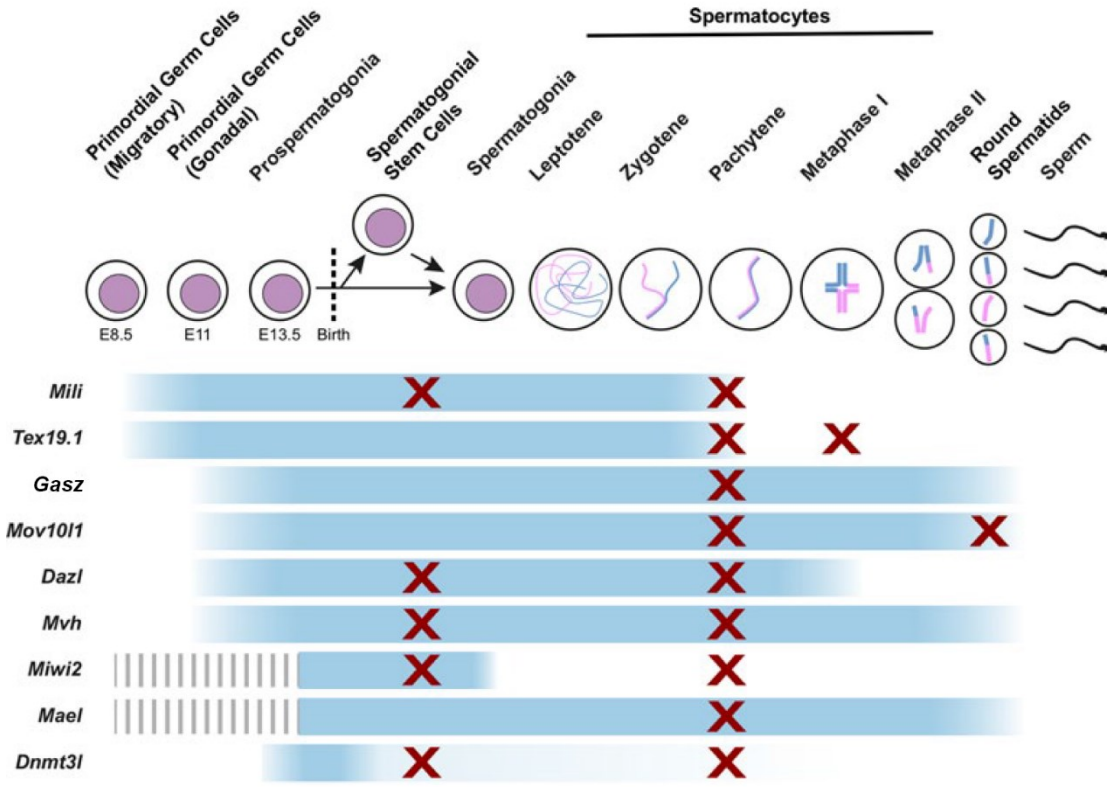

Figure 1-16. Expression patterns and mutant phenotypes of germline genome defence genes
Expression patterns of each germline genome defence gene during spermatogenesis are indicated by blue bars, with colour intensity corresponding to level of expression. Dashed grey lines indicate expression profiles which have not yet been studied. Red crosses indicate stages at which defects in progression through spermatogenesis arise. Figure from Crichton et al., 2013.

1.7.4 The piRNA retrotransposon silencing pathway

Since DNA methylation plays a key role in the transcriptional suppression of retrotransposon transcription, the global removal of DNA methylation during germline development offers a potentially vulnerable window of opportunity for the reactivation of retrotransposons. The piRNA pathway acts in part to redirect *de novo* DNA methylation to retrotransposon sequences (Crichton et al., 2013) and has a highly conserved role in preserving fertility (Cox et al., 1998). The piRNA pathway is executed by Argonaute proteins of the PIWI clade and populations of small PIWI-interacting RNAs (piRNAs). These proteins contain RNA-binding and RNaseH-like endonuclease domains (Hutvagner and Simard, 2008). Mouse homologs of PIWI include MILI, MIWI and MIWI2. The mouse PIWI proteins are largely restricted to the germline but display distinct temporal expression patterns. *Mili* is expressed from E9.5 during epigenetic reprogramming in migratory primordial germ cells, and *Miwi2*

is expressed in late foetal germ cells (Figure 1-16), hence both are present during the de novo methylation of retrotransposon sequences (Aravin et al., 2008; Hackett et al., 2012; Kuramochi-Miyagawa et al., 2001). Expression of *Mili* continues after birth, until the round spermatid stage in males and is still present in growing oocytes in females. *Miwi2* however is exclusive to male germ cells and expression ceases before meiosis (Figure 1-16) (Aravin et al., 2008). The expression of *Miwi* does not begin until pachytene and appears to substantially differ in function to the other PIWI homologues (Deng and Lin, 2002).

Miwi2 and *Mili* are both required for normal levels of piRNAs and DNA methylation of *LINE-1* and *IAP* regulatory regions (Kuramochi-Miyagawa et al., 2008), with mutation resulting in hypomethylation and corresponding upregulated expression of retrotransposons (Aravin et al., 2007; Carmell et al., 2007; Kuramochi-Miyagawa et al., 2008). MILI and MIWI2 are thought to cooperate in early germline development to amplify piRNA sequences through the "ping-pong amplification cycle", with MILI initially guiding the cleavage of mRNA complementary to an antisense guide piRNA sequence to produce a sense piRNA. These are then recognised by MIWI2 to guide cleavage of transcripts from piRNA clusters, subsequently feeding back into the system (Figure 1-17) (Aravin et al., 2008). The putative endonuclease activity of MILI is required for the amplification of retrotransposon piRNAs in foetal prospermatogonia and *de novo* methylation and transcriptional silencing of *LINE-1* but not *IAP* sequences. In contrast, MIWI2 endonuclease activity is dispensable for piRNA amplification (De Fazio et al., 2011). MIWI2 has been proposed to function in the piRNA pathway by translocation to the nucleus when bound to piRNA, these subsequently act as a guide to actively transcribing retrotransposons (Figure 1-17) (Aravin et al., 2008). The piRNA pathway targets transcriptional silencing of transposable elements in foetal gametogenesis by *de novo* DNA methylation (Kuramochi-Miyagawa et al., 2008), however a physical connection between the piRNA pathway components and the DNA methyltransferases has yet to be identified.

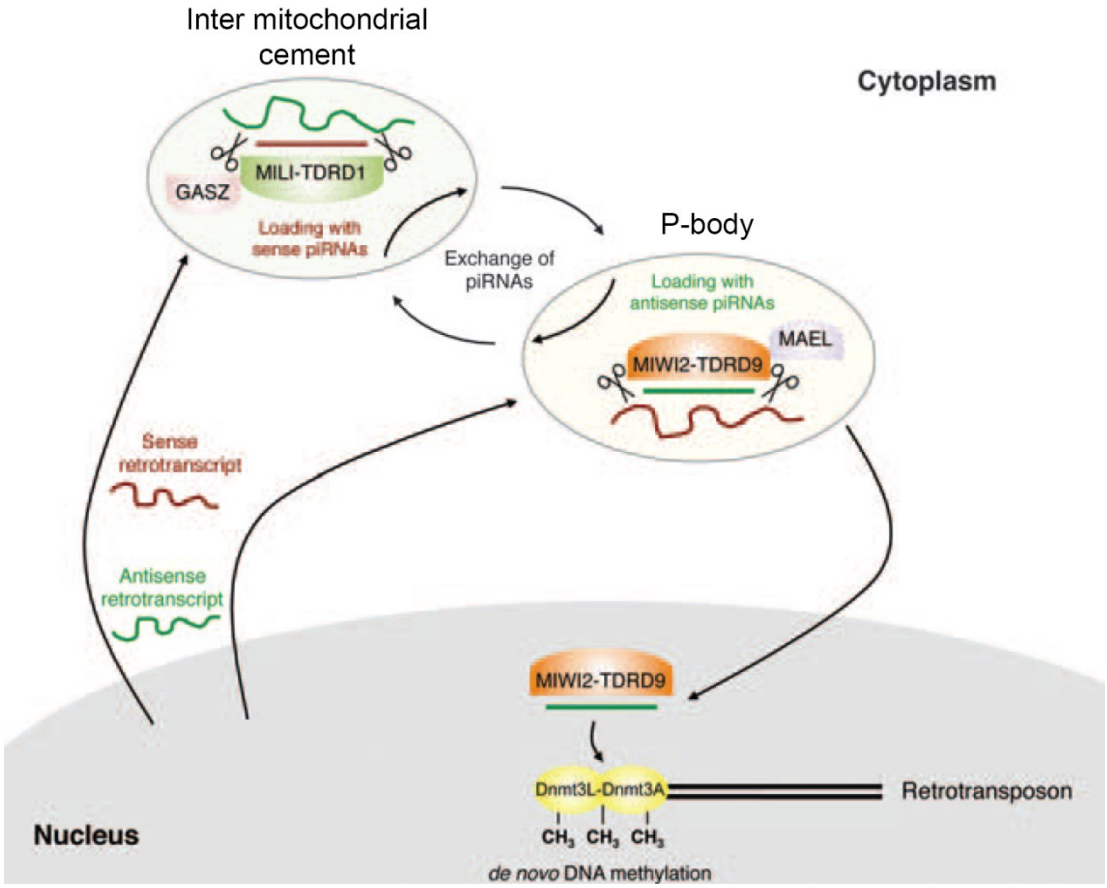

Figure 1-17. The piRNA pathway
Sense (red) and antisense (green) retrotranscripts produced from nuclear retrotransposon expression are cleaved into sense and anti-sense piRNAs respectively. Sense piRNAs associate with MILI-TDRD1 complexes in intermitochondrial cement with GASZ. Antisense piRNAs associate with MIWI2-TDRD9 complexes and localise to P-bodies with MAEL. piRNAs are used as templates to target complementary retrotranscripts which are subsequently cleaved and exchanged between the intermitochondrial cement and P-body to amplify piRNA production by the "ping-pong amplification cycle". MIWI2-TDRD9 also shuttle with associated antisense piRNAs back to the nucleus where they appear to direct de novo methylation of retrotransposons. Model modified from Zamudio and Bourc'his, 2010. (Zamudio and Bourc'his, 2010)

Mili$^{-/-}$ testes suffer reduced self-renewal of germline stem cells (Unhavaithaya et al., 2009) and the few germ cells which progress to meiosis arrest in pachytene (Figure 1-16). In the absence of MILI, MIWI2 relocalises from the nucleus and cytoplasmic granules, to become diffusely cytoplasmic (Aravin et al., 2008). Meiotic chromosome asynapsis and pachytene spermatocyte arrest is also seen in *Miwi2*$^{-/-}$ (Carmell et al., 2007). In addition to MILI, MIWI2 is also proposed to play role in maintenance of germline stem cells. This process is not initially defective in *Miwi2*$^{-/-}$ during the first round of spermatogenesis, but by 3months *Miwi2*$^{-/-}$ testes are frequently depleted of all germ cells and left with only somatic sertoli cells (Carmell et al., 2007). While both *Mili* and *Miwi2* male mutants display

defective germline stem cell maintenance and meiotic arrest at pachytene, *Mili*$^{-/-}$ female mice are fertile (Kuramochi-Miyagawa et al., 2004), once again highlighting the sexually dimorphic nature of germline genome defence.

Curiously, despite the meiotic phenotype of *Miwi2*$^{-/-}$ mutant mice, expression of *Miwi2* decreases significantly after birth and is not detected beyond 4dpp (Aravin et al., 2008), a week before meiosis begins. Conditional deletion of *Miwi2* at p5 does not cause infertility, consistent with a requirement for the pre-meiotic activity of MIWI2 to successfully complete meiosis (Bao et al., 2014). Conditional deletion of *Miwi2* at E13.5 phenocopies *Miwi2*$^{-/-}$ mice. Immunostaining of P7 testes revealed elevated levels LINE-1 ORF1 and IAP protein as well as γH2AX in pro-spermatogonial or spermatogonial stages, possibly indicating retrotransposition-related DNA damage (Bao et al., 2014). Additionally, changes in meiotic histone modification dynamics were observed, with H3K4me3 levels dropping considerably in early prophase and H3K27me3 barely detectable in similar stages in the mutant. It is not currently clear whether these changes in histone modification are primary defects due to *Miwi2* deletion or secondary defects possibly due to reduced DNA methylation and/or retrotransposon de-repression, and the consequences of these changes are also currently unknown. Together this data shows that defective embryonic function of the piRNA pathway also has severe repercussions for the regulation of retrotransposons at later stages of germ cell development and the organisation of chromatin in meiosis.

MILI and MIWI2 are thought to occupy different subcellular compartments during *de novo* DNA methylation: MILI in germ granules in the intermitochondrial cement, a form of electron-dense cytoplasmic structures termed “nuage”, typically associated with mitochondria, with other proteins including TDRD1, while MIWI2 is cytoplasmic granules known as processing bodies (P-bodies) reported to be involved in RNA degradation and translational control (Figure 1-17) (Aravin et al., 2009; Shoji et al., 2009). In addition to MILI and MIWI2, the piRNA pathway also relies on several cofactors, many of which localise to and/or organise these cellular structures. Tudor domain containing proteins interact with PIWI proteins (Chen et al., 2009; Mathioudakis et al., 2012; Vagin et al., 2009), co-localise with piRNAs and PIWI proteins in nuage and are required for the formation of these cytoplasmic structures (Figure 1-17) (Chuma et al., 2003; Shoji et al., 2009; Yabuta et al., 2011). These interactions appear to be crucial for piRNA pathway function as TDRD1, TDRD5 and TDRD9 are all required for normal *LINE-1* methylation as well as *LINE-1* silencing (Chuma et al., 2006; Reuter et al., 2009; Shoji et al., 2009; Yabuta et al., 2011). The absence of these TUDOR proteins has a more modest effect on *IAP* expression,

supporting distinctions between the regulation of this element and *LINE-1* (Aravin et al., 2009; Reuter et al., 2009; Shoji et al., 2009). Similarly to the other germline genome defence genes, these TUDOR proteins are required for male mouse fertility, with deletion typically causing a meiotic arrest in pachytene (Chuma et al., 2003; Shoji et al., 2009). However, although some *Tdrd5*$^{-/-}$ spermatocytes arrest in pachytene others progress to the round spermatid stage before arresting, indicating that TRDR5 is not absolutely essential for completion of meiotic prophase (Yabuta et al., 2011).

Maelstrom (MAEL) is also present at the nuage during early meiotic prophase as well as the chromatoid body in round spermatids (Figure 1-17**)** (Costa et al., 2006; Soper et al., 2008). Little is known about the biochemical function of MAEL other than that it possesses a domain with weak similarity to a high-mobility group (HMG) box DNA-binding domain (Costa et al., 2006). Similarly to other piRNA pathway members, MAEL is required for *LINE-1* and *IAP* suppression in testes and mutant males suffer defective chromosome synapsis, with spermatocytes arresting in pachytene (Figure 1-16). MAEL is not needed for piRNA biogenesis but is proposed to function by shuttling MIWI2-piRNA complexes between the nucleus and the nuage, similar to its role in *Drosophila* (Findley et al., 2003). *Mael*$^{-/-}$ spermatocytes appear to show indications of retrotransposition-related DNA damage being generated in prophase. LINE-1 ORF1 protein and DNA damage markers RAD51 and γH2AX are greatly elevated in *Mael*$^{-/-}$*Spo11*$^{-/-}$ when compared to *Spo11*$^{-/-}$ which lack endogenously generated meiotic DSBs, thereby revealing large amounts of SPO11-independent DNA damage associated with elevated retrotransposon protein levels (Soper et al., 2008).

The piRNA pathway is also dependent on a number of additional factors. Mouse vasa homologue (MVH) is an evolutionarily conserved helicase essential for germ cell development (Tanaka et al., 2000). MVH localises to the intermitochondrial cement and is required for the formation of this structure and hence the localisation of MILI and TDRD1. Furthermore MIWI2 fails to localise to P-bodies in *Mvh*$^{-/-}$ despite their formation. Mutant testes are defective in the production of MIWI2-associated secondary pi-RNAs, indicating a failure of ping-pong piRNA amplification and vital role for MVH in promoting this process despite not interacting with MILI or MIWI2 directly (Kuramochi-Miyagawa et al., 2010). GASZ (Germ cell-specific protein with four Ankyrin repeats, a Sterile alpha motif, and a basic leucine Zipper domain) which colocalises with MILI in the intermitochondrial cement from foetal germ cell stages through to round spermatids (Figure 1-17). In the absence of GASZ, levels of the intermitochondrial cement-associated piRNA proteins MILI, MVH,

MAEL and TDRD1 are greatly depleted and the intermitochondrial cement fails to form, revealing a vital role for GASZ in promoting the stability of these proteins (Ma et al., 2009). MILI, MIWI2 and MIWI all interact with the putative RNA helicase MOV10L1 (Frost et al., 2010; Zheng et al., 2010), and appear to interact while bound to piRNAs (Zheng et al., 2010). MOV10l1 is required for the normal amplification of ~26-28nt RNAs as well as *LINE-1* and *IAP* transcriptional silencing (Zheng et al., 2010) suggesting a vital role for MOV10L1 in piRNA biogenesis. Consistent with the piRNA-pathway related defects incurred in the absence of MVH, GASZ and MOV10L1, their mutant male reproductive phenotypes largely phenocopy those of *Mili*$^{-/-}$ and *Miwi2*$^{-/-}$, with failed retrotransposon silencing and meiotic arrest in pachytene (Figure 1-16) (Frost et al., 2010; Kuramochi-Miyagawa et al., 2010; Ma et al., 2009; Tanaka et al., 2000; Zheng et al., 2010).

Mili, *Gasz*, and *Mov10l1*, together with *Dazl* and *Tex19.1* belong to a group of genes transcriptionally silenced solely by DNA methylation and expressed during germline development in response to global DNA hypomethylation (Figure 1-15) (Hackett et al., 2012). These genes share common roles in repressing retrotransposons during male germline development. DAZL is an RNA binding protein essential for fertility in both male and female mice (Ruggiu et al., 1997), involved in promoting the expression of both *Mvh* and *Tex19.1* (Chen et al., 2011; Reynolds et al., 2005), a further germline genome defence gene which will be discussed shortly. Spermatogonial differentiation is greatly impaired in *Dazl*$^{-/-}$ testis, however a small proportion of germ cells do progress to meiosis before finally arresting at pachytene (Figure 1-16) (Schrans-Stassen et al., 2001). The misregulation of *Tex19.1* and *Mvh* is likely to be at least partially responsible for the male fertility defects incurred by *Dazl* mutation.

Although retrotransposon activity is transcriptionally repressed, retrotransposon RNAs are readily detectable in germ cells and pluripotent cells of wild type mice. However, transcript abundance does not always correlate with protein abundance, indicating the additional action of translation regulatory mechanisms, or the expression of sub-populations of elements with varying protein-coding capacities. Indeed, components of the piRNA pathway have been implicated in translational regulation in addition to their role in the DNA methylation. The Tudor domain-containing protein TDRD7 plays a role in translational regulation of LINE-1 in male germ cells (Tanaka et al., 2011), and the PIWI proteins MILI and MIWI physically associate with actively translating mRNAs in polysomes and are implicated in the control of this process (Grivna et al., 2006; Unhavaithaya et al., 2009).

1.7.5 TEX19.1 in germline genome defence

TEX19.1 (testis expressed gene 19.1) is a cytoplasmic protein crucial for male mouse fertility. The localisation of TEX19.1 protein is distinct from the intermitochondrial cement and hence the piRNA pathway. *Tex19.1* expression is initiated following germline DNA demethylation, transcript levels decrease as cells progress through meiosis, and are no longer apparent beyond early prophase (Figure 1-15, Figure 1-16) (Ollinger et al., 2008). Expression analysis of 16dpp *Tex19.1*$^{-/-}$ testes, before cell death in pachytene, has revealed limited changes in transcription largely restricted to upregulation of the LTR-retrotransposon *MMERVK10C* (Ollinger et al., 2008; Reichmann et al., 2012). Upregulated expression of this endogenous retrovirus is seen during meiosis in *Tex19.1*$^{-/-}$ testes. Similarly to other germline genome defence mutants, homologous chromosomes often fail to synapse in pachytene and spermatocytes arrest at this stage (Figure 1-16). However, unlike other germline genome defence mutants approximately half of pachytene nuclei synapse normally. 66% of nuclei subsequently progressing to metaphase I possess at least one pair of univalent chromosomes lacking a chiasma. Finally, sperm count is reduced to just 1% (Ollinger et al., 2008). Although retrotransposon upregulation, chromosome asynapsis and cell death in meiotic prophase is a feature shared by *Tex19.1*$^{-/-}$ and the other germline genome defence mutants, the mechanism by which TEX19.1 achieves retrotransposon silencing in the germline appears distinct. TEX19.1 is known to be stabilised by the E3 ubiquitin ligase UBR2 (Yang et al., 2010), but no piRNA pathway components have been connected to TEX19.1 or UBR2, and changes in *LINE-1* or *IAP* expression have not been found in *Tex19.1*$^{-/-}$ testes. Furthermore, *Tex19.1*$^{-/-}$ female mice also feature reduced fertility (Ollinger et al., 2008) suggesting that unlike many germline genome defence genes, at least some of the functions of TEX19.1 required for male fertility are also required in females.

1.7.6 How does retrotransposon activity cause infertility in males?

As all germline genome defence genes studied are essential for male mouse fertility it appears likely that the upregulated germline expression of retrotransposons shared by male mice with mutations in these genes has fatal implications for germ cells. The mutation of *Dnmt3l*, *Mili*, *Miwi2*, or *Mvh* causes defects in the renewal of germline stem cells suggesting that shared sites of resulting hypomethylation may be responsible for this aspect of their phenotype. This defect is not however a feature of all germline genome defence mutants, rather, these mutants commonly trigger meiotic arrest in male pachytene spermatocytes with

chromosome asynapsis where this has been studied (Crichton et al., 2013). The timing of this arrest is somewhat surprising given the large period following the initial activation of these genes in wild type mice: typically around three weeks. Indeed in the case of *Miwi2* expression ceases shortly after birth, hence the defects acquired must persist through several mitotic divisions before triggering arrest in meiosis. It is not currently clear how the disruption to germline genome defence would lead to the arrest observed.

The additional SPO11-independent DNA damage identified in *Mael*$^{-/-}$ spermatocytes is an indication of meiotic retrotransposition not yet demonstrated in other germline genome defence mutants (Soper et al., 2008). As previously discussed, the location and frequency of meiotic DSBs is of importance to ensure the success of the meiotic homology search central to chromosome synapsis, and excessive DSBs or misplacement of DSBs appears to be capable of compromising the homology search resulting in chromosome asynapsis (Brick et al., 2012; Lange et al., 2011). Therefore one possible mechanism by which retrotransposon expression could perturb meiotic progression is by retrotransposition events generating DNA damage which disrupts the meiotic homology search. Alternative explanations for the infertility incurred include alterations to gene expression caused by epigenetic changes or retrotransposition, and illegitimate interactions between repeat sequences unmasked by demethylation (Bourc'his and Bestor, 2004). Changes in expression and repeat demethylation are major features of most germline genome defence mutants. Data supporting this theory however is limited.

The meiotic disruption caused by the loss of TEX19.1 is of particular interest as unlike other genome defence genes it has currently been shown to cause upregulated expression apparently limited to a single low copy retrotransposon in the germline (Ollinger et al., 2008) and TEX19.1 has not been implicated in the piRNA pathway (Ollinger et al., 2008). Therefore the major features shared between *Tex19.1*$^{-/-}$ germ cells and those of other germline genome defence mutants are upregulated retrotransposon expression, chromosome asynapsis and pachytene-stage meiotic arrest. Better understanding the meiotic defects which arise in *Tex19.1*$^{-/-}$ spermatocytes may help to reveal a shared mechanism of meiotic perturbation encountered by germline genome defence mutants.

1.8 TEX19.1 and UBR2

Tex19.1 is a mammal-specific gene containing two conserved but undefined domains. In addition to the expression of *Tex19.1* in the male germ line, the gene is also expressed in embryonic stem cells (ESCs) (Kuntz et al., 2008) and the hypomethylated trophectoderm cells of the placenta (Celebi et al., 2012; Reichmann et al., 2013). TEX19.1 is essential for normal placenta development (Reichmann et al., 2013; Tarabay et al., 2013) but dispensable for ESC survival (Tarabay et al., 2013), and mutant placentas exhibit an upregulation of *LINE-1* expression (Reichmann et al., 2013). The *Tex19* gene has undergone duplication in rats and mice, to generate the a second paralog in addition to *Tex19.1*: *Tex19.2* (Kuntz et al., 2008). The pattern of *Tex19.2* expression shares some overlap with *Tex19.1* in the developing germline until E16.5, unlike *Tex19.1* from E18.5 until soon after birth *Tex19.2* is restricted to somatic cells of the male gonad (Celebi et al., 2012; Kuntz et al., 2008). These paralogs are later co-expressed in pachytene spermatocytes of adult testes (Celebi et al., 2012). Therefore it is possible that TEX19.2 could partially compensate for the absence of TEX19.1 in male germ line development.

The mechanism by which TEX19.1 represses retrotransposons is currently not known, but it is possible that the protein's strong interaction with UBR2 in the testes is involved (Yang et al., 2010). UBR2 is an E3 ubiquitin ligase in the N-end rule pathway responsible for the addition of ubiquitin to substrates (Kwon et al., 2003). Ubiquitination requires the sequential action of three enzymes, E1-activating, E2-conjugating and E3-ligating enzymes (Bannister and Kouzarides, 2011). UBR2 does not ubiquitinate TEX19.1, but rather is required for TEX19.1 protein stability (Yang et al., 2010). Hence it is possible that this interaction influences UBR2 targeting or activity.

Ubiquitin is a relatively large 76-amino acid modification that can be targeted to lysine residues in histone tails. Ubiquitination can involve the addition of an individual ubiquitin residue (mono-ubiquitination) which often influence protein function or creates binding sites for interactions, or the formation of polymeric ubiquitin chains (poly-ubiquitination) which commonly target proteins for degradation (Komander and Rape, 2012). Mono-ubiquitination of histones H2A and H2B at lysine 119 and 120 respectively has been widely studied in mitosis in association with transcriptional regulation and DNA damage response (Braun and Madhani, 2012; Cao and Yan, 2012). UbH2B levels are very low in spermatocytes (Baarends et al., 2007) and the localisation pattern has not been reported. In contrast, UbH2A levels are readily detectable in meiosis, and localise to asynapsed axes in both spermatocytes and oocytes, consistent with a role in MSUC. As

previously mentioned, UbH2A is also enriched at the sex body in pachytene spermatocytes, consistent with a role in MSCI (Baarends et al., 2005; Kouznetsova et al., 2009).

UBR2 localises to meiotic chromosomes, particularly to portions of unsynapsed chromosome axes during male meiotic prophase, colocalising with patterns of UbH2A and other sites of nuclear ubiquitination (An et al., 2010, 2012), consistent with involvement in ubiquitination during this stage. This localisation pattern has led to proposed roles in MSUC-related ubiquitination. In the absence of UBR2 male mice are infertile, with meiosis arresting at pachytene and some nuclei failing to synapse homologous chromosomes, while female *Ubr2*$^{-/-}$ mice are frequently non-viable (An et al., 2010, 2012; Kwon et al., 2003). Reduced frequency of female offspring is also a feature of *Tex19.1*$^{-/-}$ mice (Ollinger et al., 2008). It has been proposed that the male meiotic arrest in *Ubr2*$^{-/-}$ is the result of failed MSCI, indeed *Ubr2*$^{-/-}$ spermatocytes do not display UbH2A at the sex body and appear to display an increase in XY transcripts in P16 testes (An et al., 2010, 2012). However, reanalysis of gene expression data from WT and *Ubr2*$^{-/-}$ testes suggests expression changes reported could be the result of a meiotic arrest altering the maturity of the cell populations being assessed, therefore not necessarily reflecting failed MSCI (Mulugeta Achame et al., 2010). Despite its association with transcriptional repression, the role of UbH2A on asynapsed chromosomal axes and XY chromatin is not clear and as the sex body forms normally and spermatocytes complete meiosis in *Rnf8*$^{-/-}$ mutant mice which also lack UbH2A at the sex body (Lu et al., 2010). UbH2A at the sex body therefore does not appear to be required for MSCI and functions of UBR2 in addition to H2A ubiquitination at this location are likely responsible for the meiotic arrest of *Ubr2*$^{-/-}$ spermatocytes.

The distribution of ubiquitin residues (mono- or poly-ubiquitin) in spermatocytes has been assessed cytologically, providing insight into the localisation of ubiquitinated proteins in these cells. These residues become apparent in early zygotene before localising to unsynapsed axes in late zygotene. Ubiquitin is subsequently seen on unsyanpsed XY arms in early pachytene then expands through the sex body in mid-pachytene and is additionally observed across chromatin of the autosomes in late pachytene. Specific assessment of poly-ubiquitin signals revealed their appearance in pachytene, during which they largely mirror the distribution of total ubiquitin signal. These patterns largely colocalise with UBR2, other than in mid-pachytene when UBR2 remains on XY axes not throughout the sex body (An et al., 2012). Therefore UBR2 is broadly associated with ubiquitination in prophase and could be involved in the ubiquitination of numerous meiotic substrates at these locations, with the potential to affect meiotic events.

Polyubiquitin levels are reportedly dramatically reduced in *Ubr2*$^{-/-}$ pachytene spermatocytes, while a moderate reduction in sex body-associated signal are seen for total ubiquitin. Therefore in addition to H2A monoubiquitination, UBR2 is also proposed to maintain polyubiquitinated conjugates in pachytene (An et al., 2012). Furthermore, persistent axial γH2AX signals have been observed in *Ubr2*$^{-/-}$ pachytene indicating unrepaired DNA damage and suggesting a requirement of UBR2 in meiotic recombination (An et al., 2012). Comprehensive identification of UBR2 substrates for ubiquitination still remains to be achieved and the cause of the meiotic arrest in *Ubr2*$^{-/-}$ spermatocytes revealed. The dependence of TEX19.1 stability on UBR2 and similarity between aspects of the mutant phenoptypes of these two genes, such as the defective chromosome synapsis in spermatocytes and reduced mutant female viability, has led to speculation that the mutants may phenocopy one another (An et al., 2012; Yang et al., 2010). Therefore it would be of interest to further investigate the extent of phenotypic similarity between these mutants such as the apparent MSCI and ubiquitination defects which occur among synapsed spermatocytes.

In summary, deletion of *Tex19.1* in male mice is known to cause defects in chromosome synapsis in approximately half of pachytene spermatocytes, univalent chromosomes in two thirds of metaphase I spermatocytes and ultimately infertility (Ollinger et al., 2008). The methyl-sensitive expression of *Tex19.1* during germline development (Hackett et al., 2012) and upregulation of the retrotransposon *MMERVK10C* in *Tex19.1*$^{-/-}$ testis (Ollinger et al., 2008) groups *Tex19.1* with other "germline genome defence genes" also required for retrotransposon suppression in the germline. Furthermore, while the cellular function of TEX19.1 protein is not known, it has been shown to interact strongly with the E3 ubiquitin ligase UBR2 which is required for TEX19.1 protein stability (Yang et al., 2010). *Ubr2*$^{-/-}$ is proposed to phenocopy *Tex19.1*$^{-/-}$ and has additionally been reported to cause MSCI and ubiquitination defects in synapsed pachytene spermatocytes (An et al., 2010, 2012).

Unlike other germline genome defence mutants only one relatively low-copy retrotransposon appears to be altered in expression in *Tex19.1*$^{-/-}$ testes however the expression of other repetitive elements in this mutant has not been broadly analysed. This mutant may therefore have the potential to reveal the meiotic consequences of retrotransposon activity more sensitively than the other similar mutants discussed which have misregulation of retrotransposons prevalent in the genome, often other additional misregulated genes, and widespread epigenetic changes. The cause of the synaptic defects

which occur in *Tex19.1*$^{-/-}$ is not known and a better understanding of the mechanisms involved in this defect would not only help to explain the meiotic role of TEX19.1 but could also aid the understanding of the meiotic defects observed in other germline genome defence mutants. As chromosome asynapsis and metaphase I univalent chromosomes have been identified in *Tex19.1*$^{-/-}$ spermatocytes it is also of interest to investigate the progression of the intervening synapsed pachytene spermatocytes to establish whether defects also exist within this sub-population. Furthermore, similarities between *Ubr2*$^{-/-}$ and *Tex19.1*$^{-/-}$ phenotypes suggest that studying the synapsed sub-population of pachytene spermatocytes could also help to identify additional causes of meiotic arrest in *Tex19.1*$^{-/-}$ as well as inform the relationship between these two proteins. Finally, the univalent chromosomes reported in *Tex19.1*$^{-/-}$ are not a phenotypic feature shared with *Ubr2*$^{-/-}$ or the germline genome defence mutants, therefore it will be of interest to study this defect to understand whether it could reflect an additional function unique to TEX19.1.

1.9 Thesis Outline

1. Investigate the involvement of retrotransposon activity in chromosome asynapsis in *Tex19.1*$^{-/-}$ spermatocytes
2. Analyse potential causes of chromosome asynapsis in *Tex19.1*$^{-/-}$ spermatocytes
3. Study meiotic progression of synapsed *Tex19.1*$^{-/-}$ pachytene spermatocytes
4. Investigate the origin of univalent metaphase I chromosomes in *Tex19.1*$^{-/-}$

Chapter 2:

Materials and Methods

2 Materials & Methods

2.1 Embryonic Stem Cell Culture

2.1.1 Freezing and Thawing Cells Stored in Liquid Nitrogen

Cell suspensions were frozen in 1mL aliquots of 10% dimethyl sulfoxide (DMSO), 20% fetal calf serum (FCS), and standard media (DMEM (Dulbecco's Modified Eagle Medium) or GMEM (Glasgow Minimum Essential Medium)) in screw-top cyrotubes (Nunc). Cells were initially frozen in dry ice and briefly transferred to -70°C before long-term storage in liquid nitrogen. Cells were frozen at a final concentration of $2x10^6$cells/ml. Upon retrieval of cells from liquid nitrogen, cells were thawed in a 37°C water bath as quickly as possible added to 9 volumes of culture medium then spun down at 1000 rpm using a benchtop centrifuge (Beckman Coulter, Allegra X-22) to remove the DMSO, before seeding into 25cm^2 ventilated culture flasks. Flasks were pre-coated with sterile 0.1% gelatine in PBS for 15 minutes which was aspirated before the addition of media and cells.

2.1.2 Routine Cell Culture and Harvesting

ES cells were cultured in E14 media (GMEM or DMEM, 10% FCS, 1% non-essential amino acids (NEAA), 1% sodium pyruvate, 1% penicillin/streptomycin (P/S), 1% L-glutamine (L-glut), 0.001% β-mercaptoethanol (β-ME), 1mL LIF conditioned media per 500mL GMEM), in a gelatinised culture flasks at 37°C and 5% CO_2. To pass cells, cultures were washed once with PBS before thinly covering with trypsin for 2 minutes at 37°C. The reaction was terminated by the addition of 10 volumes of media containing FCS. Cells were spun at 1000 rpm for 4 minutes, resuspended in fresh media, counted and typically reseeded at a concentration of $2x10^5$cells/mL or frozen as described above.

2.1.3 Cell Counting

Both ES cells cultured and sperm assessed, were counted in suspension using a haemocytometer. The total volume defined by the counting grid was $1x10^{-4}$ ml, thus cell concentrations per ml were calculated by multiplying the total number of cells in the grid by

$1x10^4$. Cell frequency was counted in three different counting squares for two samples of each cell suspension and the mean concentration taken.

2.1.4 X-ray Irradiation

For irradiation of ESCs, cells were lifted one day after seeding at a standard concentration as described previously (2.1.2). Cell suspensions of equal volume and containing a concentration of $5x10^4$ cells per ml were placed in petri dishes and irradiated using a Faxitron X-ray cabinet. Petri dish lids were removed during irradiation. Following irradiation, cells were re-seeded in triplicate and cultured for a total of 3 days. Cells were subsequently trypsinised and counted as described previously (section 2.1.3).

2.2 Animals

2.2.1 Animals Used

Tex19.1$^{-/-}$ mice used in this study originated from the knockout line generated by Ollinger et al (Ollinger et al., 2008) in a 129/Ola x CD1 mixed genetic background. All *Tex19.1*$^{-/-}$ mouse analysis performed herein has involved mice from colonies backcrossed to C57BL/6 for 3-10 generations. Where stated, studies have been performed exclusively on third generation backcrossed mice. Other imaging analyses have involved a combination of mice from third- and tenth-generation backcrossed colonies, as observations have remained consistent between these two sources.

Spo11$^{-/-}$ mice on a C57BL/6 genetic background (Baudat et al., 2000; Mahadevaiah et al., 2008) were kindly provided by James Turner (MRC NIMR, London). *Spo11*$^{+/-}$ were crossed with third generation backcrossed *Tex19.1*$^{+/-}$ to generate the double mutant lines discussed.

2.2.2 Genotyping Polymerase Chain Reaction (PCR)

DNA was isolated from ear clips (taken from mice 12 dpp or older), or tail tips for embryos, using DNAreleasy (Anachem Ltd) according to the instructions provided by the manufacturer. PCR reactions contained 0.5 units (U) Platinum Taq (Invitrogen), 0.5mM mixed dNTPs (Invitrogen), and 1mM of each primer (Sigma). 10X PCR Buffer and 50mM

Magnesium Chloride from the corresponding Platinum Taq PCR kit were used at 1X and 2.5mM respectively, and dH_2O added to make the reaction volume up to 20µl. PCRs were performed on DNA Engine Tetrad, and G-Storm GS4 PCR machines. Typical PCR conditions for *Tex19.1* genotyping were 95°C for 5 min followed by 35 cycles of 95°C for 30 sec, annealing at 65 °C for 30 sec, 72°C for 1min. Reactions were finally incubated for 72°C for 10 min. PCR has been described by (Sambrook and Russell, 2001). *Tex19.1* genotyping was performed using primers reported by Olllinger et al (Ollinger et al., 2008) (Table 1). *Spo11* genotyping involved 40 PCR cycles with annealing at 60°C using primers reported in by Baudat et al (Baudat et al., 2000) (Table 1).

2.2.3 Agarose Gel Electrophoresis

1.5% agarose (HiPure Low EEO Agarose, Biogene UK) gels were prepared for genotyping using 1x Tris/Borate/EDTA (TBE) buffer. Ethidum Bromide was added to molten agarose for a final concentration of 0.5µg/mL before pouring to allow visualisation of DNA under ultraviolet light. A similar concentration of ethidium bromide was also added gel running buffer (1xTBE) in which gels were submerged prior to running. DNA samples were loaded to gels in combination with 6x loading buffer (15% Ficoll 400 (Amersham Biosciences), 0.25% Orange G). At least one lane was loaded with 500ng of 1kb ladder DNA size marker (Invitrogen) to gauge the DNA fragments. Stained DNA was photographed using the Biorad Universal Hood II System (Biorad) and a thermal printer (Mitsubishi). Agarose gel electrophoresis was previously described by (Sambrook and Russell, 2001)

2.2.4 Drug Treatment

Adult mice were treated with a combination of Nervirapine ($3x10^{-4}$M), Emtricitabine ($1.6x10^{-4}$M) and Tenofovir ($9.4x10^{-5}$M) ingested via drinking water as described previously by Beck-Engeser et al (Beck-Engeser et al., 2011). Mice were treated for a period of 4 weeks. Drinking water was replaced weekly and mice were weighed daily to monitor health. All water bottles were wrapped in foil to shade the solutions, including those containing untreated water used to feed control mice.

2.3 Gene Expression Analysis

2.3.1 RNA Isolation

RNA was isolated from cultured ESCs using TRIzol according to the manufacturer's instructions (Invitrogen). Cultured cells were washed in ice cold PBS and lysed in a suitable volume of TRIzol. Cell scrapers were used to maximise detachment from the floor of the culture flask, and cells were homogenised by passing the solution through a pipette several times before vortexing. Some samples were flash frozen and stored at -80°C at this stage. Homogenised samples were incubated at room temperature to allow dissociation of nucleoprotein complexes before centrifugation at 12,000g for 10mins at 4°C to remove cell debris. Supernatant was then transferred into a fresh tube, 0.2ml chloroform was added for every 1ml TRIzol, and samples were vigorously mixed, incubated at room temperature for 2-3 mins, then centrifuged for 15 mins at 12,000g at 4°C. The colourless upper phase was transferred to a fresh tube and 0.5ml isopropyl alcohol added for every 1ml TRIzol initially used. Samples were either incubated at room temperature for 10mins, or 4°C overnight, then centrifuged at 12,000g for 30 mins (10mins if precipitated overnight at 4°C) at 4°C. Pellets were washed with 75% ethanol prepared with RNase-free water (MilliQ), spun back down at 7,500 rpm/5 mins/4°C, and air dried after removing as much of the ethanol as possible. Air dried pellets were resuspended in RNase-free water.

RNA was then DNase treated to ensure removal of genomic DNA, using recombinant RNase-free DNase I (Roche) according to the manufacturer's instructions. To 20µg RNA added 10µl DNase buffer 10X, 5µl DNase I RNase-free, 0.5µl RNasein (Promega), and made the reaction volume to a total of 100µl with MilliQ dH_2O. The reaction was incubated for 1-2hrs at 37°C then purified by phenol chloroform extraction; adding 50µl phenol and 50µl chloroform, vortexing then centrifuging at 8000rpm/5mins/4°C. The upper phase was transferred to a fresh tube and RNA precipitated using 1/10 volumes of 3M pH4 sodium acetate and 2.5 volumes of 100% ethanol, then incubating for 30mins at room temperature or overnight at -20°C. The RNA was then spun down at 15,000 rpm/15 mins/4°C, pellet washed in 75% ethanol, spun down at 7500 rpm/5 mins/4°C, supernatant removed and the pellet dried and resuspended in MilliQ dH_20.

2.3.2 cDNA Synthesis

cDNA was synthesised from isolated RNA using the SuperScript III Reverse Transcriptase (Invtirogen) protocol. To obtain maximum coverage of transcripts, random primers were used in the reverse transcription reaction. To check that genomic DNA was not contaminating the RNA, additional reactions were also set up for each RNA sample without SuperScript III reverse transcriptase. 5µg RNA determined by NanoDrop analysis was added to 250ng random primers (Promega), 1µl dNTP mix (10mM each dATP, dGTP, dCTP and dTTP), and the volume made up to 13µl with MilliQ dH_2O. The reaction was heated for 5 minutes at 65°C then incubated on ice for 1 minute to remove RNA secondary structures. The contents of each tube were collected by brief centrifugation and 4µl 5X First-Strand Buffer, 1µl 0.1M DTT, and 1µl RNAsein (40U/µl, Promega) added with 1µl SuperScript III (omitted from reverse transcriptase-negative control samples). The reaction was gently mixed then spun down by centrifugation, then incubated at 25°C for 5 minutes, 50°C for 30-60 minutes and finally heated to 70°C for 5 minutes to inactivate the reaction.

2.3.3 qRT-PCR

Quantitative reverse transcription PCR (qRT-PCR) was performed to quantify the presence of various RNA transcripts. cDNA templates were first generated and diluted 1/50 for each reaction. 5µl primer mix containing the appropriate forward and reverse primers at 1mM concentrations. No-template control reactions were set up using dH_2O in place of cDNA, and cDNA reaction products in which the reverse transcriptase was replaced by dH_2O were used as no-RT controls. 10µl SYBR Green Brilliant RT-PCR master mix (Life Technologies) was finally added each reaction before running on a BioRad CFX96 Real-Time PCR detection system. PCR reactions typically consisted of 94°C for 15min, 45 cycles of (94°C for 15sec, 55°C for 30sec. 72°C for 30sec), melt curve from 65°C to 95°C with 0.5°C increment for 5min. Primers were validated to work under these conditions at 90-100% efficiency. Reactions were run in three technical replicates for each biological sample and the relative changes in gene expression calculated using the 2-ΔΔCt method (Livak and Schmittgen, 2001) using the transcript of the housekeeping gene *β-actin* to normalise the cDNAs and the expression levels. *Oct4* expression was also assessed to support ES cell status of the cells analysed. A two-tailed t-test was used to determine statistical significance of qRT-PCR gene expression changes.

2.3.4 Primer Design

Primer sequences were designed for qRT-PCR using the Primer3 online facility. Primers were designed to be 17-25nt in length and generate a 150-250bp PCR product and range in melting temperature from 54-60°C. Specificity was initially checked using the BLAT function in UCSC Genome Bioinformatics.

Gene	Purpose of Primer	Primer Sequences (5'-3')	
Tex19.1	WT allele genotyping	CTTCAGGAGGTCTGATGCCCTCT	GAGTGTTGTGTGGTGGGTGTTATGG
Tex19.1	KO allele genotyping	CTTCAGGAGGTCTGATGCCCTCT	CACCGCCTGTGCTCTAGTAGCTT
Spo11	WT allele genotyping	TGAGATACATGGAGGAAGATGG	ATGTTAGTCGGCACAGCAGTAG
Spo11	KO allele genotyping	CTGAGCCCAGAAAGCGAAGGAA	ATGTTAGTCGGCACAGCAGTAG
ß-actin	qPCR	GGCTGTATTCCCCTCCATCG	ACATGGCATTGTTACCAACTGG
Oct4	qPCR	GTGGATTCTCGAACCTGGCT	GTCTCCAGACTCCACCCAC
IAP	qPCR	GCACCCTCAAAGCCTATCTTA	TCCCTTGGTCAGTCTGGATTT
MMERVK10C	qPCR	GGTAAAGTCTCCGAGGGTCA	AACTGGTCGCAGGAGCTG
LINE1	qPCR	GGAGGGACATTTCATTCTCATC	GCTGCTCTTGTATTTGGAGCATAGA
RLTR4.int.chr8	qPCR	CATACTTCTGCCCCAGCTAA	CAGTAATCGGTGGTGAGGTC
RLTR4.int.1	qPCR	ACAAAGGCCTCCTCACTTCT	TGCCCTCATCTTCTGATAGC
RLTR4.int.2	qPCR	TGGCCCATTCTGTATCAGTT	AGTTACGGTCTGTCCCATGA
MuLV.int	qPCR	GGCAGCCATACATACAGACC	TGGTCTGCATAGAAACAGCA
MERVL2a	qPCR	GCCAGAGAGGTGCGGCAGTGGGC	GGACCCGTGGATCCTGGCTGTGGGA
RLTR45	qPCR	TGCTTTTCCGACATGGTAAT	AGTAACCCTGACCTGCTCCT

Table 1. Primer sequences

2.4 SPO11 Oligonucleotide Assay

SPO11 oligonucleotide complexes were measured as reported previously (Pan and Keeney, 2009), with minor modification:

2.4.1 Preparation of Testes Lysates

Testes were isolated from 11dpp *Tex19.1*$^{+/+}$ and *Tex19.1*$^{-/-}$ mice. Tunicas were removed and testes were individually flash frozen in liquid nitrogen at this point for storage. Two testes from a single animal were sufficient for each pull-down reaction. Testes were thawed with the addition of 450µl lysis buffer (1% Triton X-100, 400mM NaCl, 25mM HEPES-NaOH, pH7.4, 5mM EDTA, supplemented with complete, EDTA-free protease inhibitor tablets (Roche Diagnostics. 1 tablet per 10ml lysis buffer) and 2mM DTT immediately before use). Tissue was ground individually for ~30seonds using a plastic pestle in to obtain a viscous crude lysate without visible clumps. Lysates were transferred into cold ultracentrifuge tubes. Samples were spun at 100,000rpm (355,040g) in a TLA 100.3 rotor on a benchtop

ultracentrifuge for 15 minutes at 4°C to pellet insoluble material and genomic DNA. Supernatants were carefully removed by pipetting and as a precaution were spun down once again as above.

2.4.2 Immunoprecipitation

Supernatants were then carefully transferred by pipetting to 15ml Falcon tubes and the solution was pre-cleared by the addition of slurry of Sigma-Aldrich protein A agarose beads (30µL slurry per testis), incubating for 3hours at 4°C with end-over-end rotation. Beads were spun down at 1700g for 3minutes at 4°C and supernatant taken. Suspension was then incubated with SPO11 antibody (2µg per testis) for 1 hour at 4°C with end-over-end rotation. Protein A agarose beads were then added to each suspension (15µl slurry per testis) and incubated overnight at 4°C with end-over-end rotation. The beads were spun down, supernatant removed and 1ml cold wash buffer (1% Triton X-100, 150mM NaCl, 15mM Tris-HCl, pH7.4) added and used to transfer the beads to a 1.5ml tube. Beads were spun down at 2300g for 1 minute at 4°C and washed a further three times in cold wash buffer.

2.4.3 Labelling and Resolving SPO11-Oligo Complexes

Beads were next washed twice in cold 1X labelling buffer (diluted from 10X NEB4 from New England Biolabs). The labelling reaction mix for each tube comprised of 5µl 10X NEB4 buffer, 1µl terminal deoxynucleotidyl transferase (TdT) (New England Biolabs, 20,000U/ml), 42µl dH_2O, 2µl fresh [α32-P]dCTP. 50ul reaction mix was added to each tube and reactions were incubated at 37°C for 45 minutes, mixing every 5 minutes. Beads were then spun down, supernatants removed and beads washed three times in 0.5ml cold wash buffer. As much liquid as possible was removed following the final wash. 20µl 2X Laemmli sample buffer was added to each sample and heated for 2 minutes at 95°C, then chilled immediately on ice. Samples were resolved on a Ready Gel Tris-HCl, 7.5% polyacrylamide (BIO-RAD) using the advised running buffer (25mM Tris, 192mM glycine, 0.1% SDS) in a Mini-PROTEAN Tetra Cell (BIO-RAD) until the bromophenol blue dye front has just run out of the gel. Samples were run in addition to Benchmark Pre-Stained Protein Ladder (Invitrogen) for size reference. Gels were dried and wrapped in cling film. Ladders were marked on a piece of autoclave tape using a pipette tip dipped in radioactive waste to make a "hot-pen"; this was then covered with further autoclave tape. Radioactive signal was

detected by overnight exposure to a phosphor imaging plate. SPO11-oligonucleotide complexes in wild type mice migrated at between 47-59kD.

2.5 Imaging

2.5.1 Testis Spread Preparation

All testis spreads were made using plain slides first cleaned by boiling in dH2O and air drying. Testes spreads were prepared for immunoflourescence analysis in two ways, both were used due to their differing ability to enable binding of particular antibodies and preservation of cell types of interest. One method has been described previously by Peters et al (Peters et al., 1997a) and was performed with minor modification. Briefly, this involved removing the tunic albuginea in Roswell Park Memorial Institute (RPMI) media to release the seminiferous tubules. Tubules were macerated using razor blades to generate a single cell suspension. The cell suspension was left to settle for 10minutes to allow clumps of tissue to settle. Supernatant was moved to a separate tube and spun down for 5 minutes at 892g at 4°C. Media was taken off the cells and they were resuspended in hypotonic extraction buffer (30 mM Tris, 50 mM sucrose, 17 mM trisodium citrate dihydrate, 5 mM EDTA, 0.5 mM DTT and 0.5 mM phenylmethylsulphonyl fluoride (PMSF), pH 8.2) for 30–60 min. Cells were then spun down again and resuspended in 100mM sucrose solution. 10µl of the cell suspension was zig-zagged down a clean, boiled slide, previously dipped in fix (1% paraformaldehyde (PFA), pH 9.2, solution (pH set by using 10 mM sodium borate pH 9.2 buffer solution) containing 0.15% Triton X-100). Slides were then left in a humid chamber with the lid open a crack, to dry overnight. Dry slides were then stored at -80°C.

The alternative method designed by Robert Speed proceeds as follows: the tunica albuginea is removed with forceps and testes thoroughly macerated in Roswell Park Memorial Institute (RPMI) media. Suspension is made up to 3-4ml and transferred to a small Falcon tube, where remaining clumps are allowed to settle at room temperature for 10 minutes. The supernatant was transferred to a new tube and the cells pelleted for 5 minutes at 892g at 4°C then resuspended in 1ml RPMI per testis. Solutions were applied to slides using approximately 30µl drops from a Pasteur pipette. Five drops of 4.5% sucrose solution was applied to each slide and one drop of cell suspension was added from a height of roughly 15cm, followed by a single drop of 0.05% Triton-X-100. After 10 minutes nuclei were fixed

using 8 drops of 2% paraformaldehyde with 0.02%SDS in dH_2O for 20 minutes in a humid chamber. Slides were then gently washed in dH_2O and left to dry before storage at -80°C.

2.5.2 Antibody Staining

For immunostaining testis spreads, slides were first washed in PBS and blocked for 1 hour at room temperature with 50µl block solution (0.15%BSA, 0.1% Tween-20 and 5% goat serum in PBS) using a plastic coverslip for even distribution. Primary antibodies were diluted in block solution, 50µl applied to each slide, and a coverslip added before incubating in a humid chamber for 2hrs at room temperature. Slides were washed in PBS three times, for five minutes each. Secondary antibodies with 4,6-diamidino-2-phenylidole (DAPI) diluted in block solution to a final concentration of 0.002µg/µl were applied as before, incubating at room temperature in darkness for 1hour. Slides were washed 3x in PBS before adding mounting media (90% glycerol, 10% PBS, 0.1% p-phenylenediamine) and sealing below a glass coverslip with nail varnish.

To avoid cross-reaction between antibodies (typically goat anti-mouse and goat anti-guinea pig secondary antibodies with guinea pig and mouse primary antibodies respectively) staining with incompatible antibody combinations was split into two separate rounds.

Antibody	Species	Origin Reference	Concentration	Use (IF/FISH/IP)	Testes Spread-Type Used
Anti-Centromere Protein	Human	Antibodies Incorporated	1:50	IF	Peters
Anti-DMC1	Rabbit	Santa Cruz, H-100, sc-22768	1:50	IF	Speed
Anti-FK2 (Poly+MonoUbiquitin)	Mouse	ENZO Life Sciences, BML-PW8810	1:500	IF	Peters
Anti-H1t	Guinea Pig	Howard Cooke	1:1000	IF	Peters
Anti-MEI4	Rabbit	Bernard de Massy	1:200	IF	Speed
Anti-MLH1	Mouse	Pharmingen, 51-1327GR	1:50	IF	Speed
Anti-RBMY	Rabbit	David Elliott (Newcastle University)	1:100	IF	Peters
Anti-RPA	Rabbit	C. James Ingles (University of Toronto)	1:300	IF	Speed
Anti-SPO11	Mouse	Michael Thelen via Scott Keeny (Howard Hughes Medical Institute)	2µg per testis	IP	-
Anti-SYCE2	Guinea Pig	Bolcun-Filas et al. 2009	1:1000	IF	Speed + Peters
Anti-SYCP1	Rabbit	Abcam, ab15090-100	1:200	IF	Speed + Peters
Anti-SYCP3	Mouse	Santa Cruz, D-1, sc-74569	1:200	IF	Speed + Peters
Anti-SYCP3	Rabbit	Abcam, ab1592	1:300	IF	Speed + Peters
Anti-SYCP3	Rabbit	LS Bio, LS-B175	1:500	IF	Speed + Peters
Anti-γH2AX	Mouse	Millipore, JBW301	1:3000	IF	Speed
Anti-γH2AX	Rabbit	Millipore, 07-164	1:200	IF	Peters
Anto-RAD51	Rabbit	Calbiochem, PC130	1:500	IF	Speed
Biotinylated anti-avidin	Goat	Vector	1:500	FISH	Metaphase
Anti-Mouse Alexa Fluor 488	Goat	Invitrogen, A-11001	1:500	IF	Speed + Peters
Anti-Mouse Alexa Fluor 594	Goat	Invitrogen, A-11005	1:500	IF	Speed + Peters
Anti-Rabbit Alexa Fluor 488	Goat	Invitrogen, A-11008	1:500	IF	Speed + Peters
Anti-Rabbit Alexa Fluor 594	Goat	Invitrogen, A-11012	1:500	IF	Speed + Peters
Anti-Rabbit Alexa Fluor 647	Goat	Invitrogen, A-21245	1:500	IF	Speed + Peters
Anti-Guinea Pig Alexa Fluor 594	Goat	Invitrogen, A-11076	1:500	IF	Speed + Peters
Anti-Guinea Pig Alexa Fluor 647	Goat	Invitrogen, A-21450	1:500	IF	Speed + Peters

Table 2. Antibodies

2.5.3 Spermatocyte Staging

Spermatocytes were largely staged by co-staining for synaptonemal complex components and gauging the structure's progressive formation. Leptotene nuclei were identified by the presence of numerous short and incomplete axial element fragments with no apparent synapsis yet taking place. Zygotene nuclei contained fully established axial elements and some recognisable synapsis. Asynapsed pachytene nuclei were defined as having asynapsed autosomes as well as at least one fully synapsed pair of autosomes. Pachytene nuclei contained a fully synapsed set of 19 autosomes and identifiable sex chromosomes. Diplotene nuclei contained partially desynapsed autosomes with Scp3 accumulation at axial termini and bright centromeric DAPI domains. Metaphase I nuclei present a distinctive, strong centromeric accumulation of Scp3 and very low remaining signal on the chromosome axis.

2.5.4 Image Capture and Analysis

Standard three and four channel images were captured in iVision or IPlab (BioVision Technologies) using the following two imaging systems:

1. One imaging system comprises a Photometrics Coolsnap HQ2 CCD camera (Photometrics Ltd, Tucson, AZ) Zeiss Axioplan II fluorescence microscope with Plan-neofluar objectives, a 100W Hg source (Carl Zeiss, Welwyn Garden City, UK) and Chroma #89014ET three colour filter set or Chroma #89000ET four colour filter set (Chroma Technology Corp., Rockingham, VT) as appropriate. The single excitation and emission filters are installed in motorised filter wheels (Prior Scientific Instruments, Cambridge, UK). Image capture was performed using in-house scripts written for IVision (BioVision Technologies, Exton, PA).

2. The second imaging system comprises a Hamamatsu Orca AG CCD camera (Hamamatsu Photonics (UK) Ltd, Welwyn Garden City, UK) Zeiss Axioplan II fluorescence microscope with Plan-neofluar objectives, a 100W Hg source (Carl Zeiss, Welwyn Garden City, UK) and Chroma #89014ET three colour filter set or Chroma #89000ET four colour filter set (Chroma Technology Corp., Rockingham, VT) with the single excitation and emission filters installed in motorised filter

wheels (Prior Scientific Instruments, Cambridge, UK). Image capture was performed using in-house scripts written for IVision (BioVision Technologies, Exton, PA).

Only well spread nuclei were analysed throughout. Recombination foci were imaged by capturing z-stacks to include the full depth of each nucleus. Images were captured in Velocity (Perkinelmer Inc, Waltham, MA) or iVision using an imaging system comprising of a Hamamatsu Orca AG CCD camera (Hamamatsu Photonics (UK) Ltd, Welwyn Garden City, UK), Zeiss Axioplan II fluorescence microscope with Plan-neofluar or Plan apochromat objectives, a Lumen 200W metal halide light source (Prior Scientific Instruments, Cambridge, UK) and Chroma #89014ET single excitation and emission filters or Chroma #89000ET single excitation and emission filters (Chroma Technology Corp., Rockingham, VT) with the excitation and emission filters installed in Prior motorised filter wheels. A piezoelectrically driven objective mount (PIFOC model P-721, Physik Instrumente GmbH & Co, Karlsruhe) was used to control movement in the z dimension. Hardware control, image capture and analysis were performed using Volocity (Perkinelmer Inc, Waltham, MA). These images were deconvolved using a calculated PSF with the constrained iterative algorithm of Volocity (Perkinelmer Inc, Waltham, MA) and a single 2D image generated in Fiji.

All images were typically assessed in Adobe Photoshop CS6. Axial element lengths were measured using the ImageJ plugin NuronJ (Meijering et al., 2004). γH2AX signal intensity within each entire nucleus (set by DAPI signal) was quantified using ImageJ imaging software. Nearby background signal averaged from multiple readings in each image was subtracted from the mean nuclear signal per unit of area. This adjusted nuclear score was then multiplied by nuclear area to generate the total nuclear signal similarly to previously described (Mahadevaiah et al., 2008). Recombination foci were scored manually as focal staining localising to the chromosome axis, overlapping with antibody staining signal marking the axial element, and frequencies typically compared by Mann-Whitney statistical test. Some statistical analyses were performed using a Fisher's exact test as indicated in text, when used this test was two-tailed.

2.5.5 Metaphase Chromosome Spreading

Meiotic metaphase chromosomes were prepared as described in Methods in Molecular Biology Vol29; Chromosome Analysis Protocols (Gosden, 1994). Testes were isolated,

tunica removed and tubules incubated in 1% hypotonic sodium citrate for 20 minutes. Subsequently the tissue was macerated with razor blades to generate a cell suspension. Cell clumps were allowed to settle and the suspension was transferred to a fresh tube. Cells were spun down at 450g for 8 minutes. The majority of the sodium citrate was removed, leaving just enough to resuspend the cell pellet by flicking. Fix (3:1, methanol:acetic acid) was slowly added down the sides of the tube until the volume of the cell suspension is approximately trebled, the suspension was then gently but firmly pipetted to break up any cell clumps. More fix was then added to make the volume up to 5ml, and the suspension was left to stand for 1 hour at room temperature or overnight at 4°C. This solution can then be stored at -20°C. Before use, suspensions were spun down at 450g for 8 minutes and the supernatant replaced with fresh fix until a suitably cloudy suspension was obtained. Volume suitability was checked on test slides by light microscopy. Clean slides were breathed upon to create a layer of water vapour, and a drop of cell suspension was dropped onto the slide from a height of ~20cm. Slides were then allowed to air dry before FISH staining against major satellite regions to identify centromeric regions.

2.5.6 Fluorescence *in situ* hybridisation (FISH)

FISH was performed on the metaphase chromosome spreads as described previously (Boyle et al., 2001). For DNA FISH the slides (ideally 2 days after spreading) incubated in 2 x SSC, 100µg/mL RNaseA for 1 h at 37°C. The slides were then washed briefly in 2x SCC before being dehydrated using fresh 70, 90, 100% ethanol, then air dried. Slides were warmed in a 70°C oven then denatured in 70% formamide, 2x SSC pH 7.5 at 70°C for 90 seconds. They were then transferred to ice-cold 70% ethanol, and then into 90% and 100% ethanol and air dried. 15µl of 100ng biotin-labelled major satellite paint were denatured at 70°C, pre-annealed at 37°C for 15 min, then hybridized to pre-warmed slides below a rubber-sealed coverslip overnight at 37°C. Mouse major satellite probes were kindly provided by Shelagh Boyle (HGU IGMM). Slides were washed 4x 3min in 2x SSC at 45°C, 4x 3min in 0.1x SSC at 60°C and then 4x SSC/ 0.1% Tween-20 at room temperature. Slides were then covered with 40µl of blocking buffer (4x SCC, 5% Marvel) below a coverslip for 5 mins at room temperature before this is drained off and replaced by 40µl antibody/blocking buffer mix. The first antibody was FITC-conjugated avidin (Vector) to detect the biotinylated major satellite probes. After a 60min incubation at 37°C and 3x 2min washes in 4x SCC/0.1% Tween slides were stained with biotinylated anti-avidin (Vector) as with the previous antibody and this was finally repeated with a layer of FITC-conjugated avidin (Vector).

Washed slides were incubated in 1:1000DAPI/PBS for 3mins, washed then mounted in mounting media (90% glycerol, 10% PBS, 0.1% p-phenylenediamine) and sealed below a glass coverslip with nail varnish.

Chapter 3:

Retrotransposon Activity Detection by Microarray and Involvement in *Tex19.1*$^{-/-}$ Meiotic Chromosome Asynapsis

3 Retrotransposon Activity Detection by Microarray and Involvement in *Tex19.1*$^{-/-}$ Meiotic Chromosome Asynapsis

3.1 Introduction

TEX19.1 was initially proposed to be a suppressor of retrotransposons following the analysis of gene expression changes in *Tex19.1*$^{-/-}$ testes by microarray. The analysis was conducted by R. Ollinger et al using pre-pubertal 16dpp testes in which the first wave of spermatogenesis is taking place (Ollinger et al., 2008). At 16dpp the first spermatocytes are entering the pachytene stage, but mutant spermatocyte apoptosis had not yet begun, therefore the cell composition is thought to be comparable between *Tex19.1*$^{-/-}$ and controls. Microarray analysis at this stage revealed no consistent differences in the expression of single-copy genes known to be required for meiotic progression between *Tex19.1*$^{-/-}$ and controls, however a four-fold increase in the expression of probes which mapped to the LTR retrotransposon MMERVK10C was detected (Ollinger et al., 2008). Approximately 16 copies of the full-length MMERVK10C sequence are present in the genome, as well as a further 1200 fragmented sequences. Unlike mice carrying mutations in other germline genome defence genes e.g. *Mili, Dnmt3l,* the expression of more prevalent retrotransposons such as *IAP* and *LINE-1* were not seen to change in expression in *Tex19.1*$^{-/-}$ testes (Crichton et al., 2013; Ollinger et al., 2008). The apparent restriction and specificity of the gene expression changes in *Tex19.1*$^{-/-}$ testes is therefore unusual. A total of 1,221 repetitive elements identified within the Repeatmasker database exist across the mouse genome, and while the initial analysis of *Tex19.1*$^{-/-}$ testes identified misexpression of one type of element and unaltered expression of several other prominent varieties, the effect of *Tex19.1* deletion on the expression status of numerous repetitive elements in testes remains unknown. This chapter aims to investigate the reliability of a novel microarray re-annotation method used to thoroughly assess the expression of a large proportion of the diverse repetitive elements present in the mouse genome. Such a technique has the potential to provide a wider and more informative view of the global repetitive element expression in *Tex19.1*$^{-/-}$ testes. The validation of this technique that I undertake in this chapter involves its application to reanalyse embryonic stem cell (ESC) microarray datasets. The retrotransposon silencing mechanisms employed in pluripotent cells and germ cells, such as that involving TEX19.1 in spermatogenesis, are important for limiting the accumulation of repetitive elements during evolution. Hence the interrogation of mutant ESC microarray datasets for retrotransposon upregulation also has

the potential to identify factors required to restrict retrotransposon proliferation through generations.

In situ analysis of *MMERVK10C* expression in 16dpp and adult *Tex19.1*$^{-/-}$ testes indicated that the increased expression of this retrotransposon is primarily a feature of prophase-stage spermatocytes. *Tex19.1*$^{-/-}$ prophase spermatocytes also feature defective chromosome synapsis (Ollinger et al., 2008), an abnormality proposed to be attributable to meiotic retrotransposition in another mouse mutant (Soper et al., 2008), and a shared feature of mutant mice with retrotransposon upregulation (Crichton et al., 2013). In this chapter I also begin to investigate mechanisms by which retrotransposon expression might lead to the defective chromosome synapsis in *Tex19.1*$^{-/-}$ spermatocytes.

3.2 Results

3.2.1 Experimental Validation of Microarray Data Re-Annotated to Reveal Repetitive Element Expression

Probes mapping at least partially to repetitive regions of the genome as identified by the Repeatmasker database have previously been removed during re-annotation of microarray datasets, to refine expression data relating to single-copy genes (Barbosa-Morais et al., 2010). These probes are typically not designed to report retrotransposon expression, and standard microarray software will assign them to genic transcripts. In an alternative re-annotation of microarray data by I. Adams, rather than discarding probes mapping to repetitive elements, such probes were used to provide valuable information about genome-wide repetitive element expression in microarray datasets. Changes in *MMERVK10C* expression in *Tex19.1*$^{-/-}$ testes were previously detected by analysing the origin of individual upregulated microarray probe sequences (Ollinger et al., 2008). I. Adams has since developed a pipeline for the re-annotation of microarray data from a variety of platforms to assess the expression of all retrotransposons represented to reflect expression changes in a wide range of repetitive elements (between ~25% and ~50% of the 1221 repetitive elements in the Repeatmasker database depending on the platform used) (Reichmann et al., 2012). To validate this approach to identifying expression changes in repetitive-elements, I. Adams reanalysed a range of published microarray datasets from embryonic stem cell (ESC) lines carrying mutations in genes with a known involvement in transcriptional regulation to mine this data for previously overlooked changes in repetitive element expression (Reichmann et al., 2012). The polycomb repressive complex (PRC) was one such transcriptional regulatory mechanism analysed in this study. Conventional transcriptional repression by the polycomb repressive complexes PRC1 and PRC2 is thought to involve the methylation of H3K27 by PRC2, and the subsequent recruitment of PRC1 to target loci (Simon and Kingston, 2013). However, a previous study of ES cells carrying mutations in the polycomb repressive complex 1 (PRC1) subunit Ring1B or the PRC2 component Eed, and ES cells carrying mutations in both of these genes has suggested that PRC1 and PRC2 are recruited independently and act redundantly to repress the LTR retrotransposon *IAP* within this cell type (Leeb et al., 2010). Reanalysis of these ESC microarray expression datasets indeed reproduced the upregulation of *IAP* elements specifically in the *Eed*$^{-/-}$*Ring1B*$^{-/-}$ double mutants and not in the *Ring1B*$^{-/-}$ or *Eed*$^{-/-}$ single mutant cell lines (Figure 13-2) (Reichmann

et al., 2012), thus strongly supporting the value and accuracy of this re-annotation approach for identifying changes in expression of repetitive elements.

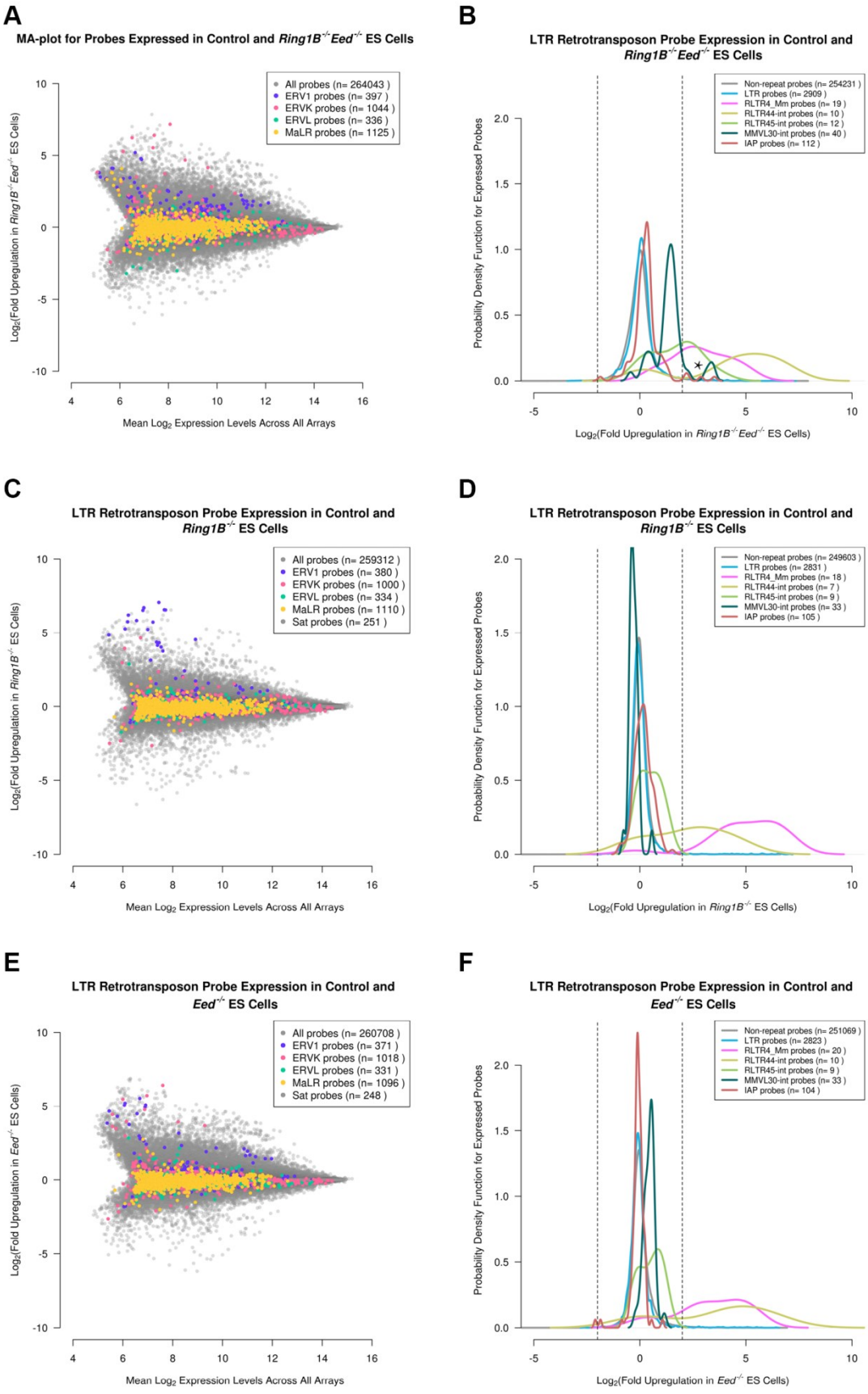

Figure 13-2. LTR retrotransposon targets of polycomb repressive complexes in ES cells.

(A, C, E) MA-plots for *Ring1B*$^{-/-}$*Eed*$^{-/-}$ double knockout, *Ring1B*$^{-/-}$ single knockout and *Eed*$^{-/-}$ single knockout ES cells showing how different classes of LTR retrotransposons change expression in these cell lines. (B, D, F) Plots showing the behaviour of selected retrotransposon probe populations in *Ring1B*$^{-/-}$*Eed*$^{-/-}$ double knockout, *Ring1B*$^{-/-}$ single knockout and *Eed*$^{-/-}$ single knockout ES cells. The selected retrotransposons are all represented by multiple upregulated probes (≥4 fold upregulation, p,0.01). Vertical lines indicate a 4 fold change. Note that some retrotransposons (e.g. *MMVL30*, *RLTR45*) are upregulated in double knockout but not in single knockout ES cells, other retrotransposons (e.g. *RLTR4*) are upregulated in all three ES cell lines. Asterisk in plot B highlights the upregulated IAP probes in this cell line. Retrotransposon probes are colour-coded as shown in the plot legends. All graphs herein attributed to I. Adams (Reichmann et al., 2012).

Dissection of upregulation revealed a subset of probes particularly mapping to shared LTR sub-families, ERVK and ERV1 (Figure 13-2 A, C, E). Further dissection of these probes indicated shared misregulation of the ERV1 element, *RLTR4*, in both the *Eed*$^{-/-}$ *Ring1B*$^{-/-}$ double knockout and single knockout cell lines, revealing *RLTR4* as a novel target for conventional transcriptional control by PRC (Figure 13-2 B, D, F) (Reichmann et al., 2012). The *RLTR4* retrotransposon probes were upregulated in all three cell lines, however close investigation in *Ring1B*$^{-/-}$ revealed that the upregulated probes corresponded mainly to the LTR region (*RLTR4_Mm*) but not usually the internal region (*RLTR4_int*) of this element (Figure 3-3). This finding suggests that the upregulated probes may only represent a subset of *RLTR4* loci, possibly corresponding to chimeric or truncated elements. I therefore mapped the genomic location of the internal-*RLTR4* upregulated probes from *Ring1B*$^{-/-}$ ESCs to the mouse genome (UCSC, NCBI37/mm9) using BLAT to assess the distribution and structure of the upregulated elements detected. Unlike the retrotransposon probes upregulated in other datasets involved in this study, I found that the *RLTR4-int* probes upregulated in *Ring1B*$^{-/-}$ do not map to multiple locations, but a single locus on chromosome 8 (chr8:125949704–125958431). Alternative *RLTR4-int* probes that did not alter in expression in *Ring1B*$^{-/-}$ ESCs mapped to multiple genomic loci, indicating that the upregulation of *RLTR4-int* probes may reflect the upregulation of a single genomic copy of this element, recognised by multiple probes. Unlike the typical structure of LTR (long terminal repeat) retrotransposons, which contain an internal protein-coding (e.g. *RLTR4-int*) sequence flanked by long terminal repeats (e.g. *RLTR4_Mm*) (Figure 3-4A), this single copy of *RLTR4-int* appears to be flanked by a single LTR containing structural rearrangements including a ~200bp deletion, and an ~6000bp truncation of the internal sequence (Figure 3-4B). To investigate whether the *RLTR4-int* upregulation is restricted to this individual genomic copy, I designed qRT-PCR primers specific to this copy and also primers designed using the *RLTR4-int* consensus sequence that recognises multiple genomic copies. qRT-PCR using these primer sets verified the upregulation of the individual copy of *RLTR4-int* on chromosome 8 in *Ring1B*$^{-/-}$ ESCs as identified by the microarray reanalysis and also verified that other common copies of

RLTR4-int are not upregulated in these mutant cells (Figure 3-4C). Furthermore, by qRT-PCR I validated the lack of expression changes at related retrotransposon sequences such as *MuLV* and prominent retrotransposons such as *LINE-1* (Figure 3-4C). As *RLTR4* is derived from *MuLV* (Changolkar et al., 2008), a redundant target sequence of PRC1 and PRC2 (Leeb et al., 2010), it is possible that the sequence changes in this single divergent copy of *RLTR4* have allowed its PRC2-independent silencing by PRC1. Overall this investigation demonstrates that re-annotation of microarray data is a sensitive, accurate and effective method for the detection of changes in the expression of repetitive elements; reproducing previously reported expression changes and often capable of discrimination between individual copies of a repetitive element.

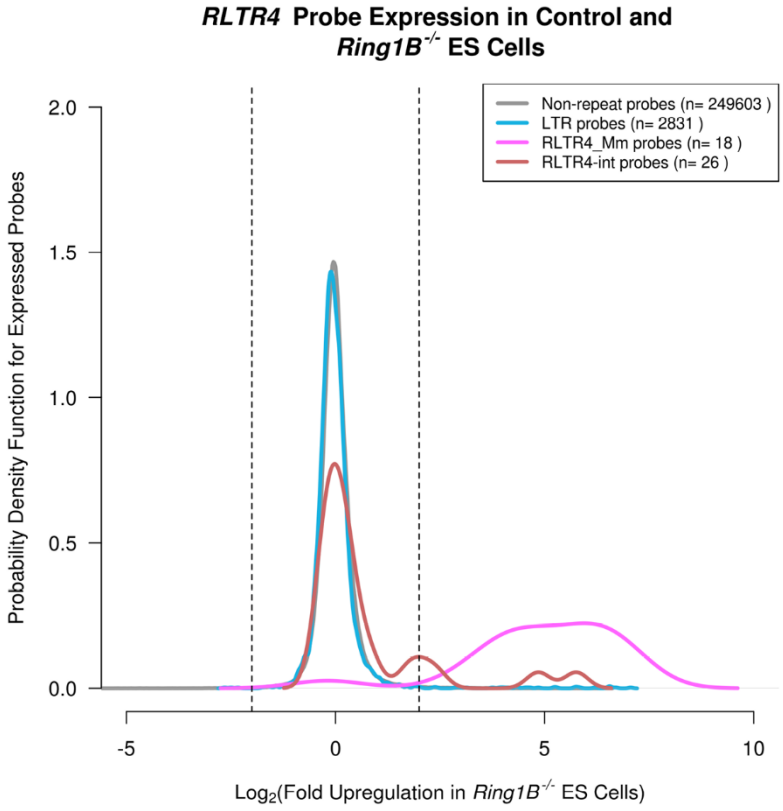

Figure 3-3. Behaviour of different *RLTR4* retrotransposon microarray probe populations in *Ring1B*$^{-/-}$ single knockout ES cells.
Different RLTR4 probe populations are colour-coded as shown in the legend, and vertical lines indicate a 4 fold change. Note that *RLTR4-Mm* probes display consistent upregulation, while *RLTR4-int* ulregulation is limited to a subset of probes. This graph is from I. Adams (Reichmann et al., 2012).

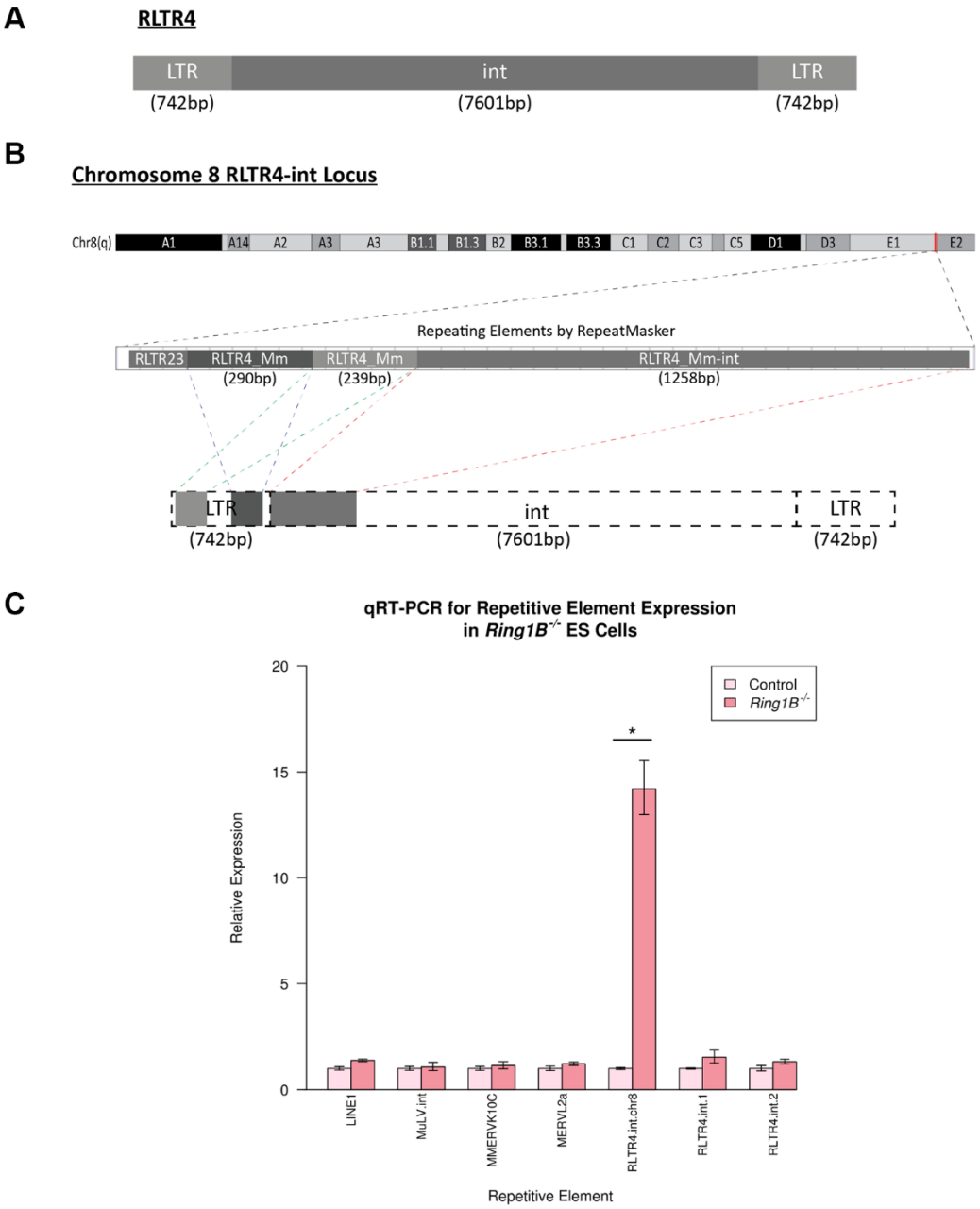

Figure 3-4. A single rearranged copy of *RLTR4-int* is upregulated in *Ring1B*$^{-/-}$ single knockout ES cells.

(A) Typical structure of RLTR4 retrotransposons consist of a 7601bp internal sequence flanked by 742bp long terminal repeat (LTR) promoter sequences. (B) Structure of the single upregulated *RLTR4-int* copy detected by microarray probes and "RLTR4.int.chr8" qRT-PCR primer sets in *Ring1B*$^{-/-}$ single knock out ESCs, as well as the surrounding retrotransposon sequences (as indicated on UCSC genome browser; mouse mm9). Mapping of these *RLTR4* sequences to the typical structure of this element, demonstrating the truncations and rearrangements exhibited. (C) qRT-PCR verification of repetitive element expression in *Ring1B*$^{-/-}$ ESCs. Expression levels (mean ± standard error) were normalized to *β-Actin* and expressed relative to wild-type control ESCs. Performed on three technical repeats. The asterisk indicates a statistically significant difference ($p<0.05$). Note that different primers for *RLTR4* elements behave differently in the qRT-PCR assay.

Published microarray data from ESCs carrying mutations in the histone deacetylase enzyme HDAC1 (Zupkovitz et al., 2006) was also reanalysed by I. Adams to further investigate the capacity and reliability of this microarray re-annotation approach to detect retrotransposon expression. The HDAC family of histone deacetylases are already implicated in retrotransposon silencing as they are targets of the drug trichostatin A, treatment with which has been demonstrated to alter retrotransposon expression (Brunmeir et al., 2010; Garcia-Perez et al., 2010; Yang and Seto, 2008). The role of HDACs in this altered regulation, and which HDACs are involved is not known. Repeat annotation of *Hdac1*$^{-/-}$ ESC microarray data revealed changes in expression particularly effecting LTR repeat probes (Figure 3-5A). These changes in expression include increases of 4-8 fold and also reductions of 2-4 fold. This re-annotation of *Hdac1*$^{-/-}$ ESC expression data by I. Adams therefore indicated a role for HDAC1 in the regulation of LTR retrotransposons. Dissection of the misregulated population of LTR probes to identify the specific misregulated retrotransposons revealed the upregulation of probes mapping *RLTR45* and *ETnERV3* retrotransposons, and the downregulation of probes corresponding to *IAP* (Figure 3-5B). Each of these misregulated elements was identified by multiple probes mapping to multiple genomic locations. *RLTR45* and *ETnERV3* share considerable sequence similarity (84% identity over 4.2kb of sequence), which may influence their shared regulation by HDAC1, or difficulties in accurately distinguishing between these two elements. To establish the reliability of these findings more accurately I obtained *Hdac1*$^{-/-}$ ESCs and used these to perform qRT-PCR using primers designed to consensus sequences mapping to *RLTR45* and *IAP*, as well as the highly prevalent retrotransposon *LINE-1*. As expected from the re-analysed microarray data, the mutation of *Hdac1* had no effect on the expression of *LINE-1* (Figure 3-6) however the expression of *RLTR45* was increased 11-fold and expression of *IAP* was reduced 2.5-fold (Figure 3-5E), again reinforcing the reliability of the changes identified in repetitive element expression via this microarray data re-annotation approach (Reichmann et al., 2012).

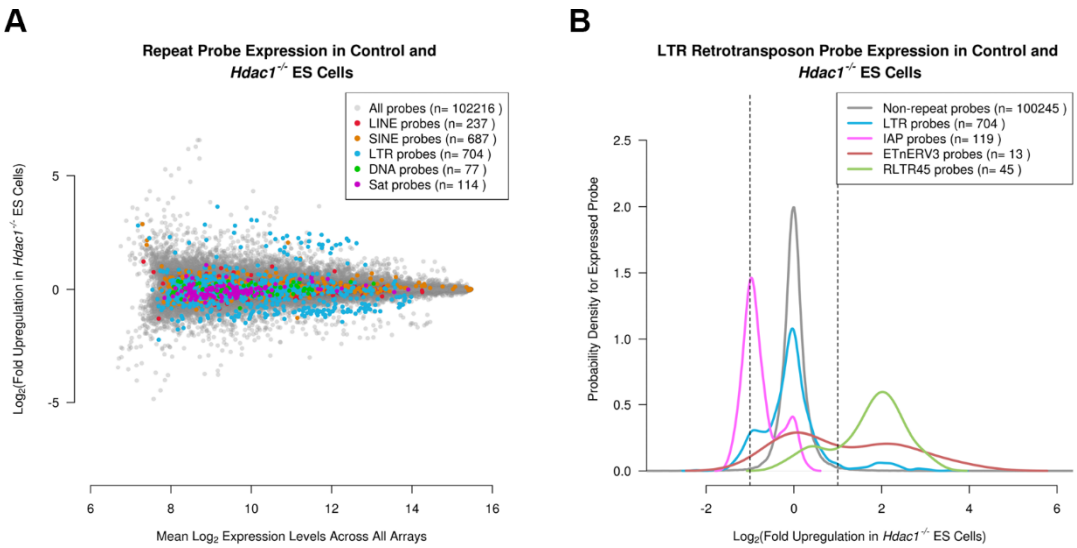

Figure 3-5. Reanalysis of *Hdac1*$^{-/-}$ ES cell microarray data to assess rerotransposon expression. (A) MA-plot for Hdac1-/- ES cell gene expression data showing how different families of repetitive element change in expression. (B) Plots showing the behaviour of selected retrotransposon probe populations in *Hdac1*$^{-/-}$ ES cells. Retrotransposons are colour-coded according to the legend. Vertical lines indicate the 2 fold change cut-off used. These graphs are attributable to I. Adams.

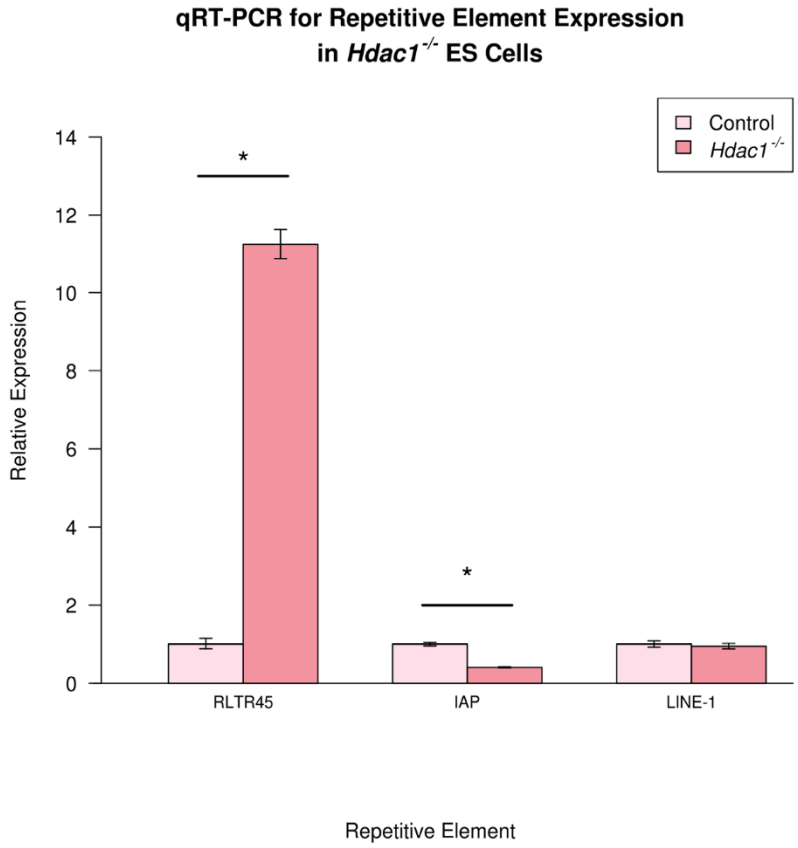

Figure 3-6. qRT-PCR validation of retrotransposon expression changes in *Hdac1*$^{-/-}$ single knockout ES cells.
qRT-PCR verification of repetitive element expression in *Hdac1*$^{-/-}$ ES cells. Expression levels (mean ± standard error) were normalized to *β-Actin* and expressed relative to wild-type control ES cells. The asterisk indicates a statistically significant difference ($p<0.05$).

Histone acetylation is typically associated with active gene transcription; therefore the deacetylase activity of the HDAC proteins is largely implicated in gene silencing (Bannister and Kouzarides, 2011). The reduction of *IAP* expression in *Hdac1*$^{-/-}$ ESCs therefore contrasts with this model. The reduction in *IAP* expression does however parallel the behaviour of some single copy targets of HDAC1 (Zupkovitz et al., 2006). It is possible that *IAP* is not directly regulated by HDAC1 but its reduced expression is a downstream consequence of upregulated primary HDAC1 targets, or alternatively HDAC1 may be directly required for *IAP* repression. To test whether HDAC1 directly interacts with both *RLTR45* and *IAP*, I reanalysed published high throughput sequencing data from HDAC1 chromatin immuno-precipitation (ChIP-seq) using mouse ESCs (Barrett et al., 2011; Whyte et al., 2012), for repetitive element binding using a separate method developed for such data by D. Day et al. (Day et al., 2010). Interestingly, *RLTR45-LTR* sequences are enriched in HDAC1 ChIP-seq relative to whole cell extract controls, suggesting that *RLTR45* is directly regulated by

HDAC1 through physical association with *RLTR45*-LTRs (Figure 3-7). In contrast, *IAP*-LTRs are depleted in HDAC1 ChIP-seq relative to whole cell extract (Figure 3-7), consistent with the downregulation of *IAP* expression being an indirect consequence of other changes in gene expression in *Hdac1*$^{-/-}$ ESCs. No consistent enrichment of HDAC1 was found at *SINE-B1* sequences, which did not change in expression in *Hdac1*$^{-/-}$ ESCs, consistent with the association between HDAC1 binding and transcriptional upregulation in the absence of HDAC1. Again, this investigation into repetitive element expression in *Hdac1*$^{-/-}$ ESCs reinforces the reliability of I. Adams' approach to reanalyse microarray expression data and assess repetitive element expression. Furthermore this technical validation identified novel repetitive elements regulated specifically by HDAC1 in ESCs, and via additional reanalysis of available ChIP-seq data provides insight into the mechanism by which HDAC1 regulates these specific repetitive elements (Reichmann et al., 2012).

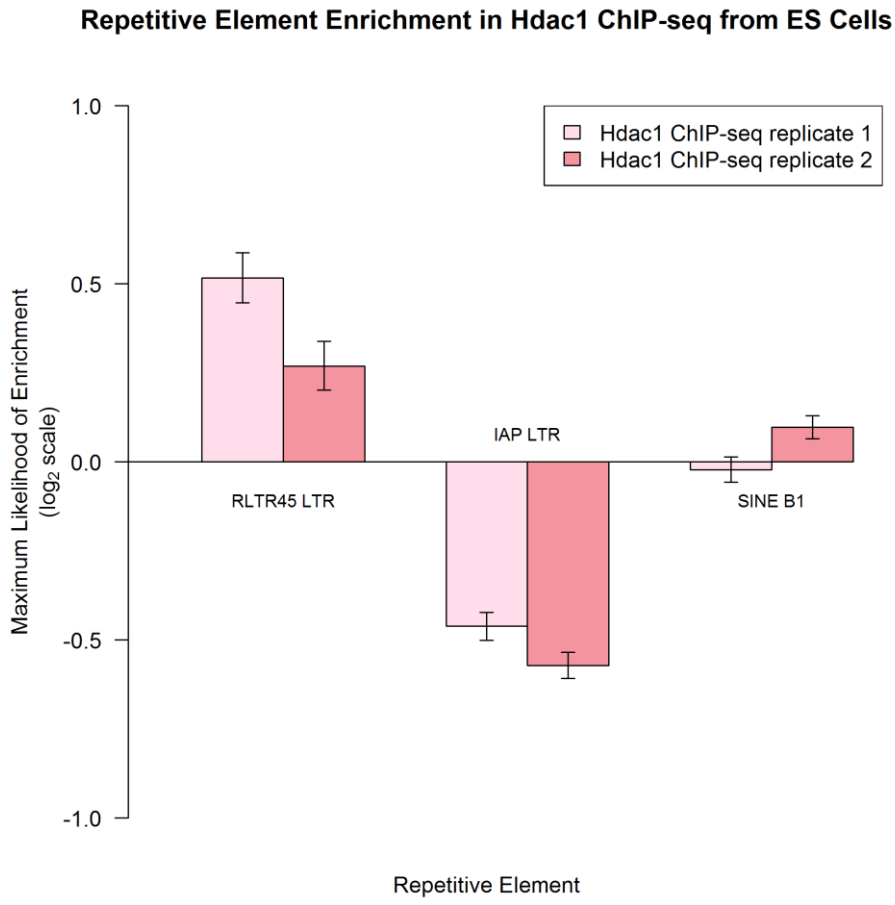

Figure 3-7. Physical association between HDAC1 and misregulated repetitive element sequences. Enrichment of LTR retrotransposon sequences in HDAC1 ChIP-seq data from mouse ES cells. The maximum likelihood of enrichment (>95% confidence intervals) for *RLTR45* LTR and *IAP* LTR sequences HDAC1 ChIP-seq relative to whole cell extract is shown. *RLTR45* LTR sequences are enriched in the HDAC1 ChIP-seq indicating a physical association between HDAC1 and RLTR45 retrotransposon chromatin, in contrast *IAP* LTR sequences are depleted.

After establishing the reliability of the microarray data re-annotation approach to detecting retrotransposon expression, this technique was employed to analyse genome-wide repetitive element expression in juvenile 16dpp *Tex19.1*$^{-/-}$ testes in mice by J. Reichmann. Mice used were from lines backcrossed three times from the 129/Ola x CD1 mixed background used for the initial analysis (Ollinger et al., 2008) to the BL/6 mouse background to reduce genetic variation. Consistent with previous findings, *MMERVK10C* was found to be upregulated in *Tex19.1*$^{-/-}$ testes, with multiple probes upregulated more than 2-fold mapping to multiple copies of *MMERVK10C-int* LTR retrotransposon sequence (Ollinger et al., 2008; Reichmann et al., 2012). Furthermore, the additional 172 different repetitive elements represented in this array analysis did not change in expression between *Tex19.1*$^{-/-}$ and control testes, demonstrating that repetitive element misexpression in the absence of TEX19.1 is limited to *MMERVK10C* in testes (Reichmann et al., 2012).

3.2.2 Investigating the Effect of Retrotransposon Activity on Events in *Tex19.1*$^{-/-}$ Spermatocyte Meiotic Prophase I

Similarly to *Tex19.1*$^{-/-}$ male mice, other mice carrying mutations in germline genome defence genes also exhibit germline upregulation of retrotransposon expression, homologous chromosome asynapsis and meiotic arrest in prophase I (Crichton et al., 2013). Mice with a null-mutation of the *Maelstrom* (*Mael*) gene are one such example. Male *Mael*$^{-/-}$ mice feature upregulation of *LINE-1* and *IAP*, and display increased levels of LINE-1 ORF1 protein during meiotic prophase (Soper et al., 2008), the same stage of germ cell development at which *MMERVK10C* is upregulated in *Tex19.1*$^{-/-}$ (Ollinger et al., 2008). ORF1 encodes a nucleic acid binding protein containing a central RNA recognition motif with nucleic acid chaperone activity, and is required for LINE-1 retrotransposition (DeBerardinis et al., 1998; Moran et al., 1996). The upregulation of ORF1 protein is associated with increased γH2AX staining in *Mael*$^{-/-}$ spermatocytes (Soper et al., 2008). Retrotransposition events have been demonstrated to generate DNA damage recognisable by γH2AX staining (Daniel et al., 2004), however additional DNA damage is difficult to assess during meiotic prophase due to the hundreds of DSBs generated by SPO11 at the initiation of meiotic recombination, which are gradually repaired as prophase progresses. *Spo11*$^{-/-}$ spermatocytes do not generate meiotic DSBs, and as such possess only low levels of DNA damage (Baudat et al., 2000; Romanienko and Camerini-Otero, 2000). A range of explanations for this low-level SPO11-independent DNA damage have been proposed, including: DSBs forming at stalled replication forks in S-phase, transcription-associated recombination, topoisomerase II

activity, retrotransposition or unknown environmental or endogenous factors such as reactive oxygen species (Carofiglio et al., 2013). Comparison of DNA damage levels in *Spo11*$^{-/-}$ and *Spo11*$^{-/-}$*Mael*$^{-/-}$ spermatocytes has revealed a dramatic increase in SPO11-independent DNA damage in the absence of MAEL (Soper et al., 2008). It has therefore been speculated that this increased SPO11-independent DNA damage represents retrotransposition events in *Mael*$^{-/-}$ spermatocytes, and may be the cause of failed chromosome synapsis in this mutant.

LTR retrotransposons typically possess protein-coding *gag*, *pro*, *pol* and sometimes *env* genes. The *pol* gene encodes the polymerase and integrase enzyme, required for retrotransposition. qRT-PCR analysis of *Tex19.1*$^{-/-}$ testes by J. Reichmann has shown upregulated expression of MMERVK10C *gag*, *pol*, and *env* genes from multiple loci, including contigs with intact copies of both *pol* and *env* (Reichmann et al., 2012). While complete MMERVK10C contigs encoding intact gag, pro, pol and env were not seen, this element may be capable of retrotransposition in *Tex19.1*$^{-/-}$ spermatocytes with the use of proteins provided in *trans* (Reichmann et al., 2012). To investigate whether retrotransposition activity could be detected as elevated SPO11-independent DNA damage in the absence of TEX19.1, as seen in *Mael*$^{-/-}$ spermatocytes, I crossed *Tex19.1*$^{+/-}$ mice with *Spo11*$^{+/-}$ mice obtained from James Turner and bred to generate *Spo11*$^{-/-}$*Tex19.1*$^{-/-}$ mutant mice (Baudat et al., 2000; Mahadevaiah et al., 2008). I then assessed the level of SPO11-independent DNA damage in the spermatocytes of these animals, initially by immuno-staining for the DNA damage marker γH2AX. Unlike *Spo11*$^{-/-}$*Mael*$^{-/-}$, any change in the level of γH2AX staining was not immediately striking in *Spo11*$^{-/-}$*Tex19.1*$^{-/-}$ in comparison to *Spo11*$^{-/-}$ (Figure 3-8A). To quantify the level of DNA damage present in these spermatocytes I measured the frequency of all distinct, focal, axis-associated γH2AX domains stained. The absence of synapsis in *Spo11*$^{-/-}$ precludes the ability to traditionally sub-stage prophase spermatocytes, therefore DNA damage was scored in zygotene-like spermatocytes with complete axial element formation recognisable as elongated linear filaments of SYCP3 antibody staining (Figure 3-8A). *Tex19.1*$^{+/-}$*Spo11*$^{-/-}$ spermatocytes contained an average of 17.35 axial γH2AX foci per nucleus, in addition to a large domain previously termed the pseudo-sex body (Figure 3-8) (Barchi et al., 2005; Bellani et al., 2005). No difference in DNA damage levels was seen in *Spo11*$^{-/-}$*Tex19.1*$^{-/-}$ (mean γH2AX foci=20.02, Mann-Whitney U test = p=0.911), indicating that unlike MAEL, the absence of TEX19.1 does not detectably affect levels of SPO11-independent DNA damage in prophase spermatocytes. Although a consistent difference in γH2AX focus frequency is not seen between spermatocytes of the three pairs of *Tex9.1*$^{+/-}$*Spo11*$^{-/-}$ and *Tex19.1*$^{-/-}$*Spo11*$^{-/-}$, a small population of spermatocytes containing >50 foci is noted to only be present in *Spo11*$^{-/-}$

Tex19.1$^{-/-}$ (Figure 3-8B). As chromosome synapsis defects are only a feature of a subpopulation of *Tex19.1*$^{-/-}$ pachytene spermatocytes (~50% (Ollinger et al., 2008)) it remains possible that a sub-population of spermatocytes with elevated SPO11-independent DSBs do proceed to become asynapsed, while others synapse normally. Due to production of very low numbers of *Spo11*$^{-/-}$*Tex19.1*$^{-/-}$ double knock out male offspring from breedings, it was not possible to extend this analysis to additional animals to better assess whether elevated SPO11-independent DNA damage is a consistent feature of a small population of *Spo11*$^{-/-}$*Tex19.1*$^{-/-}$ spermatocytes. This would however be of interest to pursue further in the future. Difficulty in breeding these mice was largely due to surprisingly low levels of all offspring homozygous for *Spo11*-null alleles. Rather than 1:2:1 ratios of WT:HET:KO *Spo11* genotypes expected by Mendelian inheritance from proven *Spo11*$^{+/-}$*Tex19.1*$^{+/-}$ matings, ratios were 75:105:34 ($p<0.001$, Chi squared test). *Tex19.1* mutant alleles were inherited with Mendelian frequency. As such only 9/214 offspring were *Spo11*$^{-/-}$*Tex19.1*$^{-/-}$ double knockouts (13 expected), and only three of these were male. This sub-Mendelian frequency of *Spo11*$^{-/-}$ offspring is unexpected and the cause of it is currently unclear.

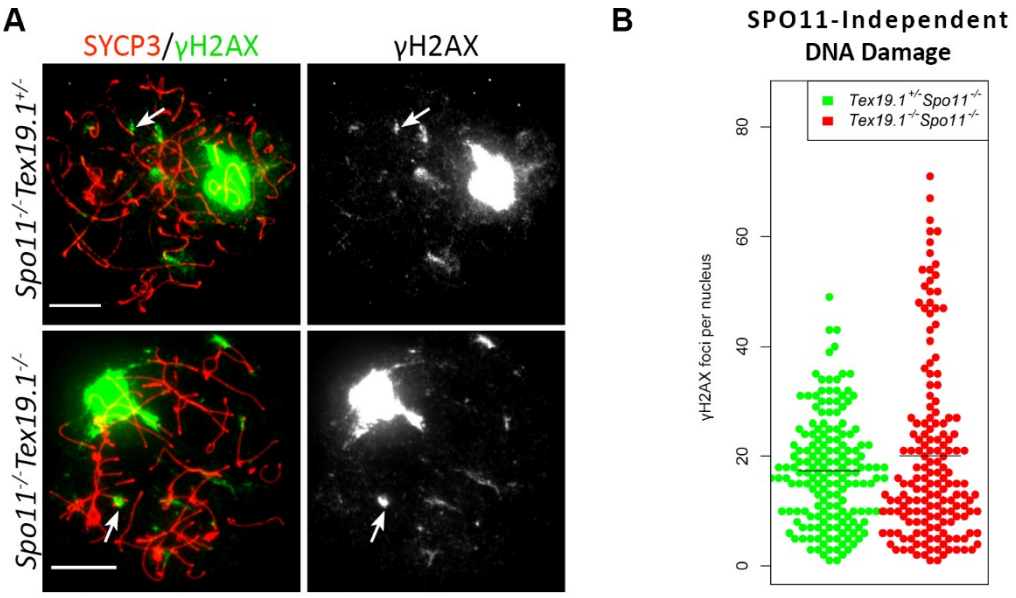

Figure 3-8. Effect of TEX19.1 on SPO11-independent meiotic DNA damage.
(A) Antibody staining of γH2AX and SYCP3 in asynapsed, zygotene-like, spermatocytes from *Spo11*$^{-/-}$*Tex19.1*$^{+/-}$ and *Spo11*$^{-/-}$*Tex19.1*$^{-/-}$ mice. Colour merges of both γH2AX (green) and SYCP3 (red), and individual monochrome images of the γH2AX staining alone are shown for representative nuclei. Arrows indicate examples of γH2AX foci scored. 10µm scale bars. (B) Beeswarm plot displaying the frequency of axis-associated γH2AX foci in each spermatocyte scored. Each point represents a nucleus scored. Mean foci for each genotype indicated by horizontal bar.

To further investigate whether additional SPO11-independent DNA DSBs participating in meiotic recombination are indeed absent in *Spo11*$^{-/-}$*Tex19.1*$^{-/-}$ spermatocytes, nuclei were stained using an antibody against the meiosis-specific homologous recombination protein DMC1, which forms axis-associated foci shortly after the formation of meiotic DSBs. Zygotene-like spermatocytes were identified using the criteria described previously, and DMC1 staining foci colocalising with SYCP3-stainied axes were counted. Unlike γH2AX foci, very few DMC1 foci were apparent in *Spo11*$^{-/-}$*Tex19.1*$^{+/-}$ or *Spo11*$^{-/-}$ *Tex19.1*$^{-/-}$ spermatocytes (Figure 3-9), however consistent with the γH2AX analysis the frequency of DMC1 foci did not differ between these mutants (mean=5.47 and 5.35 respectively, p=0.60; Mann-Whitney U test) (Figure 3-9B). Curiously, the SPO11-independent DMC1 foci present in these mutant spermatocytes were typically far fainter than SPO11-dependent foci identified using the same antibody (Figure 4-5) in later analyses of wild-type spermatocytes. It is possible that these SPO11-independent DMC1 foci represent a small proportion of SPO11-independent DSBs participating in homologous recombination but recruiting only low levels of DMC1 protein, or alternatively that this signal scored is non-specific background and thus false-positive. DMC1 foci frequencies counted were however close to those previously reported in *Spo11*$^{-/-}$ spermatocytes, which were typically observed to co-localise with γH2AX, supporting the presence of genuine DNA damage (Carofiglio et al., 2013). The consistent lack of additional SPO11-independent DNA damage in *Spo11*$^{-/-}$*Tex19.1*$^{-/-}$ spermatocytes suggests a lack of increased retrotransposition during meiotic prophase in the absence of TEX19.1. This finding distinguishes the phenotype of *Tex19.1*$^{-/-}$ from that of *Mael*$^{-/-}$ and indicates that additional SPO11-independent DNA damage during meiosis might not be responsible for the meiotic defects of *Tex19.1*$^{-/-}$ spermatocytes.

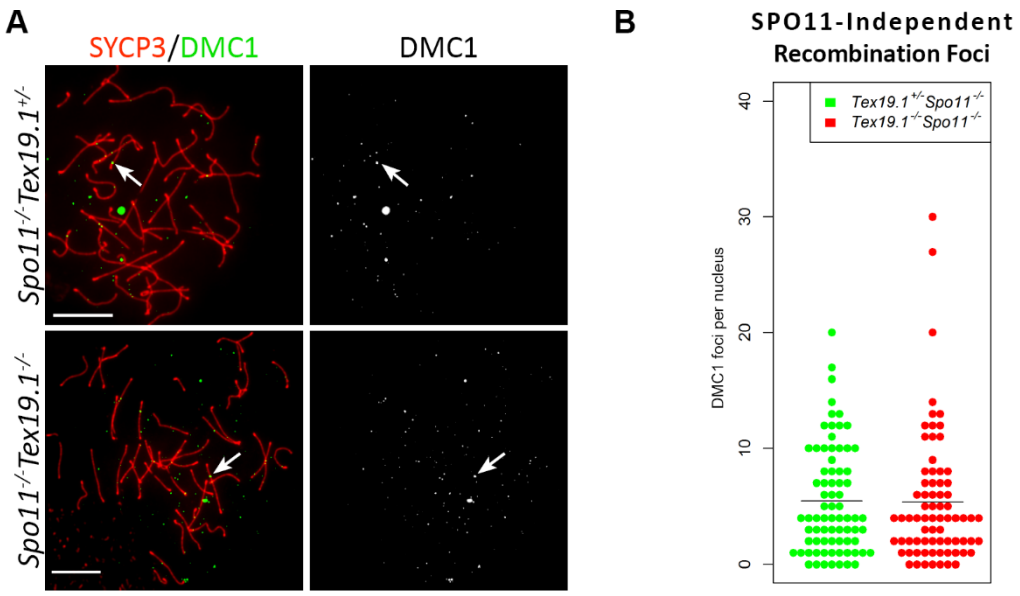

Figure 3-9. Effect of TEX19.1 on SPO11-independent recombination foci.
(A) Antibody staining of DMC1 and SYCP3 in asynapsed, zygotene-like, spermatocytes from *Spo11*$^{-/-}$ *Tex19.1*$^{+/-}$ and *Spo11*$^{-/-}$*Tex19.1*$^{-/-}$ mice. Colour merges of both DMC1 (green) and SYCP3 (red), and individual monochrome images of the DMC1 staining alone are shown for representative nuclei. Arrows indicate examples of DMC1 foci scored. (B) Beeswarm plot displaying the frequency of axis-associated DMC1 foci in each spermatocyte scored. Each point represents a nucleus scored. Mean foci for each genotype indicated by horizontal bar.

Antiretroviral drugs designed to inhibit reverse transcription are commonly used in the control of HIV infection, to block viral proliferation (Celum and Baeten, 2012). Nucleoside reverse transcription inhibitors have also been demonstrated to inhibit human LINE-1 retrotransposition (Jones et al., 2008), therefore their action is believed to extend to endogenous retrotransposons. Such drugs have been applied to *Trex1*$^{-/-}$ mice which suffer an accumulation of endogenous retroelement cDNA in cells of the heart, thought to cause or at least contribute to the sterile inflammatory myocarditis which leads to fatality in these mutant mice from 4-weeks of age. The use of combinations of antiretroviral drugs appears to target the multiple types of reverse transcriptase enzymes operating in *Trex1*$^{-/-}$ mice, and unlike the application of individual antiretroviral drugs, is able to dramatically increase survival and reduce inflammation in the heart in these mutant mice (Beck-Engeser et al., 2011). The treatment of mice with combinations of antiretroviral drugs is therefore thought to restrict the activity of retrotransposons, and limit their pathogenic impact. To investigate whether retrotransposon activity is the driving the meiotic defects observed in *Tex19.1*$^{-/-}$ spermatocyte chromosome synapsis I employed the same approach to treat mice with anti-retroviral drugs and assess the impact of this treatment on chromosome synapsis. Mice were

orally treated at approximately 2month of age with a combination of Emtricitabine, a synthetic nucleoside analogue of cytidine, Tenofovir, an acyclic nucleotide analog of adenosine 5'-monophosphate, and Viramune (nevirapine), which binds directly to reverse transcriptase and blocks the RNA-dependent and DNA-dependent DNA polymerase activities by disrupting the enzyme's catalytic site. *Tex19.1*$^{-/-}$ mice and littermate controls were treated for 30 days allowing plenty of time for drugs to take effect and for treated spermatocytes to progress to pachytene (Oakberg, 1956). Treatment was followed by immunocytological assessment of chromosome synapsis in pachytene. Levels of asynapsis were not significantly different between treated and untreated controls (19% and 11% respectively, p=0.28, Fisher's exact test) indicating the drugs are not strongly toxic to chromosome synapsis. Levels of asynapsis were also not significantly altered between treated and untreated *Tex19.1*$^{-/-}$ mice (28% and 17% respectively, n=3, Fisher's test p=0.06) demonstrating that the antiretroviral treatment was unable to rescue meiotic chromosome asynapsis in these mutant mice. A slight and non-significant increase in asynapsis was noted in treated control and mutant mice, which may indicate a slightly toxic effect of these drugs. The finding that antiretroviral treatment does not rescue *Tex19.1*$^{-/-}$ meiotic chromosome asynapsis, in addition to the lack of additional DNA damage observed, further supports the theory that retrotransposon activity during meiosis might not be responsible for the defective chromosome synapsis exhibited by this male mutant.

3.3 Discussion

This chapter aimed to establish the reliability of a microarray data re-annotation approach designed by I. Adams to identify retrotransposon expression changes. This approach has been employed by J. Reichmann to assess retrotransposon expression in *Tex19.1*$^{-/-}$ testes (Reichmann et al., 2012) more thoroughly than was performed in the initial analysis of this mutant (Ollinger et al., 2008). I further aimed to investigate the involvement of retrotransposon activity in the meiotic defects apparent in *Tex19.1*$^{-/-}$ spermatocytes. I. Adams developed a system for the re-annotation of microarray probes mapping to repetitive elements to glean expression data relating to wide ranges of such elements from microarray analyses using popular commercial platforms. Sections of this work were carried out by a number of researchers (indicated where appropriate) including myself. Together the findings demonstrate the reliability and value of this computational approach to reanalysing published datasets. The investigation of *Ring1B*$^{-/-}$ mouse ESCs replicating previous published findings, and the investigation of *Hdac1*$^{-/-}$ ESCs yielding additional novel expression changes the mechanistic basis of which were further illuminated by reanalysis of genome-wide chromatin binding by HDAC1 using a separate technique. Our analysis also highlighted the potential for misleading initial observations and the importance of validation by qRT-PCR. Upregulation of *RLTR4-int* expression in *Ring1B*$^{-/-}$ highlighted by the microarray reanalysis in ESCs was subsequently found to originate from a single genomic locus containing an individual divergent copy of this element mapped by multiple microarray probes. This locus was shown by qRT-PCR to not represent the regulation of all such elements by the RING1B-containing PRC1 complex. The use of this approach by J. Reichmann to investigate global retrotransposon expression changes in *Tex19.1*$^{-/-}$ testes replicated the initial finding of upregulated *MMERVK10C* expression and demonstrated the extreme restriction of retrotransposon upregulation to this single variety of repetitive element in this mutant mouse tissue. I assessed levels of SPO11-independent DNA damage that could relate to retorotransposition events in spermatocytes lacking TEX19.1 by imaging DNA damage-associated markers in *Spo11*$^{-/-}$*Tex19.1*$^{-/-}$ double knockout mouse spermatocytes. This demonstrated that unlike *Mael*$^{-/-}$ mutants which, like *Tex19.1*$^{-/-}$ spermatocytes feature upregulated germline retrotransposon expression and defective meiotic chromosome synapsis, *Tex19.1*$^{-/-}$*Spo11*$^{-/-}$ spermatocytes do not exhibit an increase in SPO11-independent DNA damage. Antiretroviral drug treatment of *Tex19.1*$^{-/-}$ mice also failed to rescue the chromosome asynapsis. Therefore together these findings demonstrate that detectable

indications of meiotic retrotransposition events are not elevated in spermatocytes lacking TEX19.1, and might not be responsible for the chromosome asynapsis observed.

3.3.1 Novel Retrotransposon Targets of HDAC1 Regulation in Identified in Mouse ESCs

In addition to the expanded validation of I. Adams computational approach for reanalysing microarray data to study changes in repetitive element expression, these experiments have also led to the identification of HDAC1 as a regulator of retrotransposon expression in mouse ESCs. The HDAC family of histone deacetylases have previously been implicated in retrotransposon expression in some cell lines (Brunmeir et al., 2010; Garcia-Perez et al., 2010; Yang and Seto, 2008) and HDAC1 has been demonstrated to repress the expression of avian retroviral LTRs in HeLa cells (Poleshko et al., 2008, 2010). The microarray reanalysis discussed in this chapter extends these findings by identifying *RLTR45* and *IAP* as LTR retrotransposons regulated by HDAC1 in mouse ESCs. Interestingly, while *RLTR45* is upregulated in mouse ESCs in the absence of HDAC1, the opposite was found to be true of *IAP*, with reduced expression in *Hdac1*$^{-/-}$ ESCs. Analysis of HDAC1 ChIP-seq mouse ESC data suggests that HDAC1 is recruited to *RLTR45* loci to silence this element directly, but *IAP* however does not recruit HDAC1 and is therefore likely to be regulated by HDAC1 indirectly. The downregulation of *IAP* expression observed in *Hdac1*$^{-/-}$ mouse ESCs though contrasting to the response of retrotransposons to HDACs in other systems (Brunmeir et al., 2010; Garcia-Perez et al., 2010; Poleshko et al., 2008, 2010; Yang and Seto, 2008), paralleled the behaviour of some endogenous genes in these ESCs (Zupkovitz et al., 2006). It will be of interest to determine whether the increased compensatory activity of HDAC2 in *Hdac1*$^{-/-}$ ESCs (Zupkovitz et al., 2006), or other misregulated factors, are responsible for the repression of *IAP* expression in the absence of HDAC1. Curiously, the expression of *LINE-1* elements was not altered in *Hdac1*$^{-/-}$ ESCs, which contrasts with HDAC1's role in the suppression of *LINE-1* element expression in neural stem cells (Muotri et al., 2010). Further experiments will be required to determine whether this difference reflects differences in chromatin environments in ESCs and somatic neural stem cells, or redundancy between multiple pathways acting to repress *LINE-1* activity in ESCs.

3.3.2 TEX19.1 Regulation of Reterotransposon Activity

J. Reichmann's finding that *MMERVK10C* elements, but not closely related retrotransposons such as *IAP,* are upregulated in *Tex19.1*$^{-/-}$ testes demonstrates that the sensitivity of related retrotransposons to particular regulatory mechanisms varies in the germline. It is possible that the difference in regulation of *IAP* and *MMERVK10C* are caused by the availability of transcriptional factors or by differences in the silencing mechanisms which target each of these elements. It does however appear unusual that a silencing mechanism is restricted to targeting repression of a single, relatively low-copy retrotransposon. Other germline genome defence genes identified are typically implicated in the silencing of far more prevalent multi-copy retrotransposons such as *LINE-1* and *IAP* (Crichton et al., 2013) which would be expected to pose a far greater threat to germ cell stability. Hypomethylation and expression of *Tex19.1* is initiated during the early wave of DNA methylation reprogramming in E8.5-9.5 embryonic germ cells (Hackett et al., 2012), long before the expression of the *MMERVK10C* transcripts identified in *Tex19.1*$^{-/-}$ testes in this study. It is possible that TEX19.1 plays a broader role in the regulation of more common retrotransposons at earlier stages of germ cell development, but additional levels of regulation may be employed to ensure their transcriptional repression in meiotic germ cells. Such a role for TEX19.1 is supported by the discovery of LINE-1 and IAP upregulation in *Tex19.1*$^{-/-}$ placenta (Reichmann et al., 2013). A caveat of this microarray-based approach to monitoring retrotransposon expression is that the insight gained is limited by the coverage of microarray probes mapping to repetitive elements. The coverage for LTR-retrotransposons such as *IAP* and *MMERVK10C* by the Illumina WG-6 v2.0 Beadarray used in the analysis of *Tex19.1*$^{-/-}$ is approximately 30% when compared to the Repeatmasker annotation of the mm9 assembly of the sequenced mouse genome (Reichmann et al., 2012). While this coverage is reasonable and appears sufficient to identify the majority of repetitive element expression changes, some changes may be overlooked and a greater degree of accuracy could be obtained by RNA-seq (Reichmann et al., 2012).

MMERVK10C is one of several related endogenous retroviruses known to be marked by SETDB1-deposited H3K9me3 in mESCs and to require this mark to suppress its transcriptional activity in this cell type (Karimi et al., 2011). The requirement of SETDB1 and its interaction partner KAP1 for embryonic viability has precluded the study of their involvement in germ cell development (Cammas et al., 2000; Dodge et al., 2004). It is possible that TEX19.1 is involved in regulating H3K9 trimethylation of *MMERVK10C*, however the very limited changes in expression profile in *Tex19.1*$^{-/-}$ testes (Ollinger et al.,

2008) and ESCs (Tarabay et al., 2013) indicates that the global loss of this repressive histone mark in the absence of TEX19.1 is unlikely. Reduced DNA methylation at retrotransposon sequences appears to be a major factor driving their upregulated expression in other germline genome defence mutants (Crichton et al., 2013), however DNA methylation appears to play a minor role in the silencing of *MMERVK10C* at the DNA level (J. Reichmann unpublished) and the effect of other germline genome defence gene mutations on *MMERVK10C* has not been reported. Therefore the mechanism by which TEX19.1 represses *MMERVK10C* currently remains unclear.

3.3.3 Mechanism of Chromosome Asynapsis in *Tex19.1*$^{-/-}$ Spermatocytes

Where studied, chromosome asynapsis in spermatocytes is reported in all mice carrying mutations in germline genome defence genes (Crichton et al., 2013). The mechanism of this asynapsis however has not been investigated in detail. The increase in SPO11-independent DNA damage in *Mael*$^{-/-}$ spermatocytes which is observed in correlation with increased LINE-1 ORF1 protein (Soper et al., 2008) implies that DNA damage generated by increased retrotransposition events in spermatocytes might be responsible for the failure of chromosome synapsis. Heightened levels of DNA damage are also apparent in *Miwi2*$^{-/-}$ spermatocytes (Carmell et al., 2007), however it is currently unclear if this damage reflects unrepaired SPO11-dependent DSBs due to chromosome asynapsis, or an increase in SPO11-independent DNA damage as in *Mael*$^{-/-}$. By generating *Spo11*$^{-/-}$*Tex19.1*$^{-/-}$ mice I was able to immunocytologically assess the levels of SPO11-independent DNA damage generated in the absence of TEX19.1 in spermatocytes. This chapter demonstrates that in contrast to *Mael*$^{-/-}$ spermatocytes the level of SPO11-independent DNA damage is not increased in *Spo11*$^{-/-}$ *Tex19.1*$^{-/-}$ spermatocytes. This finding indicates that despite the increased presence of *MMERVK10C* transcripts in *Tex19.1*$^{-/-}$ spermatocytes (Ollinger et al., 2008; Reichmann et al., 2012), elevated DNA damage potentially reflecting retrotransposition events cannot be detected by this assay, and therefore may not be responsible for mediating the chromosome asynapsis exhibited. Alternatively, as *Spo11*$^{-/-}$ spermatocytes arrest during prophase it is possible that this arrest in *Tex19.1*$^{-/-}$*Spo11*$^{-/-}$ precedes the stage at which retrotransposition takes place in *Tex19.1*$^{-/-}$ single mutant spermatocytes, rendering these events undetectable by this approach. Further possibilities include a situation whereby MMERVK10C exploits endogenous DNA damage generated by SPO11 to integrate new copies into the genome, or retrotransposition events dependent on the MMERVK10C endonuclease are elevated in

response to genome-wide DNA damage, as has been observed for human LINE-1 in response to gamma-irradiation induced DNA damage in cultured cells (Farkash et al., 2006). However, consistent with the theory that meiotic retrotransposition is not involved in the prophase defects of *Tex19.1*$^{-/-}$ spermatocytes, antiretroviral drugs targeting reverse transcriptase which have previously been shown to rescue cardiac defects associated with retrotransposon activity in *Trex1*$^{-/-}$ mice (Beck-Engeser et al., 2011) were unable to rescue the meiotic chromosome asynapsis of *Tex19.1*$^{-/-}$ male mice following treatment. Unfortunately this experiment does feature the caveat that I was unable to assess the effectiveness of this drug treatment on reverse transcription in the testes despite attempting several approaches to do so. If retrotransposition is indeed not increased in *Tex19.1*$^{-/-}$ this would suggest that despite the increase in *MMERVK10C* transcript abundance, this element remains silenced post-transcriptionally. Retrotransposons being the cause of the chromosome asynapsis remains a possibility even in the absence of increased retrotransposition, as increased retrotransposon protein levels may disrupt the cellular environment. Indeed, proteins encoded by human LTR retrotransposons physically interact with endogenous transcription factors present in germ cells and are capable of disrupting spermatogenesis when ectopically expressed in mice (Denne et al., 2007; Galli et al., 2005; Kaufmann et al., 2010). A further possibility is that an altered chromatin modification landscape which leads to retrotransposon expression in many germline genome defence gene mutants, causes chromosome asynapsis independent of expression changes by directly influencing the chromatin structure and ability of chromosomes to pair. This possibility will be discussed more fully in chapter 4.

Chapter 4:

Investigating the Cause of Homologous Chromosome Asynapsis in *Tex19.1*$^{-/-}$ Spermatocytes

4 Investigating the Cause of Homologous Chromosome Asynapsis in *Tex19.1*$^{-/-}$ Spermatocytes

4.1 Introduction

The aim of the work presented in this chapter was to better understand the mechanism by which homologous chromosomes fail to synapse in *Tex19.1*$^{-/-}$ pachytene spermatocytes through studying relevant key events in these mutant spermatocytes during the preceding stages of meiosis. Chromosome synapsis and meiotic recombination are two interconnected and fundamental processes which take place in parallel during meiotic prophase I and are vital for the success of this specialised cell division. Homologous chromosome pairing by recombination is initiated by the formation of hundreds of double stranded DNA breaks (DSBs) across the genome by the endonuclease SPO11 in leptotene (Baudat et al., 2000; Moens et al., 2002; Romanienko and Camerini-Otero, 2000), with particular enrichment at hotspots marked by PRDM9-dependent H3K4 trimethylation (Baudat et al., 2013; Brick et al., 2012; Smagulova et al., 2011). The formation of these breaks triggers phosphorylation of the histone variant H2AX (γH2AX), which spreads in diffuse clouds through chromatin surrounding DSBs, and is followed by the resection of DNA at the break site to generate a 5' ssDNA overhang (Figure 4-3) (Baudat et al., 2013). The ssDNA-binding protein RPA localises to break sites in addition to the recombinases RAD51 and its meiotic homologue DMC1, which promote a search for the homologous partner of the damaged chromosome, the invasion of the damaged strand and joint molecule formation with this partner (Baudat et al., 2013; Handel and Schimenti, 2010). The homologous interactions established at DSBs are stabilised by the recruitment of successive proteins including MSH4 and MSH5 which replace RAD51 and DMC1 (Her et al., 2007; de Vries et al., 1999), and the DNA damage is ultimately repaired in pachytene while homologous autosomes are completely synapsed. γH2AX domains become more restricted towards pachytene and are lost as DSBs are repaired (Chicheportiche et al., 2007). Failure to generate DSBs, to perform a homology search or to stabilise homologous interactions by recombination results in meiotic chromosome asynapsis and often also results in non-homologous interactions (Mahadevaiah et al., 2008).

The synaptonemal complex (SC) provides a structure around which the events of recombination are orchestrated. The axial element (AE) (composed of SYCP3, SYCP2) forms along the length of each homologous chromosome, anchoring chromatin loops and

colocalising with proteins involved in recombination. AE formation begins in leptotene, with the formation of short filaments, before extending along the length of chromosomes in zygotene. Chromosome synapsis also begins during zygotene, with central element (CE) (SYCP1, SYCE1, SYCE2, SYCE3, TEX12) formation between AEs of paired chromosomes bringing chromosomes into close proximity and stabilising their interaction (Fraune et al., 2012). Complete synapsis between autosomes is achieved in pachytene, and in spermatocytes synapsis between the X and Y chromosomes is limited to the pseudoautosomal region (PAR). Mutant spermatocytes lacking individual components of the SC initiate recombination and homologous chromosomes pair, however synapsis is defective and DSBs are unable to repair (Fraune et al., 2012). Therefore both defects in recombination and SC formation can result in defective meiotic chromosome synapsis. The precise nature of synapsis defects in meiotic mutants bears distinctions depending on the cause; with SC defects resulting in homologous pairing in the absence of synapsis, but recombination defects resulting in failed homologous pairing and abnormal non-homologous interactions. The mechanism of chromosome asynapsis in mutant spermatocytes can also be caused by a combination of defective SC formation and defective recombination, as proteins have been identified which influence both of these processes (Daniel et al., 2011).

Immunocytology is a valuable technique for the study of both SC formation and the progression of recombination in mouse spermatocytes, and this approach forms the majority of my investigation in this chapter. *Tex19.1*$^{-/-}$ spermatocytes appear to construct a normal AE with the recruitment of SYCP3, and partial CE formation is observed by the localisation of SYCP1 between portions of proximal AEs (Ollinger et al., 2008). Defective homologous chromosome synapsis in pachytene is the earliest meiotic defect currently reported to occur in *Tex19.1*$^{-/-}$ spermatocytes (Ollinger et al., 2008). Incomplete synapsis was seen in around half (47%) of pachytene *Tex19.1*$^{-/-}$ spermatocytes and unsynapsed chromosomes did not appear to be homologously paired. Rather, incompletely synapsed chromosomes were seen to form chains linked by apparent non-homologous synapsis (Ollinger et al., 2008). Previous immunocytological analysis of *Tex19.1*$^{-/-}$ spermatocytes revealed the presence of γH2AX and RAD51 at unsynapsed chromosome arms, indicating the presence of unrepaired DNA double strand breaks (DSBs) (Ollinger et al., 2008). The absence of additional SPO11-independent DNA damage in spermatocytes lacking TEX19.1 reported in the previous chapter (Figure 3-8) suggests that the unrepaired DNA damage in asynapsed *Tex19.1*$^{-/-}$ pachytene spermatocytes is generated by SPO11. Therefore recombination is initiated at some DSB sites in *Tex19.1*$^{-/-}$ spermatocytes by the formation of SPO11-dependent DSBs and the persistence of damage in unsynapsed regions is consistent with impaired chromosome

synapsis preventing repair (Ollinger et al., 2008). From this evidence, the meiotic defect responsible for causing the failure of chromosome synapsis in *Tex19.1*$^{-/-}$ is not clear. Pachytene asynapsis is also a shared and poorly understood feature of other male mouse germline genome defence mutants, indicating the possibility of a shared cause relating to retrotransposon upregulation (Crichton et al., 2013). In this chapter I thoroughly investigate the meiotic events preceding the pachytene-stage asynapsis of *Tex19.1*$^{-/-}$ spermatocytes to better understand the mechanism by which it arises.

4.2 Results

4.2.1 Assessing the Nature of Asynapsed Chromosomes in *Tex19.1*$^{-/-}$ Spermatocytes

The mechanism by which chromosome synapsis becomes impaired in *Tex19.1*$^{-/-}$ spermatocytes is not known. I began by investigating the nature of the chromosome asynapsis present to indicate likely mechanisms involved in its generation. Other mouse mutants with chromosome asynapsis are typically defective in one or both of the two main processes responsible for promoting meiotic chromosome synapsis: synaptonemal complex (SC) formation and recombination. The arrangement of asynapsed chromosomes in these two varieties of mutant pachytene spermatocyte is distinct, with SC mutants pairing chromosomes with similarly sized partners (presumably homologs) but failing to synapse or only synapsing partially, and recombination mutants failing to pair homologous chromosomes and often forming some aberrant non-homologous synapsis (Baudat et al., 2013; Fraune et al., 2012; Mahadevaiah et al., 2008). Non-homologous synapsis in *Tex19.1*$^{-/-}$ spermatocytes was mentioned in a previous report in outbred mice but has not been assessed in detail. I performed combined antibody staining for AE and CE components SYCP3 and SYCP1 respectively and assessed the organisation of chromosomes within *Tex19.1*$^{-/-}$ spermatocytes to investigate whether this resembles mutants defective in SC formation or recombination. This analysis was conducted on mice crossed three times back to C57BL/6 to reduce genetic variation. Mice backcrossed a minimum of 3 times were also used for all subsequent analysis of *Tex19.1*$^{-/-}$ spermatocytes discussed.

SYCP3 forms a continuous axis along the length of each homologous chromosome, marking the AE, and SYCP1 signal co-localises with the SYCP3 signal at synapsed chromosomal portions in pachytene (Figure 4-1A). In control pachytene sypermatocytes 19 pairs of synapsed autosomes are recognisable as 19 distinct axes with SYCP3 and SYCP1 signal co-localisation, and the partially synapsed XY chromosomes can be seen by their separate AEs paired and co-localising with a short filament of SYCP1 signal at the terminal PAR where they share homology and synapse (Figure 4-1A). During a masters research project I re-assessed the frequency of pachytene spermatocytes containing asynapsed autosomes in backcrossed *Tex19.1*$^{-/-}$ mice as well as heterozygous and wild type controls. Asynapsed pachytene nuclei were identified as spermatocytes with fully-formed AEs indicated by continuous SYCP3 filaments associating with chromosomes, complete synapsis

of at least one autosome pair to indicate progression to pachytene by the co-localisation of SYCP1 and SYCP3 signals along the length of an axis, and the presence of autosomal AEs failing to co-localise with SYCP1 (Figure 4-1A). I observed asynapsed autosomes in 65% of *Tex19.1*$^{-/-}$ spermatocytes and 13% of controls ($p<0.001$, Fisher's exact test, n=153, 164 respectively). This finding is comparable to the ~50% asynapsis previously reported in *Tex19.1*$^{-/-}$ outbred male mice (Ollinger et al., 2008). During my PhD I next performed a more in-depth analysis of the behaviour of asynapsed chromosomes in *Tex19.1*$^{-/-}$ pachytene spermatocytes. Nuclei were scored for the presence of "paired chromosomes" which were adjacent but not synapsed, and "partially synapsed" chromosomes of similar length, both of which are features commonly observed in mutants with defective ability to construct the SC (Fraune et al., 2012). Nuclei were also scored for the presence of "isolated chromosomes" with no clear interaction or synapsis with any other chromosome, and "non-homologous synapsis" between two or more axes of differing size and/or differing position along axes, both of which are common features of recombination-defective meiosis. No chromosomes paired adjacent to their partner but still lacking synapsis were observed in asynapsed *Tex19.1*$^{-/-}$ pachytene spermatocytes (n=62), suggesting that inability to construct the SC is not the primary cause of the asynapsis. Partially synapsed chromosomes were occasionally observed and this may indicate a slight reduction in the ability of chromosomes to synapse, however this feature was almost always observed in combination with isolated chromosomes and/or non-homologous synapsis (Figure 4-1B). The presence of isolated and/or non-homologously synapsed chromosomes in 98% of asynapsed *Tex19.1*$^{-/-}$ pachytene spermatocytes (Figure 4-1B) strongly indicates that the ability of chromosomes to successfully pair by homologous recombination is defective.

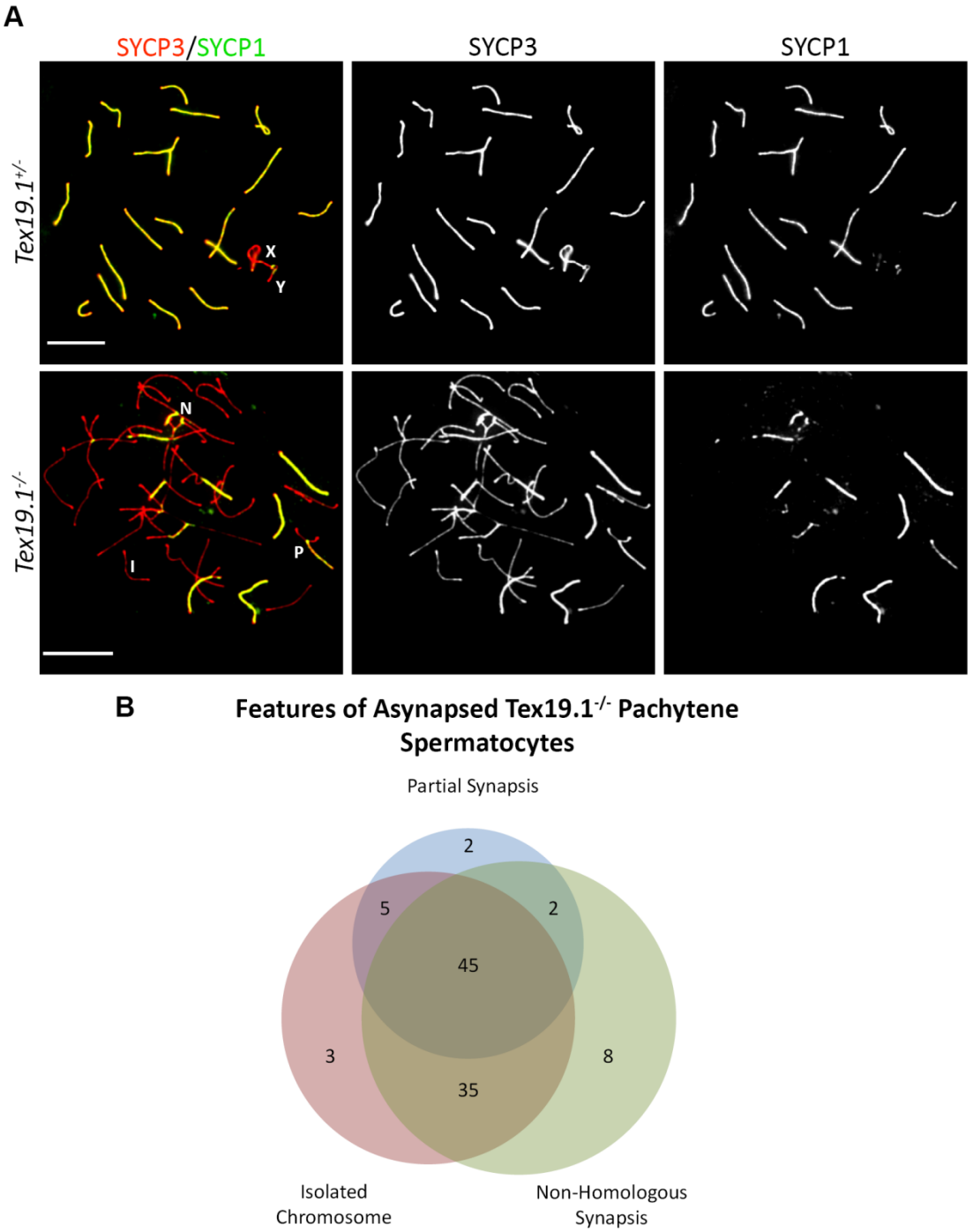

Figure 4-1. Chromosome asynapsis in *Tex19.1*$^{-/-}$ pachytene spermatocytes
(A) Pachytene spermatocytes from *Tex19.1*$^{+/-}$ and *Tex19.1*$^{-/-}$ mice, stained with AE marker SYCP3 (red) and CE marker SYCP1 (green). Genotype indicated in top left corner of merge image. Co-localisation of SYCP3 and SYCP1 indicates synapsis. "X" and "Y" indicates the partially synapsed XY chromosomes in control spermatocytes. "I" indicates a representative isolated chromosome, "P" a partially synapsed pair of homologous chromosomes, and "N" an example of non-homologous synapsis seen in asynapsed *Tex19.1*$^{-/-}$ pachytene spermatocytes. Merges and single channel images displayed. 10µm scale bars. (B) Venn diagram displaying the percentage of asynapsed *Tex19.1*$^{-/-}$ spermatocytes with individual or combinations of chromosomal features indicated (n=62).

Although the configuration of asynapsed chromosomes in *Tex19.1*$^{-/-}$ spermatocytes indicates that meiotic recombination is defective, additional subtle SC formation defects remain a possibility in this mutant. To test whether the ability of the SC to form is also impaired in *Tex19.1*$^{-/-}$ spermatocytes, I next assessed SC formation in the absence of meiotic recombination. *Spo11*$^{-/-}$ spermatocytes are unable to form the DNA double strand breaks (DSBs) which initiate meiotic recombination, and as such are defective in the pairing of homologous chromosomes (Baudat et al., 2000; Romanienko and Camerini-Otero, 2000). Although the meiotic homology search is defective in *Spo11*$^{-/-}$ spermatocytes, chromosomes still construct an AE and fragments of SC are formed between some chromosomes by the establishment of the CE, likely to largely indicate non-homologous synapsis. The frequency of these SC fragments has been used in combination with other mutations to indicate the ability of the SC to form independently of recombination (Daniel et al., 2011). I assessed the frequency of complete SC filaments demonstrated by co-localisation of SYCP3 and SYCP1 antibody staining in *Spo11*$^{-/-}$ single knockout and *Tex19.1*$^{-/-}$*Spo11*$^{-/-}$ double knockout spermatocytes (Figure 4-2A). Only spermatocytes in a zygotene-like stage were scored in this analysis: spermatocytes with fully formed AE indicated by unbroken axial SYCP3 staining on each chromosome. A similar number of SC fragments were formed in the *Spo11*$^{-/-}$ single knockout and *Spo11*$^{-/-}$*Tex19.1*$^{-/-}$ double knockout spermatocytes analysed ($p=0.35$, Mann-Whitney U test) (Figure 4-2B). Therefore in the absence of recombination the ability of SC formation to initiate is not affected by TEX19.1. Thus, chromosome asynapsis in *Tex19.1*$^{-/-}$ spermatocytes is likely to be primarily caused by defective homologous pairing of chromosomes by meiotic recombination, rather than defective SC formation.

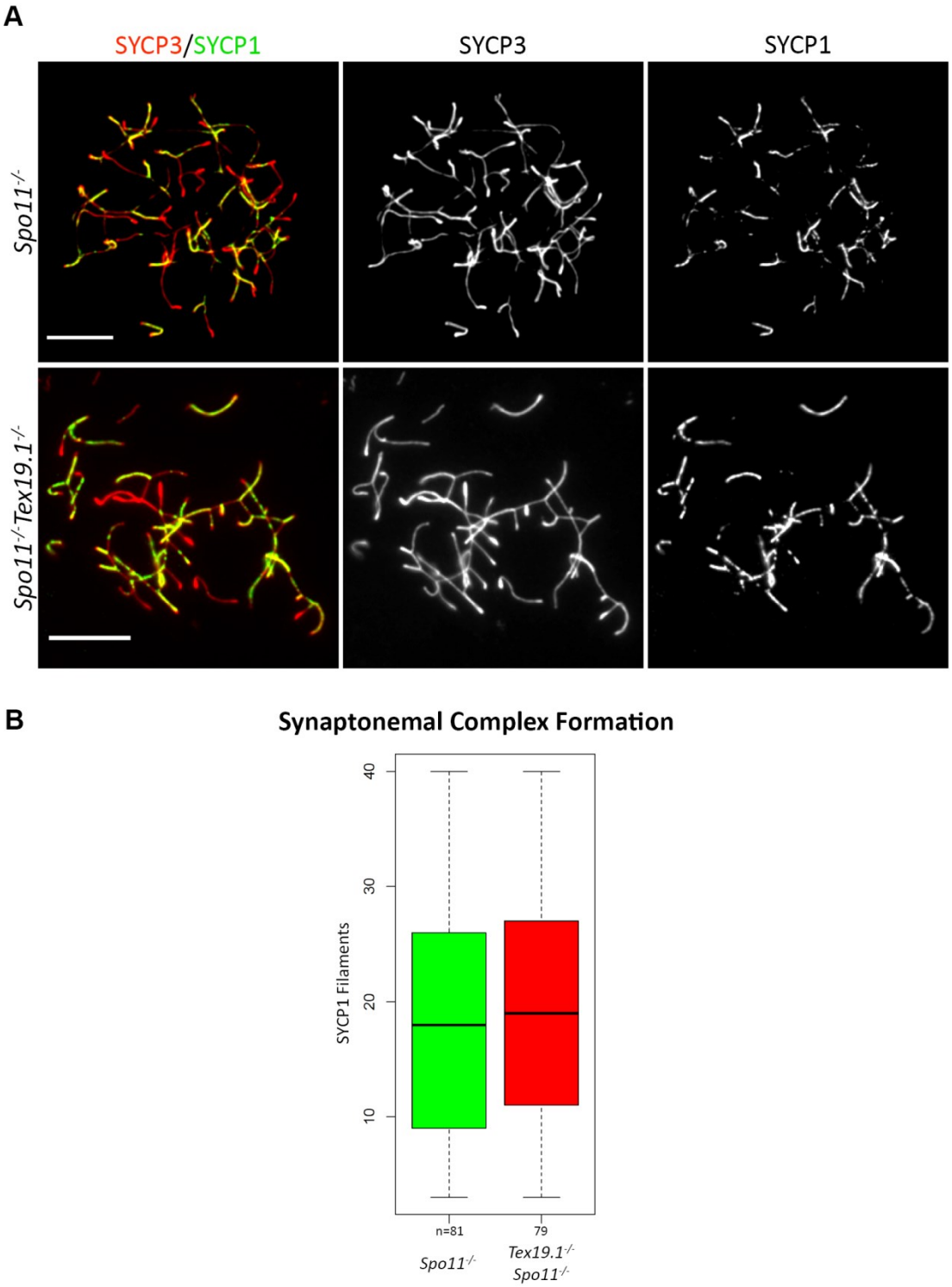

Figure 4-2. Synaptonemal complex formation in recombination-deficient spermatocytes
(A) Synaptonemal complex formation was assessed in *Spo11*$^{-/-}$ and *Spo11*$^{-/-}$*Tex19.1*$^{-/-}$ spermatocytes stained with antibodies against AE and CE proteins SYCP3 (red) and SYCP1 (green) respectively. Colocalisation of SYCP3 and SYCP1 staining patterns indicates synapsis. Merges and single channel images displayed. 10µm scale bars. (B) Box-plot displaying the frequency of synaptonemal complex formation between chromosomes in *Spo11*$^{-/-}$ single knockout and *Spo11*$^{-/-}$*Tex19.1*$^{-/-}$ double knockout zygotene-like spermatocytes.

4.2.2 Investigating the Recruitment of Early Recombination Proteins in *Tex19.1*$^{-/-}$ Spermatocytes

The meiotic homology search is largely driven by recombination. To investigate whether *Tex19.1* deletion influences meiotic recombination, and to search for recombination defects in these mutant spermatocytes which might be responsible for causing chromosome asynapsis, I next assessed the localisation of early recombination proteins in *Tex19.1*$^{-/-}$ spermatocytes. I began by investigating recombination protein localisation in zygotene by antibody staining as this is the latest meiotic stage before synapsis defects become apparent in *Tex19.1*$^{-/-}$ spermatocytes. I identified zygotene nuclei in this analysis by AE staining with an antibody against SYCP3, and CE staining using an antibody to SYCE2. Zygotene spermatocytes possess long, thin AEs which appear to be fully formed and have begun to synapse, as indicated by colocalisation with filaments of SYCE2 staining (Figure 4-4A-C). Having bound to DSBs shortly after their formation in leptotene, the ssDNA binding protein RPA and recombinases RAD51 and DMC1 remain localised to chromosome axes in zygotene, when they peak in abundance, and can be recognised on chromosome spreads as focal points of antibody staining which co-localise with SYCP3 (Figure 4-3, Figure 4-4A). The frequency of these foci rises and falls with DSB formation and progression of recombination respectively (Moens et al., 2002). As expected, antibody staining for RPA, RAD51 and DMC1 produced numerous axis-associated foci in *Tex19.1*$^{+/+}$ and *Tex19.1*$^{+/-}$ control mice (on average 217 RPA, 174 DMC1 and 116 RAD51 foci). The frequency of RPA foci observed in control zygotene spermatocytes is similar to the 150-250 foci range previously reported, as is the frequency of RAD51 and DMC1 foci, which are reported to range between 100 and 250 (Figure 4-4B) (Moens et al., 2002). RAD51 and DMC1 are thought to dissociate from DSBs earlier than RPA during zygotene, hence their foci are less abundant at this stage (Moens et al., 2002). Counts of DMC1 and RAD51 foci are often similar within control spermatocytes, however the frequency of RAD51 foci in this study is less than that of DMC1. This may reflect a genuine difference in protein localisation or alternatively a drawback to the analysis such as low sensitivity of the RAD51 antibody to its target antigen, or reduced ability to detect genuine signal due to higher levels of non-specific background signal which was a feature of staining with this antibody.

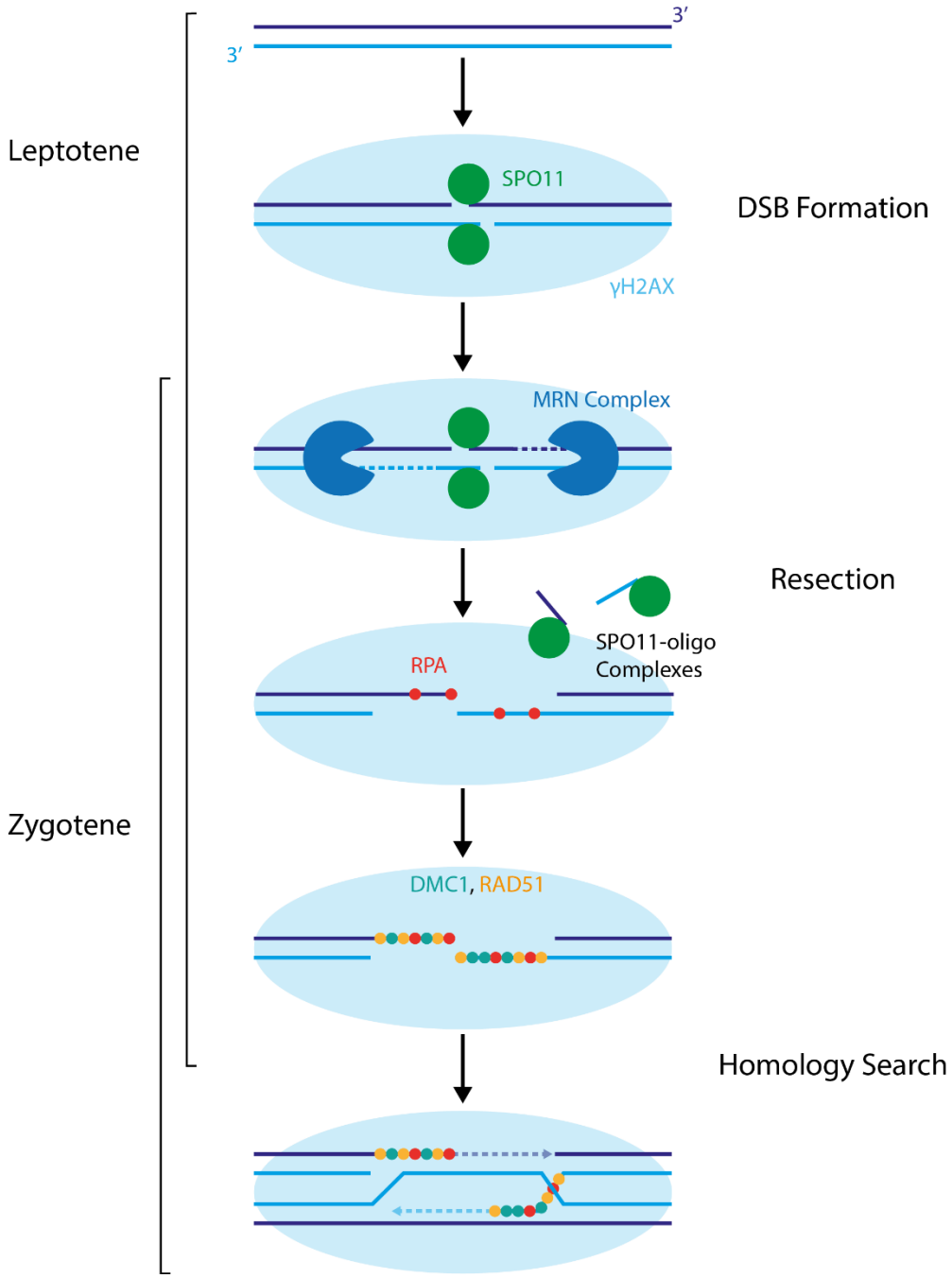

Figure 4-3. Timing of early meiotic recombination protein recruitment
Schematic displaying the formation of DNA DSBs by SPO11 dimers during leptotene, resection by the MRN complex to release SPO11-oligonucleotiude complexes and subsequent recruitment of ssDNA binding protein RPA and recombinases RAD51 and DMC1 to the resected DNA at the break site to promote the meiotic homology search and strand invasion. Precise organisation of this combination of proteins on ssDNA is not specified. For simple representation γH2AX is shown as a cloud similar to than observed cytologically, rather than as molecules bound to the DNA. Temporal dynamics of RPA localisation are based on observations made within this chapter. Dashed arrows indicate the direction of DNA synthesis to repair the DNA damage using the homologous partner DNA as a template.

Scoring antibody staining for recombination proteins in *Tex19.1*$^{-/-}$ zygotene spermatocytes revealed no significant difference in the level of RPA foci when compared with controls (mean = 203 foci, p= 0.2, Mann-Whitney U test). Assessment of the frequency of RAD51 and DMC1 foci however reveals a modest but significant reduction, with a 13% reduction in DMC1 foci (p=0.008, Mann-Whitney U test) and a 33% reduction in RAD51 (p<0.001, Mann-Whitney U test) (Figure 4-4D). This reduction reveals abnormalities in meiotic recombination in *Tex19.1*$^{-/-}$ spermatocytes. It has been proposed that RPA binds to DSBs before the localisation of RAD51 and DMC1, and after their dissociation, but not during their binding (Yang et al., 2008). However, if RPA foci are marking all early DSBs regardless of DMC1/RAD51 binding in this analysis, then unchanged RPA foci frequency in *Tex19.1*$^{-/-}$ spermatocytes at this stage suggests that normal levels of DSBs are present in these spermatocytes. This possibility will be further discussed shortly.

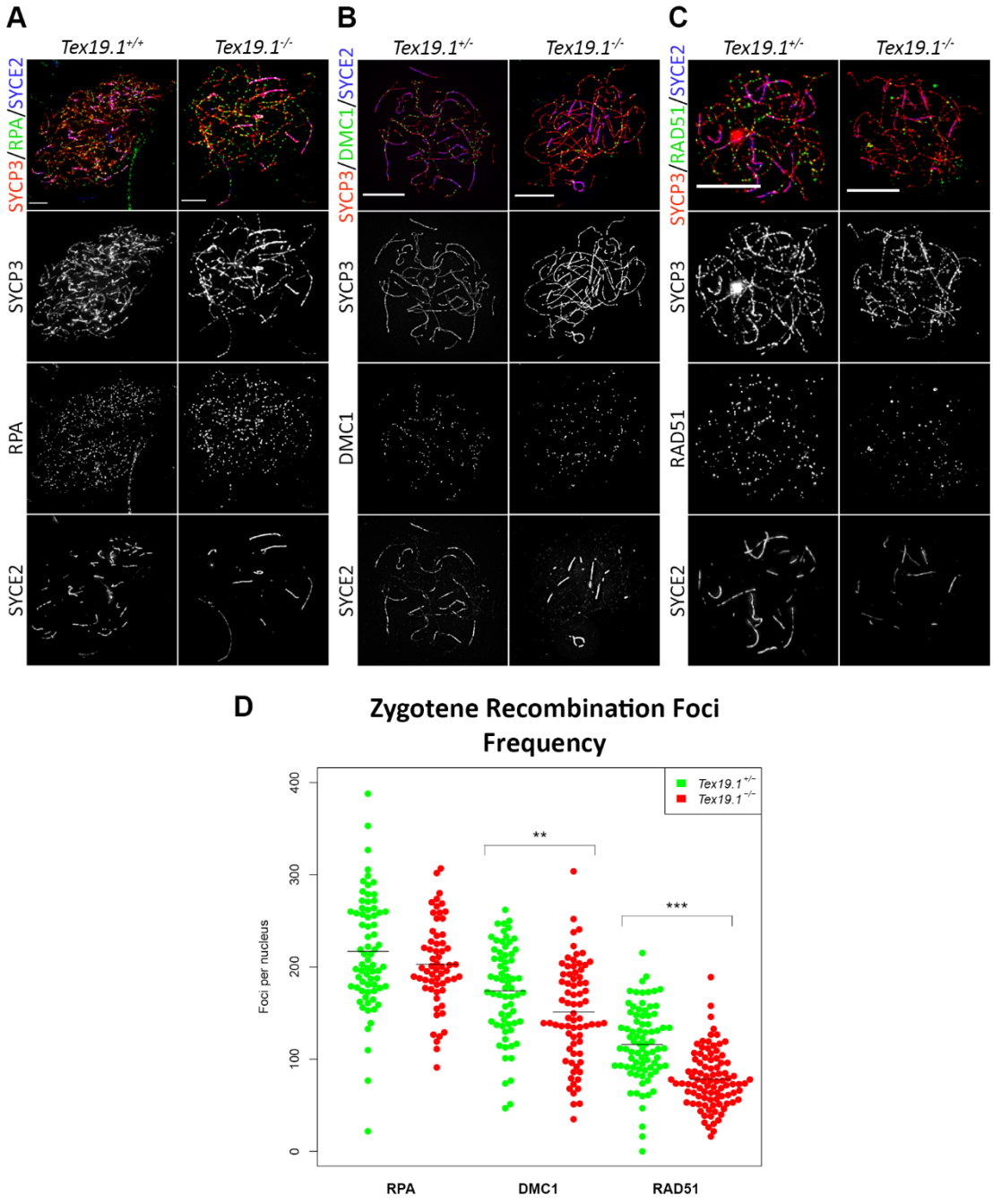

Figure 4-4. Early recombination protein localisation in zygotene spermatocytes
Representative antibody staining patterns of RPA, DMC1 and RAD51 proteins in control and *Tex19.1*$^{-/-}$ zygotene spermatocytes (A, B, C respectively – recombination protein in green channel), combined with antibody staining of SYCP3 (red) and SYCE2 (blue) to mark the axial element and central element of the synaptonemal complex respectively. Merges and single channel images displayed. 10µm scale bars. (D) Beeswarm plots displaying the frequency of axial recombination foci in each nucleus scored (plotted points) as well as the mean frequency (indicated by black bars). N=71, 61, 66, 73, 81, 93, and mean foci=217, 203, 174, 151, 116, 78 from left to right across the plot. Foci counts were compared between controls and knockout spermatocytes using a Mann-Whitney U test ($p=0.2$, $p=0.008$, $p<0.001$ respectively), asterisks denote significance.

To further investigate the recombination defect in *Tex19.1*$^{-/-}$ meiosis, I assessed the same early recombination proteins by antibody staining as previously, now in leptotene spermatocytes. Again, spermatocytes were stained with antibodies against SYCP3 and SYCE2 to mark the AE and CE. Leptotene nuclei are beginning to construct the AE and can be identified by the presence of numerous short SYCP3 fragments and the absence of SYCE2 as axes have not yet begun to synapse (Figure 4-5A-C). The foci formed by recombination proteins localise to these AE fragments during this stage. As before, I counted the frequency of RPA, RAD51 and DMC1 foci co-localising with the AE in leptotene spermatocytes. Control leptotene spermatocytes were found to have an average of 108 DMC1 foci, and 97 RAD51 foci, similar to figures widely reported at this stage (Figure 4-5D) (Cole et al., 2012; Moens et al., 2002; Roig et al., 2010). Slightly exceeding the frequency of foci formed by these proteins, an average of 133 RPA foci was observed at this stage in control spermatocytes (Figure 4-5D). Previous reports of RPA foci frequency have typically been lower than RAD51 and DMC1 during leptotene (Moens et al., 2002; Roig et al., 2010), however RPA has been shown to be capable of forming DSB-associated foci at this stage in the absence of RAD51 and DMC1 (Sharan et al., 2004; Yang et al., 2008). This inconsistency with previous analyses of RPA may reflect high sensitivity of the antibody being used here or the method by which the chromosome spreads were prepared, and appears to reveal RPA remaining bound to ssDNA at DSBs also associating with RAD51 and DMC1 as previously speculated. As antibodies used to stain RPA, RAD51 and DMC1 here are all derived from rabbits it was not possible to perform co-staining to test their co-localisation.

Antibody staining in *Tex19.1*$^{-/-}$ leptotene spermatocytes revealed a large reduction in the frequency of foci formed by all three recombination proteins. RPA foci were reduced by 38%, DMC1 foci were reduced by 70%, and RAD51 foci were reduced by 40% ($p<0.001$ for RPA, RAD51 and DMC1 foci reductions, Mann-Whitney U test) (Figure 4-5D). This dramatic reduction reveals a severe defect in the early stages of meiotic recombination in *Tex19.1*$^{-/-}$ spermatocytes. RPA is a ssDNA binding protein, therefore the reduction in the frequency of RPA foci at this stage may indicate the presence of a reduced level of resected DSBs processed to generate ssDNA (Figure 4-3). The similarly large reduction in RAD51 and DMC1 foci in leptotene *Tex19.1*$^{-/-}$ spermatocytes is consistent with this. This analysis reveals that *Tex19.1*$^{-/-}$ spermatocytes are profoundly defective in meiotic recombination, with early recombination proteins failing to localise to axes at normal levels.

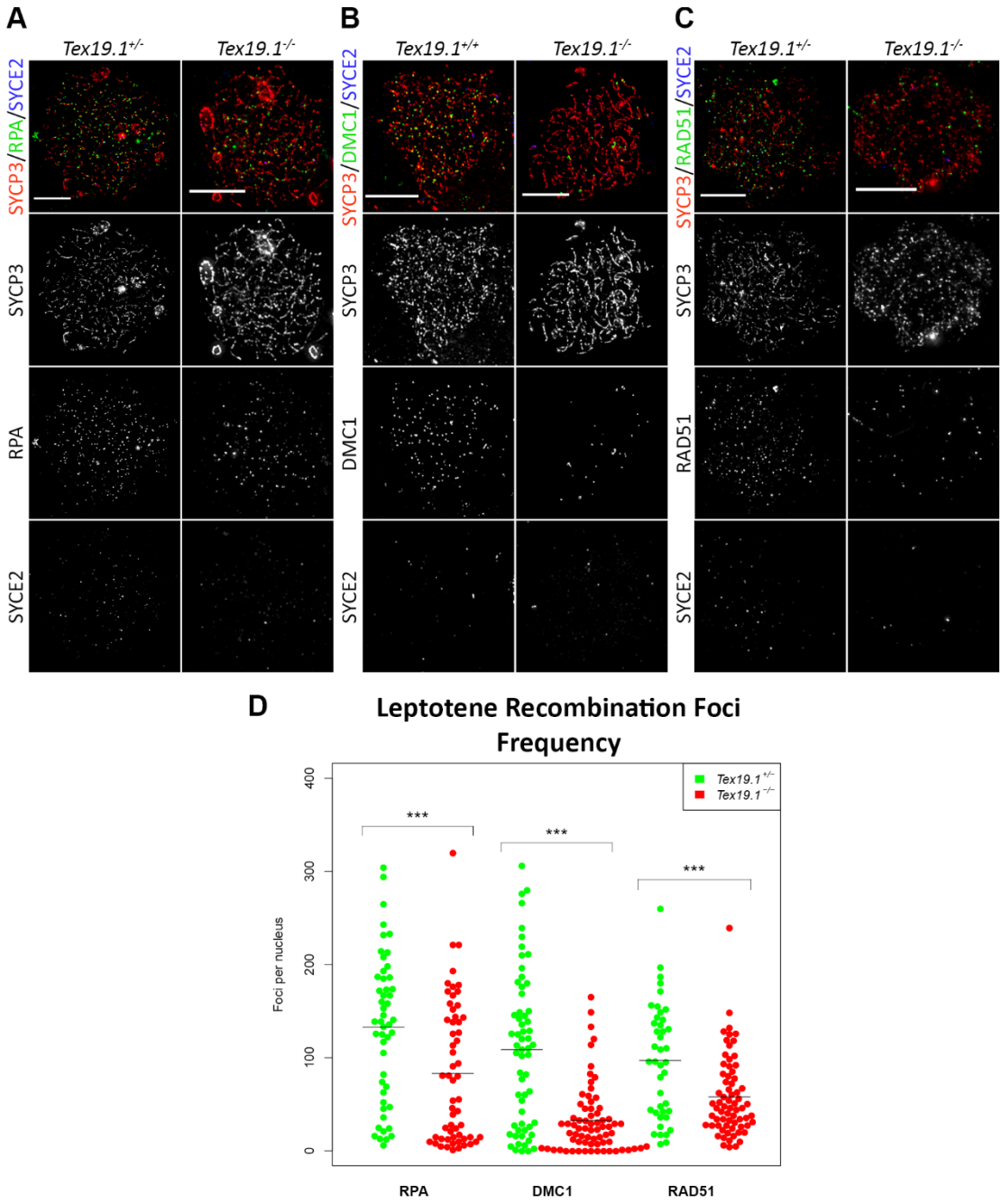

Figure 4-5. Early recombination protein localisation in leptotene spermatocytes
Representative antibody staining patterns of RPA, DMC1 and RAD51 proteins in control and *Tex19.1*$^{-/-}$ leptotene spermatocytes (A, B, C respectively – recombination protein in green channel), combined with antibody staining of SYCP3 (red) and SYCE2 (blue) to mark the axial element and central element of the synaptonemal complex respectively. Merges and single channel images displayed. 10µm scale bars. (D) Beeswarm plots displaying the frequency of axial recombination foci in each nucleus scored (plotted points) as well as the mean frequency (indicated by black bars). N=50, 58, 61, 71, 42, 69 and mean foci=133, 83, 108, 32, 97, 58 for categories from left to right across plot. Foci counts were compared between control and knockout leptotene spermatocytes using a Mann Whitney U test ($p<0.001$ for all). Asterisks indicate significance.

4.2.3 Assessing DNA Double Strand Break Processing in *Tex19.1*$^{-/-}$

The large reduction in early recombination protein foci in *Tex19.1*$^{-/-}$ spermatocytes could reflect reduced DSB frequency, altered binding of these proteins caused by defects in the processing of DSBs and their preparation for recombination protein binding, or defects in the loading of these proteins to the DSB. I first investigated whether the processing of DSBs upstream of recombination binding was defective in *Tex19.1*$^{-/-}$ spermatocytes. RPA, RAD51 and DMC1 localise to DSBs by binding to ssDNA generated at break sites (Figure 4-3) (Baudat et al., 2013). Resection of DNA to reveal ssDNA at DSBs by the MRN complex is likely to be essential to generate a substrate for the recruitment of RPA, RAD51 and DMC1 during the early stages of mouse meiotic recombination (Baudat et al., 2013; Kidane et al., 2010). Therefore defective DSB resection in *Tex19.1*$^{-/-}$ spermatocytes may be responsible for the reduction in early recombination foci observed in leptotene. Following the formation of meiotic DSBs by SPO11, this protein remains covalently bound to DNA at the break site until resection takes place, releasing SPO11 in a complex with a short oligonucleotide (oligo) fragment from this site (Figure 4-3) (Neale et al., 2005). To assess the level of resected SPO11-mediated DSBs which might be capable of binding RPA, RAD51 and DMC1 I measured the level of SPO11-oligo complexes produced in *Tex19.1*$^{-/-}$ leptotene spermatocytes. Following a technique developed by the laboratory of S. Keeney (Pan and Keeney, 2009) I immunoprecipitated SPO11 from 11dpp testis extracts, the time-point around which mouse spermatocytes are first entering leptotene (Bellvé et al., 1977) and the detectable production of SPO11-oligo complexes begins (Lange et al., 2011). Testes were taken at this age because my analysis of zygotene *Tex19.1*$^{-/-}$ spermatocytes suggested that normal levels of resected DSBs are present in this later meiotic stage, as normal levels of RPA foci can be seen (Figure 4-4B). Immunoprecipitated SPO11-oligos were detected by radiolabelling, and the level of complexes compared between control and *Tex19.1*$^{-/-}$ mice by separation with electrophoresis and subsequently imaging (Figure 4-6). This experiment was performed in duplicate and reaction products were separated by electrophoresis for different lengths of time, with one repeat achieving greater band separation (Figure 4-6A and B). Negative control reactions were performed using control 11dpp testes lysates and involving a pull-down using beads lacking SPO11 antibody. A consistent band was seen in negative controls at around 75kD as has been previously reported and is thought to be due to impurities present in the TdT enzyme used in the labelling reaction (Pan and Keeney, 2009). A further band around 70kD was also recognised specifically in the SPO11 antibody-positive test lanes and not in the negative control in one run of reaction products with greater

separation (Figure 4-6A). This second band was also detected in reactions using generic IgG antibodies and lacking testes lysate and thus appears to indicate non-specific labelling of antibodies used (data not shown). A SPO11 pull-down-specific band was detectable between 47-59kD in *Tex19.1*$^{+/+}$ lysates and not in negative controls, consistent with the size expected for SPO11-oligo complexes (Figure 4-6) (Pan and Keeney, 2009). This therefore indicates the successful resection of meiotic DSBs in *Tex19.1*$^{+/+}$ 11dpp testes. A band of this size was not detected in reactions using *Tex19.1*$^{-/-}$ testis lysates, demonstrating a large reduction in the level of SPO11-oligo complexes present in *Tex19.1*$^{-/-}$ 11dpp testes (Figure 4-6). Therefore this analysis indicates that TEX19.1 is required for normal levels of resected SPO11-dependent DSBs in leptotene spermatocytes. Thus it is likely that the reduced formation of foci by recombination proteins in *Tex19.1*$^{-/-}$ leptotene spermatocytes is due to a reduction in available resected ssDNA with which to bind, rather than a defect in the binding ability of these proteins per se.

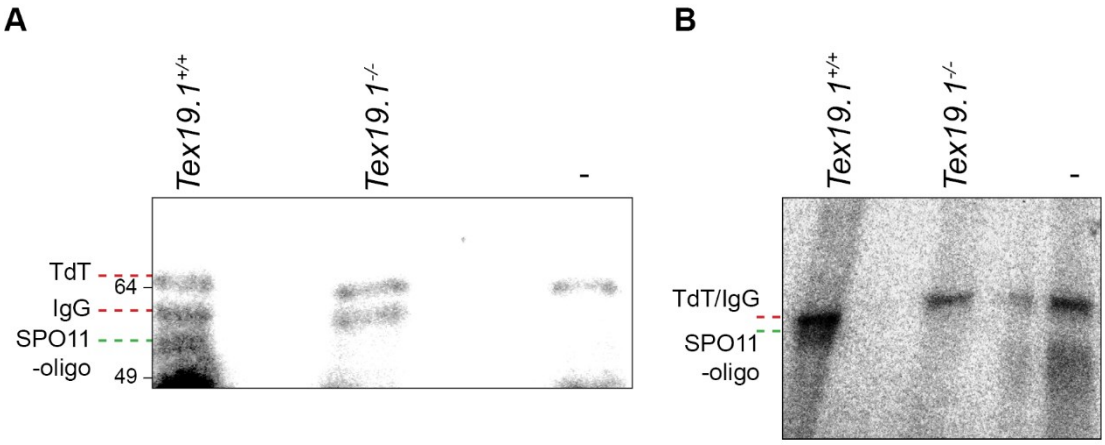

Figure 4-6. SPO11-oligonucleotide complex assessment
Two repeats (A, B) of radiolabelled SPO11-oligonucleotide complexes from *Tex19.1*$^{+/+}$ and *Tex19.1*$^{-/-}$ 11dpp testes lysates. Negative control ("-") run using *Tex19.1*$^{+/+}$ lysate and immunoprecipitation reaction followed in the absence of SPO11-antibody. SPO11-oligo complexes detectable around 55kDa in *Tex19.1*$^{+/+}$ but not *Tex19.1*$^{-/-}$ testes lysates (green dashed lines). Reaction products from repeat "A" were run for longer than repeat "B", leading to greater band separation. Non-specific bands marking TdT contaminants and apparent IgG labelling are indicated and can only be distinguished in repeat "A" (red dashed lines).

There is a large degree of overlap between the proteins involved in DSB repair in mitotic and meiotic cells, for example the MRN complex which is involved in DSB resection (Borde, 2007). As *Tex19.1* is also expressed in pluripotent and placental cells (Kuntz et al., 2008; Reichmann et al., 2013) I next investigated whether TEX19.1 might be required for the processing of DSBs formed in these mitotic cell types. I exposed two *Tex19.1*$^{-/-}$, one *Tex19.1*$^{+/-}$ and one *Tex19.1*$^{+/+}$ line of mouse embryonic stem cells (ESCs) generated by A.

Wilson to a range of levels of ionising radiation (IR) using X-ray exposure to generate DSBs, and monitored cell survival/proliferation (Krejci et al., 2012; McBurney et al., 2003). Cell survival of all genotypes tested was reduced with increasing levels of irradiation, but the degree of survival was not significantly different between wild-type E14 cells and any other genotype (Figure 4-7) (*Tex19.1*$^{+/-}$, *Tex19.1*$^{-/-}$_1 and *Tex19.1*$^{-/-}$_2, p=0.48, 0.89 and 0.52 respectively, t-test). Therefore the absence of TEX19.1 in ESCs does not affect the survival of cells following DSB formation by irradiation. Thus the requirement for TEX19.1 in DSB processing appears to be restricted to meiosis and does not extend to mitotic ESCs.

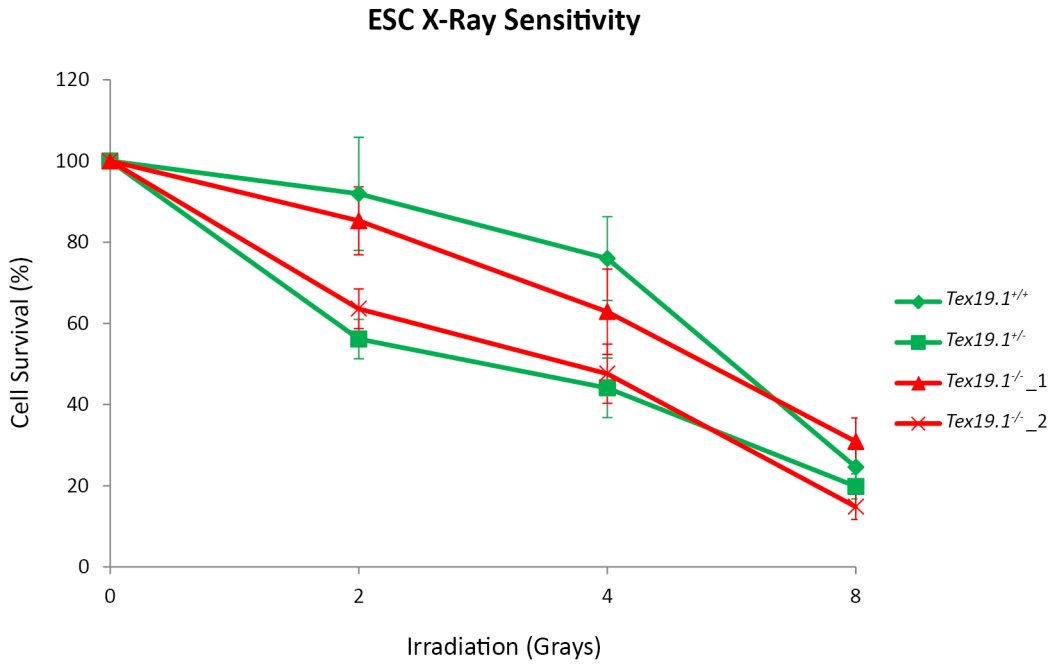

Figure 4-7. Embryonic stem cell sensitivity to DNA damage
Survival assay of embryonic stem cells following exposure to X-rays. Mean survival as a percentage of untreated cell frequencies plotted. Error bars indicate standard error. Genotype of cells assayed indicated in figure key. N=6.

4.2.4 Investigating DSB formation in *Tex19.1*$^{-/-}$

The reduced frequency of SPO11-oligo complexes and early recombination foci in *Tex19.1*$^{-/-}$ leptotene spermatocytes could be due to defective resection of the DSBs formed (Kidane et al., 2010), or this may be the result of an upstream defect in the formation of DSBs. To investigate whether the formation of DSBs in *Tex19.1*$^{-/-}$ spermatocytes appeared normal I investigated the staining pattern of phosphorylated H2AX (γH2AX) in leptotene spermatocytes. H2AX is phosphorylated in response to the formation of DSBs, and this occurs upstream of SPO11-oligo production (Figure 4-3) (Kidane et al., 2010). In control leptotene spermatocytes γH2AX staining is largely diffuse throughout the nucleus, and some enrichment colocalising with the forming AE marked by SYCP3 staining can be seen (Figure 4-8A). A similar staining pattern was also observed *Tex19.1*$^{-/-}$ leptotene spermatocytes (Figure 4-8A). However, comparison of total nuclear γH2AX staining signal between controls and *Tex19.1*$^{-/-}$ revealed a 51% reduction in the absence of TEX19.1 (Figure 4-8B). Therefore *Tex19.1*$^{-/-}$ spermatocytes appear to possess reduced levels of meiotic DNA damage in leptotene, indicating defective formation of meiotic DSBs. This reduced DSB formation is likely to be responsible for the reduced SPO11-oligo production and early recombination protein binding at this stage and reveals a very early defect in meiotic recombination in *Tex19.1*$^{-/-}$ spermatocytes.

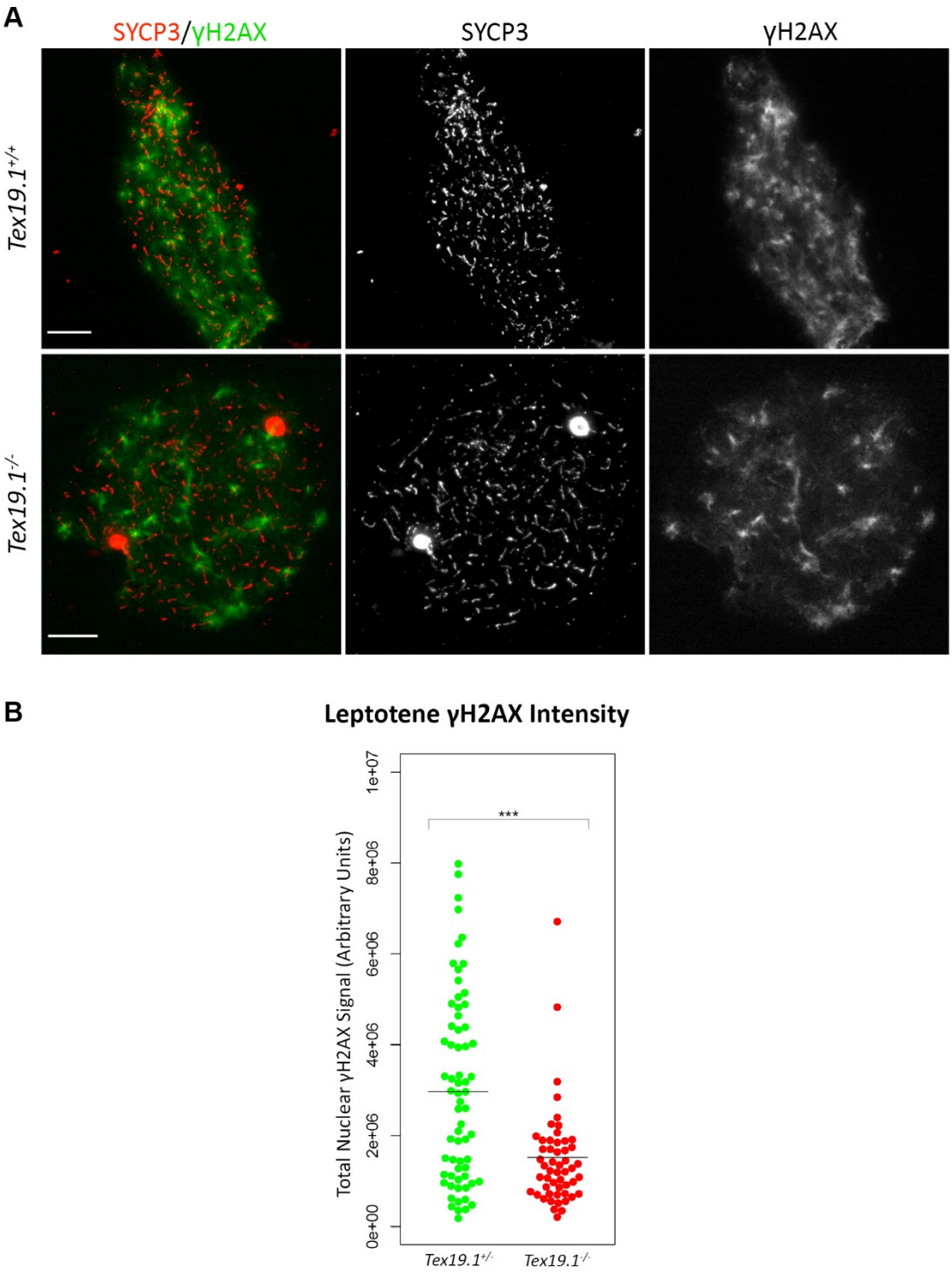

Figure 4-8. γH2AX quantification in leptotene

(A) Antibody staining against SYCP3 (red) and γH2AX (green) in control and *Tex19.1*$^{-/-}$ leptotene nuclei. Merges and single channel images displayed. 10µm scale bars. (B) Beeswarm plot for total γH2AX antibody staining signal per leptotene nucleus. N=66, 52, and mean signal = 3003597, 1477528 (arbitrary units) for control and *Tex19.1*$^{-/-}$ nuclei respectively. Significance indicated by asterisks: p<0.001, Mann-Whitney U test. Mean signal indicated by black bars.

Although the formation of meiotic DSBs is performed by SPO11 (Baudat et al., 2000; Romanienko and Camerini-Otero, 2000), this process is also reliant on the presence of various co-factors which localise to chromosome axes and function upstream of SPO11. MEI4 is one such protein, forming ~300 foci on chromosome axes in leptotene independently of SPO11 activity (Kumar et al., 2010). I next assessed the frequency of MEI4 foci in leptotene to investigate whether altered behaviour of this SPO11 co-factor might be influencing the abnormal DSB formation seen in *Tex19.1*$^{-/-}$ spermatocytes. As with the other recombination proteins analysed in this way, MEI4 was antibody stained in combination with SYCP3 to mark the AE, and foci co-localising with the AE in leptotene nuclei were counted (Figure 4-9A). Control leptotene spermatocytes were found to contain an average of 218 MEI4 foci, similar to levels previously reported (Figure 4-9B) (Kumar et al., 2010). In *Tex19.1*$^{-/-}$ leptotene spermatocytes the level of MEI4 foci was not significantly altered ($p=0.56$, Man-Whitney U test), with an average of 223 MEI4 foci detected (Figure 4-9B). Therefore the severe defect in DSB formation and production of SPO11-oligo complexes occurs in *Tex19.1*$^{-/-}$ spermatocytes independently of MEI4 localisation.

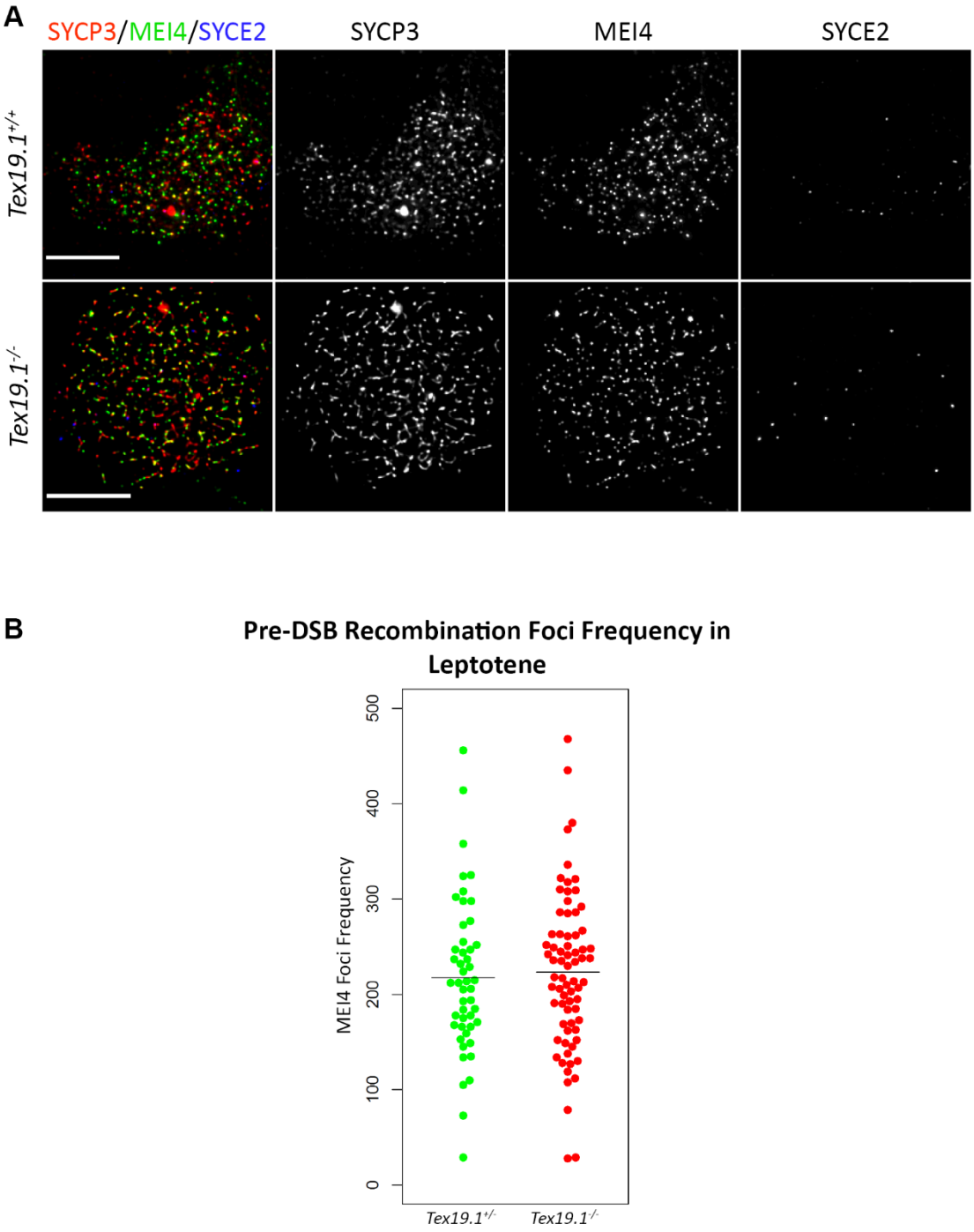

Figure 4-9. MEI4 localisation leptotene
(A) Antibody staining of SYCP3 (red) and MEI4 (green) and SYCE2 (blue) in control and *Tex19.1*$^{-/-}$ leptotene nuclei. Merges and single channel images displayed. 10µm scale bars. (B) Beeswarm plot for total MEI4 foci per leptotene nucleus. N=48, 72, and mean foci frequency = 218, 223 for control and *Tex19.1*$^{-/-}$ nuclei respectively. Mean signal indicated by black bars.

4.3 Discussion

In this chapter I have uncovered major defects in meiotic recombination which could cause the chromosome asynapsis seen in *Tex19.1*$^{-/-}$ spermatocytes. The formation of DSBs at the start of recombination is severely delayed and subsequently so is the recruitment of proteins involved in the repair of this DNA damage. The undertaking of a homology search driven by recombination is central to chromosome pairing in mammalian meiosis (Baudat et al., 2013). Unsynapsed chromosomes in *Tex19.1*$^{-/-}$ pachytene spermatocytes were noted to fail to pair against their homologous partner, therefore defects in homologous pairing of chromosomes appears to precipitate the asynapsis observed in this mutant.

4.3.1 Caveats of Immunocytological Analysis

The research in this chapter was heavily reliant on immunocytological analysis of spermatocytes prepared by chromosome spreading. Such analysis can be highly informative but also possesses inherent drawbacks. (1) The accuracy of information rendered from antibody staining is limited by the specificity of the antibodies used. This can be particularly challenging in the case of recombination proteins as focal staining recorded as specific signal is often very similar in conformation to non-specific focal background staining. I have employed strict criteria throughout my analysis to ensure reproducibility of scoring and all images have been scored blind with respect to mouse genotype to avoid the introduction of any bias. This drawback also limits the scope to which staining patterns of different recombination proteins can be compared, as quality of staining varies between antibodies. (2) Progression through meiosis is a continuum and sub-stages of prophase identified by SC staining patterns help to separate the maturity of cells analysed, but these sub-stages rely on normal progression of synapsis (which is defective in *Tex19.1*$^{-/-}$ spermatocytes) and cells will also range in progression within each sub-stage. (3) The ability to score staining patterns is also limited by the resolution of the equipment used to capture the images. While more sophisticated systems to those used do exist these are also more time consuming and were not judged to sufficiently improve the quality of the information gathered to warrant their use. (4) Finally, the preparation of testes into chromosome spreads is a method which enables parallel assessment of the wide range of cell types present within the testes. Two approaches to preparing chromosome spreads were used throughout this thesis, which possessed differing benefits to staining with particular antibodies and also retained different proportions of particular cell types (data not shown). It is important to bear in mind that only

a portion of the cells in the testis will be successfully fixed and imaged, limiting the available view of events taking place within this tissue.

While caveats do exist in the analysis of spermatogenesis by immunocytology, this approach does provides a powerful method of analysing events which cannot currently be simulated *in vitro* and are difficult to analyse biochemically using whole testes due to the tissue's heterogeneous composition. Interestingly, the analysis of ssDNA binding protein RPA during this research appears to reveal continuous binding to DNA in high levels of foci from leptotene through to zygotene. Previously only low level binding of RPA has been reported until zygotene unless the binding of RAD51 and or DMC1 was defective, thus these recombinases were thought to temporarily displace RPA from DSBs (Moens et al., 2002; Plug et al., 1997b; Roig et al., 2010; Yang et al., 2008). Unfortunately antibodies used in my analysis to stain for RPA, DMC1 and RAD51 were all raised in rabbit so colocalisation of these proteins could not be assessed. While the RPA antibody used in my analysis has been used in previous reports (Plug et al., 1997b), the method of chromosome spread preparation is different and may influence the ability of the antibody to bind, resulting in the distinction from the dynamics of this protein previously reported.

4.3.2 Meiotic Recombination Delay/Reduction and Chromosome Synapsis

Delayed meiotic recombination is an unusual phenotype and has not been reported in many mammalian mutants. One such mutant mouse is that of *Pol β*. Germline deletion of *Pol β* causes a delay and possibly an overall reduction in the resection of meiotic DSBs, resulting in a large reduction in DMC1 and RAD51 to 34% and 25% respectively in leptotene, which recover to 62% and 73% by zygotene (Kidane et al., 2010). These reductions in foci formed by proteins participating in early recombination are similar to those that I find in *Tex19.1*$^{-/-}$ spermatocytes: DMC1 and RAD51 foci reduction to 30% and 60% in leptotene, and recovery to 87% and 67% by zygotene. Unlike *Tex19.1*$^{-/-}$, *Pol β* mutant spermatocytes appear to form DSBs normally, as indicated by leptotene γH2AX localisation, therefore the mechanisms by which recombination is disrupted differ between these two mutants (Kidane et al., 2010). Similarly to *Tex19.1*$^{-/-}$ male mice however, *Pol β* mutants are defective in chromosome synapsis in the majority of pachytene spermatocytes (Kidane et al., 2010; Ollinger et al., 2008). A simple explanation for the failed chromosome synapsis in both of these mutants is that the delayed recruitment of early recombination proteins involved in the

homology search reduces the success of this search, resulting in unpaired and subsequently unsynapsed chromosomes.

Other examples of delayed meiotic recombination have also been reported, such as *Trip13* and *Zip4h* mutants, and are important to thoroughly understand the potential implication of this defect and its likelihood to be responsible for chromosome asynapsis in *Tex19.1*$^{-/-}$ spermatocytes. The moderately defective *Trip13* hypomorphic mutant, *Trip13*$^{mod/mod}$, and *Zip4h*$^{-/-}$ spermatocytes both display delayed repair of meiotic DSBs, with abnormally high levels of RAD51 and DMC1 persisting in pachytene. However, the frequency of recombination intermediates in leptotene indicates a normal level of resected DSBs and hence a normal rate of DSB formation in these mutants (Adelman and Petrini, 2008; Li and Schimenti, 2007; Roig et al., 2010). The delay to recombination in these mutants therefore begins at a later stage than in both *Tex19.1* and *Pol β* mutants. Unlike *Tex19.1*$^{-/-}$ spermatocytes, *Trip13*$^{mod/mod}$ and *Zip4*$^{-/-}$ spermatocytes successfully synapse homologous chromosomes (Kidane et al., 2010; Li and Schimenti, 2007; Roig et al., 2010), therefore the delay to meiotic recombination in these mutants does not greatly perturb the homology search. This may be because delayed progression of recombination incurred after DSB resection and recombinase recruitment is sufficient to enable chromosome pairing.

A second hypomorphic *Trip13* mutant (*Trip13*$^{sev/sev}$) with a more severe meiotic phenotype than *Trip13*$^{mod/mod}$ has also been reported. Unlike *Trip13*$^{mod/mod}$, *Trip13*$^{sev/sev}$ spermatocytes cannot synapse homologous chromosomes (Roig et al., 2010). Curiously, although *Trip13*$^{sev/sev}$ spermatocytes appear to generate normal levels of resected DSBs in leptotene, and recruit normal frequencies of DMC1 foci, the frequency of RAD51 foci formation is approximately halved at this stage. Reduction in RAD51 foci is also a feature of *Trip13*$^{mod/mod}$ though the reduction is less in this mutant than *Trip13*$^{sev/sev}$ (Roig et al., 2010). It is tempting to speculate that the highly reduced binding of the RAD51 recombinase in leptotene may be responsible for the failed chromosome synapsis in *Trip13*$^{sev/sev}$ (Roig et al., 2010), as studies in yeast lacking Rad51 have revealed that DSB repair becomes biased towards inter-sister repair and away from the inter-homolog repair which drives the meiotic homology search (Bishop, 1994; Schwacha and Kleckner, 1997; Shinohara et al., 1997). However, the mutation of *Trip13* also results in a number of other meiotic defects and, as with the *Pol β* mutant, the meiotic function(s) of these proteins are not fully understood. Thus it remains possible that pachytene chromosome asynapsis in these mutants is the result of a defect other than presence of reduced or imbalanced early recombination intermediates in leptotene. Pol β for example, appears to localise only to synapsed chromosomes, implying an additional role at this location after its requirement for early DSB processing (Kidane et

al., 2010), and TRIP13 is also required for the synapsis-dependent removal of HORMAD proteins, which are involved in detection of asynapsis (Daniel et al., 2011; Roig et al., 2010; Wojtasz et al., 2012). As so few examples of delays to meiotic recombination in mice have been reported, information about the consequences of such a defect is limited.

The reduced frequency of processed DSBs present in leptotene spermatocytes which occurs in *Pol β* mutants and *Tex19.1*$^{-/-}$ can also be achieved by reducing the expression of *Spo11*. Mice expressing reduced levels of *Spo11* from a single functional copy of the gene by controlling expression with a transgenic promoter (*Tg(Spo11β)*$^{+/-}$) causes a reduction in leptotene DMC1 foci and RAD51 foci to 60% and 44% respectively (Kauppi et al., 2013b). Furthermore, chromosome synapsis is defective in *Tg(Spo11β)*$^{+/-}$ spermatocytes indicating that reduction in DSBs results in asynapsis (Kauppi et al., 2013b). Early recombination protein foci are also reduced in *Spo11*$^{+/-}$ heterozygous spermatocytes, though to a lesser extent (leptotene DMC1 and RAD51 foci counts are 70-80% of those seen in wild-type), and this level of reduction remains compatible with chromosome synapsis (Cole et al., 2012). Therefore some reduction to DSB frequency can be tolerated in spermatocytes, but there appears to be a threshold for DSB frequency below which synapsis cannot be achieved. The reduction in processed meiotic DSBs in leptotene to ~50%, as seen in *Tg(Spo11β)*$^{+/-}$, is insufficient to promote a successful homology search, supporting the hypothesis that reduced leptotene DSB frequency causes failed chromosome synapsis in *Tex19.1*$^{-/-}$ spermatocytes. However, early recombination foci in *Tg(Spo11β)*$^{+/-}$ remain reduced to ~50% in zygotene (Kauppi et al., 2013b), unlike *Tex19.1*$^{-/-}$ which are close to wild-type levels by this stage. Thus if reduced leptotene DSBs cause asynapsis in *Tex19.1*$^{-/-}$ spermatocytes then the late-forming DSBs present in zygotene spermatocytes of *Tex19.1*$^{-/-}$ testes must possess a reduced ability to participate in the homology search and promote accurate chromosome pairing and synapsis.

4.3.3 Mechanisms of DSB Control

Meiotic DSBs are generated by the endonuclease SPO11 (Baudat et al., 2000; Romanienko and Camerini-Otero, 2000), therefore the altered DSB formation observed in *Tex19.1*$^{-/-}$ likely reflects changes in the activity of this enzyme. SPO11 exists in two isoforms with distinct temporal regulation (Bellani et al., 2010; Kauppi et al., 2011) and distinctions in genomic targeting (Brick et al., 2012). Early spermatocytes synthesise only the SPO11β isoform (Bellani et al., 2010) and this isoform alone is sufficient for DSB formation which occurs at this stage and subsequent chromosome pairing of spermatocyte autosomes (Kauppi et al.,

2011). The SPO11α isoform is not expressed until mid- to late-prophase, and is required for the formation of the majority of DSBs in the XY pseudoautosomal region (PAR) and the subsequent synapsis of most sex chromosomes, which does not begin until late zygotene (Kauppi et al., 2011). There also appears to be distinctions in mechanisms by which these two isoforms target DNA, with autosomal DSBs forming at hotspots marked with PRDM9-dependent H3K4 trimethylation (H3K4me3), but PAR DSBs lacking this mark (Brick et al., 2012). As DSB frequency is reduced in *Tex19.1*$^{-/-}$ leptotene spermatocytes, this likely reflects altered activity of the SPO11β isoform which is expressed at this time. As DSB formation at the PAR has not been specifically investigated in *Tex19.1*$^{-/-}$ spermatocytes it is not clear whether the activity of the SPO11α isoform is also reduced in this mutant. The ability of SPO11α to generate DSBs on autosomes in the absence of SPO11β is not known, however it may be possible that the delayed nature of DSB formation in *Tex19.1*$^{-/-}$ reflects impaired ability to form SPO11β-DSB in early meiosis followed by widespread DSB formation by the SPO11α isoform when it is expressed later in meiosis.

Around 200-300 DSBs are initially generated during early meiosis (Moens et al., 2002), though *Spo11* expression does not peak until pachytene (Shannon et al., 1999). The DSB forming activity of the protein therefore appears to be restricted to generation of a limited number of DNA breaks. Indeed, total SPO11 protein levels typically do not appear to be the limiting factor for DSB frequency, with a large excess of protein remaining unbound to DNA (Neale et al., 2005). The frequency of DSB formation can however be partly limited by *Spo11* expression (Kauppi et al., 2013b), and overexpression of the gene using a transgenic promoter does result in a modest elevation in DSBs (Cole et al., 2012). Therefore it appears that only a proportion of total SPO11 protein is active. The mechanisms controlling this activity are in the process of being uncovered. The kinase ATM which targets numerous proteins for phosphorylation, influences multiple pathways and is recruited by DNA damage (Shiloh and Ziv, 2013). In the absence of ATM, SPO11 DSB formation is increased approximately 10-fold (Lange et al., 2011). Therefore this mechanism of controlling SPO11 activity is a major contributor to the restriction of meiotic DSB formation. The reduction in early meiotic DSBs formed in *Tex19.1*$^{-/-}$ could relate to reduction in *Spo11* expression or SPO11 protein levels, or it is possible that mechanisms restricting SPO11 DSB forming activity are over-active in the absence of TEX19.1. A secondary wave of DSB formation has also been identified on unsynapsed axes of late-zygotene/early-pachytene spermatocytes, leading to suggestions that a negative feedback loop operates to prevent further DSB formation after local synapsis (Kauppi et al., 2013b). This mechanism

may be at least partly responsible for adding to the frequency of DSBs in early prophase *Tex19.1*$^{-/-}$ spermatocytes, enabling them to reach wild-type levels in zygotene.

The activity and targeting of SPO11 is reliant on a collection of upstream factors. SPO11 DSBs typically form at genomic hotspots marked with H3K4me3 laid down by the histone methyltransferase PRDM9 (Brick et al., 2012; Smagulova et al., 2011). In yeast, these H3K4me3-associated DSB hotspots are tethered from their original location in chromatin loops to the chromosome axis where DSB processing takes place (Acquaviva et al., 2013; Sommermeyer et al., 2013). The machinery involved in this process interacts with the axis-associated protein MEI4, which forms SPO11-independent foci and is required for DSB formation in mice (Kumar et al., 2010). While my research has shown that MEI4 foci are able to form in *Tex19.1*$^{-/-}$ spermatocytes, other components of this process may be perturbed and subsequently responsible for the reduced DSB formation observed. Indeed, while DSBs can form in the absence of PRDM9, their frequency is reduced (Hayashi et al., 2005). Therefore disruptions to PRDM9 activity upstream of SPO11 could also be responsible for the altered DSB frequency in *Tex19.1*$^{-/-}$.

4.3.4 DSB Targeting and Chromosome Synapsis

As previously discussed, it is not entirely clear whether the initial reduction in DSB frequency in *Tex19.1*$^{-/-}$ leptotene spermatocytes is sufficient to cause the chromosome asynapsis observed. This would suggest that the DSBs formed by the zygotene stage in *Tex19.1*$^{-/-}$, which are close to levels seen in controls, have a reduced ability to promote synapsis. In addition to DSB frequency, the positioning of meiotic DSBs also appears to be important for the success of the meiotic homology search. In the absence of PRDM9, DSBs form in DNA at gene promoters associated with PRDM9-independent H3K4me3, and it is this repositioning of DSBs which is proposed to lead to asynapsis in *Prdm9*$^{-/-}$ (Brick et al., 2012). Furthermore, the indiscriminate formation of DSBs by Cisplatin treatment in spermatocytes lacking SPO11 is unable to completely rescue asynapsis, supporting the importance of DSB positioning (Romanienko and Camerini-Otero, 2000). As discussed in section 3.3.2, the upregulation in expression of the retrotransposon *MMERVK10C* in *Tex19.1*$^{-/-}$ testes may reflect changes in chromatin modifications involved in transcriptional regulation. As chromatin modifications are also key in the promotion of DSB hotspots, it is possible that an altered chromatin modification landscape in *Tex19.1*$^{-/-}$ spermatocytes could be responsible for both retrotransposon upregulation and misplacement of meiotic DSBs resulting in asynapsis. This hypothesis could also be applied to the other germline genome

defence mutant male mice, which all feature retrotransposon upregulation and chromosome asynapsis, a connection between which remains to be robustly identified (Crichton et al., 2013). Indeed, widespread changes in the dynamics of various meiotic histone modifications have been identified in spermatocytes of both the *Dnmt3l*$^{-/-}$ and *Miwi2*$^{-/-}$ germline genome defence mutants (Bao et al., 2014; Webster et al., 2005). As DSBs typically form in open chromatin (Borde and de Massy, 2013), and chromatin associated with upregulated retrotransposons is likely to become more open, this may lead to an increase in DSB formation in retrotransposon-associated DNA. Formation of DSBs in repetitive DNA is predicted to be particularly unfavourable as this could lead to non-allelic homologous recombination, promoting defective pairing (Sasaki et al., 2010) and potentially asynapsis. Therefore it would be of interest to investigate whether the location in addition to the frequency of DSBs is altered in *Tex19.1*$^{-/-}$ spermatocytes to better understand the mechanism by which chromosomes fail to synapse in this mutant. Extension of this analysis to other germline genome defence mutants may also prove valuable in explaining their shared chromosome asynapsis (Crichton et al., 2013).

Chapter 5:

Investigating Synapsed *Tex19.1*$^{-/-}$ Pachytene Spermatocytes for Defects Associated with Impaired Recombination

5 Investigating Synapsed *Tex19.1*$^{-/-}$ Pachytene Spermatocytes for Defects Associated with Impaired Recombination

5.1 Introduction

The focus of this chapter's research was to investigate the behaviour and progression of *Tex19.1*$^{-/-}$ pachytene spermatocytes which achieve complete autosomal synapsis. In the previous chapter I revealed defects in *Tex19.1*$^{-/-}$ spermatocytes in the formation of DSBs which initiate meiotic recombination at the start of meiosis. While it is likely that this early recombination defect contributes to the chromosome asynapsis observed in approximately 65% of *Tex19.1*$^{-/-}$ pachytene spermatocytes, the status of the synapsed population of spermatocytes is not known. Do these represent a population of spermatocytes unaffected by recombination defects or are recombination defects insufficient to perturb synapsis but capable of disrupting later meiotic events? In this chapter I investigate key processes in pachytene to inform on the consequence of impaired recombination on the progression of synapsed pachytene *Tex19.1*$^{-/-}$ spermatocytes through meiosis.

Pachytene is a particularly long stage of meiotic prophase, lasting 3-5 days (Bellvé et al., 1977; Speed, 1982) during which numerous events take place. Meiotic DSBs are ultimately repaired during pachytene resulting in the dissociation of foci formed by the repair proteins involved, such as RPA, DMC1, and RAD51 (Moens et al., 2002). A limited number of DSBs are repaired during pachytene to produce crossovers (COs), largely via the recruitment of MLH1 at the end of recombination (Eaker et al., 2002; Holloway et al., 2008). The repair of DNA damage appears to be vital for survival beyond pachytene as *Trip13*$^{mod/mod}$ spermatocytes which synapse but possess persistent DNA damage largely arrest during this stage (Li and Schimenti, 2007; Roig et al., 2010).

An additional checkpoint also takes place during pachytene which appears to be the primary cause of spermatocyte arrest at this stage. This checkpoint is centred around the establishment of transcriptional silencing of sex chromosomes (meiotic sex chromosome inhibition: MSCI) (Mahadevaiah et al., 2008; Turner, 2007). MSCI is dependent on the formation of a large heterochromatic domain within the chromatin of the X and Y chromosomes, termed the sex body (Solari, 1974), which requires the localisation of the apparent MSCI effector, phosphorylated H2AX (γH2AX) (Fernandez-Capetillo et al., 2003; Mahadevaiah et al., 2001; Turner et al., 2004). A similar process of transcriptional silencing

also takes place at unsynapsed autosomal axes, known as meiotic silencing of unsynapsed chromatin (MSUC) (Turner et al., 2005). Asynapsis causes a titration of γH2AX from the sex body to unsynapsed autosomes, and compromises MSCI resulting in expression of XY transcripts (Mahadevaiah et al., 2008). The pachytene expression of XY transcripts can have a toxic effect on spermatocytes and is sufficient to cause arrest at this stage (Royo et al., 2010). As well as asynapsis, failed MSCI can also be caused by defects in the silencing process itself after synapsis has taken place (Fernandez-Capetillo et al., 2003; Ichijima et al., 2011; Royo et al., 2013; Turner et al., 2004). Failure of MSCI triggered by DNA damage has not been demonstrated, despite this process also sequestering γH2AX (Li and Schimenti, 2007; Roig et al., 2010). Furthermore, asynapsis-related MSCI failure operates independently of DNA damage as seen in *Spo11*$^{-/-}$ which don't generate meiotic DSBs but are incapable of chromosome synapsis and subsequently still trigger pachytene arrest following MSCI failure (Barchi et al., 2005; Mahadevaiah et al., 2008).

To summarise, during the elongated pachytene stage of meiotic prophase (Bellvé et al., 1977; Speed, 1982) numerous events take place including DSB repair (Baudat et al., 2013), massive changes in gene expression (Fallahi et al., 2010), and MSCI (Turner, 2007). While approximately half of *Tex19.1*$^{-/-}$ spermatocytes are known to achieve complete synapsis in pachytene (Ollinger et al., 2008), this population of cells has not been studied therefore the ability of these cells to proceed through this stage is unknown. During this chapter I investigate diverse key events among pachytene spermatocytes, and unless explicitly stated research in this chapter will only relate to the autosomally synapsed population of *Tex19.1*$^{-/-}$ pachytene spermatocytes. Synapsis status of X and Y chromosomes was ignored during this analysis as the dynamics of sex chromosome synapsis differs to autosomes and is not known to affect pachytene events (Kauppi et al., 2011).

5.2 Results

5.2.1 Do Recombination Defects Persist in *Tex19.1*$^{-/-}$ Synapsed Pachytene Spermatocytes?

As previously discussed, the formation and subsequent repair of meiotic DSBs is delayed during early meiotic prophase in *Tex19.1*$^{-/-}$ spermatocytes, with nuclei displaying delayed localisation and dissociation of proteins involved in early DSB processing events. To investigate whether recombination defects persist among *Tex19.1*$^{-/-}$ spermatocytes with complete autosomal synapsis I studied the level of early recombination protein foci in these pachytene nuclei. Meiotic DSBs are typically repaired during pachytene and as such the level of early recombination foci is low at the start of this stage due to their displacement by proteins involved in later stages of recombination, and foci dissociate from chromosomes completely by the end of this stage (Moens et al., 2002). Spermatocytes selected for study were judged to be fully synapsed given complete co-localisation of SYCP3 and SYCE2 staining of AEs and CEs respectively along autosomes, or by the presence of 19 bold SYCP3 axes indicating complete autosomal synapsis, and two axes of differing length with or without partial pairing indicating limited sex chromosome synapsis in the PAR (Figure 5-1A-C). Spermatocyte spreads were co-stained with RPA, DMC1 or RAD51 and the axial foci shown by this staining were counted. Control spermatocytes displayed a mean of 86 RPA, 13 DMC1 and 13 RAD51 foci per nucleus (Figure 5-1D), comparable to similar counts made at this stage in other studies (Daniel et al., 2011). The greater frequency of RPA foci than DMC1 and RAD51 foci is consistent with its presence at unrepaired DSBs after these recombinases have dissociated mid-way through recombination (Moens et al., 2002). The frequency of autosomal RPA, DMC1 and RAD51 foci in *Tex19.1*$^{-/-}$ pachytene spermatocytes was increased by 28%, 95% and 11% respectively (RPA and DMC1 foci significantly increased: $p=0.003$, $p<0.001$ respectively, Mann-Whitney U test). This data indicates that despite a portion of *Tex19.1*$^{-/-}$ spermatocytes progressing to a synapsed pachytene state, these cells possess persistent unrepaired DSBs participating in early stages of recombination. The modest and insignificant increase in RAD51 foci at this stage may reflect a genuine difference between the localisation pattern of RAD51 and its meiotic homolog DMC1 which is increased to a greater extent at this stage, due to altered DSB repair. The smaller increase in RAD51 could also relate to the higher background staining encountered with this antibody leading to genuine foci being missed when scoring, resulting in lower statistical power to detect a change in frequency.

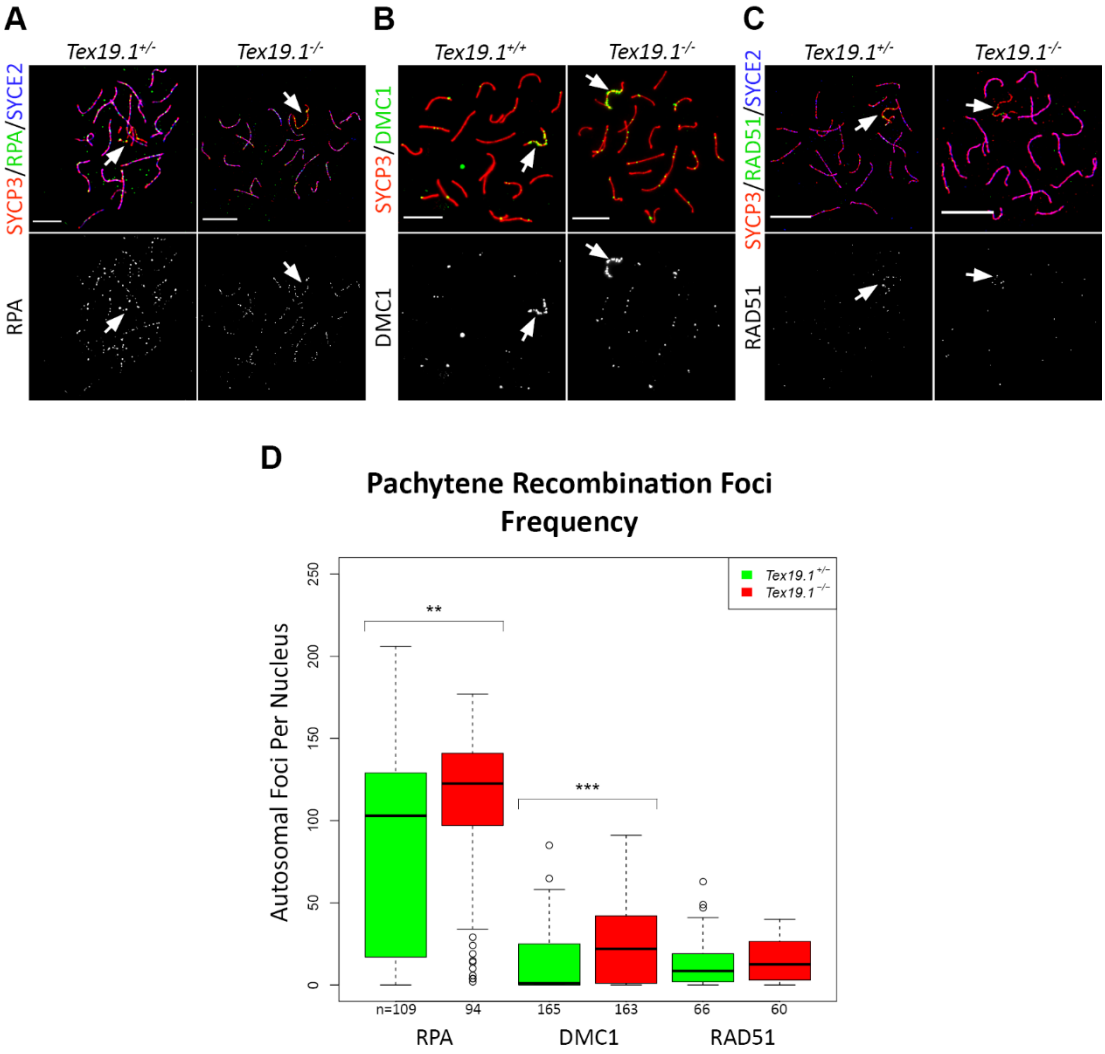

Figure 5-1. Early recombination protein localisation in pachytene spermatocytes
Representative antibody staining patterns of RPA, DMC1 and RAD51 proteins in control and *Tex19.1*$^{-/-}$ pachytene spermatocytes (A, B, C respectively – recombination protein in green channel), combined with antibody staining of SYCP3 (red) and SYCE2 (blue) to mark the axial element and central element of the synaptonemal complex respectively. Merges and single channel images displayed. 10µm scale bars. (D) Box-plots displaying the frequency of axial recombination foci in each nucleus scored. Mean foci frequencies=85, 110, 13, 25, 13, 15 from left to right across the plot. Foci counts were compared between controls and knockout spermatocytes using a Mann-Whitney U Test (p=0.002, <0.001, and 0.31 respectively), asterisks denote significance.

As recombination proceeds, DSBs progressively associate with different recombination proteins. The increased frequency of RPA and DMC1 foci indicates that more DSBs remain in early/mid stages of recombination in *Tex19.1*$^{-/-}$ pachytene spermatocytes, however this analysis can only inform on the progress of the sub-population of DSBs marked by these proteins. To gain a more complete impression of the level of DNA damage remaining in these spermatocytes I assessed the autosomal staining pattern of γH2AX, which marks unrepaired DSBs. γH2AX can be detected in condensed axial foci (S-foci) during

pachytene, which co-localise with proteins involved in early through to late stages of DSB repair (Chicheportiche et al., 2007). I co-stained spermatocytes for SYCP3 and γH2AX and counted γH2AX foci restricted to SYCP3-stained autosomal axes in pachytene nuclei (Figure 5-2A). Upon entry to pachytene wild type nuclei are known to typically contain ~120 γH2AX foci. The frequency of these foci steadily reduces during pachytene, with around one third of the number present in late pachytene nuclei and a complete loss of autosomal foci by progression to diplotene (Chicheportiche et al., 2007). γH2AX staining at the sex chromosomes meanwhile establishes a large domain known as the sex body, which will be discussed later. Therefore I scored spermatocytes as having either "high" DNA damage (>40 γH2AX foci), "moderate" damage (1-40 foci) or no damage (0 foci) to gauge the level of DNA damage present on autosomes. In control mice, 22% of pachytene spermatocytes had high levels of γH2AX foci, 62% had moderate levels, and 16% had no apparent autosomal γH2AX foci (Figure 5-2A, B). In *Tex19.1*$^{-/-}$ the frequency of pachytene nuclei with high levels of DNA damage is increased to 52% ($p<0.001$. Fisher's exact test), and correspondingly fewer nuclei than controls with moderate (38%, $p<0.001$, Fisher's exact test) or absent foci (9%, $p=0.12$, Fisher's exact test) (Figure 5-2A, B). Therefore in addition to containing elevated levels of early recombination foci, synapsed *Tex19.1*$^{-/-}$ pachytene spermatocytes more frequently contain high levels of DNA damage which has not yet been repaired. These observations may indicate that the repair of meiotic DSBs remains delayed after chromosome synapsis in *Tex19.1*$^{-/-}$ spermatocytes. An increase in SPO11-independent DNA damage was not observed in *Tex19.1*$^{-/-}$*Spo11*$^{-/-}$ spermatocytes in analyses discussed previously, therefore the formation of additional SPO11-independent DSBs at this time are not thought to account for this increase in DNA damage present. It is possible however that additional SPO11-dependent DSBs are generated. As control pachytene spermatocytes enter this stage with DNA damage which is steadily repaired, an alternative possibility is that *Tex19.1*$^{-/-}$ pachytene spermatocytes have greater DNA damage and more immature DSBs than controls because more of these spermatocytes are in an early sub-stage of pachytene. Alternatively, persistent DSBs in pachytene may also reflect a secondary defect in the repair of DNA damage in addition to the identified defect in DSB formation.

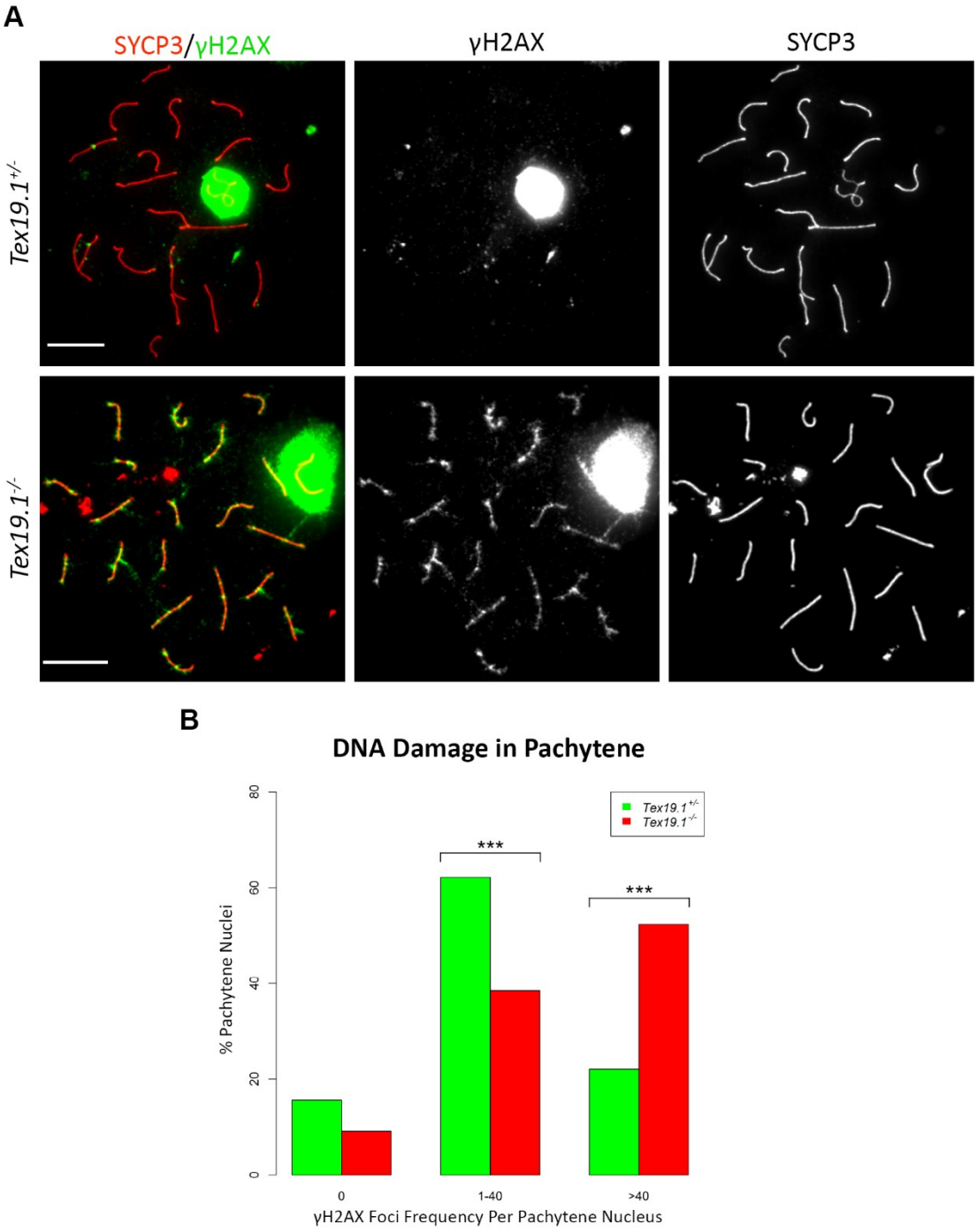

Figure 5-2. DNA damage levels in pachytene spermatocytes

(A) Representative γH2AX antibody staining patterns (green) in control and *Tex19.1*$^{-/-}$ pachytene spermatocytes, combined with antibody staining of SYCP3 (red) to mark the axial element of the synaptonemal complex for staging. The large domain of γH2AX staining in each image marks the sex body. Merges and single channel images displayed. 10µm scale bars. (B) Barplot showing the percentage of pachytene spermatocytes with either 0, 1-40 or >40 autosomal γH2AX foci. N=172, 130 for control and *Tex19.1*$^{-/-}$ counts respectively. A significant difference in the frequency of spermatocytes with each level of γH2AX foci was seen: p=0.12, <0.001, <0.001 respectively (Fisher's exact test). Asterisks denote significance.

5.2.2 Progression to Crossover Formation in *Tex19.1*$^{-/-}$ Pachytene Spermatocytes

Persistent pachytene DSBs are a feature of other mutant mice with defects in the repair of meiotic DNA damage. Such spermatocytes are often unable to repair a population of DSBs while others remain capable of progression to late recombination and a normal proportion of spermatocytes are in the process of CO formation (Adelman and Petrini, 2008; Li and Schimenti, 2007). I next investigated whether persistent DNA damage in *Tex19.1*$^{-/-}$ spermatocytes reflects a defect in DSB repair in addition to the defect in DSB formation shown previously, with impaired repair of some DSBs but not others. I assessed the ability of pachytene spermatocytes to recruit machinery required to form COs by co-staining for SYCP3 to identify suitable spermatocytes, and MLH1, which forms axial foci and is essential for the formation of the majority of CO events (Eaker et al., 2002). Pachytene spermatocytes were scored for the presence or absence of bold focal MLH1 staining on autosome axes (Figure 5-3A). 60% of control pachytene nuclei displayed axial MLH1 foci however this was reduced to just 21% among synapsed *Tex19.1*$^{-/-}$ pachytenes ($p<0.001$, Fisher's exact test) (Figure 5-3B). Therefore fewer *Tex19.1*$^{-/-}$ pachytene spermatocytes have DSBs in the late stages of recombination, forming COs by recruiting MLH1. This finding is consistent with all DSBs being in a delayed state of repair, possibly caused by their delayed formation in early prophase, and does not suggest an additional defect in the repair of meiotic DNA damage in *Tex19.1*$^{-/-}$.

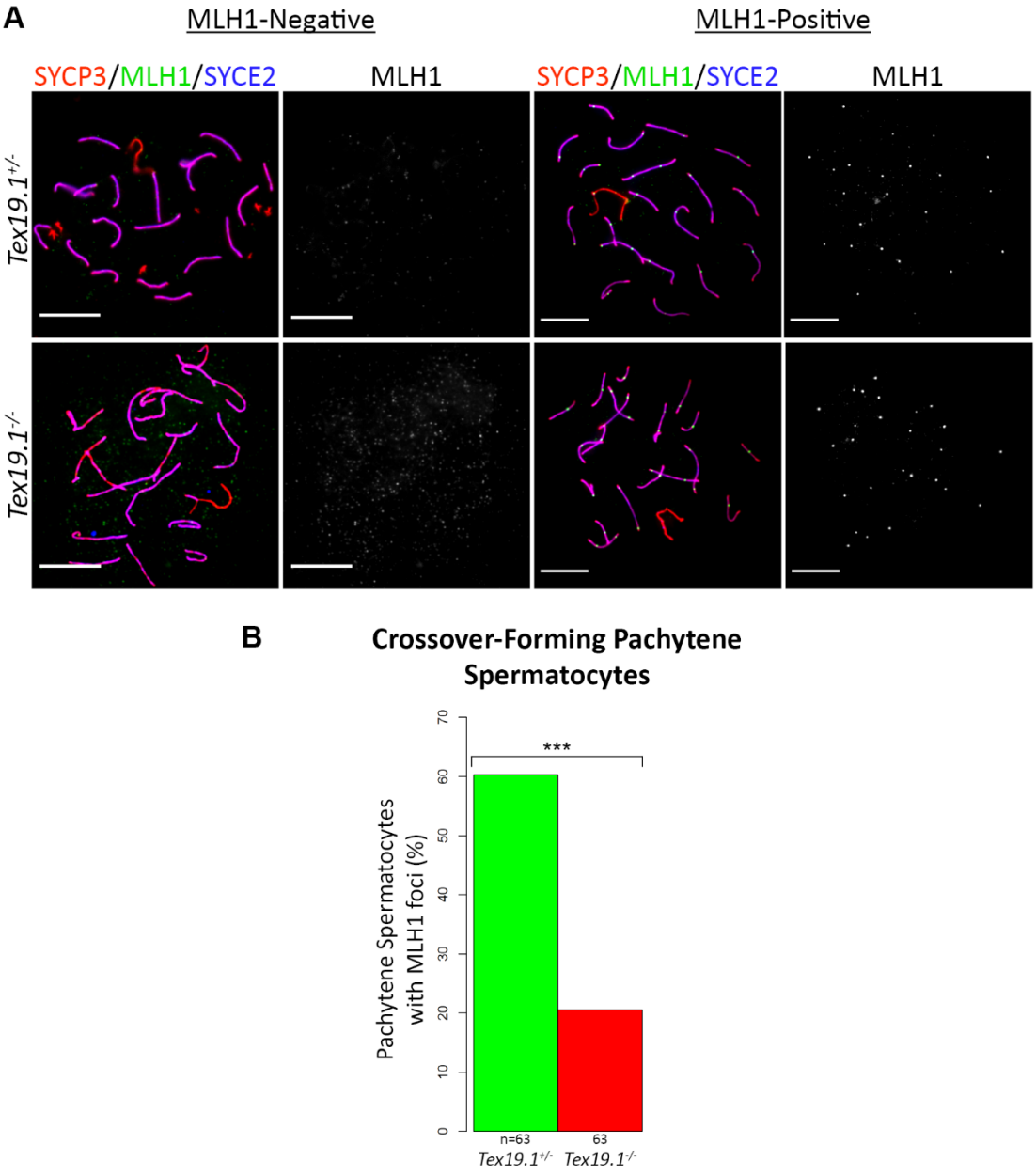

Figure 5-3. Analysis of crossover-forming pachytene spermatocytes
(A) Representative MLH1 negative and MLH1 positive (green) staining patterns present in control and *Tex19.1*$^{-/-}$ pachytene spermatocytes, combined with antibody staining of SYCP3 (red) and SYCE2 (blue) to mark the axial element and central element of the synaptonemal complex for staging. Merges and single channel images displayed. 10µm scale bars. (B) Barplot showing the percentage of pachytene spermatocytes with detected MLH1 foci. Frequency is significantly reduced in *Tex19.1*$^{-/-}$ spermatocytes ($p<0.001$, Fisher's exact test). Asterisks denote significance.

5.2.3 Expression of Pachytene Sub-stage Markers and Events in *Tex19.1*$^{-/-}$

To assess whether the altered progression of *Tex19.1*$^{-/-}$ pachytene spermatocytes is limited to the repair of DSBs I next assessed a series of other pachytene processes not known to be involved in recombination. I began by investigating the expression of the testis-specific histone H1t which has long been used as marker of mid/late pachytene in mice (Cobb et al., 1999; Inselman et al., 2003; Moens et al., 1997). H1t is also detectable in spermatocytes with mutations in recombination machinery, unable to repair DNA damage (Mahadevaiah et al., 2008), therefore it is not known to relate to recombination. H1t staining is recognisable as a cloud throughout the chromatin of a subpopulation of pachytene spermatocytes in both controls and *Tex19.1*$^{-/-}$ (Figure 5-4A). I detected such a staining pattern in 68% of synapsed control pachytene spermatocytes, however this proportion was reduced to only 27% in *Tex19.1*$^{-/-}$ ($p<0.001$, Fisher's exact test) (Figure 5-4B). This observation indicates that altered progression of events in *Tex19.1*$^{-/-}$ pachytene spermatocytes is not limited to DSB repair.

The mono-ubiquitination of histone H2A (UbH2A) at the sex body is a transient event which takes place between mid- and late-pachytene in wild-type spermatocytes and is associated with MSCI (Baarends et al., 2005; Mulugeta Achame et al., 2010). I next assessed UbH2A staining during pachytene in control and *Tex19.1*$^{-/-}$ spermatocytes to establish whether the appearance of this transient mark is also altered in the absence of TEX19.1. Co-staining spermatocytes for SYCP3 and UbH2A in control spermatocytes, revealed a similar staining pattern to that previously reported (Figure 5-5A) (Baarends et al., 2005). UbH2A staining was detected as a cloud over the XY chromosomes in 87% of control pachytene spermatocytes (Figure 5-5B). UbH2A staining was also detected over the sex chromosomes in *Tex19.1*$^{-/-}$ pachytene spermatocytes, however the proportion of cells with such staining was reduced (74%, $p=0.003$, Fisher's exact test) (Figure 5-5B). The altered frequency of this transient mark demonstrates a further pachytene event, the dynamics of which appear to be altered in *Tex19.1*$^{-/-}$, adding to the delayed repair of DSBs and appearance of H1t.

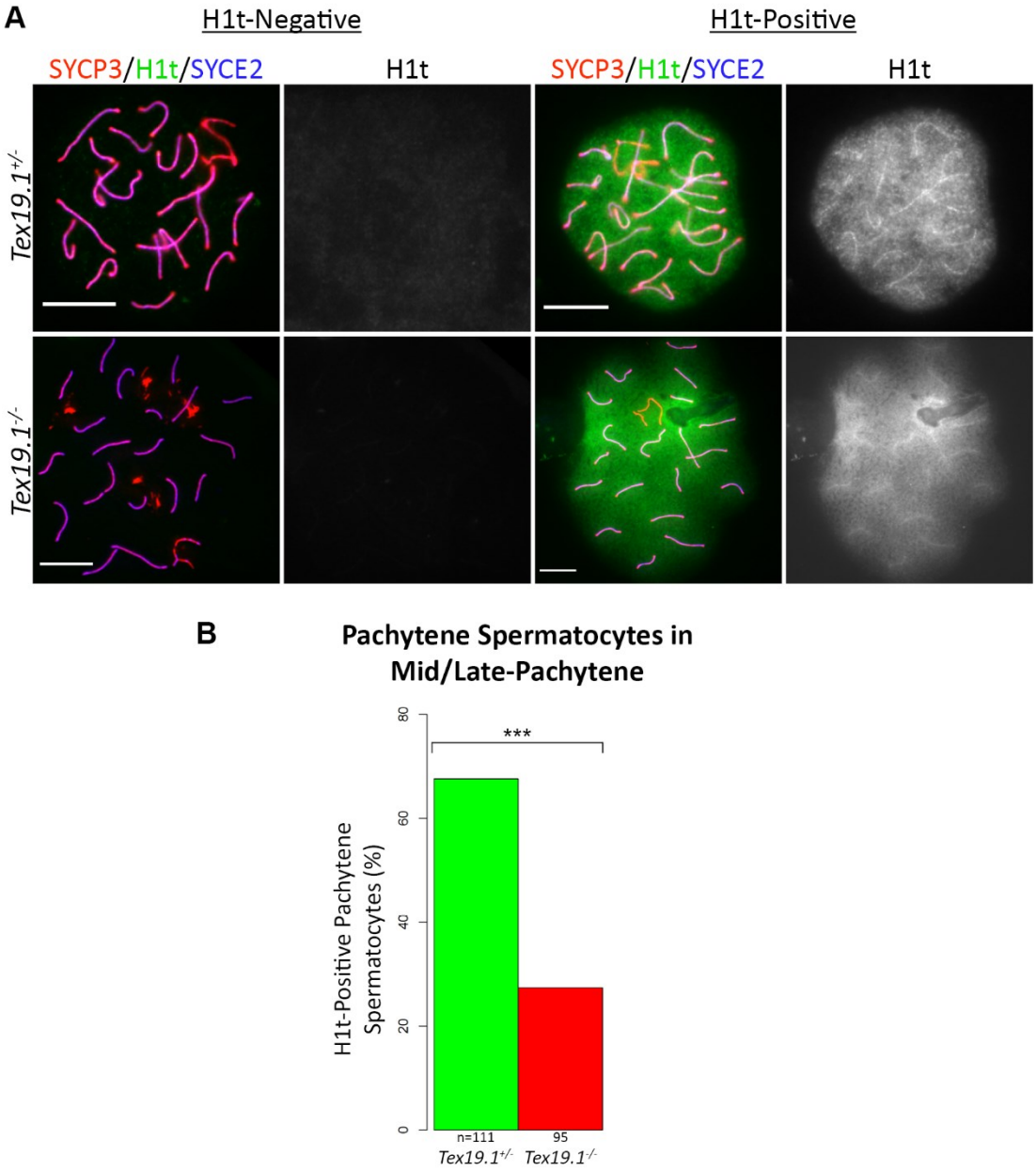

Figure 5-4. Mid-pachytene progression of spermatocytes

(A) Representative H1t negative and H1t positive (green) staining patterns present in control and *Tex19.1*$^{-/-}$ pachytene spermatocytes, combined with antibody staining of SYCP3 (red) and SYCE2 (blue) to mark the axial element and central element of the synaptonemal complex for staging. Co-localisation of SYCP3 and SYCE2 staining indicates synapsis. Merges and single channel images displayed. 10µm scale bars. (B) Barplot showing the percentage of pachytene spermatocytes with detected H1t staining. Frequency is significantly reduced in *Tex19.1*$^{-/-}$ spermatocytes ($p<0.001$, Fisher's exact test). Asterisks denote significance.

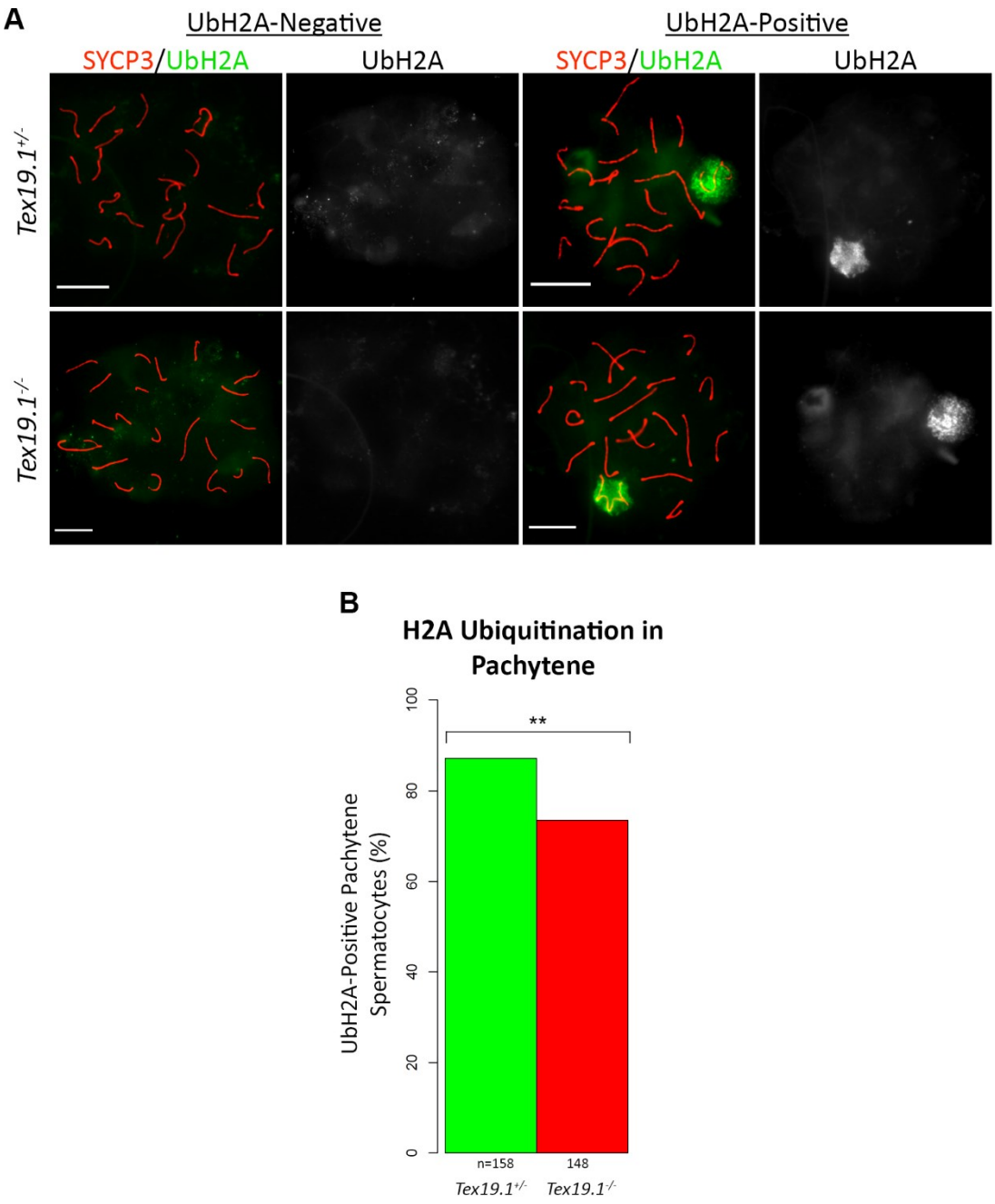

Figure 5-5. UbH2A localisation to the sex body in pachytene
(A) Representative UbH2A negative and UbH2A positive (green) staining patterns present in control and *Tex19.1*$^{-/-}$ pachytene spermatocytes, combined with antibody staining of SYCP3 (red) to mark the axial element of the synaptonemal complex for staging. Merges and single channel images displayed. 10µm scale bars. (B) Barplot showing the percentage of pachytene spermatocytes with UbH2A staining at the sex body. Frequency is significantly reduced in *Tex19.1*$^{-/-}$ (p=0.003, Fisher's exact test). Asterisks indicate significance.

In addition to the specific establishment of H2A mono-ubiquitination at the sex body, the patterns of total ubiquitination also vary as spermatocytes progress through pachytene. Ubiquitination of substrates can be broadly monitored using FK2 staining, which marks both mono- and poly-ubiquitinated residues. I investigated the progression of pachytene ubiquitination in *Tex19.1*$^{-/-}$ using a combination of FK2 and SYCP3 staining. Consistent with previous reports, FK2 staining in control pachytene spermatocytes is strikingly enriched at the sex chromosomes, in a pattern which is initially restricted to the XY axes before extending to the sex body domain as pachytene proceeds (An et al., 2012) (Figure 5-6A). For my analysis the progressive spread of FK2 staining over the sex chromosomes was divided into three visibly distinct conformations: "axial"; staining restricted to the XY chromosome axes, "loose"; staining spreading to the XY chromatin but still strongest on the axes, and "sex body"; staining is strong and evenly present over the XY chromatin and axes (Figure 5-6A). All three sex chromosome-staining conformations are detected in both control and *Tex19.1*$^{-/-}$ spermatocytes. The frequency of pachytene nuclei with axial and loose sex chromosome staining is increased in *Tex19.1*$^{-/-}$ ($p=0.05$, $p<0.001$ respectively; Fisher's exact test) (Figure 5-6B). Therefore the progression of *Tex19.1*$^{-/-}$ spermatocytes through patterns of ubiquitination at the sex chromosomes is also altered, showing an enrichment of spermatocytes displaying less mature staining patterns.

In addition to sex chromosome-associated FK2 staining, autosomal staining was also recognised. Autosomal staining was typically restricted to chromosome axes and varied between being focal or extending across the length of axes (Figure 5-6C), though it is possible that axial staining patterns consisted of numerous indistinguishable adjacent foci and is thus not a distinct pattern. This autosomal staining pattern has not been previously identified and its axial focal nature could be consistent with an association with DSB repair. Supporting this possibility, the frequency of pachytene nuclei with focal or axial FK2 staining was greatly increased in *Tex19.1*$^{-/-}$ ($p=0.0002$ and $p=0.0002$, Fisher's exact test) (Figure 5-6D). Therefore the altered patterns of ubiquitination in *Tex19.1*$^{-/-}$ are not limited to UbH2A at the sex body, but also general ubiquitination of the sex chromosomes and also extend to ubiquitination of the autosomes. These findings together with the altered levels of DSB progression through recombination, total DNA damage and expression of H1t demonstrate that an increased proportion of *Tex19.1*$^{-/-}$ pachytene spermatocytes display signs of being in immature stages of pachytene. This may reflect delayed progression through pachytene, however as MSCI-associated ubiquitination patterns are altered and MSCI must be established for progression beyond mid-pachytene. Therefore enrichment of immature

pachytene nuclei in *Tex19.1*$^{-/-}$ may reflect the loss of mid-pachytene spermatocytes due to failed MSCI.

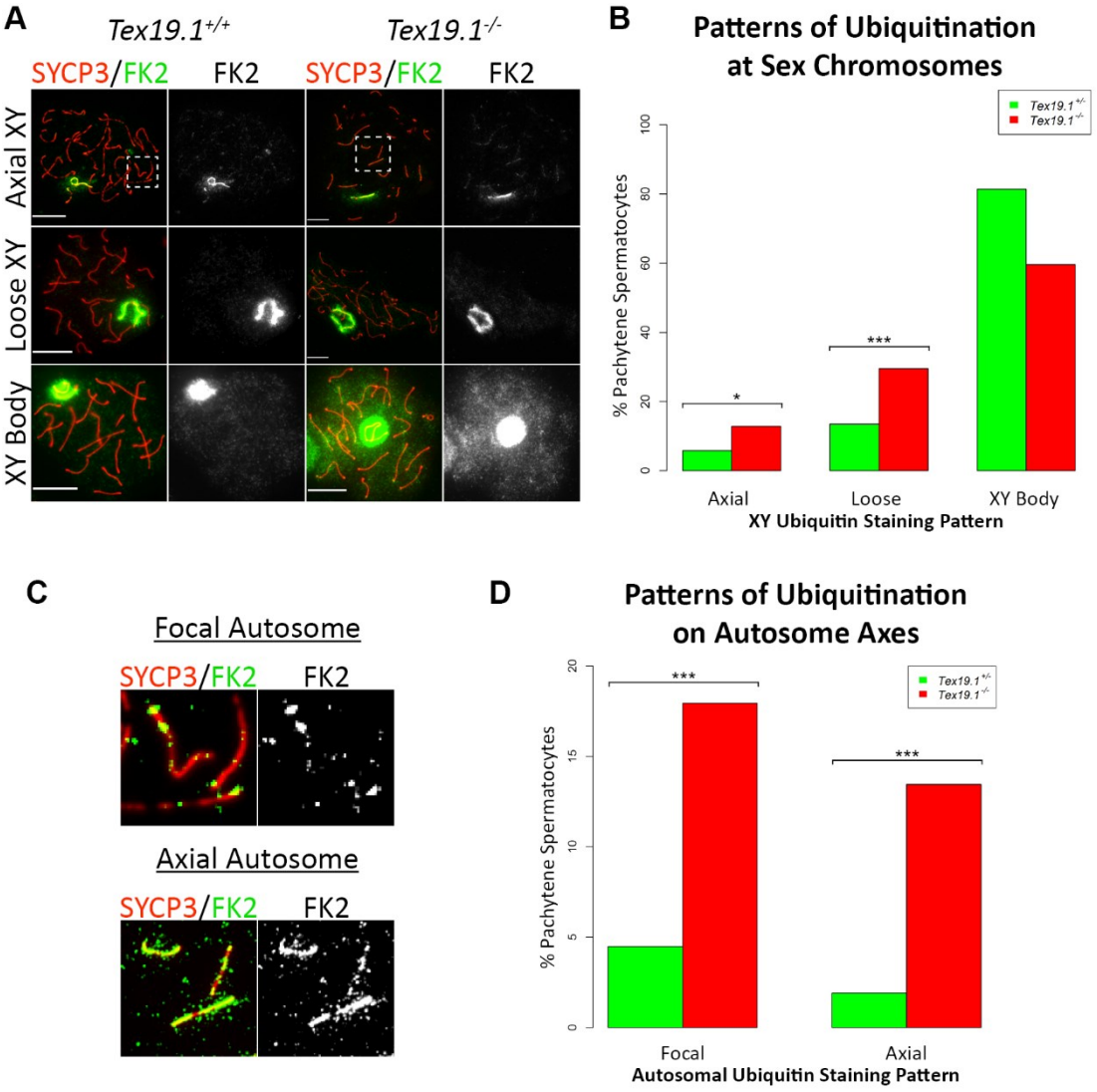

Figure 5-6. Mono- and poly-ubiquitin in pachytene spermatocytes
(A) Representative FK2 staining of mono- and poly-ubiquitin (green) in control and *Tex19.1*$^{-/-}$ pachytene spermatocytes, combined with antibody staining of SYCP3 (red) to mark the axial element of the synaptonemal complex for staging. Images with "axial", "loose", and "XY body" FK2 staining shown. Dashed boxes marked in merges are used later in section"C". Merges and single channel images displayed. 10µm scale bars. (B) Barplot showing the percentage of pachytene spermatocytes with each FK2 staining pattern at the sex body. Frequency of pachytene spermatocytes with axial and loose XY staining patterns increased in *Tex19.1*$^{-/-}$ ($p=0.05$, and $p<0.001$, Fisher's exact test). Asterisks indicate significance. (C) Representative selections of autosomal FK2 staining seen after signal amplification, taken from figure subsection "A". Focal and axial FK2 staining of autosomes shown. Merges and single channel images displayed. (D) Barplot showing the percentage of pachytene spermatocytes with each autosomal FK2 staining pattern at the sex body. Frequency of pachytene spermatocytes with focal and axial autosomal FK2 staining increased in *Tex19.1*$^{-/-}$ ($p<0.001$ for both, Fisher's exact test)

5.2.4 Assessing MSCI in *Tex19.1*$^{-/-}$

I next sought to address whether *Tex19.1*$^{-/-}$ pachytene spermatocytes were undergoing meiotic arrest despite achieving autosomal synapsis. Mid-pachytene arrest in spermatocytes appears to be typically caused by impaired MSCI (Burgoyne et al., 2009; Turner, 2007). I initially assessed whether MSCI appeared to be taking place by co-staining for SYCP3 and γH2AX (Figure 5-2A), and recording the presence/absence of a large and distinct domain of γH2AX staining over the XY chromosomes consistent with sex body formation. A cloud of γH2AX staining was detected over the XY chromosomes in all control pachytene spermatocytes. This was also the case in all *Tex19.1*$^{-/-}$ pachytene spermatocytes with full autosomal synapsis. Therefore the sex body appears to form during pachytene in the absence of TEX19.1.

To test more directly whether this γH2AX recruitment to the XY chromatin was functional in establishing MSCI I next investigated the expression of RMBY, a protein encoded by a multi-copy Y-linked gene typically silenced by MSCI during pachytene (Turner et al., 2002). RBMY can be detected in spermatocytes by immuno-staining, and should be absent from pachytene spermatocytes with successful MSCI. Spermatocytes were therefore co-stained for RMBY with SYCP3 and SYCE2 to stage nuclei. Severely asynapsed *Tex19.1*$^{-/-}$ spermatocytes were initially analysed as a positive control for this experiment and as predicted, RBMY staining was present as a diffuse nuclear signal (Figure 5-7). This reveals that severely asynapsed *Tex19.1*$^{-/-}$ spermatocytes are defective in MSCI and are likely to undergo mid-pachytene apoptosis as a result of this defect. RBMY staining was not detected in control pachytene spermatocytes, supporting successful MSCI (Figure 5-7). RBMY staining was similarly not detected in *Tex19.1*$^{-/-}$ pachytene spermatocytes with synapsed autosomes (Figure 5-7), supporting the functionality of the sex body formed in these cells and the successful establishment of MSCI. Therefore synapsed pachytene *Tex19.1*$^{-/-}$ spermatocytes do not appear to trigger mid-pachytene arrest, thus the enrichment of various features of immature pachytene spermatocytes presented appears to reflect a coordinated delay in progression of spermatocytes through this stage.

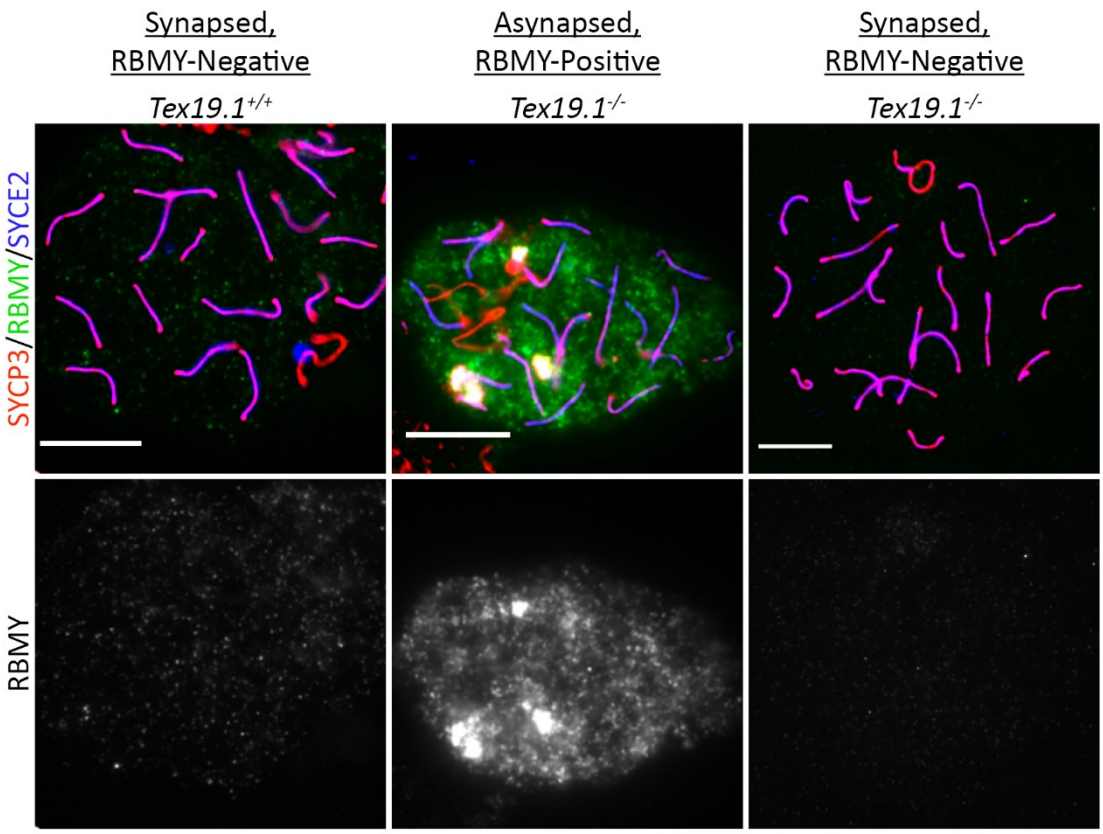

Figure 5-7. MSCI in pachytene spermatocytes
Antibody staining patterns of the Y-encoded protein RBMY, typically silenced by MSCI. Representative images of RBMY-negative control and *Tex19.1*$^{-/-}$ synapsed spermatocytes, and RBMY-positive (green) *Tex19.1*$^{-/-}$ spermatocyte with several asynapsed chromosomes. Staining combined with antibody staining of SYCP3 (red) and SYCE2 (blue) to mark the axial element and central element of the synaptonemal complex for staging. Co-localisation of SYCP3 and SYCE2 staining indicates synapsis. Merges and single channel images displayed. 10µm scale bars.

5.2.5 Investigating the Coordination of Delayed Pachytene Progression in *Tex19.1*$^{-/-}$

Data presented so far in this chapter has demonstrated that several processes which occur during pachytene progression are delayed in *Tex19.1*$^{-/-}$, however it is currently unclear if the relative progression of these processes remains synchronised and what is driving this delay. A further feature of pachytene progression is the elongation of autosomal axes between early and late pachytene, though the cause of this elongation is unknown (Vranis et al., 2010). Axis length has the advantage of being a feature which is easy to measure and likely to alter gradually during pachytene, enabling sensitive comparison between sub-populations of spermatocytes previously identified. I investigated axis length in *Tex19.1*$^{-/-}$ pachytene

spermatocytes to establish whether axial elongation is a further pachytene feature delayed in this mutant, and initially did so only in MLH1-postive spermatocytes to select for those undergoing crossover formation in late pachytene. Comparison of total axis length between control and *Tex19.1*$^{-/-}$ spermatocytes revealed a 6.5% reduction in length (p=0.01, t-test) (Figure 5-8A, C), and comparison between individual (Figure 5-1B) and groups of axes ranked by size (Figure 5-8C) as has been performed in similar analyses (Roig et al., 2010) demonstrated that all chromosomes were equally affected. A significant reduction in length was not achieved for the smallest group of axes, though this is likely due to a greater degree of measurement error relative to total length. This finding suggests that in addition to the other pachytene features discussed, elongation of the axial element also appears to be delayed in *Tex19.1*$^{-/-}$ pachytene spermatocytes. Furthermore the observation of this delay between MLH1-positive spermatocytes undergoing late stages of recombination indicates that even after progression to this late stage other processes remain delayed. Therefore the delays to processes in *Tex19.1*$^{-/-}$ pachytene spermatocytes are not entirely synchronous. An alternative possibility however is that axis length is indeed reduced in *Tex19.1*$^{-/-}$ spermatocytes, for example due to altered cohesin composition of the chromosome core (Novak et al., 2008).

A

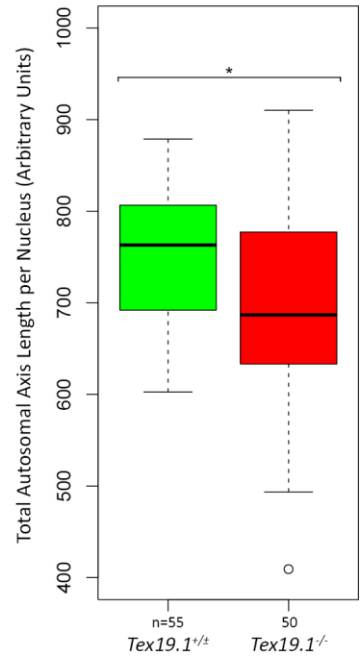

B

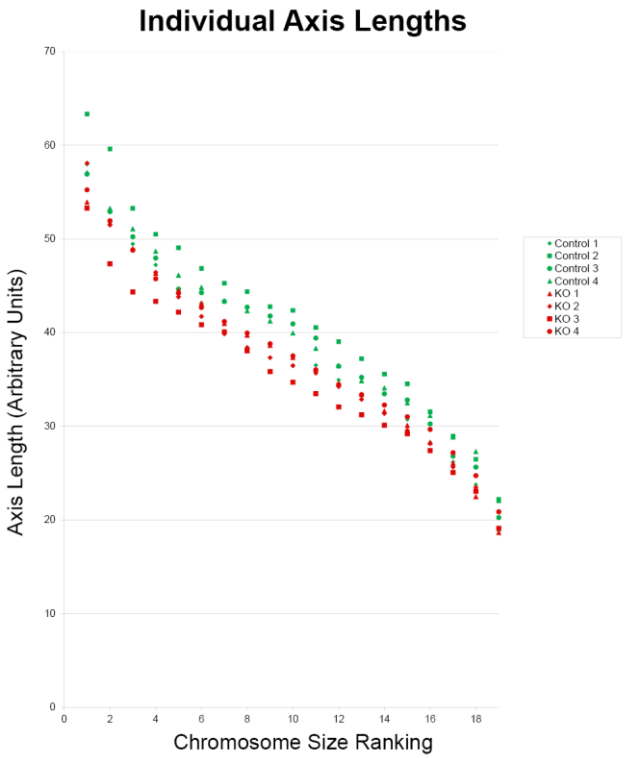

C

Grouped Axis Ranks	Sum mean axes lengths (arbitrary units)		% Reduction in Length
	Control	KO	
1-2	113.69	105.79	6.95*
3-5	146.20	137.04	6.27*
6-11	248.31	231.90	6.61*
12-16	166.92	155.49	6.84*
17-19	73.53	69.80	5.08
Total	748.64	700.01	6.50*

Figure 5-8. Synapsed pachytene spermatocyte axis length.
(A) Boxplot showing total autosomal axis length per MLH1-positive nucleus in control and *Tex19.1*$^{-/-}$ synapsed pachytene nuclei, calculated by measuring SYCP3-stained filaments. (B) Individual ranked axis lengths for each animal. Mean lengths for four pairs of animals plotted. (C) Table of grouped axis lengths. Significance of p≤0.05 indicated by a single asterisk.

I next assessed the possibilities that differences in the continuous trait of axis length could reflect fundamental changes in axis composition or changes in pachytene stage dynamics, and also investigated whether this process correlates more closely with other delayed features of *Tex19.1*$^{-/-}$ pachytene to better understand the relationships between the events studied. As I have already shown a dramatic delay in the formation of DSBs in early

prophase and this is likely to be responsible for the delayed DSB repair in pachytene. It is an attractive possibility that recombination delays are central in orchestrating delays in other processes in *Tex19.1*$^{-/-}$. Therefore I next investigated the coordination between axis elongation and DSB repair in pachytene by comparing axis length between spermatocytes previously found to possess different degrees of DNA damage identified by autosomal γH2AX foci (Figure 5-2B, Figure 5-9. As before, pachytene spermatocytes were grouped by ranges of γH2AX foci: no DNA damage (0 γH2AX foci) moderate damage (1-40 foci) or high damage (>40 foci). Axis length in control pachytene spermatocytes showed a steady and significant increase between the three levels of reducing DNA damage ($p<0.001$ between each level of DNA damage, Mann-Whitney U test), demonstrating that the increase in axis length does occur gradually during pachytene (Figure 5-9). *Tex19.1*$^{-/-}$ spermatocytes demonstrated a similar pattern of increasing axis length with decreasing DNA damage, consistent with meiotic progression. The reduction in axis length between spermatocytes with moderate levels and no DNA damage was not significant however, likely because very few *Tex19.1*$^{-/-}$ spermatocytes with no DNA damage could be found to include in this analysis due to their scarcity. Remarkably, when the length of axes was compared between control and *Tex19.1*$^{-/-}$ spermatocytes grouped based on DNA damage levels, no significant difference was apparent. Therefore protein composition of the chromosome core is unlikely to be fundamentally altered in *Tex19.1*$^{-/-}$, and the process of elongation shows a closer association to DNA damage than to CO formation. This close association may be caused by a direct relationship, as changes in chromosome core composition are implicated in DSB repair (Lightfoot et al., 2011). The close relationship between recombination and axis length, and less direct relationship with CO formation inferred, does not exclude the possibility that delays to recombination could also be responsible for causing delays to other pachytene processes though such delays may be less tightly synchronised. For example it is possible that a DNA damage checkpoint(s) during pachytene could coordinate progression of other events at sub-stages.

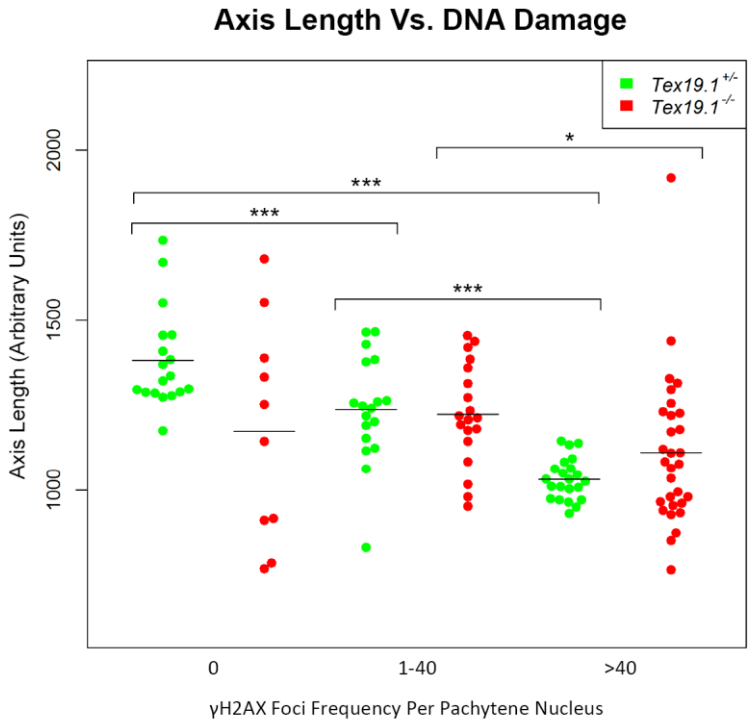

Figure 5-9. Pachytene autosomal axis length compared to DNA damage
Beeswarm plot comparing the total length of pachytene autosomal synaptonemal complex axes between spermatocytes with either 0, 1-40, or >40 autosomal γH2AX foci indicative of DNA damage (no damage, "moderate" damage, "high" damage respectively). Genotypes indicated in key. Significant differences indicated by brackets and asterisks.

To investigate directly whether the delayed pachytene progression in *Tex19.1*$^{-/-}$ is caused by recombination defects or by an additional recombination-independent meiotic role for TEX19.1, I assessed pachytene progression in the absence of meiotic recombination. *Spo11*$^{-/-}$ spermatocytes fail to generate meiotic DSBs and as such are unable to undergo meiotic recombination and synapsis is defective (Baudat et al., 2000; Romanienko and Camerini-Otero, 2000). Despite this, *Spo11*$^{-/-}$ spermatocytes are able to progress to mid-pachytene and recruit H1t (Barchi et al., 2005), an event which I have shown to be delayed in *Tex19.1*$^{-/-}$. By assessing the frequency of H1t positive asynapsed zygotene-like spermatocytes with fully formed axes but only partial synapsis in *Spo11*$^{-/-}$ and *Spo11*$^{-/-}$ *Tex19.1*$^{-/-}$ mice I was able to assess the effect of TEX19.1 on pachytene progression independently of its effect on DSB formation (Figure 5-10A). H1t staining was detected in approximately 50% of *Spo11*$^{-/-}$ single mutant spermatocytes analysed (Figure 5-10B), and in *Tex19.1*$^{-/-}$*Spo11*$^{-/-}$ double knockout mice a similar frequency of H1t positive zygotene-like spermatocytes were observed (p=1.00; Fisher's exact test) (Figure 5-10B). Therefore the reduced ability of spermatocytes to progress to an H1t-positive mid-pachytene stage of

meiosis in the absence of TEX19.1 is dependent on the meiotic DSB forming endonuclease SPO11. This finding indicates that the delayed pachytene progression observed in *Tex19.1*$^{-/-}$ is related to the meiotic recombination defects incurred in this mutant and is consistent with the presence of recombination-related checkpoints during pachytene.

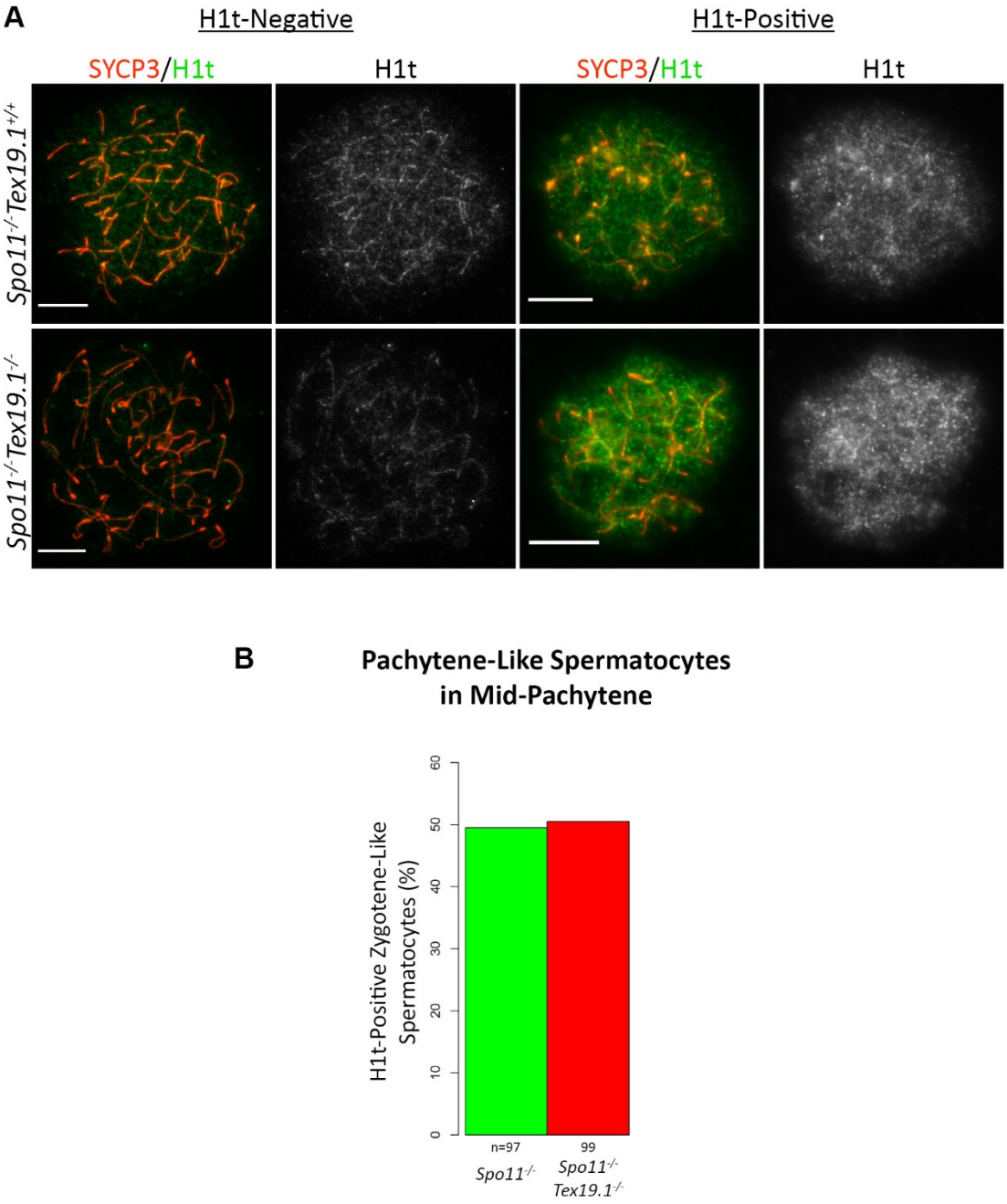

Figure 5-10. Mid-pachytene progression of spermatocytes Lacking SPO11
(A) Representative H1t-negative and H1t-positive (green) staining patterns present in *Spo11*$^{-/-}$ and *Tex19.1*$^{-/-}$*Spo11*$^{-/-}$ zygotene-like asynapsed spermatocytes, combined with antibody staining of SYCP3 (red) to mark the axial element of the synaptonemal complex for staging. Merges and single channel images displayed. 10µm scale bars. (B) Barplot showing the percentage of zygotene-like spermatocytes with detected H1t staining.

5.3 Discussion

My research presented in this chapter reveals that despite 65% of *Tex19.1*$^{-/-}$ pachytene spermatocytes achieving successful autosomal synapsis, this sub-population still displays abnormalities. *Tex19.1*$^{-/-}$ pachytene spermatocytes display elevated levels of unrepaired DSBs, characteristic of early pachytene cells, and a reduction in nuclei displaying markers of mid/late pachytene such as H1t, MLH1 and sex body associated UbH2A. Furthermore the gradual establishment of ubiquitination associated with sex body chromatin as well as the dissociation of axis-associated ubiquitination from autosomes is also delayed. The enrichment in pachytene spermatocytes displaying diverse immature features in *Tex19.1*$^{-/-}$ is not caused by mid-pachytene meiotic arrest eliminating more mature cells as MSCI, the major cause of such arrest, remains effective. These findings point to a delay in the progression of *Tex19.1*$^{-/-}$ spermatocytes through pachytene. Elongation of chromosome axes during pachytene was found to be a gradual process associating closely with levels of DNA damage, but less so with CO formation. Therefore some delayed features of *Tex19.1*$^{-/-}$ pachytene spermatocytes are more closely coordinated than others, possibly indicating more direct relationships. However, delayed expression of H1t in the absence of TEX19.1 was found to be dependent on SPO11 and therefore is likely to also be related to recombination. It is possible that the delayed initiation of recombination of *Tex19.1*$^{-/-}$ spermatocytes presented in chapter 4 also has implications for pachytene spermatocytes which achieve full synapsis, with delays to recombination resulting in delayed progression of diverse events in this stage. These findings may indicate the presence of recombination-related checkpoint(s) during pachytene to coordinate progression.

5.3.1 *Tex19.1*$^{-/-}$ Spermatocytes Survive Pachytene after Autosomal Synapsis is Achieved

Tex19.1$^{-/-}$ testes display autosomal asynapsis in approximately 65% of pachytene spermatocytes. In the original analysis on outbred *Tex19.1*$^{-/-}$ mice univalent chromosomes were observed in 66% of the remaining spermatocytes which progress to metaphase I, and the final sperm count of *Tex19.1*$^{-/-}$ male mice was ~1% (Ollinger et al., 2008). The rate of the meiotic defects identified in *Tex19.1*$^{-/-}$ spermatocytes thus far is currently insufficient to fully account for the reduction in sperm observed. It is possible that additional fatal defects exist during *Tex19.1*$^{-/-}$ spermatogenesis which account for cell loss. Mid-pachytene is a common arrest-point for defective spermatocytes, primarily due to failed MSCI (Barchi et al., 2005;

Mahadevaiah et al., 2008). The successful localisation of γH2AX to sex body chromatin and the absence of detectable protein encoded by the Y-linked *Rbmy* gene however, are consistent with successful MSCI in *Tex19.1*$^{-/-}$ pachytene spermatocytes. Failed MSCI is the most widely reported cause of pachytene spermatocyte arrest, though a DNA damage checkpoint also appears to exist (Li and Schimenti, 2007; Roig et al., 2010). Cell counts of synapsed pachytene and diplotene spermatocytes have not shown any indication of spermatocyte arrest between these stages in *Tex19.1*$^{-/-}$ (data not shown), therefore the DNA damage checkpoint also does not appear to be triggered in this mutant. It is possible that additional cell loss occurring later in spermatogenesis, or some degree of error in the measurement of asynapsis, metaphase univalent chromosomes or sperm counts accounts for the reduction in sperm initially recorded in *Tex19.1*$^{-/-}$ (Ollinger et al., 2008).

5.3.2 Progression through Pachytene is Delayed in *Tex19.1*$^{-/-}$ Spermatocytes

Curiously, the progression of *Tex19.1*$^{-/-}$ spermatocytes through pachytene was found to be delayed, with fewer spermatocytes staining positive for the mid-pachytene marker H1t, the late recombination marker MLH1, or the MSCI-associated ubiquitination of histone H2A. Furthermore, the general dynamics of mono/poly ubiquitination at the sex chromosomes and on autosomal axes, as well as chromosome elongation also appeared to be delayed. None of the pachytene events investigated appeared to proceed with normal dynamics in *Tex19.1*$^{-/-}$. This shared delay strongly indicates the presence of a system coordinating the processes taking place during this stage. Pachytene is a particularly long stage of meiotic prophase, lasting 3-5 days (Bellvé et al., 1977; Speed, 1982) during which numerous events take place which likely have important roles in promoting continued progression through spermatogenesis. Cell-cycle coordination during this stage would therefore be of great value to ensure controlled spermatocyte development.

Delayed progression of spermatocytes to mid-pachytene and expression of H1t in *Tex19.1*$^{-/-}$ was found to be dependent on SPO11. As the main known function of SPO11 is to generate meiotic DSBs at the start of meiosis (Baudat et al., 2000; Romanienko and Camerini-Otero, 2000), this suggests that the delay in pachytene progression in *Tex19.1*$^{-/-}$ spermatocytes is dependent on meiotic DSBs. Research in a range of meiotic mutant mice has shown that the ability of spermatocytes to reach an H1t-positive state is not dependent on chromosome synapsis and can also be reached in mutant spermatocytes with a large amount

of unrepaired DNA damage such as *Dmc1*$^{-/-}$ and *Msh5*$^{-/-}$ (Mahadevaiah et al., 2008). While both *Dmc1*$^{-/-}$ and *Msh5*$^{-/-}$ spermatocytes can become H1t-positive, H1t staining is weaker in *Dmc1*$^{-/-}$ spermatocytes than *Msh5*$^{-/-}$ suggesting that cells arrest at a slightly earlier stage (Mahadevaiah et al., 2008), possibly due to retarded progression. While both mutants contain persistent unrepaired DSBs, those in *Dmc1*$^{-/-}$ spermatocytes are unable to progress as far through meiotic recombination as DSBs in *Msh5*$^{-/-}$ spermatocytes (Pittman et al., 1998; de Vries et al., 1999). Therefore partial progression of recombination may be sufficient to permit pachytene expression of H1t.

Zip4h$^{-/-}$ and *Trip13*$^{mod/mod}$ spermatocytes have an impaired ability to repair meiotic DSBs, and high levels of immature recombination intermediates persist in synapsed pachytene spermatocytes (Adelman and Petrini, 2008; Li and Schimenti, 2007) in an apparently similar manner to *Tex19.1*$^{-/-}$. However unlike *Tex19.1*$^{-/-}$ pachytene spermatocytes, the formation of COs by MLH1 does not appear to be delayed in *Trip13*$^{mod/mod}$ or *Zip4h*$^{-/-}$ (Adelman and Petrini, 2008; Li and Schimenti, 2007). Therefore as with the expression of H1t, unrepaired DNA damage per se is not sufficient to delay CO formation. Axis length was found to coordinate closely with DNA damage but less so with ability to recruit MLH1, and axis length remains reduced in MLH1-positive cells implying that levels of DNA damage are also elevated in crossover-forming *Tex19.1*$^{-/-}$ spermatocytes. This is consistent with the theory that elevated DNA damage per se does not inhibit crossover formation. It is possible however that due to the aberrant initial formation of meiotic DSBs in *Tex19.1*$^{-/-}$ spermatocytes some DNA damage present after synapsis remains in a highly immature state of progression through recombination which is not present in *Trip13*^{modmod} or *Zip4h*$^{-/-}$ at this stage, and is capable of triggering a delay in H1t expression and CO formation, as well as the other delays discussed. Alternatively, the delayed formation of DSBs may more directly result in the absence of sufficiently mature DSBs to undergo CO formation until later in pachytene in *Tex19.1*$^{-/-}$.

It is interesting to note that the elongation of chromosome axes is a process which was shown to associate very closely with DNA damage in control and *Tex19.1*$^{-/-}$ spermatocytes, suggesting that axial elongation and repair of DNA damage could be directly related. This is an association that has not previously been reported. A reduction in axis length is widely linked with reduced cohesin (Fukuda et al., 2014; Murdoch et al., 2013; Novak et al., 2008; Revenkova et al., 2004; Vranis et al., 2010), therefore a reduction in axis length in response to DNA damage may indicate a removal of cohesin. Conversely, cohesin loading has been demonstrated in response to DNA damage in mammalian cells (Kim et al.,

2002) and is required for repair of meiotic DNA damage in *C. elegans* (Lightfoot et al., 2011). Therefore the cause of axis length reduction in response to DNA damage is currently unclear and will require much further investigation.

DNA damage influences the mitotic cell-cycle and is capable of triggering a delayed cell-cycle progression in such cells (Bartek and Lukas, 2001). My findings indicate that a similar system(s) is likely to be involved in regulating spermatocyte progression through the lengthy pachytene stage. Two key classes of regulatory molecules typically control cell cycle progression, cyclins and cyclin-dependent kinases (CDKs) (Satyanarayana and Kaldis, 2009). CDK2 is known to localise to MLH1-positive sites of crossover formation in pachytene and the phosphorylation of CDK2 appears to trigger transition from pachytene to diplotene in mouse spermatocytes (Liu et al., 2014; Ward et al., 2007). As I have shown that axis length associates with DNA damage levels, the reduction in axis length of MLH1-positive *Tex19.1*$^{-/-}$ spermatocytes suggests the presence of greater unrepaired DNA damage than controls. As this DNA damage is repaired before progression of *Tex19.1*$^{-/-}$ spermatocytes to diplotene (data not shown) it is likely that the presence of DNA damage in late pachytene inhibits CDK2 phosphorylation and the subsequent initiation of spermatocyte transition into diplotene. This proposal fits with reports that despite the presence of high levels of unrepaired DNA damage in MLH1-positive *Zip4h*$^{-/-}$ spermatocytes, cells do not progress to diplotene until DNA damage is repaired (Adelman and Petrini, 2008). There does appear to be a DNA damage checkpoint at the end of pachytene which is capable of triggering arrest of spermatocytes with DNA damage that is unable to repair (Li and Schimenti, 2007). In oocytes this checkpoint is dependent on CHK2, however this is not the case in spermatocytes (Bolcun-Filas et al., 2014). A similar meiotic DNA-damage checkpoint has also been thoroughly studied in yeast (Marston and Amon, 2004). The mechanisms of cell cycle control which might be operating to regulate earlier stages of pachytene that are delayed in *Tex19.1*$^{-/-}$ are currently unclear.

5.3.3 Ubiquitination in *Tex19.1*$^{-/-}$ Pachytene Spermatocytes

The mechanism by which TEX19.1 affects meiosis is not known, though its role as a major interaction partner of the E3 ubiquitin ligase UBR2 (Yang et al., 2010) suggests involvement in meiotic ubiquitination. *Ubr2*$^{-/-}$ spermatocytes are defective in chromosome synapsis, possess elevated levels of DNA damage in pachytene, appear to be unable to mono-ubiquitinate histone H2A at the sex body and arrest in pachytene (An et al., 2010, 2012). Furthermore, UBR2 is required for the stability of TEX19.1 in testes (Yang et al., 2010). As

this is the case, and because several of the published features of *Ubr2*$^{-/-}$ mice and *Tex19.1*$^{-/-}$ share similarities, these two mutants have been proposed to phenocopy (Yang et al., 2010). During this chapter I have demonstrated that unlike *Ubr2*$^{-/-}$, *Tex19.1*$^{-/-}$ pachytene spermatocytes are able to ubiquitinate histone H2A at the sex body and as such these mutants do not phenocopy. It remains a possibility that the role of TEX19.1 in meiosis relates to that of UBR2, however the meiotic phenotype of *Ubr2*$^{-/-}$ is at least partially due to TEX19.1-independent defects.

Investigation into the ubiquitination of meiotic substrates during pachytene in my analysis has revealed that in addition to the previously identified patterns associated with the sex body (An et al., 2012), ubiquitination also occurs at focal locations along autosomal axes. This pattern was present in control and *Tex19.1*$^{-/-}$ spermatocytes and is therefore a pattern associated with normal meiotic events. As this pattern was enriched in *Tex19.1*$^{-/-}$ pachytene spermatocytes it is likely to relate to events normally occurring early in this stage, consistent with delayed progression. The focal nature of the staining is reminiscent of recombination foci, therefore ubiquitination at this location may relate to the progression of DNA damage repair. It is possible that such staining relates to the HEI10-mediated ubiquitination which promotes the resolution of recombination intermediates in pachytene (Qiao et al., 2014).

Chapter 6:

Investigating the Source of Univalent Metaphase I Chromosomes in *Tex19.1*$^{-/-}$ Testes

6 Investigating the Source of Univalent Metaphase I Chromosomes in *Tex19.1*$^{-/-}$ Testes

6.1 Introduction

The question I sought to answer in the final results chapter of my thesis was how univalent chromosomes arise in *Tex19.1*$^{-/-}$ metaphase I spermatocytes (Ollinger et al., 2008). Meiotic recombination ultimately culminates in the pairing of homologous chromosomes and the repair of DNA DSBs, with at least one repair event per chromosome pair being resolved in a manner which generates a genetic exchange. These genetic exchanges are known as crossovers (COs). CO formation introduces genetic diversity into germ cells produced and also establishes a physical linkage between homologous chromosomes which is maintained by the cohesin complex and manifest in metaphase I as chiasmata, holding homologous chromosomes in a bivalent conformation (Hodges et al., 2005). The bivalent state of homologous chromosomes is required to ensure bidirectional segregation of homologs in the first meiotic division. In the absence of chiasmata homologous chromosomes are present in metaphase I in a univalent state and are unable to reliably segregate, leading to aneuploidy (Handel and Schimenti, 2010).

The 200-300 DSBs normally made during meiotic recombination (Moens et al., 2002) are eventually resolved either to produce a non-crossover (NCO) (~90% of DSBs), where the repaired DNA strand returns to its chromosome of origin, or to produce a CO by exchanging DNA flanking the break site between each chromosome. CO formation is largely dependent on the MLH1-MLH3 endonuclease (Eaker et al., 2002; Edelmann et al., 1996; Lipkin et al., 2002; Rogacheva et al., 2014). The frequency and positioning of axial foci formed by MLH1 and MLH3 in pachytene closely corresponds with that of chiasmata in metaphase I (Anderson et al., 1999; Lipkin et al., 2002). Typically around 23 COs/chiasmata are formed per mouse spermatocyte, with their distribution tightly controlled. At least one CO must form on each chromosome pair for chromosome segregation to be successful (Fledel-Alon et al., 2009). While the majority of COs are generated by an MLH1/3-dependent pathway (Class I CO pathway) a small number (~3) of COs per mouse spermatocyte are generated in the absence of these proteins (Eaker et al., 2002). These COs are generated by the MUS81-dependent Class II CO pathway, and are insensitive to CO interference (Holloway et al., 2008). Univalent metaphase I chromosomes can be produced by reduced recruitment of Class I CO forming machinery (Adelman and Petrini, 2008; Eaker

et al., 2002; Roig et al., 2010) however a reduction in Class II CO formation is compensated for by additional Class I CO formation and bivalency in metaphase is not affected (Holloway et al., 2008).

Chromosome synapsis is also vital for CO formation (Kauppi et al., 2011; de Vries et al., 2005), hence asynapsis may also be capable of causing univalent chromosomes in metaphase I. Spermatocyte progression to metaphase I is dependent on the successful establishment of MSCI (meiotic sex chromosome inhibition) in pachytene. MSCI is antagonised by extensive asynapsis as unsynapsed autosomes undergo a similar process of silencing (MSUC – meiotic silencing of unsynapsed chromatin) which sequesters the machinery involved (Mahadevaiah et al., 2008). MSCI failure results in mid-pachytene arrest. While extensive asynapsis has lethal consequences for pachytene spermatocytes due to failed MSCI, asynapsed sex chromosomes are tolerated until metaphase, where they are seen as univalents (Kauppi et al., 2011). Some additional asynapsis can be tolerated without disrupting MSCI, as spermatocytes carrying a single unsynapsed copy of human chromosome 21 progress to at least late pachytene (Mahadevaiah et al., 2008). It is important to note that while an unsynapsed surplus chromosome appears to be tolerated for prophase progression, the ability of a single pair of unsynapsed autosomes in a normal quadruploid spermatocyte to do so has not been assessed. It is possible that a low level of asynapsis could be endured without perturbing MSCI, however the establishment of MSUC on such chromosomes would alter autosomal gene expression and could silence essential genes (Burgoyne et al., 2009). Asynapsis only affects around 50% of *Tex19.1*$^{-/-}$ spermatocytes and these asynapsed nuclei also contain synapsed chromosomes (Ollinger et al., 2008), suggesting that the severity of the synapsis defect may vary. If spermatocytes with low-level asynapsis exist in *Tex19.1*$^{-/-}$ it may be possible for these to progress to metaphase I and generate the individual univalent chromosomes reported (Ollinger et al., 2008).

The initial report of the *Tex19.1*$^{-/-}$ mutant mouse phenotype revealed the presence of univalent chromosomes in 66% of metaphase I spermatocytes, with 56% containing univalent sex chromosomes and 33% containing a univalent autosome (Ollinger et al., 2008). This defect is likely to be partially responsible for the infertility incurred in the absence of TEX19.1 in male mice. It is currently unknown whether these univalent chromosomes are generated by spermatocytes with low-level asynapsis progressing to metaphase, or by an unidentified defect in CO formation, distribution or maintenance on synapsed chromosomes. In this chapter I investigate the possibility that defective CO formation or chromosome asynapsis could account for univalent chromosomes in *Tex19.1*$^{-/-}$ metaphase I spermatocytes.

6.2 Results

6.2.1 Validating the Metaphase I Defect in Backcrossed *Tex19.1*$^{-/-}$ Spermatocytes

The original report of elevated levels of univalent metaphase I chromosomes in *Tex19.1*$^{-/-}$ spermatocytes was made following analysis of mice from a mixed 129/Ola x CD1 background (Ollinger et al., 2008). This mouse line has since been backcrossed to C57/B6. I began this investigation into the cause of the univalent chromosomes by assessing their frequency in metaphase I spermatocytes from control and *Tex19.1*$^{-/-}$ testes to establish the presence and severity of this defect in the backcrossed mouse population. Only nuclei with a complete set of 20 homologous chromosome pairs were scored. DNA was stained with DAPI and DNA FISH was performed for major satellites: very large arrays of tandemly repeating non-coding DNA which constitute the main component of functional centromeres (Figure 6-1A). Major satellite FISH was used to identify centromeres and orientate chromosomes analysed. Bivalent pairs of chromosomes were typically recognisable as two lengths of closely aligned DAPI-stained DNA domains, sharing a visible mirrored connection. Chromosomes uniformly aligned opposite one another but lacking a visible connection were suspected to share terminal exchanges. Sex chromosomes were recognised by their similarly shared pairing and alignment, but greatly differing length, and the absence of major satellite staining on the Y chromosome (Figure 6-1A) (Broccoli et al., 1990). Univalent chromosomes were scored as those lacking recognisable pairings or homologous interactions (Figure 6-1A). Univalent chromosomes were observed in 22% of control metaphase I nuclei, with 19% of nuclei containing univalent sex chromosomes, 7% containing univalent autosomes, and the frequency of univalent autosomes never rising above one per nucleus (Figure 6-1B). As has been previously reported, the frequency of univalent XY chromosomes is much higher than that of autosomes (Léotard et al., 1987). The total frequency of control nuclei with univalent chromosomes is higher than previously reported (5% of *Tex19.1*$^{-/-}$ metaphase I contain univalent chromosomes. 5% XY, 1% autosomal) (Léotard et al., 1987; Ollinger et al., 2008), this may be a consequence of the spread preparation approach or differences in the scoring of nuclei between researchers.

In *Tex19.1*$^{-/-}$ testes the rate of metaphase I nuclei containing univalent chromosomes was increased to 53% ($p<0.001$ Fisher's exact test) in backcrossed mice (Figure 6-1B). 36% of nuclei analysed contain univalent sex chromosomes ($p=0.03$; Fisher's exact test) and 19%

contain univalent autosomes (p=0.01; Fisher's exact test), with no nuclei containing more than one univalent pair of autosomes. These rates are slightly lower than those previously reported in *Tex19.1*$^{-/-}$ outbred mice (56% nuclei with univalent XY, 33% with a univalent autosome (Ollinger et al., 2008)). This finding demonstrates a consistent increase in univalent chromosomes among metaphase I spermatocytes in the absence of TEX19.1, with small numbers of chromosomes affected in each nucleus and the sex chromosomes being particularly susceptible.

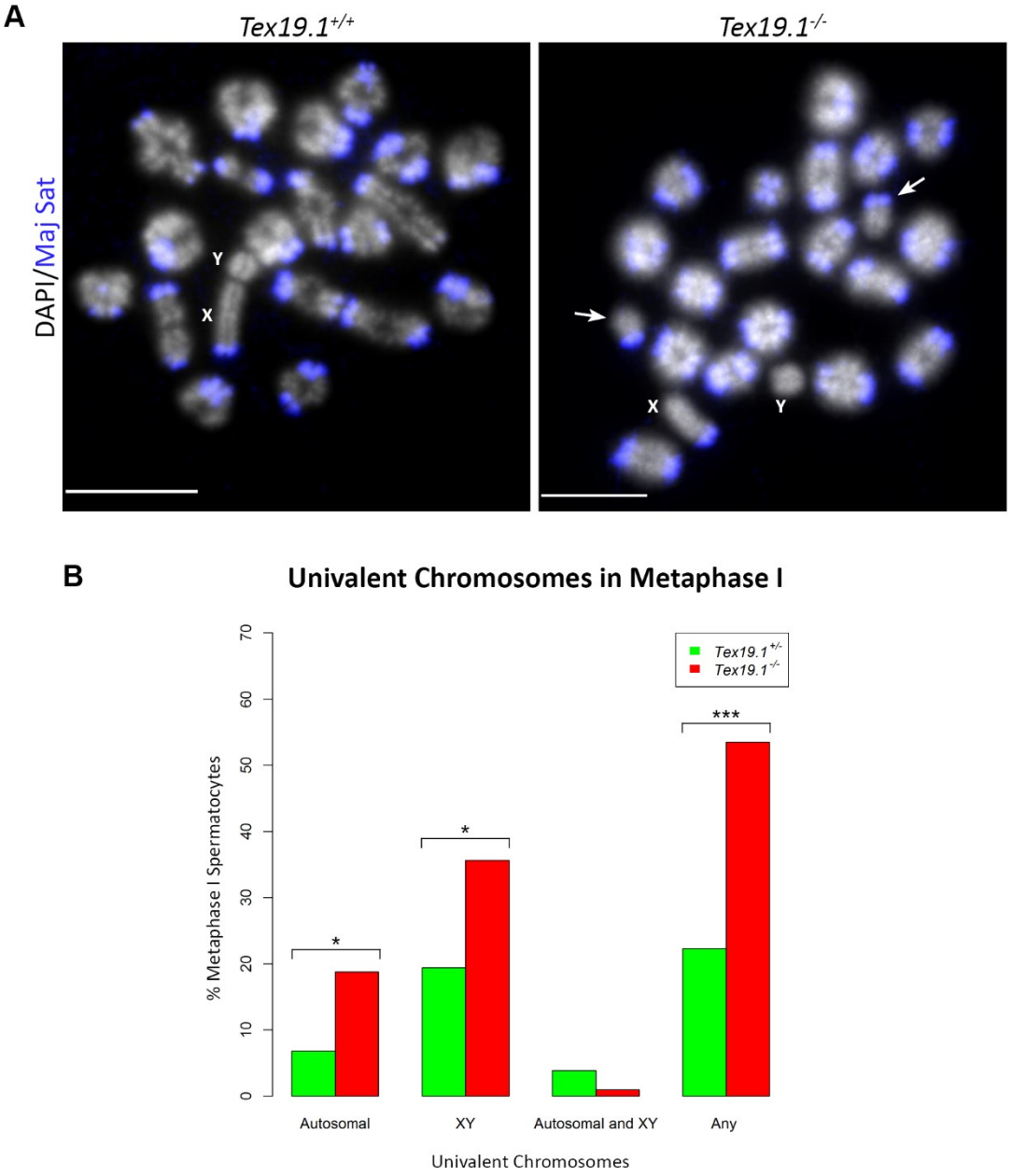

Figure 6-1. Analysis of univalent metaphase I chromosomes
(A) Representative *Tex19.1*$^{+/+}$ and *Tex19.1*$^{-/-}$ metaphase I spermatocytes. DNA stained with DAPI (monochrome) and centromeres marked by major satellite DNA FISH (blue). Arrows indicate univalent autosomes, and the X and Y sex chromosomes are labelled. 10µm scale bars. (B) Bar graph displaying the percentage of metaphase I spermatocytes with univalent chromosomes. The specific nature of the univalent chromosomes identified is indicated. *Tex19.1*$^{+/\pm}$ N=103, *Tex19.1*$^{-/-}$ N=101. Asterisks denote significance.

6.2.2 Autosomal Crossover Formation in Pachytene *Tex19.1*$^{-/-}$ Spermatocytes

I next investigated whether a reduction in CO formation could be responsible for the elevated level of univalent chromosomes in *Tex19.1*$^{-/-}$ metaphase I spermatocytes. COs are generated during pachytene, and are largely dependent on MLH1 which localises to axial foci at this stage (Eaker et al., 2002). The frequency and positioning of MLH1 foci closely correspond to that of chiasmata and is widely used as a marker for CO formation (Anderson et al., 1999). To investigate whether fewer COs are formed in *Tex19.1*$^{-/-}$ spermatocytes I scored the frequency of MLH1 foci on autosomal axes in pachytene spermatocytes with autosomal synapsis (Figure 6-2A). I recorded the mean of 21.7 MLH1 foci per nucleus across the 19 autosomes of control pachytene spermatocytes (Figure 6-2B), similar to some previously reported MLH1 foci counts for C57BL/6 mice (Anderson et al., 1999), but slightly lower than others (Koehler et al., 2002) (~24 autosomal foci in this strain of mouse). My analysis of MLH1 foci frequency in *Tex19.1*$^{-/-}$ pachytene spermatocytes revealed a similar mean of 21.2 autosomal MLH1 foci per pachytene nucleus ($p=0.46$; Mann-Whitney U test) (Figure 6-2B). Therefore as there is not a detectable reduction in the total frequency of MLH1 foci in *Tex19.1*$^{-/-}$ spermatocytes, a reduction in total autosomal CO frequency does not appear to cause the achiasmate autosomes in metaphase I.

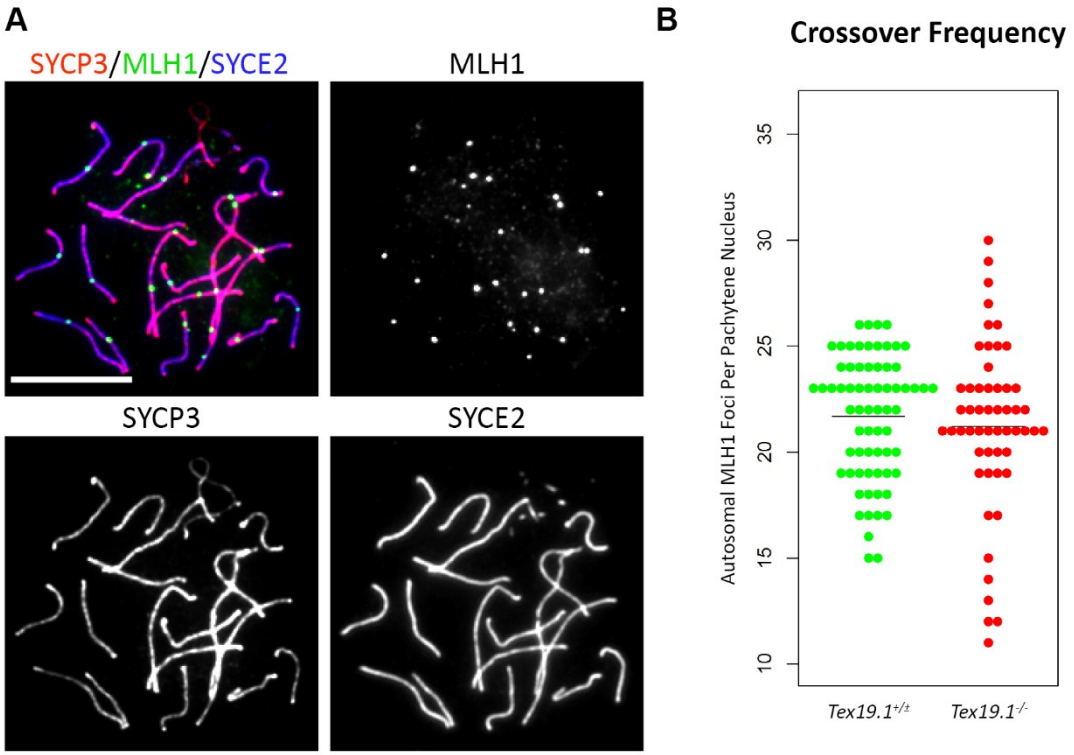

Figure 6-2. MLH1 analysis of crossover formation
(A) MLH1-positive synapsed pachytene nucleus, typical of those analysed. MLH1 (green), SYCP3 (red) and SYCE2 (blue) shown in merge and single colour monochrome images. 10µm scale bar. (B) Beeswarm plot showing total frequency of MLH1 antibody stained foci on autosomes per nucleus of control and *Tex19.1*$^{-/-}$ pachytene spermatocytes. N=65, 54 respectively. Black bars indicate mean frequency.

6.2.3 Autosomal Crossover Distribution

As one CO per autosome pair is necessary for each pair of homologous chromosomes to form a bivalent, the distribution of the COs is critical. I next investigated the number of COs being formed on each autosome to establish whether an increase in autosomes lacking COs could account for the univalents in *Tex19.1*$^{-/-}$ metaphase I spermatocytes. I scored the frequency of MLH1 foci per autosomal axis in control and mutant pachytene spermatocytes. Control pachytene spermatocytes lacked MLH1 foci on 4.6% of autosomes and such axes were observed in 54% of nuclei (Figure 6-3A, B). This was a surprisingly high frequency given that a single pair of univalent autosomes was only detected in 7% of metaphase I nuclei, and likely reflects the asynchronous recruitment and/or dissociation of MLH1 foci. Previous analyses by Anderson *et al* observe an absence of MLH1 foci on 4% of autosomes (Anderson et al., 1999), a frequency close to that which I observe in my analysis. Autosomes lacking MLH1 foci may be overestimated in these analyses due to the transience of MLH1

staining. Furthermore, as a portion of COs are MLH1-independent some COs are not detectable by this approach therefore MLH1 counts are always expected to be a slight underestimate of CO frequency (Holloway et al., 2008).

Analysis of MLH1 focus frequency on *Tex19.1*$^{-/-}$ pachytene autosomes revealed that 55% of synapsed MLH1 positive nuclei possess an autosome without an MLH1 focus (p=1, Fisher's exact test) (Figure 6-3A), with 6.66% of autosomes affected (p=0.17, Fisher's exact test) (Figure 6-3B). Similar analysis into the frequency of autosomes with 1, 2, or 3 MLH1 foci also did not show a significant difference between control and *Tex19.1*$^{-/-}$ spermatocytes (Figure 6-2B). Therefore there is not a detectable change in the distribution of COs among autosomes in *Tex19.1*$^{-/-}$, and as such failure to form COs does not appear to cause the increase in univalent metaphase I autosomes in *Tex19.1*$^{-/-}$ testes.

Finally I assessed the positioning of COs along autosomes as they are known to be consistently enriched and depleted at certain chromosomal locations and misplacement can impair chromosome segregation (Martinez-Perez and Colaiácovo, 2009). To investigate whether altered positioning of crossover sites in *Tex19.1*$^{-/-}$ could contribute to the generation of univalent chromosomes, I assessed the proximity of MLH1 foci to the centromere on autosomes with single MLH1 focus. Centromeres were identified by intense DAPI staining as previously performed by Anderson *et al* (Anderson et al., 1999). The position of each MLH1 focus was calculated as a percentage of the total axis length and divided into 10 equally spaced groups. As expected, MLH1 frequency in control spermatocytes was low in the portion of chromosome axes closest to the centromeres and the telomeres, peaking near the sub-telomeric interval (Figure 6-2C) (Anderson et al., 1999). The distribution of MLH1 foci was not seen to differ in *Tex19.1*$^{-/-}$ spermatocytes (p=1, t-test). Therefore the positioning of individual crossovers with regards to axial spacing from the centromere is unchanged in *Tex19.1*$^{-/-}$ and is not the cause of univalent chromosomes in mutant metaphase I nuclei. Together these data demonstrate that perturbation of MLH1 foci formation is not responsible for generating univalent autosomes in *Tex19.1*$^{-/-}$ metaphase I spermatocytes.

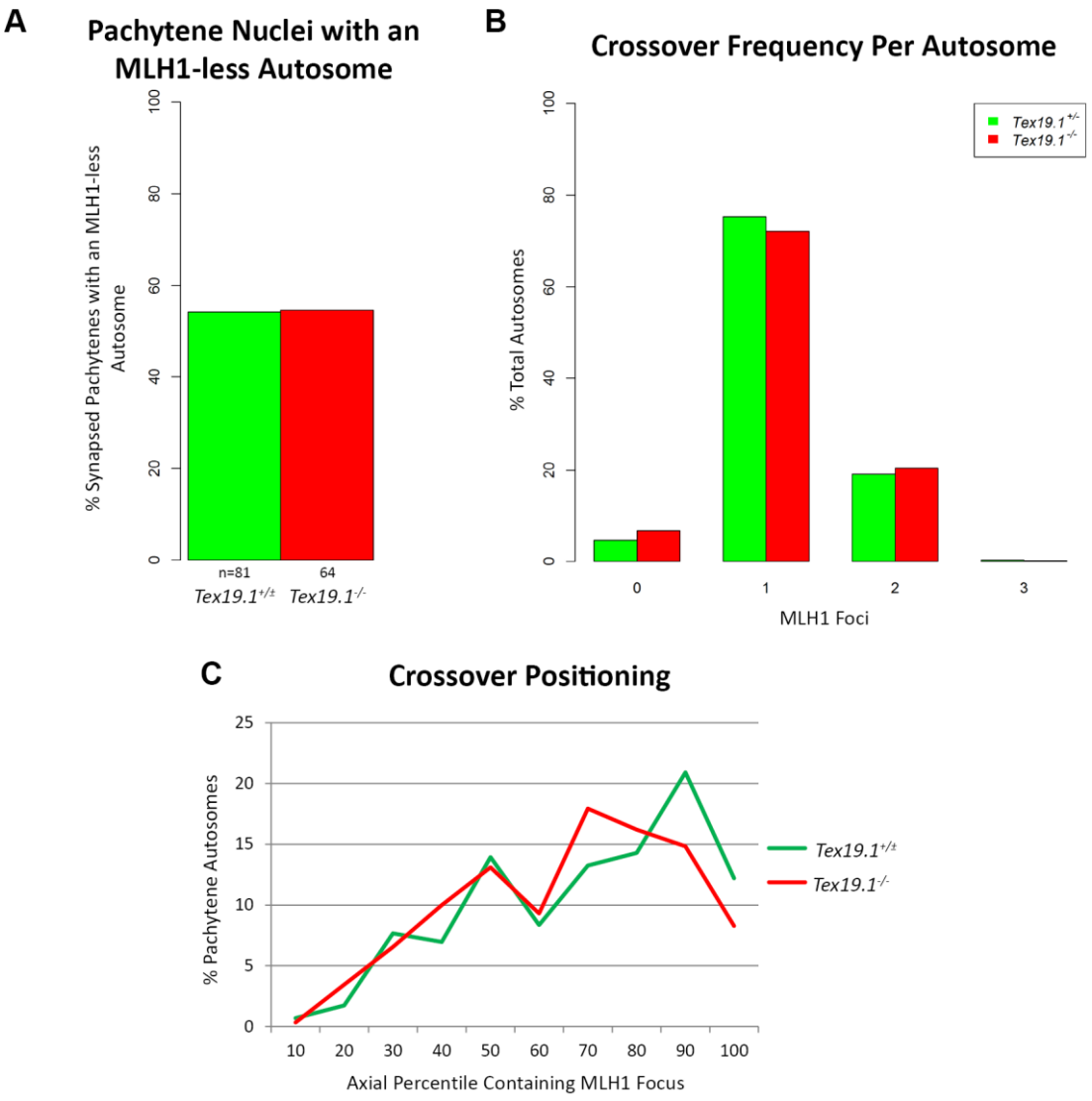

Figure 6-3. Autosomal MLH1 distribution and positioning
(A) Bar graph showing the percentage of pachytene spermatocytes with an autosome lacking an MLH1-marked crossover (CO) in control and *Tex19.1*$^{-/-}$. (B) Bar graph showing the frequency of MLH1-marked COs formed on each autosome. (C) Line graph showing the frequency of MLH1-marked CO formation positioned within 10 equal segments between the centromere and telomere.

6.2.4 Autosomal Asynapsis as a Source of Univalent Metaphase I Chromosomes in *Tex19.1*$^{-/-}$

Extensive chromosome asynapsis in spermatocytes impairs MSCI resulting in mid-pachytene arrest, however it may be possible for spermatocytes with low-level asynapsis to progress to metaphase I (Mahadevaiah et al., 2008). As no more than one univalent autosome was observed in any *Tex19.1*$^{-/-}$ nuclei (Figure 6-1B), only a single asynapsed autosome would be

expected to pass through from pachytene. To investigate whether this could occur in *Tex19.1*$^{-/-}$ I scored the extent of asynapsis in asynapsed pachytene spermatocytes during my earlier Masters research project. Counting the frequency of asynapsed autosomes revealed that 28% of defective pachytene nuclei had just one asynapsed autosome (Figure 6-4A, B). Therefore low-level asynapsis is indeed frequently observed among *Tex19.1*$^{-/-}$ spermatocytes.

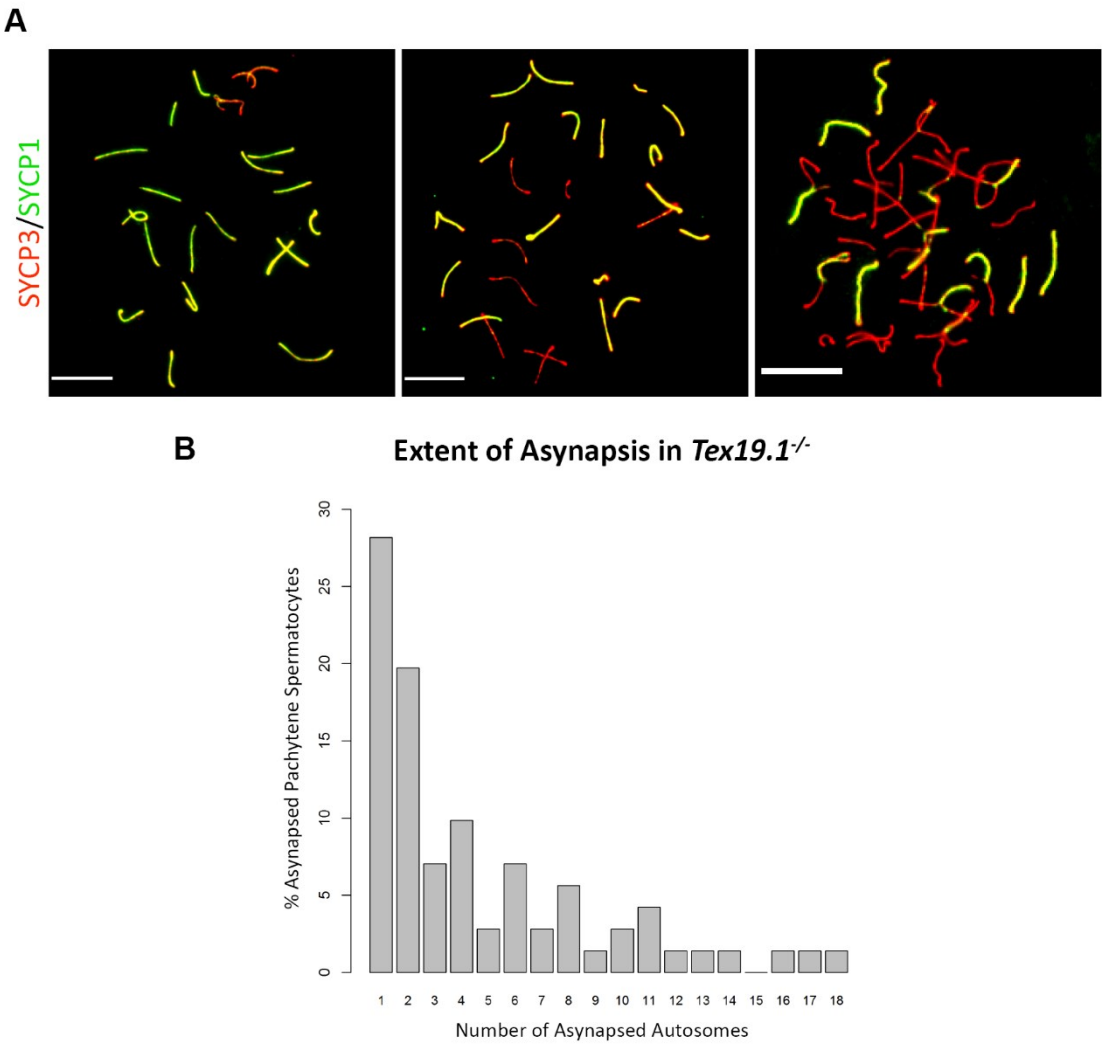

Figure 6-4. Extent of asynapsis in *Tex19.1*$^{-/-}$ Spermatocytes
(A) Representative images displaying the variation in severity of chromosome asynapsis in *Tex19.1*$^{-/-}$ spermatocytes. Axial element and central element stained with SYCP3 (red) and SYCP1 (green) respectively. (B) Barchart showing number of asynapsed autosomes in asynapsed *Tex19.1*$^{-/-}$ pachytene spermatocytes.

As only single autosomes are found to be univalent in *Tex19.1*$^{-/-}$ metaphase I spermatocytes, all cells progressing to this stage must form COs on the majority of autosomes, resulting in chiasmata. Therefore any asynapsed spermatocytes progressing to metaphase are expected to recruit CO forming machinery. To test whether this was the case I co-stained spermatocytes for SYCP3 and SYCE2 to gauge autosomal synapsis and MLH1 to

assess CO forming ability (Figure 6-5A). Analysis of control spermatocytes revealed no MLH1-positive asynapsed spermatocytes (Figure 6-5B). Analysis of *Tex19.1*$^{-/-}$ spermatocytes however found that 9.3% of MLH1-positive spermatocytes contain autosomal asynapsis (p=0.03, Fisher's exact test). These MLH1-positive asynapsed spermatocytes represent just 8.3% of the asynapsed spermatocytes in *Tex19.1*$^{-/-}$ (Figure 6-5B). Therefore the majority of asynapsed spermatocytes in this mutant appear to arrest prior to MLH1 recruitment, however a small sub-population do appear to progress to form COs. As MLH1 is a marker of late pachytene, these asynapsed spermatocytes also appear to avoid MSCI disruption and related meiotic arrest (Burgoyne et al., 2009; Ichijima et al., 2011). These asynapsed MLH1-positive nuclei typically exhibit limited asynapsis with a single autosome totally asynapsed (50%) (Figure 6-5A), thus unable to form a CO, consistent with the increase in metaphase I spermatocytes with a single univalent autosome in *Tex19.1*$^{-/-}$ (Figure 6-1B). Therefore asynapsis in pachytene appears to be able to account for the increase in univalent autosomes at metaphase I in *Tex19.1*$^{-/-}$ testes.

A

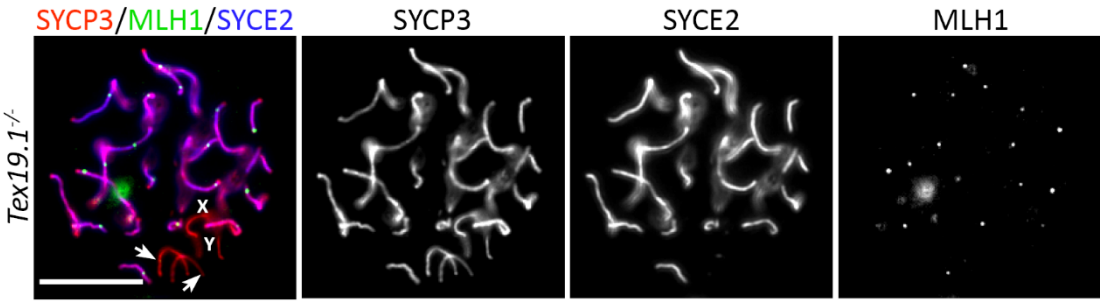

B

Genotype	% MLH1 Positive Nuclei with Asynapsed Autosome/s (n)	% Autosomally Asynapsed Nuclei with MLH1 Foci (n)
Tex19.1$^{+/\pm}$	0.00 (58)	0.00 (13)
Tex19.1$^{-/-}$	9.30* (43)	8.33 (48)

Figure 6-5. Autosomal asynapsis in MLH1 positive spermatocytes
(A) MLH1-positive *Tex19.1*$^{-/-}$ spermatocyte with a single pair of asynapsed autosomes (arrows) following antibody staining against MLH1 (green) in combination with SYCP3 (red) and SYCE2 (blue) to mark the axial element and central element of the synaptonemal complex respectively to stage spermatocytes and inform the status of synapsis. SYCP3 and SYCE2 staining co-localisation indicative of synapsis. X and Y chromosomes marked on merges. Merges and single channel images shown. 10µm scale bars. (B) Table showing the frequency of autosomal asynapsis in MLH1-positive spermatocytes and the frequency of MLH1 recruitment in asynapsed spermatocytes. Asterisks indicate significance when compared between genotypes (p≤0.05, Fisher's exact test).

6.2.5 Crossover Formation between Sex Chromosomes in *Tex19.1*$^{-/-}$ Spermatocytes

Defective *Tex19.1*$^{-/-}$ metaphase I spermatocytes most frequently contain univalent sex chromosomes. CO formation between the sex chromosomes was not analysed together with the autosomes as they display distinct pairing and recombination dynamics (Kauppi et al., 2011). To assess whether defective CO formation between sex chromosomes is responsible for their frequent lack of chiasmata in *Tex19.1*$^{-/-}$ I next assessed the frequency of crossover formation at the synapsed sex chromosome pseudoautosomal region (PAR). I did so by scoring for the presence of an MLH1 focus at the synapsed PAR in spermatocytes with synapsed MLH1-positive autosomes. Spermatocytes were co-stained with antibodies against MLH1 as well as SYCP3 and SYCE2 to mark the AE and CE respectively as previously described (Figure 6-6A). Sex chromosomes were judged to be synapsed if SYCP3 staining of the X and Y was connected at a single terminus, as SYCE2 could not always be detected at this location (Figure 6-6A). The point of this connection was judged to be the PAR. In control mice I found that 59% of synapsed PARs possess a detectable MLH1 focus (Figure 6-6B), which fits with the dynamics of recombination on the sex chromosomes being delayed relative to autosomes. I observed no significant change in synapsed PAR MLH1 focus formation in *Tex19.1*$^{-/-}$ spermatocytes (49% MLH1-positive, p=0.71, Fisher's exact test) (Figure 6-6B). Therefore, as seen in autosomal assessment, impaired ability to form crossovers at the PAR of synapsed sex chromosomes is also not responsible for the generation of univalent sex chromosomes in *Tex19.1*$^{-/-}$ metaphase I spermatocytes.

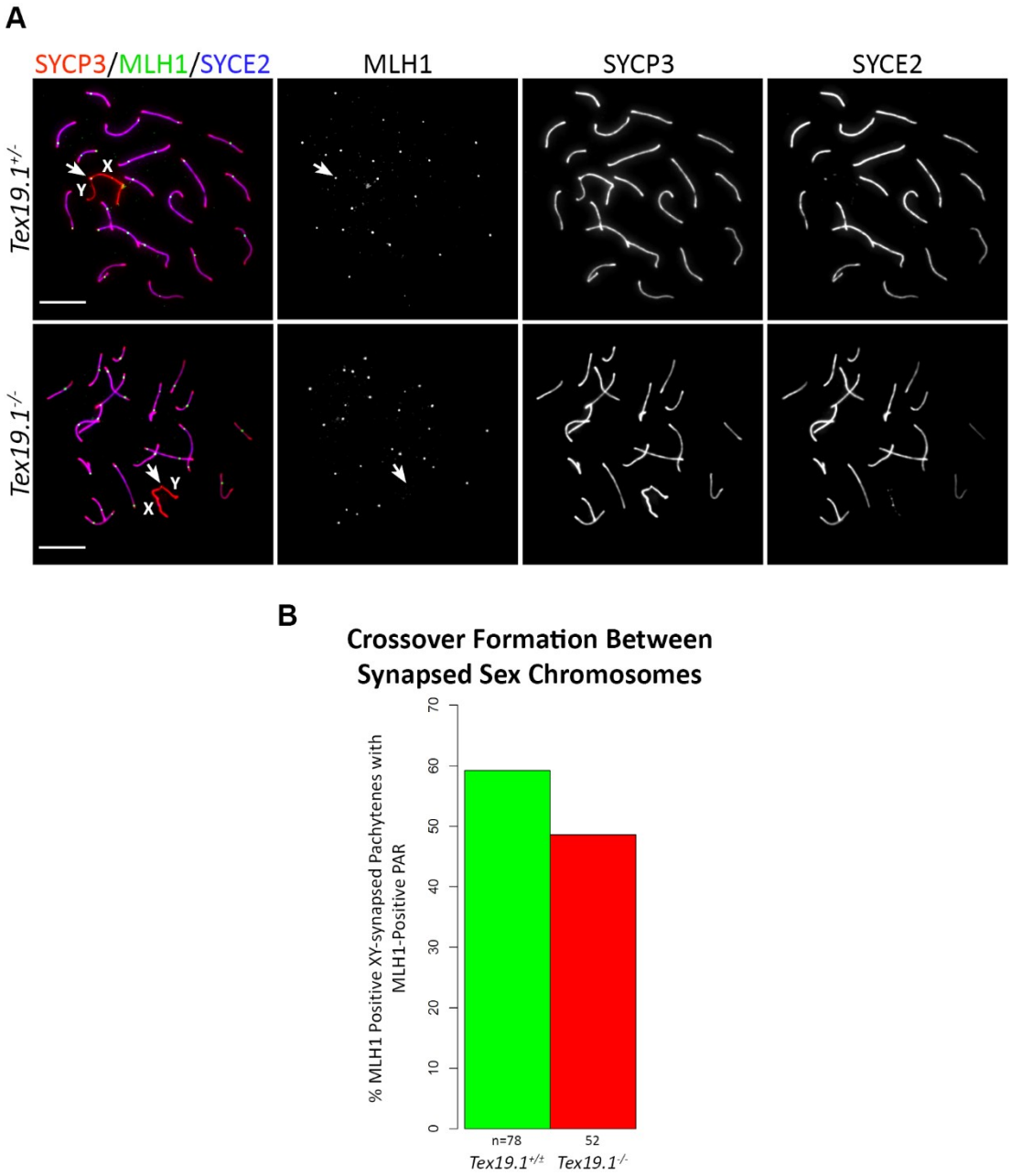

Figure 6-6. Crossover formation between sex chromosomes

(A) Representative images of control and *Tex19.1*$^{-/-}$ MLH1-positive pachytene spermatocytes with synapsed autosomes and sex chromosomes. AE and CE stained with antibodies against SYCP3 (red) and SYCE2 (blue) respectively, crossovers marked with MLH1 staining (green). Merges and single channel monochrome images shown. X and Y chromosomes indicated. Arrows indicate the synapsed pseudoautosomal region (PAR) where crossover formation is expected to take place. PAR is MLH1 positive in top images and negative in bottom images. (B) Bar graph showing the percentage of synapsed PARs with MLH1 foci in spermatocytes with synapsed MLH1-positive autosomes from control and *Tex19.1*$^{-/-}$ mice.

6.2.6 Sex Chromosome Asynapsis as a Source of Univalent Metaphase I Chromosomes

As the progression of asynapsed autosomes to metaphase I appears to account for the increase in such univalent chromosomes I next assessed whether failure to synapse could also account for the increase in univalent sex chromosomes in *Tex19.1*$^{-/-}$. Indeed, failure to synapse sex chromosomes has been demonstrated previously to result in corresponding univalent sex chromosomes in metaphase I (Kauppi et al., 2011). I assessed the synapsis of the sex chromosomes only in MLH1 positive spermatocytes with complete autosomal synapsis, scoring sex chromosomes as asynapsed if their AEs fail to make a terminal connection (Figure 6-7A). In control spermatocytes the sex chromosomes were seen to be asynapsed in 3.7% of cases (Figure 6-7B), similar to frequencies previously reported (Kauppi et al., 2011). In *Tex19.1*$^{-/-}$ MLH1-positive spermatocytes the frequency of asynapsed sex chromosomes was dramatically elevated to 18.8% ($p=0.0047$, Fisher's exact test) (Figure 6-7B). This large increase demonstrates a defect in chromosome synapsis in *Tex19.1*$^{-/-}$ spermatocytes is not restricted to autosomes. Taken together with the MLH1 counts showing normal frequency of CO formation on synapsed autosomes and sex chromosomes, this data indicates that the high rate of univalent sex chromosomes in *Tex19.1*$^{-/-}$ spermatocytes is likely attributable to asynapsis.

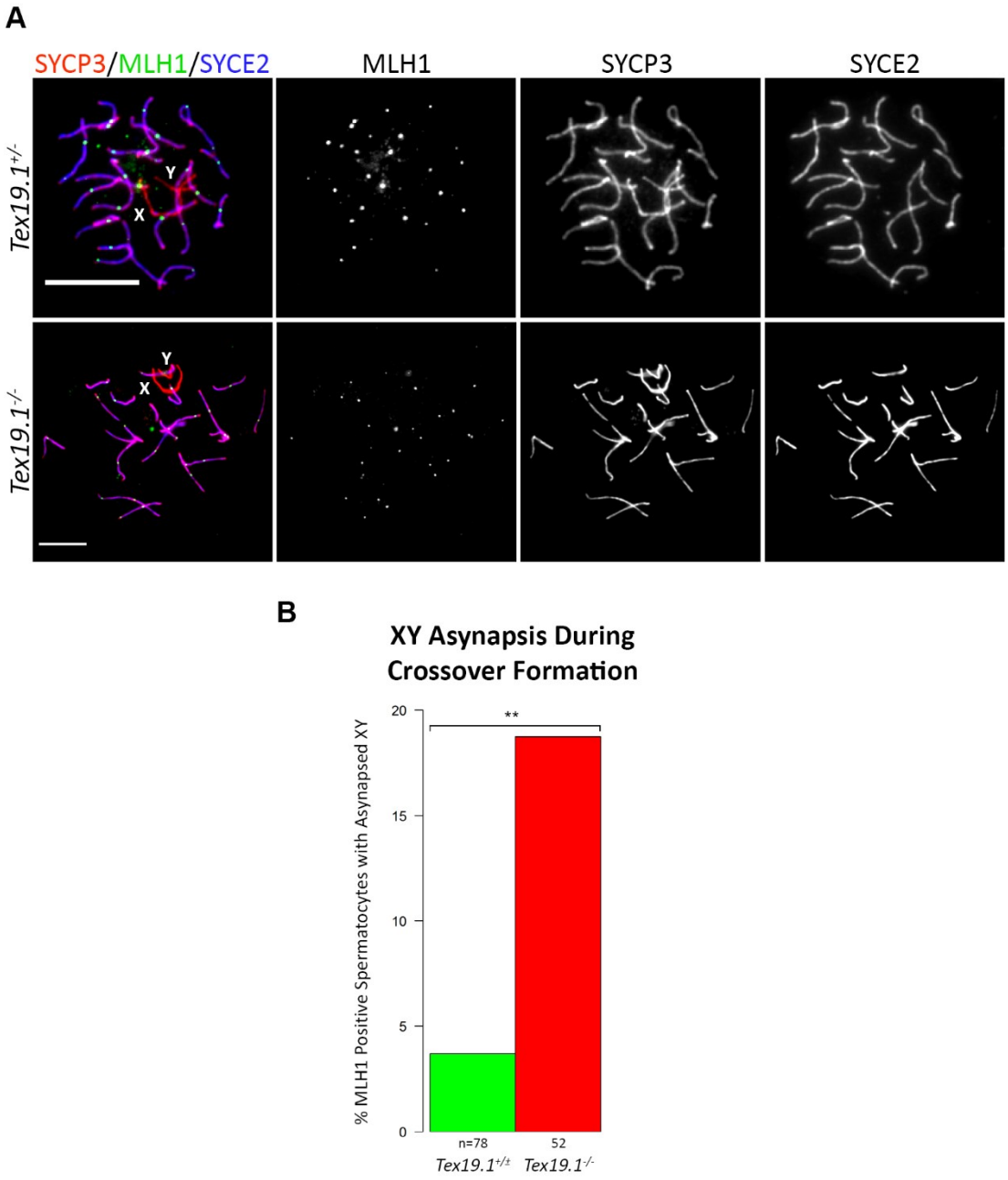

Figure 6-7. XY asynapsis in MLH1 positive spermatocytes

(A) Representative MLH1-positive images with asynapsed sex chromosomes from control and *Tex19.1*$^{-/-}$ pachytene spermatocytes. Spermatocytes stained with antibodies against MLH1 (green) to mark crossover formation as well as SYCP3 (red) and SYCE2 (blue) to mark the axial element and central element of the synaptonemal complex respectively to stage spermatocytes and inform the status of synapsis. X and Y chromosomes marked on merges. Merges and single channel images shown. 10µM scale bars. (B) Barplot showing the frequency of sex chromosome asynapsis among spermatocytes with autosomal MLH1 staining. Asterisks indicate significance.

6.3 Discussion

In this chapter I investigated potential sources of the univalent chromosomes present in *Tex19.1*$^{-/-}$ metaphase I spermatocytes. Heightened frequency of metaphase I univalent chromosomes in *Tex19.1*$^{-/-}$ was originally reported in mice from an outbred colony (Ollinger et al., 2008). I have shown that this remains a consistent feature of backcrossed *Tex19.1*$^{-/-}$ mice, largely affecting the sex chromosomes and occasionally also individual autosomes. I have shown that CO frequency, distribution and positioning are not altered in synapsed *Tex19.1*$^{-/-}$ spermatocytes and as such defective CO formation does not appear to be responsible for the generation of univalent chromosomes in this mutant. Rather, a small proportion of *Tex19.1*$^{-/-}$ spermatocytes possess asynapsed autosomes during CO formation which are likely unable to form COs and may account for the generation of univalent autosomes. Similarly I also revealed a large increase in the frequency of asynapsed sex chromosomes during crossover formation, which are likely to account for the increase in univalent sex chromosomes. Therefore univalent chromosomes in *Tex19.1*$^{-/-}$ metaphase I spermatocytes appear to be a late consequence of defective chromosome synapsis in pachytene.

6.3.1 Defects in Crossover Formation do not Cause Univalent Chromosomes in *Tex19.1*$^{-/-}$ Metaphase I Spermatocytes

The absence of a change in MLH1 foci frequency, distribution and positioning in *Tex19.1*$^{-/-}$ spermatocytes is consistent with normal CO formation. This analysis did however record a surprisingly high frequency of autosomes without MLH1 foci in control spermatocytes (4.6% of total autosomes scored), with at least one observed in 54% of spermatocytes. This frequency is much higher than the frequency of metaphase I spermatocytes containing univalent autosomes in control animals (7%), therefore the true frequency of COs formed is not entirely reflected by MLH1 foci frequency in this analysis. A rate of 4% autosomes lacking MLH1 foci has also been reported previously (Anderson et al., 1999) and as such is not unprecedented. In analysis by Anderson et al autosomes lacking MLH1 foci often had shorter axes and were thought to represent the smaller autosomes, which are more frequently univalent in metaphase I. Therefore at least a portion of these were predicted to reflect a genuine failure to form a CO. Interestingly this was not the case in my analysis, with autosomes lacking MLH1 foci failing to show any consistent difference in size (data not shown), thus suggesting that CO formation is occurring on most of these chromosomes but is

not detected. Failure to detect CO formation by MLH1 staining may reflect the asynchronous nature of this event (Anderson et al., 1999). To avoid under-representation of CO formation by MLH1 counts, some researchers only include spermatocytes with ≥19 foci in analyses so that every autosome has the potential to recruit one focus. I did not use this approach in my analysis as I was looking for spermatocytes with a reduction in MLH1 foci, therefore more spermatocytes in the process of recruiting and dissociating MLH1 will be included. Sensitivity of the antibody used, preparation of the spermatocytes spreads used or the scoring criteria employed may also contribute to differences in counts. While Class II COs are MLH1 independent and not detected by this assay, these are not expected to be reduced in *Tex19.1*$^{-/-}$ as this has been shown to result in a compensatory increase in Class I MLH1-dependent COs (Holloway et al., 2008). Finally, the maintenance of COs by the cohesin complex is vital for chiasmata formation and I cannot exclude the possibility that chiasmata maintenance is defective in *Tex19.1*$^{-/-}$ and contributes to the generation of univalent chromosomes.

6.3.2 Sex Chromosome Asynapsis in *Tex19.1*$^{-/-}$ Crossover-Forming Spermatocytes

DSB formation and subsequent pairing of male sex chromosomes at the PAR begins later than the same process on autosomes, at late zygotene rather than leptotene (Kauppi et al., 2011), and subsequent CO formation indicated by MLH1 localisation is also altered relative to autosomes and as such XY MLH1 foci are typically excluded from CO counts (Anderson et al., 1999). While XY synapsis is delayed relative to that of autosomes, it is typically thought to have occurred by pachytene and asynapsed sex chromosomes at this stage closely reflect frequencies of univalent sex chromosomes later in metaphase I (Kauppi et al., 2011). Therefore the large increase in asynapsed sex chromosomes in crossover-forming *Tex19.1*$^{-/-}$ pachytene spermatocytes is likely to be accountable for the increase in univalent sex chromosomes in this mutant.

Interestingly, the fact that XY synapsis is severely impaired in *Tex19.1*$^{-/-}$ spermatocytes indicates that the meiotic mechanisms perturbed in this mutant are not restricted to autosomes. Such autosome-specific mechanisms appear to include DSB formation by the SPO11 isoform SPO11β (Kauppi et al., 2011), and DSB hotspot promotion by PRDM9 (Brick et al., 2012). As autosomal DSB formation dynamics are altered in *Tex19.1*$^{-/-}$ spermatocytes and potentially responsible for the autosomal asynapsis incurred, it

will be of interest to investigate the progression of recombination at the PAR in *Tex19.1*$^{-/-}$ spermatocytes. As a delay in DSB formation is associated with the asynapsis of *Tex19.1*$^{-/-}$ autosomes it is possible that a similar defect in the timing of DSB formation involving the sex chromosomes could delay XY synapsis and DSB formation. Given this, I cannot exclude the possibility that synapsis and CO formation is severely delayed *Tex19.1*$^{-/-}$ spermatocytes and therefore not detected.

6.3.3 Autosomal Asynapsis in *Tex19.1*$^{-/-}$ Crossover-Forming Spermatocytes

Surprisingly, asynapsis also appears to be the source of increased univalent autosomes in metaphase I *Tex19.1*$^{-/-}$ spermatocytes. Previous studies of the consequences of autosomal asynapsis have indicated that spermatocytes arrest in mid-pachytene as the result of failed MSCI (Barchi et al., 2005; Mahadevaiah et al., 2008), and as such indirectly fail to recruit MLH1 foci (Ichijima et al., 2011). Therefore MLH1-positive asynapsed *Tex19.1*$^{-/-}$ spermatocytes do not appear to arrest as the result of failed MSCI. Such nuclei are however a small proportion of the asynapsed *Tex19.1*$^{-/-}$ spermatocyte population, therefore the majority of such nuclei appear to arrest prior to MLH1 recruitment (Figure 6-8). The precise nature of the autosomal asynapsis in CO-forming *Tex19.1*$^{-/-}$ spermatocytes is not currently clear but typically (though not exclusively) involves a single completely asynapsed autosome located near the sex chromosomes. Consistent with the establishment of MSCI in such *Tex19.1*$^{-/-}$ spermatocytes, γH2AX staining in nuclei with a single asynapsed autosome has shown a strongly stained domain covering the sex chromosomes (data not shown). It is likely that asynapsed autosomes will be silenced by an MSUC response (Turner et al., 2005). Studies of spermatocytes with some individual additional chromosomes have demonstrated the ability to tolerate an extra unsynapsed chromosome in prophase (Burgoyne et al., 2009; Mahadevaiah et al., 2008). However, these analyses have involved surplus chromosomes, therefore the transcriptional silencing of a pair of autosomes in a euploid spermatocytes may have inconsistent consequences depending on the meiotic requirement of genes encoded (Figure 6-8). Indeed, spermatocytes which are double heterozygous for two reciprocal translocations of chromosomes 1 and 13 often results in limited asynapsis, apparently compatible with the establishment of MSCI, however these spermatocytes appear to arrest before maturing to spermatozoa (Peters et al., 1997b). The mechanism responsible for this germ cell arrest is not known but speculated to be due to silencing of crucial meiotic genes by MSUC on the asynapsed chromosomes (Burgoyne et al., 2009; van der Laan et al., 2004).

Furthermore, although the MSCI-related arrest of pachytene spermatocytes appears to occur before MLH1 recruitment, the apparent DNA damage-dependent checkpoint does not (Li and Schimenti, 2007). Thus it is possible that CO-forming *Tex19.1*$^{-/-}$ spermatocytes with asynapsed autosomes may yet arrest in late pachytene as a result of DNA damage. This is a possibility which is likely to be more closely reflected by unsynapsed surplus trisomic chromosomes previously mentioned, the DNA damage on which is tolerated in prophase and ultimately repaired by non-intersister mechanisms (Burgoyne et al., 2009; Mahadevaiah et al., 2008). Therefore while autosomal asynapsis appears to be a likely source of metaphase I univalent autosomes in *Tex19.1*$^{-/-}$ this is a novel observation of such a phenomenon and the complete understanding of the consequences of its occurrence require greater study.

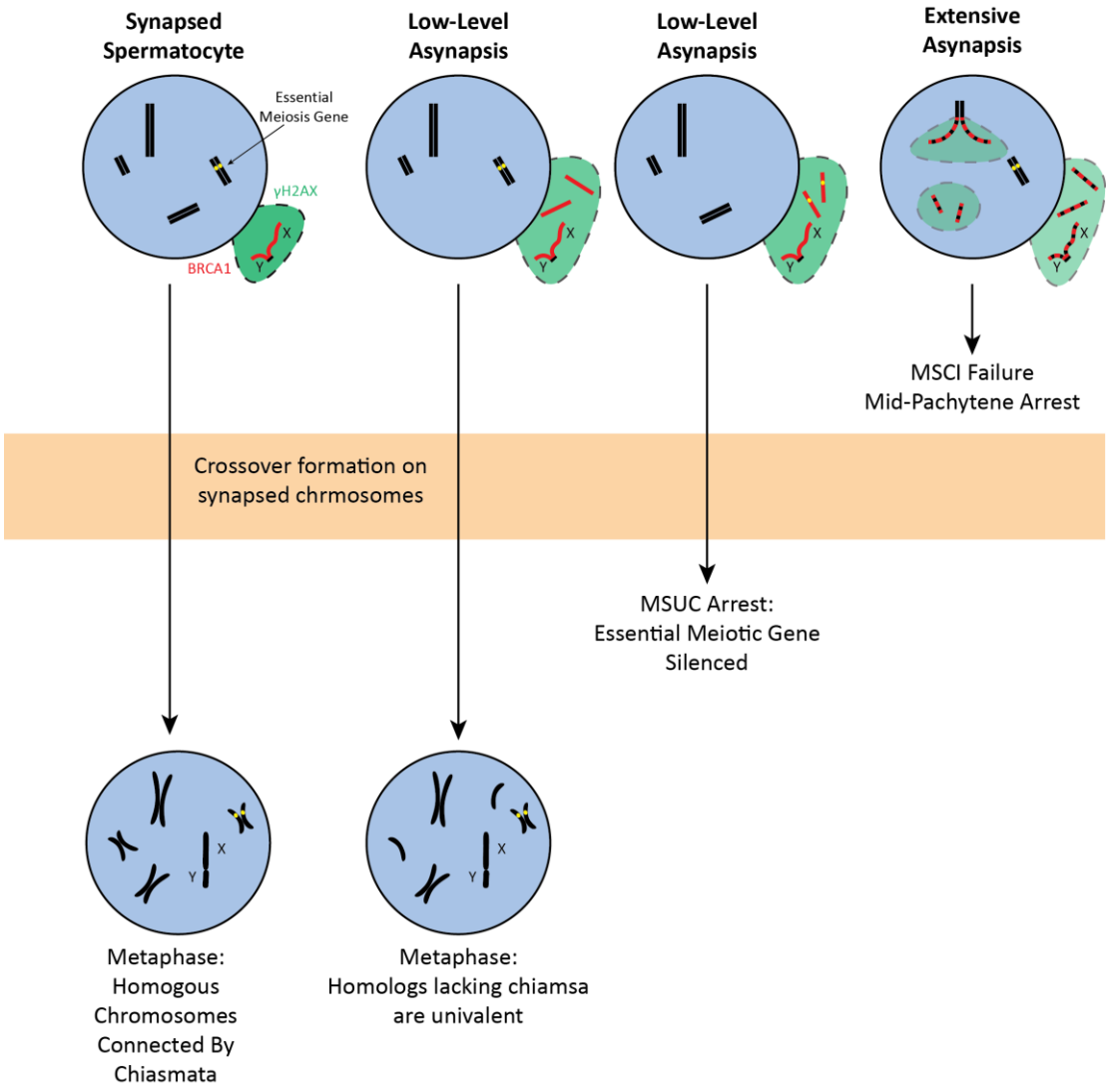

Figure 6-8. Model for generation of univalent chromosomes by low-level asynapsis
Paired black bars indicate synapsed homologous chromosomes in pachytene. One pair of autosomes contains an essential gene for meiotic progression (yellow). Partially synapsed sex chromosomes recruit BRCA1 (red) to axes and exist in the transcriptionally silenced sex body, covered by a domain of γH2AX. Asynapsed autosomes also recruit BRCA1 and γH2AX, sequestering these from the sex chromosomes and impairing MSCI in the case of extensive asynapsis. Low-level asynapsis is compatible with MSCI and crossover formation but progression to metaphase may depend on whether essential meiosis genes are silenced by MSUC on unsynapsed autosomes.

Chapter 7:

Discussion

7 Discussion

The main aim of the research presented in this thesis was to understand the meiotic phenotype of *Tex19.1*$^{-/-}$ spermatocytes. Specifically I aimed to investigate the possibility that derepression of retrotransposons could cause the chromosome asynapsis present in this mutant, as well as studying other potential mechanisms by which this defect could arise. I also aimed to establish whether pachytene spermatocytes achieving synapsis progress normally through this stage, as well as the origin of the univalent chromosomes present at metaphase I in this mutant.

7.1 Defective Events in Early Recombination Cause Pachytene Chromosome Asynapsis in *Tex19.1*$^{-/-}$

The initial report into the phenotype of *Tex19.1*$^{-/-}$ male mice showed that approximately 50% of pachytene spermatocytes contained asynapsed chromosomes and a wave of apoptosis at this stage was consistent with this defect being largely responsible for the infertility incurred. Furthermore, *Tex19.1*$^{-/-}$ testes were found to display upregulated expression of the retrotransposon *MMERVK10C* (Ollinger et al., 2008). *Tex19.1* has since been grouped with a number of other genes which are all activated during embryonic germline development in response to global loss of methylation which occurs during epigenetic reprogramming (Hackett et al., 2012). This group of "germline genome defence genes" are all required for retrotransposon silencing in the male germ line (*Mili, Miwi2, Gasz, Mael, Mvh, Mov10l1, Dnmt3l, Tex19.1*) (Crichton et al., 2013; Hackett et al., 2012). Similarly, mutations in these genes all result in chromosome asynapsis, demonstrating an association between retrotransposon activity and failed synapsis, however the mechanism behind this shared defect is unknown (Crichton et al., 2013). Investigation into *Mael*$^{-/-}$ spermatocytes has revealed an increase in SPO11-independent DNA damage during meiosis (Soper et al., 2008), which may represent retrotransposition events. The introduction of such additional DNA damage could be capable of perturbing the meiotic homology search, resulting in asynapsis. During chapter 3 I demonstrated that *Tex19.1*$^{-/-}$ spermatocytes fail to show any increase in SPO11-independent DNA damage, therefore no potentially retrotransposition-related DNA damage was detected. Furthermore the treatment of mice with antiretroviral drugs capable of inhibiting retrotransposon activity did not rescue the asynapsis phenotype of *Tex19.1*$^{-/-}$ spermatocytes. These findings suggest that large amounts of retrotransposition-related DNA damage do not arise in this mutant during meiosis and are not responsible for

the chromosome asynapsis. Therefore it is possible that the mechanism responsible for failed chromosome synapsis differs between germline genome defence mutants. Alternatively the additional SPO11-independent DNA damage reported in *Mael*$^{-/-}$ spermatocytes may not drive asynapsis in this mutant. Rather, a separate unidentified mechanism relating to retrotransposon derepression could be involved in asynapsis and shared among germline genome defence mutants.

Further investigation into the cause of *Tex19.1*$^{-/-}$ asynapsis in chapter 4 revealed severe defects in early recombination. Immunocytological analysis of early prophase spermatocytes demonstrated that the formation of DNA double strand breaks (DSBs) in leptotene is greatly reduced, as γH2AX signal intensity falls to around 50%. Consistent with this observation, the subsequent recruitment of proteins involved in early recombination (RPA, DMC1, RAD51) to DSB foci is dramatically reduced at this stage to around 50%. Furthermore, this immunocytological data was supported by the biochemical assessment of SPO11-oligonucleotide complexes which are reduced to undetectable levels during leptotene in *Tex19.1*$^{-/-}$, consistent with a major reduction in DSB frequency. Therefore early meiotic recombination in this mutant is profoundly defective. Remarkably, despite this large reduction in DSB frequency in leptotene, by zygotene *Tex19.1*$^{-/-}$ spermatocytes appear to possess a normal level of DSBs although the progression of these DSBs through early stages of recombination remains delayed.

It is currently unclear whether the initial reduced frequency of DSBs in *Tex19.1*$^{-/-}$ would be sufficient to cause asynapsis. Reduction in DSB frequency to 70% in *Spo11*$^{+/-}$ heterozygotes does not result in asynapsis (Cole et al., 2012), however the reduction of DSB frequency to 50% as seen in spermatocytes expressing reduced levels of *Spo11* from a transgenic promoter (*Tg(Spo11β)*$^{+/-}$) is not compatible with synapsis (Kauppi et al., 2013b). Therefore there appears to be a threshold for DSB frequency which must be exceeded for successful synapsis to take place. The reduction in leptotene DSB frequency in *Tg(Spo11β)*$^{+/-}$ spermatocytes is similar to the 50% reduction seen in *Tex19.1*$^{-/-}$ at this stage, however, unlike *Tex19.1*$^{-/-}$ spermatocytes *Tg(Spo11β)*$^{+/-}$, spermatocytes do not catch up to normal levels of DSB frequency in zygotene, but remain reduced to ~50% (Kauppi et al., 2013b). Therefore if the initial reduction in DSB frequency causes asynapsis in *Tex19.1*$^{-/-}$ then the additional DSBs formed in zygotene in this mutant must possess a greatly reduced capacity to promote synapsis. The germline deletion of *Polβ* is one mouse mutant with an apparently similar delay in the dynamics of recombination to *Tex19.1*$^{-/-}$ (DSB foci reduced to ~50% in leptotene and recovery to ~70% in zygotene). Chromosome synapsis is defective in this mutant,

potentially supporting the reduced ability of late-forming DSBs to promote synapsis. However the meiotic function of Polβ is not completely understood and as the protein localises to axes after synapsis it may have another more direct role in promoting synapsis (Kidane et al., 2010). Formation of additional DSBs by cisplatin treatment in *Spo11*$^{-/-}$ spermatoctytes has been shown to improve synapsis in this asynapsed mutant (Romanienko and Camerini-Otero, 2000). It would be of interest to treat *Tex19.1*$^{-/-}$ mice with cisplatin to investigate whether additional DSB formation in leptotene could rescue asynapsis by raising the frequency of DSBs participating in the initial stages of the homology search.

While my finding that large levels of SPO11-independent meiotic DNA damage are not generated in *Tex19.1*$^{-/-}$ suggests that meiotic retrotransposition-related damage might not cause the asynapsis in this mutant it remains an attractive possibility that the asynapsis and increased retrotransposon activity shared by germline genome defence mutants are related. This is also a likely possibility since TEX19.1 function identified so far has been limited to retrotransposon silencing, and this extends to the placenta (Reichmann et al., 2013; Tarabay et al., 2013), therefore a direct role in meiotic recombination would require an additional meiosis-specific function of this protein. As well as DSB frequency, the positioning of DSBs appears to be of great importance for the success of chromosome synapsis (Brick et al., 2012). A simple model, in which the activation of *MMERVK10C* expression resulted in recruitment of meiotic DSB forming machinery to these loci, perturbing the homology search by introducing non-unique search material, could account for *Tex19.1*$^{-/-}$ asynapsis. However it is not clear how such a process would have a broad impact on synapsis, affecting numerous autosomes and the PAR, as few functional copies of *MMERVK10C* are present in the genome and none reside in the PAR. Furthermore it is not clear why an actively expressed infrequent retrotransposon sequence would be more attractive to DSB-forming machinery than DSB hotspots or non-retrotransposon genes undergoing expression. Therefore a mechanism connecting retrotransposon expression and asynapsis would require a broader influence over recombination.

DSBs typically form at hotspots throughout the genome which are marked by PRDM9-dependent H3K4me3 (Baudat et al., 2013), and such sites in yeast typically exist in euchromatin in the loops extending from the axial element (Blat et al., 2002; Borde and de Massy, 2013). Investigation into the genetic content of the axial element by SYCP3 ChIP-seq has demonstrated a particular enrichment of the repetitive element SINE B1 (Johnson et al., 2013), FISH analysis of LINE1 element distribution has also shown axial enrichment (Hernández-Hernández et al., 2008) and the synaptonemal complex of DNase digested

pachytene spermatocytes has demonstrated considerable enrichment for both LINE1 and SINE element DNA (Pearlman et al., 1992). Therefore several lines of evidence support the enrichment of retrotransposon DNA in the meiotic chromosome axis. As repetitive elements comprise around 40% of the mouse genome, these potentially pose a considerable threat to the meiotic homology search if they become involved as they are non-unique and will likely result in non-allelic recombination and/or failure of chromosome pairing (Crichton et al., 2013; Ollinger et al., 2010; Sasaki et al., 2010). It is possible that repetitive sequences are hidden in the chromosome axis during meiosis so as to minimise targeting of meiotic DSB formation (Figure 7-1). Transcriptional activity of retrotransposons in germline genome defence mutants (Crichton et al., 2013) would be predicted to associate with the establishment of an open chromatin environment at such loci. Reorganisation of meiotic chromatin related with retrotransposon expression could make repetitive DNA more accessible/attractive to DSB-forming machinery and/or impair targeting of such machinery to DSB hotspots (Figure 7-1). Consistent with the idea of major reorganisation of meiotic chromatin in germline genome defence mutants, *Dnmt3l*$^{-/-}$ spermatocytes are reported to possess altered histone modification dynamics resulting in a more open meiotic chromatin state (Webster et al., 2005), and *Miwi2*$^{-/-}$ spermatocytes display reduced levels of H3K27me3 and H3K4me3 during early meiosis (Bao et al., 2014). As previously mentioned, the upregulation of *MMERVK10C* in *Tex19.1*$^{-/-}$ spermatocytes is likely to cause only a minor change in chromatin conformation due to its limited frequency. *Tex19.1* expressed in the developing germline begins at ~E8.5-E9.5 (Hackett et al., 2012), although how and when TEX19.1 functions is not known. TEX19.1 may play a larger role in transcriptional suppression of retrotransposons during pre-meiotic stages of germ cell development than in meiosis, and it is possible that embryonic retrotransposition events in *Tex19.1*$^{-/-}$ germ cells cause widespread alterations to the chromatin landscape which persist into meiosis and perturb recombination. Insertion of retrotransposon sequence into a DSB hotspot in yeast has indeed been shown to lead to chromatin compaction and hotspot inactivation (Ben-Aroya et al., 2004). An alternative/additional possibility is that TEX19.1 promotes retrotransposon silencing by via suppressive chromatin modifications, and the majority of retrotransposons affected are silenced by alternative backup mechanisms in meiosis, but some degree of altered chromatin organisation remains across the genome. The embryonic function of germline genome defence genes can clearly have greatly detrimental impact on meiosis as *Miwi2* is only expressed until shortly after birth (Aravin et al., 2008), long before meiosis is initiated, yet *Miwi2*$^{-/-}$ spermatocytes are greatly defective in chromosome synapsis (Carmell et al., 2007). Therefore defects incurred embryonically can be tolerated through several cell

divisions, but have fatal consequences in meiosis. To investigate the requirement of the pre-meiotic function of TEX19.1 for spermatocyte progression through meiosis it would be of interest to study the meiotic consequences of conditional *Tex19.1* deletion at different stages during germline development.

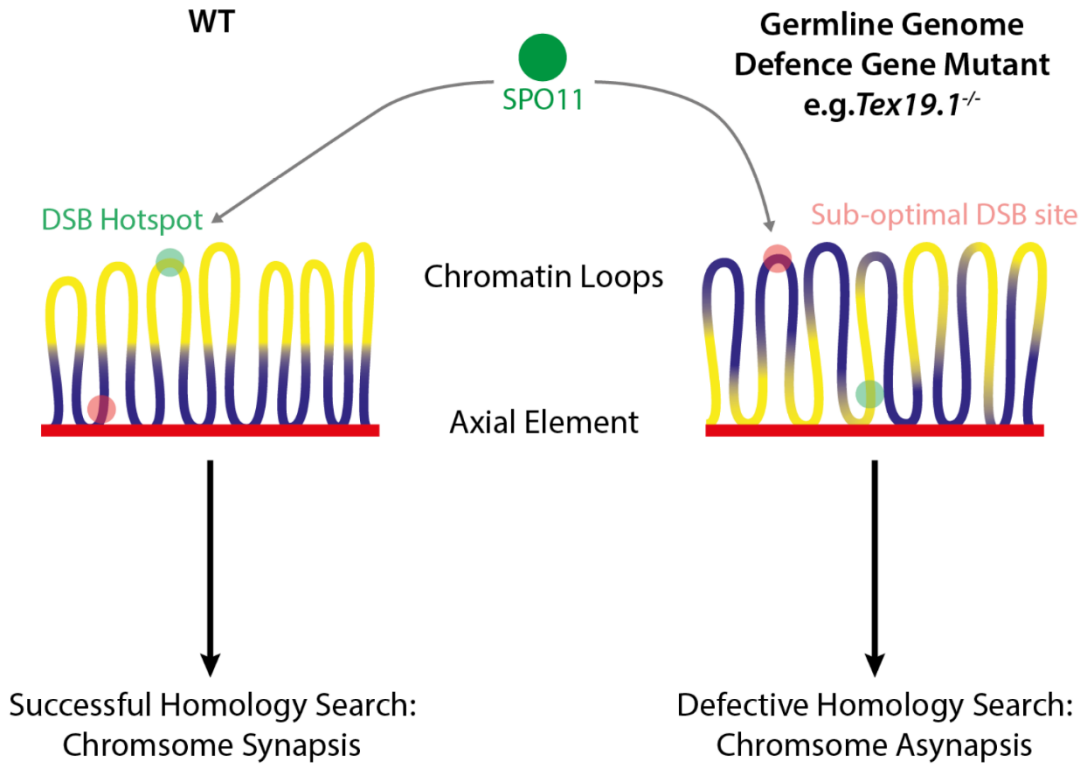

Figure 7-1. Model for shared mechanism of asynapsis in germline genome defence mutants
Chromatin loops (yellow/blue) are anchored in the chromosome core (red) during meiotic prophase. SPO11 (green) initiates recombination by forming DSBs in early meiotic prophase. DSB hotspots (green locus) at DNA optimal for promotion of the homology search is normally in accessible loop-associated DNA (yellow), while DNA sub-optimal for DSB formation (red locus) and promotion of the homology search such as retrotransposons, are enriched in axis-associated locations (blue). Altered chromatin organisation in germline genome defence mutants reduces access and DSB formation at optimal DSB hotspots and/or increases access and DSB formation at sub-optimal DSB sites such as retrotransposons. The non-unique nature of DNA in such sub-optimal locations causes a failed homology search and chromosome asynapsis.

The use of sub-optimal DSB locations could also be the cause of the initial reduction DSB formation in *Tex19.1*$^{-/-}$ spermatocytes, as alternative DSB positioning in *Prdm9*$^{-/-}$ is also associated with a reduction in DMC1 foci recorded across all spermatocytes (Brick et al., 2012; Hayashi et al., 2005), possibly indicating reduced formation of meiotic DSBs. It would

be of great interest to investigate this possible alteration of DSB positioning in *Tex19.1*$^{-/-}$ spermatocytes by DMC1 ChIP-seq, as well as the possibility of altered distribution of chromatin marks associated with DSB formation by H3K4me3 ChIP-seq. The distribution of H3K9me3 would also be of interest as this has been previously implicated in the silencing of *MMERVK10C* (Karimi et al., 2011) and therefore may provide insight into to TEX9.1 function in transcriptional silencing. Furthermore, it would be interesting to characterise the progression of meiotic recombination in other germline genome defence mutants as investigation into this is currently limited, and to also extend ChIP-seq analysis of DSB positioning to such mutants to potentially establish whether this mechanism of synaptic perturbation is shared.

7.2 Defective Recombination Delays Progression of Synapsed *Tex19.1*$^{-/-}$ Spermatocytes through Pachytene

My research presented in chapter 5 revealed that despite the successful synapsis of 35% of *Tex19.1*$^{-/-}$ spermatocytes, progression through pachytene is defective in these cells. Spermatocytes display delayed progression of numerous events including DSB repair and crossover formation, expression of the mid-pachytene marker H1t, ubiquitination of histone H2A at the sex body and delayed dynamics of other ubiquitination events associated with both sex chromosomes and autosomal axes. This finding appears to demonstrate the presence of a cell-cycle control mechanism(s) which co-regulates these diverse events. Furthermore, the finding that delayed progression to mid-pachytene expression of H1t does not occur in *Tex19.1*$^{-/-}$*Spo11*$^{-/-}$ double knockout spermatocytes relative to *Spo11*$^{-/-}$ single knockouts shows that this delay is dependent on SPO11 and therefore likely related to SPO11-dependent DSBs. I have previously shown the formation of SPO11 DSBs to be delayed in early prophase in *Tex19.1*$^{-/-}$ spermatocytes. Therefore together this evidence indicates that the delayed progression through pachytene in synapsed *Tex19.1*$^{-/-}$ spermatocytes is a secondary consequence of abnormal meiotic DSB formation. It is likely that such a defect is not observed in other germline genome defence mutants as perturbations to synapsis are too severe to achieve any complete synapsis, therefore all spermatocytes arrest due to failed MSCI (Mahadevaiah et al., 2008). Following the model previously proposed for the mechanism of chromosome asynapsis in germline genome defence mutants, the more severe asynapsis seen in other mutants may reflect a greater disruption of chromatin organisation, consistent with the more severe dysregulation of retrotransposon silencing reported

(Crichton et al., 2013). Additionally the ability of some *Tex19.1*$^{-/-}$ spermatocytes to synapse indicates the involvement of some stochasticity in the processes involved.

Unrepaired DNA damage per se is not sufficient to inhibit spermatocytes progression to mid-pachytene and expression of H1t as *Dmc1*$^{-/-}$ and *Msh5*$^{-/-}$ spermatocytes reach this stage despite the presence of numerous unrepaired DSBs (Mahadevaiah et al., 2008). However, H1t staining is weaker in *Dmc1*$^{-/-}$ spermatocytes possibly indicating meiotic arrest at an earlier stage (Mahadevaiah et al., 2008) potentially due to impaired pachytene progression. Additionally, DSBs in *Dmc1*$^{-/-}$ do not progress as far through recombination as those in *Msh5*$^{-/-}$ (Pittman et al., 1998; de Vries et al., 1999). Therefore the increased presence of DSBs in an immature state of repair in pachytene may be responsible for promoting a delay in progression of *Dmc1*$^{-/-}$ and also *Tex19.1*$^{-/-}$ spermatocytes through this stage.

Similarly, a delay in progression to CO formation is not seen in synapsed pachytene *Zip4h*$^{-/-}$ and *Trip13*$^{mod/mod}$ spermatocytes, both of which possess elevated levels of unrepaired DSBs (Adelman and Petrini, 2008; Li and Schimenti, 2007; Roig et al., 2010) suggesting this is not inhibited by the presence of DNA damage per se. *Tex19.1*$^{-/-}$ pachytene spermatocytes also possess elevated levels of unrepaired DSBs but do show delayed CO formation, therefore a distinction must exist between this phenotype and those of *Zip4h*$^{-/-}$ and *Trip13*$^{mod/mod}$ male mice. Unlike *Tex19.1*$^{-/-}$ spermatocytes the initial formation of DSBs occurs normally in *Zip4h*$^{-/-}$ and *Trip13*$^{mod/mod}$, therefore it is possible that progression to CO formation in *Tex19.1*$^{-/-}$ could also be impeded by the presence of DSBs in immature stages of recombination, as appears to be the case for H1t expression. It is also possible however that rather than controlling a checkpoint to monitor progression to CO formation, all DSBs may be insufficiently mature to be processed to form COs until later in pachytene in *Tex19.1*$^{-/-}$ due to their delayed formation. Therefore my findings indicate that the initial delay in DSB formation in early prophase in *Tex19.1*$^{-/-}$ is likely to be responsible for retarding progression of synapsed spermatocytes through pachytene. Some processes are likely to be directly effected as they relate to recombination, however others appear to be restrained by a recombination-related checkpoint which coordinates cell-cycle progression through pachytene and remains to be identified.

7.3 Pachytene Asynapsis Causes Univalent Chromosomes in *Tex19.1*$^{-/-}$ Metaphase I Spermatocytes

My research into the source of univalent chromosomes which arise in metaphase I in *Tex19.1*$^{-/-}$ testes indicates that the formation of crossovers between synapsed chromosomes is unaltered and not responsible for this defect. Rather, univalent chromosomes appear to originate from individual unsynapsed chromosomes present during crossover formation in pachytene which are consequently unable to form a crossover. Therefore, once again this finding relates to the defective events in early recombination and perturbed chromosome synapsis in *Tex19.1*$^{-/-}$, demonstrating that the effects of this original defect vary in severity and resonate throughout subsequent meiotic stages. The finding that sex chromosome synapsis is frequently defective in pachytene spermatocytes suggests the recombination defect responsible is not limited to autosomes. This is of particular interest as the timing and machinery involved in DSB formation appears to differ between the autosomes and the pseudoautosomal region (PAR) of the sex chromosomes: autosomal DSBs are made in leptotene by SPO11β at PRDM9-promoted hotspots, PAR DSBs are made in late zygotene by SPO11α at PRDM9-independent sites (Brick et al., 2012; Kauppi et al., 2011). Therefore this finding is consistent with recombination being perturbed on a global scale by reorganisation of the chromatin substrate (Figure 7-1). It will be of interest to specifically investigate the dynamics of PAR recombination in *Tex19.1*$^{-/-}$ by immuno-FISH for the PAR DNA and recombination proteins, to better understand the cause of the recombination defect in this mutant and also the control of DSB regulation on the PAR.

The observation of unsynapsed autosomes in crossover-forming spermatocytes in *Tex19.1*$^{-/-}$ is a particularly unusual observation borne of the variable degree to which chromosome synapsis is disrupted between spermatocytes in this mutant. Crossover formation in spermatocytes with such low-level asynapsis indicates they have not triggered MSCI failure and mid-pachytene arrest (Burgoyne et al., 2009; Ichijima et al., 2011), however DSBs unable to repair on such chromosomes may yet trigger the DSB checkpoint in late pachytene (Li and Schimenti, 2007). Furthermore, transcriptional silencing by MSUC is likely to take place on these unsynapsed autosomes (Turner et al., 2005), so progression of such spermatocytes to metaphase I would depend on the absence of any essential genes involved in the interim residing on the affected chromosome (Burgoyne et al., 2009). Therefore it appears possible that asynapsed chromosomes present in late pachytene could account for univalent chromosomes in metaphase I, however affected nuclei would need to pass several other hurdles before reaching this stage and it is possible that only a sub-

population these spermatocytes would survive. It would be of interest to investigate this defect more closely and establish how the progression/elimination of spermatocytes between pachytene and metaphase I relate to levels of persistent DNA damage and gene content of chromosomes involved.

7.4 Retrotransposon Regulation and Fertility Through Evolution

Repetitive elements account for a vast portion of the genetic sequence in most eukaryotic genomes (Jurka et al., 2007). Repetitive elements can be major drivers of genetic change across the genome: introducing genomic variation by acting as sites for recombination-mediated deletions and rearrangements, influencing expression of nearby genes, and by retrotransposition events disrupting pre-existing genetic information in the host genome (Romanish et al., 2010). While a limited amount of genetic instability is essential to drive evolution, if the germline mutation rate is too high this will compromise offspring viability. Flies and mammals have both been found to possess mechanisms of silencing retrotransposons in the germline, demonstrating the importance of such defence for species' survival, furthermore these systems are also essential for fertility (Crichton et al., 2013; Siomi et al., 2008). There is also a growing body of evidence that in addition to silencing the activity of retrotransposons in the germline, it is also a priority to avoid using repetitive DNA in meiotic recombination as this is likely to motivate non-allelic pairing of chromosomes and could cause major genetic reorganisation and/or meiotic failure (Sasaki et al., 2010). The omission of repetitive sequences from meiotic recombination is achieved by avoiding DSB formation at such loci. Precise analysis of DSB positioning in yeast has shown that this is indeed the case (Pan et al., 2011). Furthermore, the insertion of retrotransposon DNA into a DSB hotspot in yeast results in compaction of that location and avoidance of DSB formation in that previously highly active site (Ben-Aroya et al., 2004). This indicates the existence of mechanisms which recognise repetitive elements and redirect recombination machinery away from them, possibly relying on chromatin reorganisation. It is likely that similar mechanisms also take place in humans, as active LINE-1 retrotransposons are commonly located in regions of linkage disequilibrium, indicating a lack of involvement in meiotic recombination (Kuhn et al., 2014). As LINE-1 transcript and ORF1 protein levels peak in the postnatal male mouse germline during leptotene and zygotene (Branciforte and Martin, 1994), it is attractive to postulate that mechanisms acting after translation may prevent disruption of meiotic recombination by LINE-1 activity. Surprisingly, a negative relationship between meiotic recombination and repetitive DNA does not always appear to

be encouraged, with some hotspots in yeast relying on the presence of nearby repeats (Sasaki et al., 2013) and the consensus hotspot sequence in humans, thought to be involved in at least 40% of crossovers, being found in minisatellite sequences implicated in disease causing non-allelic sites of recombination (Myers et al., 2008). It has been proposed that recombination at retrotransposon sequences within diploid organisms heterozygous for a retrotransposon insertion could favour the element's elimination, thus reducing future genomic threat (Sasaki et al., 2013). Therefore while repetitive sequences are likely to be avoided in general during recombination, some repeat-related locations are favoured for DSB formation in evolutionarily distant species, suggesting limited encouragement to promote genetic variation.

Meiotic recombination machinery is typically highly conserved through evolution; hence my finding that the mammal-specific gene *Tex19.1* is a vital requirement for normal meiotic recombination in male mice is an unusual observation. As the repetitive elements enriched across different eukaryotic genomes vary widely between species, it may be expected that although their control remains a conserved priority for meiotic success, the methods by which this is achieved must also vary as they are tailored to the particular threat present. My findings in *Tex19.1*$^{-/-}$ spermatocytes reveal a defect in both retrotransposon silencing and meiotic recombination, suggesting a potential dual function of TEX19.1 activity both for silencing retrotransposon expression in the germ line and potentially for preventing its involvement in recombination. Such a role may also extend to other germline genome defence mutants in mice and systems in other species, possibly mediating both protective effects by influencing surrounding chromatin organisation.

7.5 Conclusion

The data presented in this thesis identifies a primary defect in the formation of meiotic DSBs in *Tex19.1*$^{-/-}$ spermatocytes, with DSB frequency initially reduced to ~50% in leptotene, before reaching normal levels in zygotene. It is likely that this recombination defect is responsible for the chromosome asynapsis incurred in this mutant, though it is currently unclear whether the initial reduced frequency of DSBs itself is sufficient to account for asynapsis or if altered DSB dynamics reflect a more complex perturbation such as sub-optimal DSB positioning which is incompatible with a successful homology search. I propose a model in which changes in chromatin organisation relating to upregulated retrotransposon expression result in DSB formation in repetitive DNA and/or the reduced DSB formation in normal hotspot DNA. This novel model provides a link between the

retrotransposon expression and chromosome asynapsis which are shared features of all male germline genome defence mutant mice (Crichton et al., 2013). The consequences of this recombination defect in *Tex19.1*$^{-/-}$ spermatocytes are variable. Many spermatocytes exhibit large amounts of asynapsis and appear to arrest in pachytene, while some exhibit only low levels of asynapsis affecting sex chromosomes or individual autosomes and appear to progress to metaphase I where such chromosomes are univalent. Furthermore, *Tex19.1*$^{-/-}$ spermatocytes which achieve autosomal synapsis exhibit a delayed progression though numerous processes in pachytene, dependent on SPO11, revealing the presence of a meiotic cell-cycle control mechanism which coordinates events in pachytene and is influenced by meiotic recombination. Therefore the unique and heterogeneous meiotic phenotype of *Tex19.1*$^{-/-}$ male mice has the potential to inform the understanding of multiple processes including meiotic DSB formation, regulation of pachytene progression and prophase checkpoint control. The association demonstrated herein between failure to suppress retrotransposon expression and defective meiotic recombination connects two fundamental processes of great importance for controlling genetic variation between generations. It is possible that shared mechanisms controlling these processes exist within diverse organisms, regulating genetic reorganisation during germ cell production to balance meiotic success and offspring survival against evolutionary drive.

Bibliography

Bibliography

Aboussekhra, A., Chanet, R., Adjiri, A., and Fabre, F. (1992). Semidominant suppressors of Srs2 helicase mutations of Saccharomyces cerevisiae map in the RAD51 gene, whose sequence predicts a protein with similarities to procaryotic RecA proteins. Mol. Cell. Biol. *12*, 3224–3234.

Acquaviva, L., Székvölgyi, L., Dichtl, B., Dichtl, B.S., de La Roche Saint André, C., Nicolas, A., and Géli, V. (2013). The COMPASS subunit Spp1 links histone methylation to initiation of meiotic recombination. Science *339*, 215–218.

Adelman, C.A., and Petrini, J.H. (2008). ZIP4H (TEX11) deficiency in the mouse impairs meiotic double strand break repair and the regulation of crossing over. PLoS Genet *4*, e1000042.

Alsheimer, M., Baier, A., Schramm, S., Schütz, W., and Benavente, R. (2010). Synaptonemal complex protein SYCP3 exists in two isoforms showing different conservation in mammalian evolution. Cytogenet. Genome Res. *128*, 162–168.

An, J.Y., Kim, E.-A., Jiang, Y., Zakrzewska, A., Kim, D.E., Lee, M.J., Mook-Jung, I., Zhang, Y., and Kwon, Y.T. (2010). UBR2 mediates transcriptional silencing during spermatogenesis via histone ubiquitination. Proc. Natl. Acad. Sci. U. S. A. *107*, 1912–1917.

An, J.Y., Kim, E., Zakrzewska, A., Yoo, Y.D., Jang, J.M., Han, D.H., Lee, M.J., Seo, J.W., Lee, Y.J., Kim, T.-Y., et al. (2012). UBR2 of the N-end rule pathway is required for chromosome stability via histone ubiquitylation in spermatocytes and somatic cells. PloS One *7*, e37414.

Anderson, D.E., Losada, A., Erickson, H.P., and Hirano, T. (2002). Condensin and cohesin display different arm conformations with characteristic hinge angles. J Cell Biol *156*, 419–424.

Anderson, L.K., Reeves, A., Webb, L.M., and Ashley, T. (1999). Distribution of crossing over on mouse synaptonemal complexes using immunofluorescent localization of MLH1 protein. Genetics *151*, 1569–1579.

Aravin, A.A., Sachidanandam, R., Girard, A., Fejes-Toth, K., and Hannon, G.J. (2007). Developmentally regulated piRNA clusters implicate MILI in transposon control. Science *316*, 744–747.

Aravin, A.A., Sachidanandam, R., Bourc'his, D., Schaefer, C., Pezic, D., Toth, K.F., Bestor, T., and Hannon, G.J. (2008). A piRNA pathway primed by individual transposons is linked to de novo DNA methylation in mice. Mol. Cell *31*, 785–799.

Aravin, A.A., van der Heijden, G.W., Castañeda, J., Vagin, V.V., Hannon, G.J., and Bortvin, A. (2009). Cytoplasmic compartmentalization of the fetal piRNA pathway in mice. PLoS Genet. *5*, e1000764.

Arnheim, N., Calabrese, P., and Tiemann-Boege, I. (2007). Mammalian meiotic recombination hot spots. Annu. Rev. Genet. *41*, 369–399.

Ben-Aroya, S., Mieczkowski, P.A., Petes, T.D., and Kupiec, M. (2004). The compact chromatin structure of a Ty repeated sequence suppresses recombination hotspot activity in Saccharomyces cerevisiae. Mol. Cell *15*, 221–231.

Arumugam, P., Gruber, S., Tanaka, K., Haering, C.H., Mechtler, K., and Nasmyth, K. (2003). ATP hydrolysis is required for cohesin's association with chromosomes. Curr. Biol. CB *13*, 1941–1953.

Ashley, T., Walpita, D., and de Rooij, D.G. (2001). Localization of two mammalian cyclin dependent kinases during mammalian meiosis. J. Cell Sci. *114*, 685–693.

Auton, A., Fledel-Alon, A., Pfeifer, S., Venn, O., Ségurel, L., Street, T., Leffler, E.M., Bowden, R., Aneas, I., Broxholme, J., et al. (2012). A fine-scale chimpanzee genetic map from population sequencing. Science *336*, 193–198.

Baarends, W.M., Wassenaar, E., van der Laan, R., Hoogerbrugge, J., Sleddens-Linkels, E., Hoeijmakers, J.H.J., de Boer, P., and Grootegoed, J.A. (2005). Silencing of unpaired chromatin and histone H2A ubiquitination in mammalian meiosis. Mol. Cell. Biol. *25*, 1041–1053.

Baarends, W.M., Wassenaar, E., Hoogerbrugge, J.W., Schoenmakers, S., Sun, Z.-W., and Grootegoed, J.A. (2007). Increased phosphorylation and dimethylation of XY body histones in the Hr6b-knockout mouse is associated with derepression of the X chromosome. J. Cell Sci. *120*, 1841–1851.

Bannister, A.J., and Kouzarides, T. (2011). Regulation of chromatin by histone modifications. Cell Res. *21*, 381–395.

Bao, J., Zhang, Y., Schuster, A.S., Ortogero, N., Nilsson, E.E., Skinner, M.K., and Yan, W. (2014). Conditional inactivation of Miwi2 reveals that MIWI2 is only essential for prospermatogonial development in mice. Cell Death Differ.

Barbosa-Morais, N.L., Dunning, M.J., Samarajiwa, S.A., Darot, J.F.J., Ritchie, M.E., Lynch, A.G., and Tavaré, S. (2010). A re-annotation pipeline for Illumina BeadArrays: improving the interpretation of gene expression data. Nucleic Acids Res. *38*, e17.

Barchi, M., Mahadevaiah, S., Di Giacomo, M., Baudat, F., de Rooij, D.G., Burgoyne, P.S., Jasin, M., and Keeney, S. (2005). Surveillance of different recombination defects in mouse spermatocytes yields distinct responses despite elimination at an identical developmental stage. Mol. Cell. Biol. *25*, 7203–7215.

Barlow, A.L., Benson, F.E., West, S.C., and Hultén, M.A. (1997). Distribution of the Rad51 recombinase in human and mouse spermatocytes. EMBO J. *16*, 5207–5215.

Barlow, C., Liyanage, M., Moens, P.B., Tarsounas, M., Nagashima, K., Brown, K., Rottinghaus, S., Jackson, S.P., Tagle, D., Ried, T., et al. (1998). Atm deficiency results in severe meiotic disruption as early as leptonema of prophase I. Dev. Camb. Engl. *125*, 4007–4017.

Barrett, T., Troup, D.B., Wilhite, S.E., Ledoux, P., Evangelista, C., Kim, I.F., Tomashevsky, M., Marshall, K.A., Phillippy, K.H., Sherman, P.M., et al. (2011). NCBI GEO: archive for functional genomics data sets--10 years on. Nucleic Acids Res. *39*, D1005–D1010.

Bartek, J., and Lukas, J. (2001). Mammalian G1- and S-phase checkpoints in response to DNA damage. Curr. Opin. Cell Biol. *13*, 738–747.

Baudat, F., Manova, K., Yuen, J.P., Jasin, M., and Keeney, S. (2000). Chromosome synapsis defects and sexually dimorphic meiotic progression in mice lacking Spo11. Mol Cell *6*, 989–998.

Baudat, F., Buard, J., Grey, C., Fledel-Alon, A., Ober, C., Przeworski, M., Coop, G., and de Massy, B. (2010). PRDM9 is a major determinant of meiotic recombination hotspots in humans and mice. Science *327*, 836–840.

Baudat, F., Imai, Y., and de Massy, B. (2013). Meiotic recombination in mammals: localization and regulation. Nat. Rev. Genet. *14*, 794–806.

Beck-Engeser, G.B., Eilat, D., and Wabl, M. (2011). An autoimmune disease prevented by anti-retroviral drugs. Retrovirology *8*, 91.

Bellani, M.A., Romanienko, P.J., Cairatti, D.A., and Camerini-Otero, R.D. (2005). SPO11 is required for sex-body formation, and Spo11 heterozygosity rescues the prophase arrest of Atm-/- spermatocytes. J. Cell Sci. *118*, 3233–3245.

Bellani, M.A., Boateng, K.A., McLeod, D., and Camerini-Otero, R.D. (2010). The expression profile of the major mouse SPO11 isoforms indicates that SPO11beta introduces double strand breaks and suggests that SPO11alpha has an additional role in prophase in both spermatocytes and oocytes. Mol. Cell. Biol. *30*, 4391–4403.

Bellvé, A.R., Cavicchia, J.C., Millette, C.F., O'Brien, D.A., Bhatnagar, Y.M., and Dym, M. (1977). Spermatogenic cells of the prepuberal mouse. Isolation and morphological characterization. J. Cell Biol. *74*, 68–85.

Birtle, Z., and Ponting, C.P. (2006). Meisetz and the birth of the KRAB motif. Bioinforma. Oxf. Engl. *22*, 2841–2845.

Bishop, D.K. (1994). RecA homologs Dmc1 and Rad51 interact to form multiple nuclear complexes prior to meiotic chromosome synapsis. Cell *79*, 1081–1092.

Bishop, D.K., Park, D., Xu, L., and Kleckner, N. (1992). DMC1: a meiosis-specific yeast homolog of E. coli recA required for recombination, synaptonemal complex formation, and cell cycle progression. Cell *69*, 439–456.

Blat, Y., Protacio, R.U., Hunter, N., and Kleckner, N. (2002). Physical and functional interactions among basic chromosome organizational features govern early steps of meiotic chiasma formation. Cell *111*, 791–802.

Blatch, G.L., and Lässle, M. (1999). The tetratricopeptide repeat: a structural motif mediating protein-protein interactions. BioEssays News Rev. Mol. Cell. Dev. Biol. *21*, 932–939.

Boateng, K.A., Bellani, M.A., Gregoretti, I.V., Pratto, F., and Camerini-Otero, R.D. (2013). Homologous pairing preceding SPO11-mediated double-strand breaks in mice. Dev. Cell *24*, 196–205.

Bolcun-Filas, E., Costa, Y., Speed, R., Taggart, M., Benavente, R., De Rooij, D.G., and Cooke, H.J. (2007). SYCE2 is required for synaptonemal complex assembly, double strand break repair, and homologous recombination. J. Cell Biol. *176*, 741–747.

Bolcun-Filas, E., Hall, E., Speed, R., Taggart, M., Grey, C., de Massy, B., Benavente, R., and Cooke, H.J. (2009). Mutation of the mouse Syce1 gene disrupts synapsis and suggests a link between synaptonemal complex structural components and DNA repair. PLoS Genet. *5*, e1000393.

Bolcun-Filas, E., Rinaldi, V.D., White, M.E., and Schimenti, J.C. (2014). Reversal of female infertility by Chk2 ablation reveals the oocyte DNA damage checkpoint pathway. Science *343*, 533–536.

Borde, V. (2007). The multiple roles of the Mre11 complex for meiotic recombination. Chromosome Res. Int. J. Mol. Supramol. Evol. Asp. Chromosome Biol. *15*, 551–563.

Borde, V., and de Massy, B. (2013). Programmed induction of DNA double strand breaks during meiosis: setting up communication between DNA and the chromosome structure. Curr. Opin. Genet. Dev. *23*, 147–155.

Borde, V., Wu, T.C., and Lichten, M. (1999). Use of a recombination reporter insert to define meiotic recombination domains on chromosome III of Saccharomyces cerevisiae. Mol. Cell. Biol. *19*, 4832–4842.

Boulton, S.J. (2006). Cellular functions of the BRCA tumour-suppressor proteins. Biochem. Soc. Trans. *34*, 633–645.

Bourc'his, D., and Bestor, T.H. (2004). Meiotic catastrophe and retrotransposon reactivation in male germ cells lacking Dnmt3L. Nature *431*, 96–99.

Bourc'his, D., Xu, G.L., Lin, C.S., Bollman, B., and Bestor, T.H. (2001). Dnmt3L and the establishment of maternal genomic imprints. Science *294*, 2536–2539.

Boyle, S., Gilchrist, S., Bridger, J.M., Mahy, N.L., Ellis, J.A., and Bickmore, W.A. (2001). The spatial organization of human chromosomes within the nuclei of normal and emerin-mutant cells. Hum. Mol. Genet. *10*, 211–219.

Branciforte, D., and Martin, S.L. (1994). Developmental and cell type specificity of LINE-1 expression in mouse testis: implications for transposition. Mol. Cell. Biol. *14*, 2584–2592.

Braun, S., and Madhani, H.D. (2012). Shaping the landscape: mechanistic consequences of ubiquitin modification of chromatin. EMBO Rep. *13*, 619–630.

Brick, K., Smagulova, F., Khil, P., Camerini-Otero, R.D., and Petukhova, G.V. (2012). Genetic recombination is directed away from functional genomic elements in mice. Nature *485*, 642–645.

Broccoli, D., Miller, O.J., and Miller, D.A. (1990). Relationship of mouse minor satellite DNA to centromere activity. Cytogenet. Cell Genet. *54*, 182–186.

Brown, E.J., and Baltimore, D. (2000). ATR disruption leads to chromosomal fragmentation and early embryonic lethality. Genes Dev. *14*, 397–402.

Brunmeir, R., Lagger, S., Simboeck, E., Sawicka, A., Egger, G., Hagelkruys, A., Zhang, Y., Matthias, P., Miller, W.J., and Seiser, C. (2010). Epigenetic regulation of a murine retrotransposon by a dual histone modification mark. PLoS Genet. *6*, e1000927.

Brunschwig, H., Levi, L., Ben-David, E., Williams, R.W., Yakir, B., and Shifman, S. (2012). Fine-scale maps of recombination rates and hotspots in the mouse genome. Genetics *191*, 757–764.

Buard, J., and de Massy, B. (2007). Playing hide and seek with mammalian meiotic crossover hotspots. Trends Genet. TIG *23*, 301–309.

Burgoyne, P.S., Mahadevaiah, S.K., and Turner, J.M.A. (2009). The consequences of asynapsis for mammalian meiosis. Nat. Rev. Genet. *10*, 207–216.

Cammas, F., Mark, M., Dollé, P., Dierich, A., Chambon, P., and Losson, R. (2000). Mice lacking the transcriptional corepressor TIF1beta are defective in early postimplantation development. Dev. Camb. Engl. *127*, 2955–2963.

Cao, J., and Yan, Q. (2012). Histone ubiquitination and deubiquitination in transcription, DNA damage response, and cancer. Front. Oncol. *2*, 26.

Carmell, M.A., Girard, A., van de Kant, H.J., Bourc'his, D., Bestor, T.H., de Rooij, D.G., and Hannon, G.J. (2007). MIWI2 is essential for spermatogenesis and repression of transposons in the mouse male germline. Dev Cell *12*, 503–514.

Carofiglio, F., Inagaki, A., de Vries, S., Wassenaar, E., Schoenmakers, S., Vermeulen, C., van Cappellen, W.A., Sleddens-Linkels, E., Grootegoed, J.A., Te Riele, H.P.J., et al. (2013).

SPO11-independent DNA repair foci and their role in meiotic silencing. PLoS Genet. *9*, e1003538.

Cedar, H., and Bergman, Y. (2012). Programming of DNA methylation patterns. Annu. Rev. Biochem. *81*, 97–117.

Celebi, C., van Montfoort, A., Skory, V., Kieffer, E., Kuntz, S., Mark, M., and Viville, S. (2012). Tex 19 paralogs exhibit a gonad and placenta-specific expression in the mouse. J. Reprod. Dev. *58*, 360–365.

Celeste, A., Petersen, S., Romanienko, P.J., Fernandez-Capetillo, O., Chen, H.T., Sedelnikova, O.A., Reina-San-Martin, B., Coppola, V., Meffre, E., Difilippantonio, M.J., et al. (2002). Genomic instability in mice lacking histone H2AX. Science *296*, 922–927.

Celum, C., and Baeten, J.M. (2012). Antiretroviral-based HIV-1 prevention: antiretroviral treatment and pre-exposure prophylaxis. Antivir. Ther. *17*, 1483–1493.

Chambon, J.-P., Touati, S.A., Berneau, S., Cladière, D., Hebras, C., Groeme, R., McDougall, A., and Wassmann, K. (2013). The PP2A inhibitor I2PP2A is essential for sister chromatid segregation in oocyte meiosis II. Curr. Biol. CB *23*, 485–490.

Chan, K.-L., Roig, M.B., Hu, B., Beckouët, F., Metson, J., and Nasmyth, K. (2012). Cohesin's DNA exit gate is distinct from its entrance gate and is regulated by acetylation. Cell *150*, 961–974.

Changolkar, L.N., Singh, G., and Pehrson, J.R. (2008). macroH2A1-dependent silencing of endogenous murine leukemia viruses. Mol. Cell. Biol. *28*, 2059–2065.

Chatterjee, A., Zakian, S., Hu, X.-W., and Singleton, M.R. (2013). Structural insights into the regulation of cohesion establishment by Wpl1. EMBO J. *32*, 677–687.

Chen, C., Jin, J., James, D.A., Adams-Cioaba, M.A., Park, J.G., Guo, Y., Tenaglia, E., Xu, C., Gish, G., Min, J., et al. (2009). Mouse Piwi interactome identifies binding mechanism of Tdrkh Tudor domain to arginine methylated Miwi. Proc. Natl. Acad. Sci. U. S. A. *106*, 20336–20341.

Chen, J., Melton, C., Suh, N., Oh, J.S., Horner, K., Xie, F., Sette, C., Blelloch, R., and Conti, M. (2011). Genome-wide analysis of translation reveals a critical role for deleted in azoospermia-like (Dazl) at the oocyte-to-zygote transition. Genes Dev. *25*, 755–766.

Chen, X.B., Melchionna, R., Denis, C.M., Gaillard, P.H., Blasina, A., Van de Weyer, I., Boddy, M.N., Russell, P., Vialard, J., and McGowan, C.H. (2001). Human Mus81-associated endonuclease cleaves Holliday junctions in vitro. Mol. Cell *8*, 1117–1127.

Cherry, S.M., Adelman, C.A., Theunissen, J.W., Hassold, T.J., Hunt, P.A., and Petrini, J.H.J. (2007). The Mre11 complex influences DNA repair, synapsis, and crossing over in murine meiosis. Curr. Biol. CB *17*, 373–378.

Chi, P., San Filippo, J., Sehorn, M.G., Petukhova, G.V., and Sung, P. (2007). Bipartite stimulatory action of the Hop2-Mnd1 complex on the Rad51 recombinase. Genes Dev. *21*, 1747–1757.

Chiang, T., Duncan, F.E., Schindler, K., Schultz, R.M., and Lampson, M.A. (2010). Evidence that weakened centromere cohesion is a leading cause of age-related aneuploidy in oocytes. Curr. Biol. CB *20*, 1522–1528.

Chicheportiche, A., Bernardino-Sgherri, J., de Massy, B., and Dutrillaux, B. (2007). Characterization of Spo11-dependent and independent phospho-H2AX foci during meiotic prophase I in the male mouse. J. Cell Sci. *120*, 1733–1742.

Chuma, S., Hiyoshi, M., Yamamoto, A., Hosokawa, M., Takamune, K., and Nakatsuji, N. (2003). Mouse Tudor Repeat-1 (MTR-1) is a novel component of chromatoid bodies/nuages in male germ cells and forms a complex with snRNPs. Mech. Dev. *120*, 979–990.

Chuma, S., Hosokawa, M., Kitamura, K., Kasai, S., Fujioka, M., Hiyoshi, M., Takamune, K., Noce, T., and Nakatsuji, N. (2006). Tdrd1/Mtr-1, a tudor-related gene, is essential for male germ-cell differentiation and nuage/germinal granule formation in mice. Proc. Natl. Acad. Sci. U. S. A. *103*, 15894–15899.

Ciosk, R., Shirayama, M., Shevchenko, A., Tanaka, T., Toth, A., Shevchenko, A., and Nasmyth, K. (2000). Cohesin's binding to chromosomes depends on a separate complex consisting of Scc2 and Scc4 proteins. Mol. Cell *5*, 243–254.

Cloud, V., Chan, Y.-L., Grubb, J., Budke, B., and Bishop, D.K. (2012). Rad51 is an accessory factor for Dmc1-mediated joint molecule formation during meiosis. Science *337*, 1222–1225.

Cobb, J., Cargile, B., and Handel, M.A. (1999). Acquisition of competence to condense metaphase I chromosomes during spermatogenesis. Dev Biol *205*, 49–64.

Cole, F., Kauppi, L., Lange, J., Roig, I., Wang, R., Keeney, S., and Jasin, M. (2012). Homeostatic control of recombination is implemented progressively in mouse meiosis. Nat. Cell Biol. *14*, 424–430.

Costa, Y., Speed, R., Ollinger, R., Alsheimer, M., Semple, C.A., Gautier, P., Maratou, K., Novak, I., Höög, C., Benavente, R., et al. (2005). Two novel proteins recruited by synaptonemal complex protein 1 (SYCP1) are at the centre of meiosis. J. Cell Sci. *118*, 2755–2762.

Costa, Y., Speed, R.M., Gautier, P., Semple, C.A., Maratou, K., Turner, J.M.A., and Cooke, H.J. (2006). Mouse MAELSTROM: the link between meiotic silencing of unsynapsed chromatin and microRNA pathway? Hum. Mol. Genet. *15*, 2324–2334.

Covo, S., Westmoreland, J.W., Gordenin, D.A., and Resnick, M.A. (2010). Cohesin Is limiting for the suppression of DNA damage-induced recombination between homologous chromosomes. PLoS Genet. *6*, e1001006.

Cox, D.N., Chao, A., Baker, J., Chang, L., Qiao, D., and Lin, H. (1998). A novel class of evolutionarily conserved genes defined by piwi are essential for stem cell self-renewal. Genes Dev. *12*, 3715–3727.

Crichton, J.H., Dunican, D.S., Maclennan, M., Meehan, R.R., and Adams, I.R. (2013). Defending the genome from the enemy within: mechanisms of retrotransposon suppression in the mouse germline. Cell. Mol. Life Sci. CMLS.

Crichton, J.H., Playfoot, C.J., and Adams, I.R. (2014). The role of chromatin modifications in progression through mouse meiotic prophase. J. Genet. Genomics Yi Chuan Xue Bao *41*, 97–106.

Daniel, K., Lange, J., Hached, K., Fu, J., Anastassiadis, K., Roig, I., Cooke, H.J., Stewart, A.F., Wassmann, K., Jasin, M., et al. (2011). Meiotic homologue alignment and its quality surveillance are controlled by mouse HORMAD1. Nat. Cell Biol. *13*, 599–610.

Daniel, R., Ramcharan, J., Rogakou, E., Taganov, K.D., Greger, J.G., Bonner, W., Nussenzweig, A., Katz, R.A., and Skalka, A.M. (2004). Histone H2AX is phosphorylated at sites of retroviral DNA integration but is dispensable for postintegration repair. J Biol Chem *279*, 45810–45814.

Davies, O.R., Maman, J.D., and Pellegrini, L. (2012). Structural analysis of the human SYCE2-TEX12 complex provides molecular insights into synaptonemal complex assembly. Open Biol. *2*, 120099.

Day, D.S., Luquette, L.J., Park, P.J., and Kharchenko, P.V. (2010). Estimating enrichment of repetitive elements from high-throughput sequence data. Genome Biol. *11*, R69.

Deaton, A.M., and Bird, A. (2011). CpG islands and the regulation of transcription. Genes Dev. *25*, 1010–1022.

DeBerardinis, R.J., Goodier, J.L., Ostertag, E.M., and Kazazian, H.H., Jr (1998). Rapid amplification of a retrotransposon subfamily is evolving the mouse genome. Nat. Genet. *20*, 288–290.

Dehé, P.-M., Dichtl, B., Schaft, D., Roguev, A., Pamblanco, M., Lebrun, R., Rodríguez-Gil, A., Mkandawire, M., Landsberg, K., Shevchenko, A., et al. (2006). Protein interactions within the Set1 complex and their roles in the regulation of histone 3 lysine 4 methylation. J. Biol. Chem. *281*, 35404–35412.

Deng, W., and Lin, H. (2002). miwi, a murine homolog of piwi, encodes a cytoplasmic protein essential for spermatogenesis. Dev Cell *2*, 819–830.

Denne, M., Sauter, M., Armbruester, V., Licht, J.D., Roemer, K., and Mueller-Lantzsch, N. (2007). Physical and functional interactions of human endogenous retrovirus proteins Np9 and rec with the promyelocytic leukemia zinc finger protein. J. Virol. *81*, 5607–5616.

Dennis, K., Fan, T., Geiman, T., Yan, Q., and Muegge, K. (2001). Lsh, a member of the SNF2 family, is required for genome-wide methylation. Genes Dev. *15*, 2940–2944.

Deshaies, R.J., and Joazeiro, C.A.P. (2009). RING domain E3 ubiquitin ligases. Annu. Rev. Biochem. *78*, 399–434.

Dodge, J.E., Kang, Y.-K., Beppu, H., Lei, H., and Li, E. (2004). Histone H3-K9 methyltransferase ESET is essential for early development. Mol. Cell. Biol. *24*, 2478–2486.

Dodson, G.E., Shi, Y., and Tibbetts, R.S. (2004). DNA replication defects, spontaneous DNA damage, and ATM-dependent checkpoint activation in replication protein A-deficient cells. J. Biol. Chem. *279*, 34010–34014.

Eaker, S., Cobb, J., Pyle, A., and Handel, M.A. (2002). Meiotic prophase abnormalities and metaphase cell death in MLH1-deficient mouse spermatocytes: insights into regulation of spermatogenic progress. Dev Biol *249*, 85–95.

Edelmann, W., Cohen, P.E., Kane, M., Lau, K., Morrow, B., Bennett, S., Umar, A., Kunkel, T., Cattoretti, G., Chaganti, R., et al. (1996). Meiotic pachytene arrest in MLH1-deficient mice. Cell *85*, 1125–1134.

Edelmann, W., Cohen, P.E., Kneitz, B., Winand, N., Lia, M., Heyer, J., Kolodner, R., Pollard, J.W., and Kucherlapati, R. (1999). Mammalian MutS homologue 5 is required for chromosome pairing in meiosis. Nat Genet *21*, 123–127.

Eijpe, M., Heyting, C., Gross, B., and Jessberger, R. (2000a). Association of mammalian SMC1 and SMC3 proteins with meiotic chromosomes and synaptonemal complexes. J. Cell Sci. *113 (Pt 4)*, 673–682.

Eijpe, M., Offenberg, H., Goedecke, W., and Heyting, C. (2000b). Localisation of RAD50 and MRE11 in spermatocyte nuclei of mouse and rat. Chromosoma *109*, 123–132.

Eijpe, M., Offenberg, H., Jessberger, R., Revenkova, E., and Heyting, C. (2003). Meiotic cohesin REC8 marks the axial elements of rat synaptonemal complexes before cohesins SMC1beta and SMC3. J. Cell Biol. *160*, 657–670.

Fallahi, M., Getun, I.V., Wu, Z.K., and Bois, P.R.J. (2010). A Global Expression Switch Marks Pachytene Initiation during Mouse Male Meiosis. Genes *1*, 469–483.

Farkash, E.A., Kao, G.D., Horman, S.R., and Prak, E.T.L. (2006). Gamma radiation increases endonuclease-dependent L1 retrotransposition in a cultured cell assay. Nucleic Acids Res. *34*, 1196–1204.

De Fazio, S., Bartonicek, N., Di Giacomo, M., Abreu-Goodger, C., Sankar, A., Funaya, C., Antony, C., Moreira, P.N., Enright, A.J., and O'Carroll, D. (2011). The endonuclease activity of Mili fuels piRNA amplification that silences LINE1 elements. Nature *480*, 259–263.

Fernandez-Capetillo, O., Mahadevaiah, S.K., Celeste, A., Romanienko, P.J., Camerini-Otero, R.D., Bonner, W.M., Manova, K., Burgoyne, P., and Nussenzweig, A. (2003). H2AX is required for chromatin remodeling and inactivation of sex chromosomes in male mouse meiosis. Dev. Cell *4*, 497–508.

Findley, S.D., Tamanaha, M., Clegg, N.J., and Ruohola-Baker, H. (2003). Maelstrom, a Drosophila spindle-class gene, encodes a protein that colocalizes with Vasa and RDE1/AGO1 homolog, Aubergine, in nuage. Dev. Camb. Engl. *130*, 859–871.

Fledel-Alon, A., Wilson, D.J., Broman, K., Wen, X., Ober, C., Coop, G., and Przeworski, M. (2009). Broad-scale recombination patterns underlying proper disjunction in humans. PLoS Genet. *5*, e1000658.

Foley, E.A., and Kapoor, T.M. (2013). Microtubule attachment and spindle assembly checkpoint signalling at the kinetochore. Nat. Rev. Mol. Cell Biol. *14*, 25–37.

Fraune, J., Schramm, S., Alsheimer, M., and Benavente, R. (2012). The mammalian synaptonemal complex: protein components, assembly and role in meiotic recombination. Exp. Cell Res. *318*, 1340–1346.

Frost, R.J.A., Hamra, F.K., Richardson, J.A., Qi, X., Bassel-Duby, R., and Olson, E.N. (2010). MOV10L1 is necessary for protection of spermatocytes against retrotransposons by Piwi-interacting RNAs. Proc. Natl. Acad. Sci. U. S. A. *107*, 11847–11852.

Fukuda, T., Fukuda, N., Agostinho, A., Hernández-Hernández, A., Kouznetsova, A., and Höög, C. (2014). STAG3-mediated stabilization of REC8 cohesin complexes promotes chromosome synapsis during meiosis. EMBO J. *33*, 1243–1255.

Galli, U.M., Sauter, M., Lecher, B., Maurer, S., Herbst, H., Roemer, K., and Mueller-Lantzsch, N. (2005). Human endogenous retrovirus rec interferes with germ cell development in mice and may cause carcinoma in situ, the predecessor lesion of germ cell tumors. Oncogene *24*, 3223–3228.

Garcia-Cruz, R., Brieño, M.A., Roig, I., Grossmann, M., Velilla, E., Pujol, A., Cabero, L., Pessarrodona, A., Barbero, J.L., and Garcia Caldés, M. (2010). Dynamics of cohesin proteins REC8, STAG3, SMC1 beta and SMC3 are consistent with a role in sister chromatid cohesion during meiosis in human oocytes. Hum. Reprod. Oxf. Engl. *25*, 2316–2327.

Garcia-Perez, J.L., Morell, M., Scheys, J.O., Kulpa, D.A., Morell, S., Carter, C.C., Hammer, G.D., Collins, K.L., O'Shea, K.S., Menendez, P., et al. (2010). Epigenetic silencing of engineered L1 retrotransposition events in human embryonic carcinoma cells. Nature *466*, 769–773.

Gerlich, D., Koch, B., Dupeux, F., Peters, J.-M., and Ellenberg, J. (2006). Live-cell imaging reveals a stable cohesin-chromatin interaction after but not before DNA replication. Curr. Biol. CB *16*, 1571–1578.

Goedecke, W., Eijpe, M., Offenberg, H.H., van Aalderen, M., and Heyting, C. (1999). Mre11 and Ku70 interact in somatic cells, but are differentially expressed in early meiosis. Nat. Genet. *23*, 194–198.

Gómez, R., Valdeolmillos, A., Parra, M.T., Viera, A., Carreiro, C., Roncal, F., Rufas, J.S., Barbero, J.L., and Suja, J.A. (2007). Mammalian SGO2 appears at the inner centromere domain and redistributes depending on tension across centromeres during meiosis II and mitosis. EMBO Rep. *8*, 173–180.

Gorr, I.H., Boos, D., and Stemmann, O. (2005). Mutual inhibition of separase and Cdk1 by two-step complex formation. Mol. Cell *19*, 135–141.

Gosden, J.R. (1994). Chromosome Analysis Protocols (Humana Press).

Grey, C., Baudat, F., and de Massy, B. (2009). Genome-wide control of the distribution of meiotic recombination. PLoS Biol. *7*, e35.

Grivna, S.T., Pyhtila, B., and Lin, H. (2006). MIWI associates with translational machinery and PIWI-interacting RNAs (piRNAs) in regulating spermatogenesis. Proc Natl Acad Sci U A *103*, 13415–13420.

Guacci, V., Koshland, D., and Strunnikov, A. (1997). A direct link between sister chromatid cohesion and chromosome condensation revealed through the analysis of MCD1 in S. cerevisiae. Cell *91*, 47–57.

Haarhuis, J.H.I., Elbatsh, A.M.O., van den Broek, B., Camps, D., Erkan, H., Jalink, K., Medema, R.H., and Rowland, B.D. (2013). WAPL-mediated removal of cohesin protects against segregation errors and aneuploidy. Curr. Biol. CB *23*, 2071–2077.

Hackett, J.A., Reddington, J.P., Nestor, C.E., Dunican, D.S., Branco, M.R., Reichmann, J., Reik, W., Surani, M.A., Adams, I.R., and Meehan, R.R. (2012). Promoter DNA methylation couples genome-defence mechanisms to epigenetic reprogramming in the mouse germline. Development *139*, 3623–3632.

Haering, C.H., Löwe, J., Hochwagen, A., and Nasmyth, K. (2002). Molecular architecture of SMC proteins and the yeast cohesin complex. Mol. Cell *9*, 773–788.

Hajkova, P., Erhardt, S., Lane, N., Haaf, T., El-Maarri, O., Reik, W., Walter, J., and Surani, M.A. (2002). Epigenetic reprogramming in mouse primordial germ cells. Mech. Dev. *117*, 15–23.

Hamer, G., Gell, K., Kouznetsova, A., Novak, I., Benavente, R., and Höög, C. (2006). Characterization of a novel meiosis-specific protein within the central element of the synaptonemal complex. J. Cell Sci. *119*, 4025–4032.

Hamer, G., Wang, H., Bolcun-Filas, E., Cooke, H.J., Benavente, R., and Höög, C. (2008). Progression of meiotic recombination requires structural maturation of the central element of the synaptonemal complex. J. Cell Sci. *121*, 2445–2451.

Handel, M.A., and Schimenti, J.C. (2010). Genetics of mammalian meiosis: regulation, dynamics and impact on fertility. Nat. Rev. Genet. *11*, 124–136.

Hata, K., Okano, M., Lei, H., and Li, E. (2002). Dnmt3L cooperates with the Dnmt3 family of de novo DNA methyltransferases to establish maternal imprints in mice. Dev. Camb. Engl. *129*, 1983–1993.

Hauf, S., Waizenegger, I.C., and Peters, J.M. (2001). Cohesin cleavage by separase required for anaphase and cytokinesis in human cells. Science *293*, 1320–1323.

Hayashi, K., Yoshida, K., and Matsui, Y. (2005). A histone H3 methyltransferase controls epigenetic events required for meiotic prophase. Nature *438*, 374–378.

Henderson, K.A., Kee, K., Maleki, S., Santini, P.A., and Keeney, S. (2006). Cyclin-dependent kinase directly regulates initiation of meiotic recombination. Cell *125*, 1321–1332.

Hendrich, B., and Bird, A. (1998). Identification and characterization of a family of mammalian methyl-CpG binding proteins. Mol. Cell. Biol. *18*, 6538–6547.

Her, C., Wu, X., Wan, W., and Doggett, N.A. (1999). Identification and characterization of the mouse MutS homolog 5: Msh5. Mamm. Genome Off. J. Int. Mamm. Genome Soc. *10*, 1054–1061.

Her, C., Zhao, N., Wu, X., and Tompkins, J.D. (2007). MutS homologues hMSH4 and hMSH5: diverse functional implications in humans. Front. Biosci. J. Virtual Libr. *12*, 905–911.

Hernández-Hernández, A., Rincón-Arano, H., Recillas-Targa, F., Ortiz, R., Valdes-Quezada, C., Echeverría, O.M., Benavente, R., and Vázquez-Nin, G.H. (2008). Differential distribution and association of repeat DNA sequences in the lateral element of the synaptonemal complex in rat spermatocytes. Chromosoma *117*, 77–87.

Herrán, Y., Gutiérrez-Caballero, C., Sánchez-Martín, M., Hernández, T., Viera, A., Barbero, J.L., de Álava, E., de Rooij, D.G., Suja, J.Á., Llano, E., et al. (2011). The cohesin subunit RAD21L functions in meiotic synapsis and exhibits sexual dimorphism in fertility. EMBO J. *30*, 3091–3105.

Hirano, T. (2006). At the heart of the chromosome: SMC proteins in action. Nat. Rev. Mol. Cell Biol. *7*, 311–322.

Hirano, M., and Hirano, T. (2002). Hinge-mediated dimerization of SMC protein is essential for its dynamic interaction with DNA. EMBO J. *21*, 5733–5744.

Hirota, K., Steiner, W.W., Shibata, T., and Ohta, K. (2007). Multiple modes of chromatin configuration at natural meiotic recombination hot spots in fission yeast. Eukaryot. Cell *6*, 2072–2080.

Hodges, C.A., Revenkova, E., Jessberger, R., Hassold, T.J., and Hunt, P.A. (2005). SMC1beta-deficient female mice provide evidence that cohesins are a missing link in age-related nondisjunction. Nat Genet *37*, 1351–1355.

Holloman, W.K. (2011). Unraveling the mechanism of BRCA2 in homologous recombination. Nat. Struct. Mol. Biol. *18*, 748–754.

Holloway, J.K., Booth, J., Edelmann, W., McGowan, C.H., and Cohen, P.E. (2008). MUS81 generates a subset of MLH1-MLH3-independent crossovers in mammalian meiosis. PLoS Genet *4*, e1000186.

Holloway, J.K., Morelli, M.A., Borst, P.L., and Cohen, P.E. (2010). Mammalian BLM helicase is critical for integrating multiple pathways of meiotic recombination. J. Cell Biol. *188*, 779–789.

Hu, B., Itoh, T., Mishra, A., Katoh, Y., Chan, K.-L., Upcher, W., Godlee, C., Roig, M.B., Shirahige, K., and Nasmyth, K. (2011). ATP hydrolysis is required for relocating cohesin from sites occupied by its Scc2/4 loading complex. Curr. Biol. CB *21*, 12–24.

Hunter, N. (2011). Double duty for Exo1 during meiotic recombination. Cell Cycle Georget. Tex *10*, 2607–2609.

Hunter, N., and Kleckner, N. (2001). The single-end invasion: an asymmetric intermediate at the double-strand break to double-holliday junction transition of meiotic recombination. Cell *106*, 59–70.

Hutvagner, G., and Simard, M.J. (2008). Argonaute proteins: key players in RNA silencing. Nat. Rev. Mol. Cell Biol. *9*, 22–32.

Ichijima, Y., Ichijima, M., Lou, Z., Nussenzweig, A., Camerini-Otero, R.D., Chen, J., Andreassen, P.R., and Namekawa, S.H. (2011). MDC1 directs chromosome-wide silencing of the sex chromosomes in male germ cells. Genes Dev. *25*, 959–971.

Inselman, A., Eaker, S., and Handel, M.A. (2003). Temporal expression of cell cycle-related proteins during spermatogenesis: establishing a timeline for onset of the meiotic divisions. Cytogenet. Genome Res. *103*, 277–284.

Ishiguro, K., Kim, J., Fujiyama-Nakamura, S., Kato, S., and Watanabe, Y. (2011). A new meiosis-specific cohesin complex implicated in the cohesin code for homologous pairing. EMBO Rep. *12*, 267–275.

Ishiguro, K.-I., Kim, J., Shibuya, H., Hernández-Hernández, A., Suzuki, A., Fukagawa, T., Shioi, G., Kiyonari, H., Li, X.C., Schimenti, J., et al. (2014). Meiosis-specific cohesin mediates homolog recognition in mouse spermatocytes. Genes Dev.

Ishiguro, T., Tanaka, K., Sakuno, T., and Watanabe, Y. (2010). Shugoshin-PP2A counteracts casein-kinase-1-dependent cleavage of Rec8 by separase. Nat. Cell Biol. *12*, 500–506.

Ivanov, D., Schleiffer, A., Eisenhaber, F., Mechtler, K., Haering, C.H., and Nasmyth, K. (2002). Eco1 is a novel acetyltransferase that can acetylate proteins involved in cohesion. Curr. Biol. CB *12*, 323–328.

Jackson, S.P., and Bartek, J. (2009). The DNA-damage response in human biology and disease. Nature *461*, 1071–1078.

Jensen-Seaman, M.I., Furey, T.S., Payseur, B.A., Lu, Y., Roskin, K.M., Chen, C.-F., Thomas, M.A., Haussler, D., and Jacob, H.J. (2004). Comparative recombination rates in the rat, mouse, and human genomes. Genome Res. *14*, 528–538.

Johnson, M.E., Rowsey, R.A., Shirley, S., VandeVoort, C., Bailey, J., and Hassold, T. (2013). A specific family of interspersed repeats (SINEs) facilitates meiotic synapsis in mammals. Mol. Cytogenet. *6*, 1.

Jonason, A.S., Baker, S.M., and Sweasy, J.B. (2001). Interaction of DNA polymerase beta with GRIP1 during meiosis. Chromosoma *110*, 402–410.

Jones, R.B., Garrison, K.E., Wong, J.C., Duan, E.H., Nixon, D.F., and Ostrowski, M.A. (2008). Nucleoside analogue reverse transcriptase inhibitors differentially inhibit human LINE-1 retrotransposition. PloS One *3*, e1547.

Jurka, J., Kapitonov, V.V., Kohany, O., and Jurka, M.V. (2007). Repetitive sequences in complex genomes: structure and evolution. Annu. Rev. Genomics Hum. Genet. *8*, 241–259.

Kaneda, M., Okano, M., Hata, K., Sado, T., Tsujimoto, N., Li, E., and Sasaki, H. (2004). Essential role for de novo DNA methyltransferase Dnmt3a in paternal and maternal imprinting. Nature *429*, 900–903.

Karimi, M.M., Goyal, P., Maksakova, I.A., Bilenky, M., Leung, D., Tang, J.X., Shinkai, Y., Mager, D.L., Jones, S., Hirst, M., et al. (2011). DNA methylation and SETDB1/H3K9me3 regulate predominantly distinct sets of genes, retroelements, and chimeric transcripts in mESCs. Cell Stem Cell *8*, 676–687.

Katis, V.L., Lipp, J.J., Imre, R., Bogdanova, A., Okaz, E., Habermann, B., Mechtler, K., Nasmyth, K., and Zachariae, W. (2010). Rec8 phosphorylation by casein kinase 1 and Cdc7-Dbf4 kinase regulates cohesin cleavage by separase during meiosis. Dev. Cell *18*, 397–409.

Kato, Y., Kaneda, M., Hata, K., Kumaki, K., Hisano, M., Kohara, Y., Okano, M., Li, E., Nozaki, M., and Sasaki, H. (2007). Role of the Dnmt3 family in de novo methylation of imprinted and repetitive sequences during male germ cell development in the mouse. Hum. Mol. Genet. *16*, 2272–2280.

Kaufmann, S., Sauter, M., Schmitt, M., Baumert, B., Best, B., Boese, A., Roemer, K., and Mueller-Lantzsch, N. (2010). Human endogenous retrovirus protein Rec interacts with the testicular zinc-finger protein and androgen receptor. J. Gen. Virol. *91*, 1494–1502.

Kauppi, L., Barchi, M., Baudat, F., Romanienko, P.J., Keeney, S., and Jasin, M. (2011). Distinct properties of the XY pseudoautosomal region crucial for male meiosis. Science *331*, 916–920.

Kauppi, L., Jasin, M., and Keeney, S. (2013a). How much is enough? Control of DNA double-strand break numbers in mouse meiosis. Cell Cycle Georget. Tex *12*, 2719–2720.

Kauppi, L., Barchi, M., Lange, J., Baudat, F., Jasin, M., and Keeney, S. (2013b). Numerical constraints and feedback control of double-strand breaks in mouse meiosis. Genes Dev.

Keegan, K.S., Holtzman, D.A., Plug, A.W., Christenson, E.R., Brainerd, E.E., Flaggs, G., Bentley, N.J., Taylor, E.M., Meyn, M.S., Moss, S.B., et al. (1996). The Atr and Atm protein kinases associate with different sites along meiotically pairing chromosomes. Genes Dev. *10*, 2423–2437.

Keeney, S. (2001). Mechanism and control of meiotic recombination initiation. Curr. Top. Dev. Biol. *52*, 1–53.

Keeney, S., Giroux, C.N., and Kleckner, N. (1997). Meiosis-specific DNA double-strand breaks are catalyzed by Spo11, a member of a widely conserved protein family. Cell *88*, 375–384.

Khalil, A.M., Boyar, F.Z., and Driscoll, D.J. (2004). Dynamic histone modifications mark sex chromosome inactivation and reactivation during mammalian spermatogenesis. Proc. Natl. Acad. Sci. U. S. A. *101*, 16583–16587.

Kidane, D., Jonason, A.S., Gorton, T.S., Mihaylov, I., Pan, J., Keeney, S., de Rooij, D.G., Ashley, T., Keh, A., Liu, Y., et al. (2010). DNA polymerase beta is critical for mouse meiotic synapsis. EMBO J. *29*, 410–423.

Kim, J.-S., Krasieva, T.B., LaMorte, V., Taylor, A.M.R., and Yokomori, K. (2002). Specific recruitment of human cohesin to laser-induced DNA damage. J. Biol. Chem. *277*, 45149–45153.

Kleckner, N., Storlazzi, A., and Zickler, D. (2003). Coordinate variation in meiotic pachytene SC length and total crossover/chiasma frequency under conditions of constant DNA length. Trends Genet. TIG *19*, 623–628.

Kneitz, B., Cohen, P.E., Avdievich, E., Zhu, L., Kane, M.F., Hou, H., Kolodner, R.D., Kucherlapati, R., Pollard, J.W., and Edelmann, W. (2000). MutS homolog 4 localization to meiotic chromosomes is required for chromosome pairing during meiosis in male and female mice. Genes Dev *14*, 1085–1097.

Koehler, K.E., Cherry, J.P., Lynn, A., Hunt, P.A., and Hassold, T.J. (2002). Genetic control of mammalian meiotic recombination. I. Variation in exchange frequencies among males from inbred mouse strains. Genetics *162*, 297–306.

Kolas, N.K., Yuan, L., Hoog, C., Heng, H.H.Q., Marcon, E., and Moens, P.B. (2004). Male mouse meiotic chromosome cores deficient in structural proteins SYCP3 and SYCP2 align by homology but fail to synapse and have possible impaired specificity of chromatin loop attachment. Cytogenet. Genome Res. *105*, 182–188.

Komander, D., and Rape, M. (2012). The ubiquitin code. Annu. Rev. Biochem. *81*, 203–229.

Kong, A., Gudbjartsson, D.F., Sainz, J., Jonsdottir, G.M., Gudjonsson, S.A., Richardsson, B., Sigurdardottir, S., Barnard, J., Hallbeck, B., Masson, G., et al. (2002). A high-resolution recombination map of the human genome. Nat. Genet. *31*, 241–247.

Kong, A., Thorleifsson, G., Gudbjartsson, D.F., Masson, G., Sigurdsson, A., Jonasdottir, A., Walters, G.B., Jonasdottir, A., Gylfason, A., Kristinsson, K.T., et al. (2010). Fine-scale recombination rate differences between sexes, populations and individuals. Nature *467*, 1099–1103.

Koszul, R., and Kleckner, N. (2009). Dynamic chromosome movements during meiosis: a way to eliminate unwanted connections? Trends Cell Biol. *19*, 716–724.

Kouznetsova, A., Wang, H., Bellani, M., Camerini-Otero, R.D., Jessberger, R., and Höög, C. (2009). BRCA1-mediated chromatin silencing is limited to oocytes with a small number of asynapsed chromosomes. J. Cell Sci. *122*, 2446–2452.

Kouznetsova, A., Benavente, R., Pastink, A., and Höög, C. (2011). Meiosis in mice without a synaptonemal complex. PloS One *6*, e28255.

Krejci, L., Altmannova, V., Spirek, M., and Zhao, X. (2012). Homologous recombination and its regulation. Nucleic Acids Res. *40*, 5795–5818.

Kudo, N.R., Wassmann, K., Anger, M., Schuh, M., Wirth, K.G., Xu, H., Helmhart, W., Kudo, H., McKay, M., Maro, B., et al. (2006). Resolution of chiasmata in oocytes requires separase-mediated proteolysis. Cell *126*, 135–146.

Kudo, N.R., Anger, M., Peters, A.H., Stemmann, O., Theussl, H.C., Helmhart, W., Kudo, H., Heyting, C., and Nasmyth, K. (2009). Role of cleavage by separase of the Rec8 kleisin subunit of cohesin during mammalian meiosis I. J Cell Sci *122*, 2686–2698.

Kuhn, A., Ong, Y.M., Cheng, C.-Y., Wong, T.Y., Quake, S.R., and Burkholder, W.F. (2014). Linkage disequilibrium and signatures of positive selection around LINE-1 retrotransposons in the human genome. Proc. Natl. Acad. Sci. U. S. A. *111*, 8131–8136.

Kuleszewicz, K., Fu, X., and Kudo, N.R. (2013). Cohesin loading factor Nipbl localizes to chromosome axes during mammalian meiotic prophase. Cell Div. *8*, 12.

Kumar, R., Bourbon, H.-M., and de Massy, B. (2010). Functional conservation of Mei4 for meiotic DNA double-strand break formation from yeasts to mice. Genes Dev. *24*, 1266–1280.

Kuntz, S., Kieffer, E., Bianchetti, L., Lamoureux, N., Fuhrmann, G., and Viville, S. (2008). Tex19, a mammalian-specific protein with a restricted expression in pluripotent stem cells and germ line. Stem Cells *26*, 734–744.

Kuramochi-Miyagawa, S., Kimura, T., Yomogida, K., Kuroiwa, A., Tadokoro, Y., Fujita, Y., Sato, M., Matsuda, Y., and Nakano, T. (2001). Two mouse piwi-related genes: miwi and mili. Mech Dev *108*, 121–133.

Kuramochi-Miyagawa, S., Kimura, T., Ijiri, T.W., Isobe, T., Asada, N., Fujita, Y., Ikawa, M., Iwai, N., Okabe, M., Deng, W., et al. (2004). Mili, a mammalian member of piwi family gene, is essential for spermatogenesis. Development *131*, 839–849.

Kuramochi-Miyagawa, S., Watanabe, T., Gotoh, K., Totoki, Y., Toyoda, A., Ikawa, M., Asada, N., Kojima, K., Yamaguchi, Y., Ijiri, T.W., et al. (2008). DNA methylation of retrotransposon genes is regulated by Piwi family members MILI and MIWI2 in murine fetal testes. Genes Dev *22*, 908–917.

Kuramochi-Miyagawa, S., Watanabe, T., Gotoh, K., Takamatsu, K., Chuma, S., Kojima-Kita, K., Shiromoto, Y., Asada, N., Toyoda, A., Fujiyama, A., et al. (2010). MVH in piRNA processing and gene silencing of retrotransposons. Genes Dev *24*, 887–892.

Kwon, Y.T., Xia, Z., An, J.Y., Tasaki, T., Davydov, I.V., Seo, J.W., Sheng, J., Xie, Y., and Varshavsky, A. (2003). Female lethality and apoptosis of spermatocytes in mice lacking the UBR2 ubiquitin ligase of the N-end rule pathway. Mol. Cell. Biol. *23*, 8255–8271.

Van der Laan, R., Uringa, E.-J., Wassenaar, E., Hoogerbrugge, J.W., Sleddens, E., Odijk, H., Roest, H.P., de Boer, P., Hoeijmakers, J.H.J., Grootegoed, J.A., et al. (2004). Ubiquitin

ligase Rad18Sc localizes to the XY body and to other chromosomal regions that are unpaired and transcriptionally silenced during male meiotic prophase. J. Cell Sci. *117*, 5023–5033.

De La Fuente, R., Baumann, C., Fan, T., Schmidtmann, A., Dobrinski, I., and Muegge, K. (2006). Lsh is required for meiotic chromosome synapsis and retrotransposon silencing in female germ cells. Nat Cell Biol *8*, 1448–1454.

Lammers, J.H., Offenberg, H.H., van Aalderen, M., Vink, A.C., Dietrich, A.J., and Heyting, C. (1994). The gene encoding a major component of the lateral elements of synaptonemal complexes of the rat is related to X-linked lymphocyte-regulated genes. Mol. Cell. Biol. *14*, 1137–1146.

Lander, E.S., Linton, L.M., Birren, B., Nusbaum, C., Zody, M.C., Baldwin, J., Devon, K., Dewar, K., Doyle, M., FitzHugh, W., et al. (2001). Initial sequencing and analysis of the human genome. Nature *409*, 860–921.

Lange, J., Pan, J., Cole, F., Thelen, M.P., Jasin, M., and Keeney, S. (2011). ATM controls meiotic double-strand-break formation. Nature *479*, 237–240.

Lee, J., and Hirano, T. (2011). RAD21L, a novel cohesin subunit implicated in linking homologous chromosomes in mammalian meiosis. J. Cell Biol. *192*, 263–276.

Lee, J., Kitajima, T.S., Tanno, Y., Yoshida, K., Morita, T., Miyano, T., Miyake, M., and Watanabe, Y. (2008). Unified mode of centromeric protection by shugoshin in mammalian oocytes and somatic cells. Nat. Cell Biol. *10*, 42–52.

Leeb, M., Pasini, D., Novatchkova, M., Jaritz, M., Helin, K., and Wutz, A. (2010). Polycomb complexes act redundantly to repress genomic repeats and genes. Genes Dev. *24*, 265–276.

Léotard, D., Kirsch-Volders, M., Alexandre, H., Poma, K., and Susanne, C. (1987). Relationship between frequencies of univalents and meiotic segregation in different mouse strains and their hybrids. Genetica *75*, 189–198.

Lewis, J.D., Meehan, R.R., Henzel, W.J., Maurer-Fogy, I., Jeppesen, P., Klein, F., and Bird, A. (1992). Purification, sequence, and cellular localization of a novel chromosomal protein that binds to methylated DNA. Cell *69*, 905–914.

Li, X.C., and Schimenti, J.C. (2007). Mouse pachytene checkpoint 2 (trip13) is required for completing meiotic recombination but not synapsis. PLoS Genet *3*, e130.

Libby, B.J., De La Fuente, R., O'Brien, M.J., Wigglesworth, K., Cobb, J., Inselman, A., Eaker, S., Handel, M.A., Eppig, J.J., and Schimenti, J.C. (2002). The mouse meiotic mutation mei1 disrupts chromosome synapsis with sexually dimorphic consequences for meiotic progression. Dev. Biol. *242*, 174–187.

Libby, B.J., Reinholdt, L.G., and Schimenti, J.C. (2003). Positional cloning and characterization of Mei1, a vertebrate-specific gene required for normal meiotic chromosome synapsis in mice. Proc. Natl. Acad. Sci. U. S. A. *100*, 15706–15711.

Lightfoot, J., Testori, S., Barroso, C., and Martinez-Perez, E. (2011). Loading of meiotic cohesin by SCC-2 is required for early processing of DSBs and for the DNA damage checkpoint. Curr. Biol. CB *21*, 1421–1430.

Lim, D.S., and Hasty, P. (1996). A mutation in mouse rad51 results in an early embryonic lethal that is suppressed by a mutation in p53. Mol. Cell. Biol. *16*, 7133–7143.

Lin, W., Jin, H., Liu, X., Hampton, K., and Yu, H.-G. (2011). Scc2 regulates gene expression by recruiting cohesin to the chromosome as a transcriptional activator during yeast meiosis. Mol. Biol. Cell *22*, 1985–1996.

Lipkin, S.M., Moens, P.B., Wang, V., Lenzi, M., Shanmugarajah, D., Gilgeous, A., Thomas, J., Cheng, J., Touchman, J.W., Green, E.D., et al. (2002). Meiotic arrest and aneuploidy in MLH3-deficient mice. Nat. Genet. *31*, 385–390.

Lister, L.M., Kouznetsova, A., Hyslop, L.A., Kalleas, D., Pace, S.L., Barel, J.C., Nathan, A., Floros, V., Adelfalk, C., Watanabe, Y., et al. (2010). Age-related meiotic segregation errors in mammalian oocytes are preceded by depletion of cohesin and Sgo2. Curr. Biol. CB *20*, 1511–1521.

Liu, H., Rankin, S., and Yu, H. (2013a). Phosphorylation-enabled binding of SGO1-PP2A to cohesin protects sororin and centromeric cohesion during mitosis. Nat. Cell Biol. *15*, 40–49.

Liu, H., Jia, L., and Yu, H. (2013b). Phospho-H2A and cohesin specify distinct tension-regulated Sgo1 pools at kinetochores and inner centromeres. Curr. Biol. CB *23*, 1927–1933.

Liu, J.G., Yuan, L., Brundell, E., Björkroth, B., Daneholt, B., and Höög, C. (1996). Localization of the N-terminus of SCP1 to the central element of the synaptonemal complex and evidence for direct interactions between the N-termini of SCP1 molecules organized head-to-head. Exp. Cell Res. *226*, 11–19.

Liu, W., Wang, L., Zhao, W., Song, G., Xu, R., Wang, G., Wang, F., Li, W., Lian, J., Tian, H., et al. (2014). Phosphorylation of CDK2 at threonine 160 regulates meiotic pachytene and diplotene progression in mice. Dev. Biol. *392*, 108–116.

Livak, K.J., and Schmittgen, T.D. (2001). Analysis of relative gene expression data using real-time quantitative PCR and the 2(-Delta Delta C(T)) Method. Methods San Diego Calif *25*, 402–408.

Llano, E., Gómez, R., Gutiérrez-Caballero, C., Herrán, Y., Sánchez-Martín, M., Vázquez-Quiñones, L., Hernández, T., de Alava, E., Cuadrado, A., Barbero, J.L., et al. (2008). Shugoshin-2 is essential for the completion of meiosis but not for mitotic cell division in mice. Genes Dev. *22*, 2400–2413.

Llano, E., Herrán, Y., García-Tuñón, I., Gutiérrez-Caballero, C., de Álava, E., Barbero, J.L., Schimenti, J., de Rooij, D.G., Sánchez-Martín, M., and Pendás, A.M. (2012). Meiotic cohesin complexes are essential for the formation of the axial element in mice. J. Cell Biol. *197*, 877–885.

Llano, E., Gomez-H, L., García-Tuñón, I., Sánchez-Martín, M., Caburet, S., Barbero, J.L., Schimenti, J.C., Veitia, R.A., and Pendas, A.M. (2014). STAG3 is a strong candidate gene for male infertility. Hum. Mol. Genet.

Lu, L.-Y., Wu, J., Ye, L., Gavrilina, G.B., Saunders, T.L., and Yu, X. (2010). RNF8-dependent histone modifications regulate nucleosome removal during spermatogenesis. Dev. Cell *18*, 371–384.

Lynn, A., Ashley, T., and Hassold, T. (2004). Variation in human meiotic recombination. Annu. Rev. Genomics Hum. Genet. *5*, 317–349.

Ma, L., Buchold, G.M., Greenbaum, M.P., Roy, A., Burns, K.H., Zhu, H., Han, D.Y., Harris, R.A., Coarfa, C., Gunaratne, P.H., et al. (2009). GASZ is essential for male meiosis and suppression of retrotransposon expression in the male germline. PLoS Genet *5*, e1000635.

Mahadevaiah, S.K., Turner, J.M., Baudat, F., Rogakou, E.P., de Boer, P., Blanco-Rodríguez, J., Jasin, M., Keeney, S., Bonner, W.M., and Burgoyne, P.S. (2001). Recombinational DNA double-strand breaks in mice precede synapsis. Nat. Genet. *27*, 271–276.

Mahadevaiah, S.K., Bourc'his, D., de Rooij, D.G., Bestor, T.H., Turner, J.M., and Burgoyne, P.S. (2008). Extensive meiotic asynapsis in mice antagonises meiotic silencing of

unsynapsed chromatin and consequently disrupts meiotic sex chromosome inactivation. J Cell Biol *182*, 263–276.

Marston, A.L., and Amon, A. (2004). Meiosis: cell-cycle controls shuffle and deal. Nat. Rev. Mol. Cell Biol. *5*, 983–997.

Martinez-Perez, E., and Colaiácovo, M.P. (2009). Distribution of meiotic recombination events: talking to your neighbors. Curr. Opin. Genet. Dev. *19*, 105–112.

Mathioudakis, N., Palencia, A., Kadlec, J., Round, A., Tripsianes, K., Sattler, M., Pillai, R.S., and Cusack, S. (2012). The multiple Tudor domain-containing protein TDRD1 is a molecular scaffold for mouse Piwi proteins and piRNA biogenesis factors. RNA N. Y. N *18*, 2056–2072.

McBurney, M.W., Yang, X., Jardine, K., Bieman, M., Th'ng, J., and Lemieux, M. (2003). The absence of SIR2alpha protein has no effect on global gene silencing in mouse embryonic stem cells. Mol. Cancer Res. MCR *1*, 402–409.

McVean, G.A.T., Myers, S.R., Hunt, S., Deloukas, P., Bentley, D.R., and Donnelly, P. (2004). The fine-scale structure of recombination rate variation in the human genome. Science *304*, 581–584.

Mehta, G.D., Kumar, R., Srivastava, S., and Ghosh, S.K. (2013). Cohesin: functions beyond sister chromatid cohesion. FEBS Lett. *587*, 2299–2312.

Meijering, E., Jacob, M., Sarria, J.-C.F., Steiner, P., Hirling, H., and Unser, M. (2004). Design and validation of a tool for neurite tracing and analysis in fluorescence microscopy images. Cytom. Part J. Int. Soc. Anal. Cytol. *58*, 167–176.

Meissner, A., Mikkelsen, T.S., Gu, H., Wernig, M., Hanna, J., Sivachenko, A., Zhang, X., Bernstein, B.E., Nusbaum, C., Jaffe, D.B., et al. (2008). Genome-scale DNA methylation maps of pluripotent and differentiated cells. Nature *454*, 766–770.

Meuwissen, R.L., Offenberg, H.H., Dietrich, A.J., Riesewijk, A., van Iersel, M., and Heyting, C. (1992). A coiled-coil related protein specific for synapsed regions of meiotic prophase chromosomes. EMBO J. *11*, 5091–5100.

Michaelis, C., Ciosk, R., and Nasmyth, K. (1997). Cohesins: chromosomal proteins that prevent premature separation of sister chromatids. Cell *91*, 35–45.

Mihola, O., Trachtulec, Z., Vlcek, C., Schimenti, J.C., and Forejt, J. (2009). A mouse speciation gene encodes a meiotic histone H3 methyltransferase. Science *323*, 373–375.

Mizuno, K., Emura, Y., Baur, M., Kohli, J., Ohta, K., and Shibata, T. (1997). The meiotic recombination hot spot created by the single-base substitution ade6-M26 results in remodeling of chromatin structure in fission yeast. Genes Dev. *11*, 876–886.

Moens, P.B., Chen, D.J., Shen, Z., Kolas, N., Tarsounas, M., Heng, H.H., and Spyropoulos, B. (1997). Rad51 immunocytology in rat and mouse spermatocytes and oocytes. Chromosoma *106*, 207–215.

Moens, P.B., Tarsounas, M., Morita, T., Habu, T., Rottinghaus, S.T., Freire, R., Jackson, S.P., Barlow, C., and Wynshaw-Boris, A. (1999). The association of ATR protein with mouse meiotic chromosome cores. Chromosoma *108*, 95–102.

Moens, P.B., Kolas, N.K., Tarsounas, M., Marcon, E., Cohen, P.E., and Spyropoulos, B. (2002). The time course and chromosomal localization of recombination-related proteins at meiosis in the mouse are compatible with models that can resolve the early DNA-DNA interactions without reciprocal recombination. J. Cell Sci. *115*, 1611–1622.

Moran, J.V., Holmes, S.E., Naas, T.P., DeBerardinis, R.J., Boeke, J.D., and Kazazian, H.H., Jr (1996). High frequency retrotransposition in cultured mammalian cells. Cell *87*, 917–927.

Mouse Genome Sequencing Consortium, Waterston, R.H., Lindblad-Toh, K., Birney, E., Rogers, J., Abril, J.F., Agarwal, P., Agarwala, R., Ainscough, R., Alexandersson, M., et al. (2002). Initial sequencing and comparative analysis of the mouse genome. Nature *420*, 520–562.

Mulugeta Achame, E., Wassenaar, E., Hoogerbrugge, J.W., Sleddens-Linkels, E., Ooms, M., Sun, Z.-W., van IJcken, W.F.J., Grootegoed, J.A., and Baarends, W.M. (2010). The ubiquitin-conjugating enzyme HR6B is required for maintenance of X chromosome silencing in mouse spermatocytes and spermatids. BMC Genomics *11*, 367.

Muotri, A.R., Marchetto, M.C.N., Coufal, N.G., Oefner, R., Yeo, G., Nakashima, K., and Gage, F.H. (2010). L1 retrotransposition in neurons is modulated by MeCP2. Nature *468*, 443–446.

Murdoch, B., Owen, N., Stevense, M., Smith, H., Nagaoka, S., Hassold, T., McKay, M., Xu, H., Fu, J., Revenkova, E., et al. (2013). Altered cohesin gene dosage affects Mammalian meiotic chromosome structure and behavior. PLoS Genet. *9*, e1003241.

Musacchio, A., and Salmon, E.D. (2007). The spindle-assembly checkpoint in space and time. Nat. Rev. Mol. Cell Biol. *8*, 379–393.

Musselman, C.A., Lalonde, M.-E., Côté, J., and Kutateladze, T.G. (2012). Perceiving the epigenetic landscape through histone readers. Nat. Struct. Mol. Biol. *19*, 1218–1227.

Myant, K., and Stancheva, I. (2008). LSH cooperates with DNA methyltransferases to repress transcription. Mol. Cell. Biol. *28*, 215–226.

Myers, S., Bottolo, L., Freeman, C., McVean, G., and Donnelly, P. (2005). A fine-scale map of recombination rates and hotspots across the human genome. Science *310*, 321–324.

Myers, S., Freeman, C., Auton, A., Donnelly, P., and McVean, G. (2008). A common sequence motif associated with recombination hot spots and genome instability in humans. Nat. Genet. *40*, 1124–1129.

Myers, S., Bowden, R., Tumian, A., Bontrop, R.E., Freeman, C., MacFie, T.S., McVean, G., and Donnelly, P. (2010). Drive against hotspot motifs in primates implicates the PRDM9 gene in meiotic recombination. Science *327*, 876–879.

Nasmyth, K. (2005). How do so few control so many? Cell *120*, 739–746.

Nasmyth, K. (2011). Cohesin: a catenase with separate entry and exit gates? Nat. Cell Biol. *13*, 1170–1177.

Nasmyth, K., and Haering, C.H. (2009). Cohesin: its roles and mechanisms. Annu. Rev. Genet. *43*, 525–558.

Neale, M.J., Pan, J., and Keeney, S. (2005). Endonucleolytic processing of covalent protein-linked DNA double-strand breaks. Nature *436*, 1053–1057.

Neumann, R., and Jeffreys, A.J. (2006). Polymorphism in the activity of human crossover hotspots independent of local DNA sequence variation. Hum. Mol. Genet. *15*, 1401–1411.

Nichols, M.D., DeAngelis, K., Keck, J.L., and Berger, J.M. (1999). Structure and function of an archaeal topoisomerase VI subunit with homology to the meiotic recombination factor Spo11. EMBO J. *18*, 6177–6188.

Nicolas, A. (1998). Relationship between transcription and initiation of meiotic recombination: toward chromatin accessibility. Proc. Natl. Acad. Sci. U. S. A. *95*, 87–89.

Nishiyama, T., Ladurner, R., Schmitz, J., Kreidl, E., Schleiffer, A., Bhaskara, V., Bando, M., Shirahige, K., Hyman, A.A., Mechtler, K., et al. (2010). Sororin mediates sister chromatid cohesion by antagonizing Wapl. Cell *143*, 737–749.

Novak, I., Wang, H., Revenkova, E., Jessberger, R., Scherthan, H., and Höög, C. (2008). Cohesin Smc1beta determines meiotic chromatin axis loop organization. J. Cell Biol. *180*, 83–90.

Oakberg, E.F. (1956). Duration of spermatogenesis in the mouse and timing of stages of the cycle of the seminiferous epithelium. Am. J. Anat. *99*, 507–516.

Offenberg, H.H., Schalk, J.A., Meuwissen, R.L., van Aalderen, M., Kester, H.A., Dietrich, A.J., and Heyting, C. (1998). SCP2: a major protein component of the axial elements of synaptonemal complexes of the rat. Nucleic Acids Res. *26*, 2572–2579.

Okano, M., Bell, D.W., Haber, D.A., and Li, E. (1999). DNA methyltransferases Dnmt3a and Dnmt3b are essential for de novo methylation and mammalian development. Cell *99*, 247–257.

Ollinger, R., Alsheimer, M., and Benavente, R. (2005). Mammalian protein SCP1 forms synaptonemal complex-like structures in the absence of meiotic chromosomes. Mol. Biol. Cell *16*, 212–217.

Ollinger, R., Childs, A.J., Burgess, H.M., Speed, R.M., Lundegaard, P.R., Reynolds, N., Gray, N.K., Cooke, H.J., and Adams, I.R. (2008). Deletion of the pluripotency-associated Tex19.1 gene causes activation of endogenous retroviruses and defective spermatogenesis in mice. PLoS Genet. *4*, e1000199.

Ollinger, R., Reichmann, J., and Adams, I.R. (2010). Meiosis and retrotransposon silencing during germ cell development in mice. Differ. Res. Biol. Divers. *79*, 147–158.

Ortega, S., Prieto, I., Odajima, J., Martín, A., Dubus, P., Sotillo, R., Barbero, J.L., Malumbres, M., and Barbacid, M. (2003). Cyclin-dependent kinase 2 is essential for meiosis but not for mitotic cell division in mice. Nat. Genet. *35*, 25–31.

Ouyang, Z., Zheng, G., Song, J., Borek, D.M., Otwinowski, Z., Brautigam, C.A., Tomchick, D.R., Rankin, S., and Yu, H. (2013). Structure of the human cohesin inhibitor Wapl. Proc. Natl. Acad. Sci. U. S. A. *110*, 11355–11360.

Paigen, K., and Petkov, P. (2010). Mammalian recombination hot spots: properties, control and evolution. Nat. Rev. Genet. *11*, 221–233.

Paigen, K., Szatkiewicz, J.P., Sawyer, K., Leahy, N., Parvanov, E.D., Ng, S.H.S., Graber, J.H., Broman, K.W., and Petkov, P.M. (2008). The recombinational anatomy of a mouse chromosome. PLoS Genet. *4*, e1000119.

Pan, J., and Keeney, S. (2009). Detection of SPO11-oligonucleotide complexes from mouse testes. Methods Mol. Biol. Clifton NJ *557*, 197–207.

Pan, J., Sasaki, M., Kniewel, R., Murakami, H., Blitzblau, H.G., Tischfield, S.E., Zhu, X., Neale, M.J., Jasin, M., Socci, N.D., et al. (2011). A hierarchical combination of factors shapes the genome-wide topography of yeast meiotic recombination initiation. Cell *144*, 719–731.

Parelho, V., Hadjur, S., Spivakov, M., Leleu, M., Sauer, S., Gregson, H.C., Jarmuz, A., Canzonetta, C., Webster, Z., Nesterova, T., et al. (2008). Cohesins functionally associate with CTCF on mammalian chromosome arms. Cell *132*, 422–433.

Parra, M.T., Viera, A., Gómez, R., Page, J., Benavente, R., Santos, J.L., Rufas, J.S., and Suja, J.A. (2004). Involvement of the cohesin Rad21 and SCP3 in monopolar attachment of sister kinetochores during mouse meiosis I. J. Cell Sci. *117*, 1221–1234.

Parvanov, E.D., Ng, S.H.S., Petkov, P.M., and Paigen, K. (2009). Trans-regulation of mouse meiotic recombination hotspots by Rcr1. PLoS Biol. *7*, e36.

Parvanov, E.D., Petkov, P.M., and Paigen, K. (2010). Prdm9 controls activation of mammalian recombination hotspots. Science *327*, 835.

Pauli, A., Althoff, F., Oliveira, R.A., Heidmann, S., Schuldiner, O., Lehner, C.F., Dickson, B.J., and Nasmyth, K. (2008). Cell-type-specific TEV protease cleavage reveals cohesin functions in Drosophila neurons. Dev. Cell *14*, 239–251.

Pearlman, R.E., Tsao, N., and Moens, P.B. (1992). Synaptonemal complexes from DNase-treated rat pachytene chromosomes contain (GT)n and LINE/SINE sequences. Genetics *130*, 865–872.

Pelttari, J., Hoja, M.R., Yuan, L., Liu, J.G., Brundell, E., Moens, P., Santucci-Darmanin, S., Jessberger, R., Barbero, J.L., Heyting, C., et al. (2001). A meiotic chromosomal core consisting of cohesin complex proteins recruits DNA recombination proteins and promotes synapsis in the absence of an axial element in mammalian meiotic cells. Mol. Cell. Biol. *21*, 5667–5677.

Perry, J., Kleckner, N., and Börner, G.V. (2005). Bioinformatic analyses implicate the collaborating meiotic crossover/chiasma proteins Zip2, Zip3, and Spo22/Zip4 in ubiquitin labeling. Proc. Natl. Acad. Sci. U. S. A. *102*, 17594–17599.

Peters, A.H., Plug, A.W., van Vugt, M.J., and de Boer, P. (1997a). A drying-down technique for the spreading of mammalian meiocytes from the male and female germline. Chromosome Res. Int. J. Mol. Supramol. Evol. Asp. Chromosome Biol. *5*, 66–68.

Peters, A.H., Plug, A.W., and de Boer, P. (1997b). Meiosis in carriers of heteromorphic bivalents: sex differences and implications for male fertility. Chromosome Res. Int. J. Mol. Supramol. Evol. Asp. Chromosome Biol. *5*, 313–324.

Petukhova, G.V., Romanienko, P.J., and Camerini-Otero, R.D. (2003). The Hop2 protein has a direct role in promoting interhomolog interactions during mouse meiosis. Dev. Cell *5*, 927–936.

Pezza, R.J., Voloshin, O.N., Vanevski, F., and Camerini-Otero, R.D. (2007). Hop2/Mnd1 acts on two critical steps in Dmc1-promoted homologous pairing. Genes Dev. *21*, 1758–1766.

Pezza, R.J., Camerini-Otero, R.D., and Bianco, P.R. (2010). Hop2-Mnd1 condenses DNA to stimulate the synapsis phase of DNA strand exchange. Biophys. J. *99*, 3763–3772.

Pezza, R.J., Voloshin, O.N., Volodin, A.A., Boateng, K.A., Bellani, M.A., Mazin, A.V., and Camerini-Otero, R.D. (2014). The dual role of HOP2 in mammalian meiotic homologous recombination. Nucleic Acids Res. *42*, 2346–2357.

Pezzi, N., Prieto, I., Kremer, L., Pérez Jurado, L.A., Valero, C., Del Mazo, J., Martínez-A, C., and Barbero, J.L. (2000). STAG3, a novel gene encoding a protein involved in meiotic chromosome pairing and location of STAG3-related genes flanking the Williams-Beuren syndrome deletion. FASEB J. Off. Publ. Fed. Am. Soc. Exp. Biol. *14*, 581–592.

Pittman, D.L., Cobb, J., Schimenti, K.J., Wilson, L.A., Cooper, D.M., Brignull, E., Handel, M.A., and Schimenti, J.C. (1998). Meiotic prophase arrest with failure of chromosome synapsis in mice deficient for Dmc1, a germline-specific RecA homolog. Mol Cell *1*, 697–705.

Plug, A.W., Clairmont, C.A., Sapi, E., Ashley, T., and Sweasy, J.B. (1997a). Evidence for a role for DNA polymerase beta in mammalian meiosis. Proc. Natl. Acad. Sci. U. S. A. *94*, 1327–1331.

Plug, A.W., Peters, A.H., Xu, Y., Keegan, K.S., Hoekstra, M.F., Baltimore, D., de Boer, P., and Ashley, T. (1997b). ATM and RPA in meiotic chromosome synapsis and recombination. Nat. Genet. *17*, 457–461.

Poleshko, A., Palagin, I., Zhang, R., Boimel, P., Castagna, C., Adams, P.D., Skalka, A.M., and Katz, R.A. (2008). Identification of cellular proteins that maintain retroviral epigenetic silencing: evidence for an antiviral response. J. Virol. *82*, 2313–2323.

Poleshko, A., Einarson, M.B., Shalginskikh, N., Zhang, R., Adams, P.D., Skalka, A.M., and Katz, R.A. (2010). Identification of a functional network of human epigenetic silencing factors. J. Biol. Chem. *285*, 422–433.

Prieto, I., Suja, J.A., Pezzi, N., Kremer, L., Martínez-A, C., Rufas, J.S., and Barbero, J.L. (2001). Mammalian STAG3 is a cohesin specific to sister chromatid arms in meiosis I. Nat. Cell Biol. *3*, 761–766.

Prokhortchouk, A., Hendrich, B., Jørgensen, H., Ruzov, A., Wilm, M., Georgiev, G., Bird, A., and Prokhortchouk, E. (2001). The p120 catenin partner Kaiso is a DNA methylation-dependent transcriptional repressor. Genes Dev. *15*, 1613–1618.

Qiao, H., Prasada Rao, H.B.D., Yang, Y., Fong, J.H., Cloutier, J.M., Deacon, D.C., Nagel, K.E., Swartz, R.K., Strong, E., Holloway, J.K., et al. (2014). Antagonistic roles of ubiquitin ligase HEI10 and SUMO ligase RNF212 regulate meiotic recombination. Nat. Genet. *46*, 194–199.

Ranjha, L., Anand, R., and Cejka, P. (2014). The Saccharomyces cerevisiae Mlh1-Mlh3 heterodimer is an endonuclease that preferentially binds to Holliday junctions. J. Biol. Chem. *289*, 5674–5686.

Reddington, J.P., Pennings, S., and Meehan, R.R. (2013). Non-canonical functions of the DNA methylome in gene regulation. Biochem. J. *451*, 13–23.

Reichmann, J., Crichton, J.H., Madej, M.J., Taggart, M., Gautier, P., Garcia-Perez, J.L., Meehan, R.R., and Adams, I.R. (2012). Microarray analysis of LTR retrotransposon silencing identifies Hdac1 as a regulator of retrotransposon expression in mouse embryonic stem cells. PLoS Comput. Biol. *8*, e1002486.

Reichmann, J., Reddington, J.P., Best, D., Read, D., Ollinger, R., Meehan, R.R., and Adams, I.R. (2013). The genome-defence gene Tex19.1 suppresses LINE-1 retrotransposons in the placenta and prevents intra-uterine growth retardation in mice. Hum Mol Genet *22*, 1791–1806.

Reinholdt, L.G., and Schimenti, J.C. (2005). Mei1 is epistatic to Dmc1 during mouse meiosis. Chromosoma *114*, 127–134.

Reuter, M., Chuma, S., Tanaka, T., Franz, T., Stark, A., and Pillai, R.S. (2009). Loss of the Mili-interacting Tudor domain-containing protein-1 activates transposons and alters the Mili-associated small RNA profile. Nat Struct Mol Biol *16*, 639–646.

Revenkova, E., Eijpe, M., Heyting, C., Gross, B., and Jessberger, R. (2001). Novel meiosis-specific isoform of mammalian SMC1. Mol. Cell. Biol. *21*, 6984–6998.

Revenkova, E., Eijpe, M., Heyting, C., Hodges, C.A., Hunt, P.A., Liebe, B., Scherthan, H., and Jessberger, R. (2004). Cohesin SMC1 beta is required for meiotic chromosome dynamics, sister chromatid cohesion and DNA recombination. Nat. Cell Biol. *6*, 555–562.

Reynolds, A., Qiao, H., Yang, Y., Chen, J.K., Jackson, N., Biswas, K., Holloway, J.K., Baudat, F., de Massy, B., Wang, J., et al. (2013). RNF212 is a dosage-sensitive regulator of crossing-over during mammalian meiosis. Nat. Genet. *45*, 269–278.

Reynolds, N., Collier, B., Maratou, K., Bingham, V., Speed, R.M., Taggart, M., Semple, C.A., Gray, N.K., and Cooke, H.J. (2005). Dazl binds in vivo to specific transcripts and can regulate the pre-meiotic translation of Mvh in germ cells. Hum Mol Genet *14*, 3899–3909.

Rieder, C.L., and Salmon, E.D. (1998). The vertebrate cell kinetochore and its roles during mitosis. Trends Cell Biol. *8*, 310–318.

Robine, N., Uematsu, N., Amiot, F., Gidrol, X., Barillot, E., Nicolas, A., and Borde, V. (2007). Genome-wide redistribution of meiotic double-strand breaks in Saccharomyces cerevisiae. Mol. Cell. Biol. *27*, 1868–1880.

Rogacheva, M.V., Manhart, C.M., Chen, C., Guarne, A., Surtees, J., and Alani, E. (2014). Mlh1-Mlh3, a meiotic crossover and DNA mismatch repair factor, is a Msh2-Msh3-stimulated endonuclease. J. Biol. Chem. *289*, 5664–5673.

Rogakou, E.P., Pilch, D.R., Orr, A.H., Ivanova, V.S., and Bonner, W.M. (1998). DNA double-stranded breaks induce histone H2AX phosphorylation on serine 139. J. Biol. Chem. *273*, 5858–5868.

Roig, I., Dowdle, J.A., Toth, A., de Rooij, D.G., Jasin, M., and Keeney, S. (2010). Mouse TRIP13/PCH2 is required for recombination and normal higher-order chromosome structure during meiosis. PLoS Genet. *6*.

Rolef Ben-Shahar, T., Heeger, S., Lehane, C., East, P., Flynn, H., Skehel, M., and Uhlmann, F. (2008). Eco1-dependent cohesin acetylation during establishment of sister chromatid cohesion. Science *321*, 563–566.

Romanienko, P.J., and Camerini-Otero, R.D. (2000). The mouse Spo11 gene is required for meiotic chromosome synapsis. Mol. Cell *6*, 975–987.

Romanish, M.T., Cohen, C.J., and Mager, D.L. (2010). Potential mechanisms of endogenous retroviral-mediated genomic instability in human cancer. Semin. Cancer Biol. *20*, 246–253.

Royo, H., Polikiewicz, G., Mahadevaiah, S.K., Prosser, H., Mitchell, M., Bradley, A., de Rooij, D.G., Burgoyne, P.S., and Turner, J.M.A. (2010). Evidence that meiotic sex chromosome inactivation is essential for male fertility. Curr. Biol. CB *20*, 2117–2123.

Royo, H., Prosser, H., Ruzankina, Y., Mahadevaiah, S.K., Cloutier, J.M., Baumann, M., Fukuda, T., Höög, C., Tóth, A., de Rooij, D.G., et al. (2013). ATR acts stage specifically to regulate multiple aspects of mammalian meiotic silencing. Genes Dev. *27*, 1484–1494.

Ruggiu, M., Speed, R., Taggart, M., McKay, S.J., Kilanowski, F., Saunders, P., Dorin, J., and Cooke, H.J. (1997). The mouse Dazla gene encodes a cytoplasmic protein essential for gametogenesis. Nature *389*, 73–77.

La Salle, S., Mertineit, C., Taketo, T., Moens, P.B., Bestor, T.H., and Trasler, J.M. (2004). Windows for sex-specific methylation marked by DNA methyltransferase expression profiles in mouse germ cells. Dev. Biol. *268*, 403–415.

La Salle, S., Oakes, C.C., Neaga, O.R., Bourc'his, D., Bestor, T.H., and Trasler, J.M. (2007). Loss of spermatogonia and wide-spread DNA methylation defects in newborn male mice deficient in DNMT3L. BMC Dev. Biol. *7*, 104.

Sambrook, J., and Russell, D.W. (2001). Molecular Cloning: A Laboratory Manual (Cold Spring Harbor Laboratory Press).

De los Santos, T., Hunter, N., Lee, C., Larkin, B., Loidl, J., and Hollingsworth, N.M. (2003). The Mus81/Mms4 endonuclease acts independently of double-Holliday junction resolution to promote a distinct subset of crossovers during meiosis in budding yeast. Genetics *164*, 81–94.

Sasaki, M., Lange, J., and Keeney, S. (2010). Genome destabilization by homologous recombination in the germ line. Nat. Rev. Mol. Cell Biol. *11*, 182–195.

Sasaki, M., Tischfield, S.E., van Overbeek, M., and Keeney, S. (2013). Meiotic recombination initiation in and around retrotransposable elements in Saccharomyces cerevisiae. PLoS Genet. *9*, e1003732.

Satyanarayana, A., and Kaldis, P. (2009). Mammalian cell-cycle regulation: several Cdks, numerous cyclins and diverse compensatory mechanisms. Oncogene *28*, 2925–2939.

Schmekel, K., Meuwissen, R.L., Dietrich, A.J., Vink, A.C., van Marle, J., van Veen, H., and Heyting, C. (1996). Organization of SCP1 protein molecules within synaptonemal complexes of the rat. Exp. Cell Res. *226*, 20–30.

Schramm, S., Fraune, J., Naumann, R., Hernandez-Hernandez, A., Höög, C., Cooke, H.J., Alsheimer, M., and Benavente, R. (2011). A novel mouse synaptonemal complex protein is essential for loading of central element proteins, recombination, and fertility. PLoS Genet. *7*, e1002088.

Schrans-Stassen, B.H., Saunders, P.T., Cooke, H.J., and de Rooij, D.G. (2001). Nature of the spermatogenic arrest in Dazl -/- mice. Biol Reprod *65*, 771–776.

Schwacha, A., and Kleckner, N. (1997). Interhomolog bias during meiotic recombination: meiotic functions promote a highly differentiated interhomolog-only pathway. Cell *90*, 1123–1135.

Sebastian, J., Ravi, M., Andreuzza, S., Panoli, A.P., Marimuthu, M.P.A., and Siddiqi, I. (2009). The plant adherin AtSCC2 is required for embryogenesis and sister-chromatid cohesion during meiosis in Arabidopsis. Plant J. Cell Mol. Biol. *59*, 1–13.

Sedelnikova, O.A., Pilch, D.R., Redon, C., and Bonner, W.M. (2003). Histone H2AX in DNA damage and repair. Cancer Biol. Ther. *2*, 233–235.

Seki, Y., Hayashi, K., Itoh, K., Mizugaki, M., Saitou, M., and Matsui, Y. (2005). Extensive and orderly reprogramming of genome-wide chromatin modifications associated with specification and early development of germ cells in mice. Dev. Biol. *278*, 440–458.

Serrentino, M.-E., and Borde, V. (2012). The spatial regulation of meiotic recombination hotspots: are all DSB hotspots crossover hotspots? Exp. Cell Res. *318*, 1347–1352.

Shannon, M., Richardson, L., Christian, A., Handel, M.A., and Thelen, M.P. (1999). Differential gene expression of mammalian SPO11/TOP6A homologs during meiosis. FEBS Lett. *462*, 329–334.

Sharan, S.K., Pyle, A., Coppola, V., Babus, J., Swaminathan, S., Benedict, J., Swing, D., Martin, B.K., Tessarollo, L., Evans, J.P., et al. (2004). BRCA2 deficiency in mice leads to meiotic impairment and infertility. Dev. Camb. Engl. *131*, 131–142.

Sheridan, S., and Bishop, D.K. (2006). Red-Hed regulation: recombinase Rad51, though capable of playing the leading role, may be relegated to supporting Dmc1 in budding yeast meiosis. Genes Dev. *20*, 1685–1691.

Shiloh, Y. (2003). ATM and related protein kinases: safeguarding genome integrity. Nat. Rev. Cancer *3*, 155–168.

Shiloh, Y., and Ziv, Y. (2013). The ATM protein kinase: regulating the cellular response to genotoxic stress, and more. Nat. Rev. Mol. Cell Biol. *14*, 197–210.

Shinohara, A., Ogawa, H., and Ogawa, T. (1992). Rad51 protein involved in repair and recombination in S. cerevisiae is a RecA-like protein. Cell *69*, 457–470.

Shinohara, A., Gasior, S., Ogawa, T., Kleckner, N., and Bishop, D.K. (1997). Saccharomyces cerevisiae recA homologues RAD51 and DMC1 have both distinct and overlapping roles in meiotic recombination. Genes Cells Devoted Mol. Cell. Mech. *2*, 615–629.

Shoji, M., Tanaka, T., Hosokawa, M., Reuter, M., Stark, A., Kato, Y., Kondoh, G., Okawa, K., Chujo, T., Suzuki, T., et al. (2009). The TDRD9-MIWI2 complex is essential for piRNA-mediated retrotransposon silencing in the mouse male germline. Dev. Cell *17*, 775–787.

Simon, J.A., and Kingston, R.E. (2013). Occupying chromatin: Polycomb mechanisms for getting to genomic targets, stopping transcriptional traffic, and staying put. Mol. Cell *49*, 808–824.

Siomi, M.C., Saito, K., and Siomi, H. (2008). How selfish retrotransposons are silenced in Drosophila germline and somatic cells. FEBS Lett. *582*, 2473–2478.

Skibbens, R.V., Colquhoun, J.M., Green, M.J., Molnar, C.A., Sin, D.N., Sullivan, B.J., and Tanzosh, E.E. (2013). Cohesinopathies of a feather flock together. PLoS Genet. *9*, e1004036.

Smagulova, F., Gregoretti, I.V., Brick, K., Khil, P., Camerini-Otero, R.D., and Petukhova, G.V. (2011). Genome-wide analysis reveals novel molecular features of mouse recombination hotspots. Nature *472*, 375–378.

Smallwood, S.A., and Kelsey, G. (2012). De novo DNA methylation: a germ cell perspective. Trends Genet. TIG *28*, 33–42.

Snowden, T., Acharya, S., Butz, C., Berardini, M., and Fishel, R. (2004). hMSH4-hMSH5 recognizes Holliday Junctions and forms a meiosis-specific sliding clamp that embraces homologous chromosomes. Mol. Cell *15*, 437–451.

Sobol, R.W., and Wilson, S.H. (2001). Mammalian DNA beta-polymerase in base excision repair of alkylation damage. Prog. Nucleic Acid Res. Mol. Biol. *68*, 57–74.

Solari, A.J. (1974). The behavior of the XY pair in mammals. Int. Rev. Cytol. *38*, 273–317.

Sommermeyer, V., Béneut, C., Chaplais, E., Serrentino, M.E., and Borde, V. (2013). Spp1, a member of the Set1 Complex, promotes meiotic DSB formation in promoters by tethering histone H3K4 methylation sites to chromosome axes. Mol. Cell *49*, 43–54.

Song, R., Ro, S., Michaels, J.D., Park, C., McCarrey, J.R., and Yan, W. (2009). Many X-linked microRNAs escape meiotic sex chromosome inactivation. Nat. Genet. *41*, 488–493.

Soper, S.F., van der Heijden, G.W., Hardiman, T.C., Goodheart, M., Martin, S.L., de Boer, P., and Bortvin, A. (2008). Mouse maelstrom, a component of nuage, is essential for spermatogenesis and transposon repression in meiosis. Dev Cell *15*, 285–297.

Speed, R.M. (1982). Meiosis in the foetal mouse ovary. I. An analysis at the light microscope level using surface-spreading. Chromosoma *85*, 427–437.

Stemmann, O., Zou, H., Gerber, S.A., Gygi, S.P., and Kirschner, M.W. (2001). Dual inhibition of sister chromatid separation at metaphase. Cell *107*, 715–726.

Stracker, T.H., Theunissen, J.-W.F., Morales, M., and Petrini, J.H.J. (2004). The Mre11 complex and the metabolism of chromosome breaks: the importance of communicating and holding things together. DNA Repair *3*, 845–854.

Suetake, I., Shinozaki, F., Miyagawa, J., Takeshima, H., and Tajima, S. (2004). DNMT3L stimulates the DNA methylation activity of Dnmt3a and Dnmt3b through a direct interaction. J. Biol. Chem. *279*, 27816–27823.

Sun, L.-Q., Lee, D.W., Zhang, Q., Xiao, W., Raabe, E.H., Meeker, A., Miao, D., Huso, D.L., and Arceci, R.J. (2004). Growth retardation and premature aging phenotypes in mice with disruption of the SNF2-like gene, PASG. Genes Dev. *18*, 1035–1046.

Sun, Y., Kucej, M., Fan, H.-Y., Yu, H., Sun, Q.-Y., and Zou, H. (2009). Separase is recruited to mitotic chromosomes to dissolve sister chromatid cohesion in a DNA-dependent manner. Cell *137*, 123–132.

Syrjänen, J.L., Pellegrini, L., and Davies, O.R. (2014). A molecular model for the role of SYCP3 in meiotic chromosome organisation. eLife e02963.

Tachibana-Konwalski, K., Godwin, J., van der Weyden, L., Champion, L., Kudo, N.R., Adams, D.J., and Nasmyth, K. (2010). Rec8-containing cohesin maintains bivalents without turnover during the growing phase of mouse oocytes. Genes Dev. *24*, 2505–2516.

Takada, Y., Naruse, C., Costa, Y., Shirakawa, T., Tachibana, M., Sharif, J., Kezuka-Shiotani, F., Kakiuchi, D., Masumoto, H., Shinkai, Y., et al. (2011). HP1γ links histone methylation marks to meiotic synapsis in mice. Dev. Camb. Engl. *138*, 4207–4217.

Tanaka, S.S., Toyooka, Y., Akasu, R., Katoh-Fukui, Y., Nakahara, Y., Suzuki, R., Yokoyama, M., and Noce, T. (2000). The mouse homolog of Drosophila Vasa is required for the development of male germ cells. Genes Dev *14*, 841–853.

Tanaka, T., Hosokawa, M., Vagin, V.V., Reuter, M., Hayashi, E., Mochizuki, A.L., Kitamura, K., Yamanaka, H., Kondoh, G., Okawa, K., et al. (2011). Tudor domain containing 7 (Tdrd7) is essential for dynamic ribonucleoprotein (RNP) remodeling of chromatoid bodies during spermatogenesis. Proc. Natl. Acad. Sci. U. S. A. *108*, 10579–10584.

Tarabay, Y., Kieffer, E., Teletin, M., Celebi, C., Van Montfoort, A., Zamudio, N., Achour, M., El Ramy, R., Gazdag, E., Tropel, P., et al. (2013). The mammalian-specific Tex19.1 gene plays an essential role in spermatogenesis and placenta-supported development. Hum. Reprod. Oxf. Engl. *28*, 2201–2214.

Tedeschi, A., Wutz, G., Huet, S., Jaritz, M., Wuensche, A., Schirghuber, E., Davidson, I.F., Tang, W., Cisneros, D.A., Bhaskara, V., et al. (2013). Wapl is an essential regulator of chromatin structure and chromosome segregation. Nature *501*, 564–568.

Thorslund, T., Esashi, F., and West, S.C. (2007). Interactions between human BRCA2 protein and the meiosis-specific recombinase DMC1. EMBO J. *26*, 2915–2922.

Tóth, A., Ciosk, R., Uhlmann, F., Galova, M., Schleiffer, A., and Nasmyth, K. (1999). Yeast cohesin complex requires a conserved protein, Eco1p(Ctf7), to establish cohesion between sister chromatids during DNA replication. Genes Dev. *13*, 320–333.

Tsubouchi, H., and Roeder, G.S. (2006). Budding yeast Hed1 down-regulates the mitotic recombination machinery when meiotic recombination is impaired. Genes Dev. *20*, 1766–1775.

Turner, J.M.A. (2007). Meiotic sex chromosome inactivation. Dev. Camb. Engl. *134*, 1823–1831.

Turner, J.M.A., Mahadevaiah, S.K., Elliott, D.J., Garchon, H.-J., Pehrson, J.R., Jaenisch, R., and Burgoyne, P.S. (2002). Meiotic sex chromosome inactivation in male mice with targeted disruptions of Xist. J. Cell Sci. *115*, 4097–4105.

Turner, J.M.A., Aprelikova, O., Xu, X., Wang, R., Kim, S., Chandramouli, G.V.R., Barrett, J.C., Burgoyne, P.S., and Deng, C.-X. (2004). BRCA1, histone H2AX phosphorylation, and male meiotic sex chromosome inactivation. Curr. Biol. CB *14*, 2135–2142.

Turner, J.M.A., Mahadevaiah, S.K., Fernandez-Capetillo, O., Nussenzweig, A., Xu, X., Deng, C.-X., and Burgoyne, P.S. (2005). Silencing of unsynapsed meiotic chromosomes in the mouse. Nat. Genet. *37*, 41–47.

Uhlmann, F., Lottspeich, F., and Nasmyth, K. (1999). Sister-chromatid separation at anaphase onset is promoted by cleavage of the cohesin subunit Scc1. Nature *400*, 37–42.

Uhlmann, F., Wernic, D., Poupart, M.A., Koonin, E.V., and Nasmyth, K. (2000). Cleavage of cohesin by the CD clan protease separin triggers anaphase in yeast. Cell *103*, 375–386.

Unal, E., Heidinger-Pauli, J.M., Kim, W., Guacci, V., Onn, I., Gygi, S.P., and Koshland, D.E. (2008). A molecular determinant for the establishment of sister chromatid cohesion. Science *321*, 566–569.

Unhavaithaya, Y., Hao, Y., Beyret, E., Yin, H., Kuramochi-Miyagawa, S., Nakano, T., and Lin, H. (2009). MILI, a PIWI-interacting RNA-binding protein, is required for germ line stem cell self-renewal and appears to positively regulate translation. J Biol Chem *284*, 6507–6519.

Vagin, V.V., Wohlschlegel, J., Qu, J., Jonsson, Z., Huang, X., Chuma, S., Girard, A., Sachidanandam, R., Hannon, G.J., and Aravin, A.A. (2009). Proteomic analysis of murine Piwi proteins reveals a role for arginine methylation in specifying interaction with Tudor family members. Genes Dev. *23*, 1749–1762.

Visnes, T., Giordano, F., Kuznetsova, A., Suja, J.A., Lander, A.D., Calof, A.L., and Ström, L. (2013). Localisation of the SMC loading complex Nipbl/Mau2 during mammalian meiotic prophase I. Chromosoma.

Vranis, N.M., Van der Heijden, G.W., Malki, S., and Bortvin, A. (2010). Synaptonemal complex length variation in wild-type male mice. Genes *1*, 505–520.

De Vries, F.A., de Boer, E., van den Bosch, M., Baarends, W.M., Ooms, M., Yuan, L., Liu, J.G., van Zeeland, A.A., Heyting, C., and Pastink, A. (2005). Mouse Sycp1 functions in synaptonemal complex assembly, meiotic recombination, and XY body formation. Genes Dev *19*, 1376–1389.

De Vries, S.S., Baart, E.B., Dekker, M., Siezen, A., de Rooij, D.G., de Boer, P., and te Riele, H. (1999). Mouse MutS-like protein Msh5 is required for proper chromosome synapsis in male and female meiosis. Genes Dev. *13*, 523–531.

Waizenegger, I.C., Hauf, S., Meinke, A., and Peters, J.M. (2000). Two distinct pathways remove mammalian cohesin from chromosome arms in prophase and from centromeres in anaphase. Cell *103*, 399–410.

Wang, P.J., McCarrey, J.R., Yang, F., and Page, D.C. (2001). An abundance of X-linked genes expressed in spermatogonia. Nat. Genet. *27*, 422–426.

Ward, J.O., Reinholdt, L.G., Motley, W.W., Niswander, L.M., Deacon, D.C., Griffin, L.B., Langlais, K.K., Backus, V.L., Schimenti, K.J., O'Brien, M.J., et al. (2007). Mutation in mouse hei10, an e3 ubiquitin ligase, disrupts meiotic crossing over. PLoS Genet. *3*, e139.

Weber, M., Hellmann, I., Stadler, M.B., Ramos, L., Pääbo, S., Rebhan, M., and Schübeler, D. (2007). Distribution, silencing potential and evolutionary impact of promoter DNA methylation in the human genome. Nat. Genet. *39*, 457–466.

Webster, K.E., O'Bryan, M.K., Fletcher, S., Crewther, P.E., Aapola, U., Craig, J., Harrison, D.K., Aung, H., Phutikanit, N., Lyle, R., et al. (2005). Meiotic and epigenetic defects in Dnmt3L-knockout mouse spermatogenesis. Proc. Natl. Acad. Sci. U. S. A. *102*, 4068–4073.

Wei, K., Clark, A.B., Wong, E., Kane, M.F., Mazur, D.J., Parris, T., Kolas, N.K., Russell, R., Hou, H., Jr, Kneitz, B., et al. (2003). Inactivation of Exonuclease 1 in mice results in DNA mismatch repair defects, increased cancer susceptibility, and male and female sterility. Genes Dev. *17*, 603–614.

Whyte, W.A., Bilodeau, S., Orlando, D.A., Hoke, H.A., Frampton, G.M., Foster, C.T., Cowley, S.M., and Young, R.A. (2012). Enhancer decommissioning by LSD1 during embryonic stem cell differentiation. Nature *482*, 221–225.

Wiench, M., John, S., Baek, S., Johnson, T.A., Sung, M.-H., Escobar, T., Simmons, C.A., Pearce, K.H., Biddie, S.C., Sabo, P.J., et al. (2011). DNA methylation status predicts cell type-specific enhancer activity. EMBO J. *30*, 3028–3039.

Winkel, K., Alsheimer, M., Ollinger, R., and Benavente, R. (2009). Protein SYCP2 provides a link between transverse filaments and lateral elements of mammalian synaptonemal complexes. Chromosoma *118*, 259–267.

Wojtasz, L., Daniel, K., Roig, I., Bolcun-Filas, E., Xu, H., Boonsanay, V., Eckmann, C.R., Cooke, H.J., Jasin, M., Keeney, S., et al. (2009). Mouse HORMAD1 and HORMAD2, two conserved meiotic chromosomal proteins, are depleted from synapsed chromosome axes with the help of TRIP13 AAA-ATPase. PLoS Genet. *5*, e1000702.

Wojtasz, L., Cloutier, J.M., Baumann, M., Daniel, K., Varga, J., Fu, J., Anastassiadis, K., Stewart, A.F., Reményi, A., Turner, J.M.A., et al. (2012). Meiotic DNA double-strand breaks and chromosome asynapsis in mice are monitored by distinct HORMAD2-independent and -dependent mechanisms. Genes Dev. *26*, 958–973.

Wu, T.C., and Lichten, M. (1994). Meiosis-induced double-strand break sites determined by yeast chromatin structure. Science *263*, 515–518.

Wu, L., Bachrati, C.Z., Ou, J., Xu, C., Yin, J., Chang, M., Wang, W., Li, L., Brown, G.W., and Hickson, I.D. (2006). BLAP75/RMI1 promotes the BLM-dependent dissolution of homologous recombination intermediates. Proc. Natl. Acad. Sci. U. S. A. *103*, 4068–4073.

Xu, H., Beasley, M., Verschoor, S., Inselman, A., Handel, M.A., and McKay, M.J. (2004). A new role for the mitotic RAD21/SCC1 cohesin in meiotic chromosome cohesion and segregation in the mouse. EMBO Rep. *5*, 378–384.

Xu, H., Beasley, M.D., Warren, W.D., van der Horst, G.T.J., and McKay, M.J. (2005). Absence of mouse REC8 cohesin promotes synapsis of sister chromatids in meiosis. Dev. Cell *8*, 949–961.

Xu, X., Aprelikova, O., Moens, P., Deng, C.-X., and Furth, P.A. (2003). Impaired meiotic DNA-damage repair and lack of crossing-over during spermatogenesis in BRCA1 full-length isoform deficient mice. Dev. Camb. Engl. *130*, 2001–2012.

Yabuta, Y., Ohta, H., Abe, T., Kurimoto, K., Chuma, S., and Saitou, M. (2011). TDRD5 is required for retrotransposon silencing, chromatoid body assembly, and spermiogenesis in mice. J. Cell Biol. *192*, 781–795.

Yaman, R., and Grandjean, V. (2006). Timing of entry of meiosis depends on a mark generated by DNA methyltransferase 3a in testis. Mol. Reprod. Dev. *73*, 390–397.

Yang, X.-J., and Seto, E. (2008). The Rpd3/Hda1 family of lysine deacetylases: from bacteria and yeast to mice and men. Nat. Rev. Mol. Cell Biol. *9*, 206–218.

Yang, F., De La Fuente, R., Leu, N.A., Baumann, C., McLaughlin, K.J., and Wang, P.J. (2006). Mouse SYCP2 is required for synaptonemal complex assembly and chromosomal synapsis during male meiosis. J. Cell Biol. *173*, 497–507.

Yang, F., Eckardt, S., Leu, N.A., McLaughlin, K.J., and Wang, P.J. (2008). Mouse TEX15 is essential for DNA double-strand break repair and chromosomal synapsis during male meiosis. J. Cell Biol. *180*, 673–679.

Yang, F., Cheng, Y., An, J.Y., Kwon, Y.T., Eckardt, S., Leu, N.A., McLaughlin, K.J., and Wang, P.J. (2010). The ubiquitin ligase Ubr2, a recognition E3 component of the N-end rule pathway, stabilizes Tex19.1 during spermatogenesis. PloS One *5*, e14017.

Yang, H., Jeffrey, P.D., Miller, J., Kinnucan, E., Sun, Y., Thoma, N.H., Zheng, N., Chen, P.-L., Lee, W.-H., and Pavletich, N.P. (2002). BRCA2 function in DNA binding and recombination from a BRCA2-DSS1-ssDNA structure. Science *297*, 1837–1848.

Yin, J., Sobeck, A., Xu, C., Meetei, A.R., Hoatlin, M., Li, L., and Wang, W. (2005). BLAP75, an essential component of Bloom's syndrome protein complexes that maintain genome integrity. EMBO J. *24*, 1465–1476.

Yoshida, K., Kondoh, G., Matsuda, Y., Habu, T., Nishimune, Y., and Morita, T. (1998). The mouse RecA-like gene Dmc1 is required for homologous chromosome synapsis during meiosis. Mol Cell *1*, 707–718.

Yuan, L., Pelttari, J., Brundell, E., Björkroth, B., Zhao, J., Liu, J.G., Brismar, H., Daneholt, B., and Höög, C. (1998). The synaptonemal complex protein SCP3 can form multistranded, cross-striated fibers in vivo. J. Cell Biol. *142*, 331–339.

Yuan, L., Liu, J.G., Zhao, J., Brundell, E., Daneholt, B., and Höög, C. (2000). The murine SCP3 gene is required for synaptonemal complex assembly, chromosome synapsis, and male fertility. Mol. Cell *5*, 73–83.

Yuan, L., Liu, J.-G., Hoja, M.-R., Wilbertz, J., Nordqvist, K., and Höög, C. (2002). Female germ cell aneuploidy and embryo death in mice lacking the meiosis-specific protein SCP3. Science *296*, 1115–1118.

Zamudio, N., and Bourc'his, D. (2010). Transposable elements in the mammalian germline: a comfortable niche or a deadly trap? Heredity *105*, 92–104.

Zeng, W., Baumann, C., Schmidtmann, A., Honaramooz, A., Tang, L., Bondareva, A., Dores, C., Fan, T., Xi, S., Geiman, T., et al. (2011). Lymphoid-specific helicase (HELLS) is essential for meiotic progression in mouse spermatocytes. Biol. Reprod. *84*, 1235–1241.

Zentner, G.E., and Henikoff, S. (2013). Regulation of nucleosome dynamics by histone modifications. Nat. Struct. Mol. Biol. *20*, 259–266.

Zheng, K., Xiol, J., Reuter, M., Eckardt, S., Leu, N.A., McLaughlin, K.J., Stark, A., Sachidanandam, R., Pillai, R.S., and Wang, P.J. (2010). Mouse MOV10L1 associates with Piwi proteins and is an essential component of the Piwi-interacting RNA (piRNA) pathway. Proc. Natl. Acad. Sci. U. S. A. *107*, 11841–11846.

Zou, Y., Liu, Y., Wu, X., and Shell, S.M. (2006). Functions of human replication protein A (RPA): from DNA replication to DNA damage and stress responses. J. Cell. Physiol. *208*, 267–273.

Zupkovitz, G., Tischler, J., Posch, M., Sadzak, I., Ramsauer, K., Egger, G., Grausenburger, R., Schweifer, N., Chiocca, S., Decker, T., et al. (2006). Negative and positive regulation of gene expression by mouse histone deacetylase 1. Mol Cell Biol *26*, 7913–7928.

Appendix